

Past, Present and Future of the Scaling Relations of Galaxies and Active Galactic Nuclei

Mauro D'Onofrio^{1,2}, Paola Marziani² and Cesare Chiosi¹

¹*Department of Physics and Astronomy "G. Galilei", University of Padua, Italy*

²*INAF-Osservatorio Astronomico di Padova, Italy*

Correspondence*:

D'Onofrio Mauro

mauro.donofrio@unipd.it

ABSTRACT

We review the properties of the established Scaling Relations (SRs) of galaxies and active galactic nuclei (AGN), focusing on their origin and expected evolution back in time, providing a short history of the most important progresses obtained up to now and discussing the possible future studies. We also try to connect the observed SRs with the physical mechanisms behind them, examining to what extent current models reproduce the observational data.

The emerging picture clarifies the complexity intrinsic to the galaxy formation and evolution process as well as the basic uncertainties still affecting our knowledge of the AGN phenomenon. At the same time, however, it suggests that the detailed analysis of the SRs can profitably contribute to our understanding of galaxies and AGN.

Keywords: Galaxies, structure, evolution, scale relations, simulations. AGN, structure, evolution, scale relations

1 INTRODUCTION

With the term "Scaling Relations" (hereafter, SRs) astronomers indicate a series of correlations between the parameters describing the physical characteristics of galaxies. These can be radii, mean velocities of stars and gas, stellar population proxies as colors or mass-to-light ratios, density and total amount of gas and dust, black-hole masses, etc.

The study of SRs started when Edwin Hubble presented his famous tuning fork diagram for the morphological classification of galaxy types [1]. Very soon this beautiful scheme prompted the idea that the morphological sequence is driven by some physical parameters, such as mass, luminosity, color, angular momentum and gas content, that progressively change along the sequence determining the observed types. Attempts to build a "physical" classification of galaxies characterized the following years [see e.g. 2, 3, 4, 5, 6].

The first questions arising from the morphological sequence concerned the different flattening observed among galaxies [7]. In this work the authors tried to answer why some galaxies have a flat disk while others do not and, in connection with this, why the spheroidal components of all galaxies contain only old stars, why S0's and early-type spirals have lost their spiral arms and why up to 50% of galaxies are barred.

The basic idea was that the Hubble sequence is essentially an angular momentum sequence [8, 7], where star formation (SF) occurs at increasing gas density. The spread of color within the morphological types was attributed to the different star formation rates (SFR) inside galaxies [9] and to the different stellar populations inside them [10].

Quite soon however, it was clear that the parameters describing the properties of galaxies can be considered a mathematical manifold [3], because several correlations among them are in place. If we consider for example the galaxy luminosity (L), we observe that it correlates with: the effective radius (R_e ; the radius enclosing half the total luminosity) [11], the central velocity dispersion of the stars (σ) (hereafter Faber-Jackson FJ relation [12]), the effective surface brightness (I_e ; the mean surface brightness inside R_e) [13, 14], color [15] and line-strength index (M_{g_2}) [16].

The great number of observed correlations promptly arose other fundamental questions. What are the most fundamental correlations? What parameters better describe their physics? How do the SRs evolve with time?

In an attempt to answer these questions Guzman, R. et al. [17] claimed that only three fundamental relations are necessary to describe all global SRs among the spheroidal systems, while Disney et al. [18] found a striking correlation among five basic parameters that govern the galactic dynamics (R_{50} , R_{90} , M_{HI} , M_d , L : respectively the 90%-light radius, the 50%-light radius, the H I mass, the dynamical mass and the luminosity) and the color. The principal component analysis (PCA) further showed that the first eigenvector dominates the correlations among the parameters and can explain up to 83% of the variance in the data.

Unfortunately, the next investigations demonstrated that the SRs cannot be used as a basis for a theoretical understanding of galaxy formation and evolution. They can be used only 'a posteriori' to verify the ability of theories in reproducing the observed correlations. Galaxies are complex and evolving systems requiring much complex statistical tools than simple PCA [19].

In other words the Hubble classification is only a qualitative scheme, influenced by subjective decisions and difficult to use for distant galaxies. The sequence rests only on the morphological parameters measured in the visual bands, while galaxies are complex systems that can be observed from X-rays to radio wavelengths. In addition a lot of information, such as chemical compositions, stellar populations, central black hole masses, kinematics of stars and gas, etc., can be obtained from the spectral analysis [20].

Recently new support to the study of the SRs was gained thanks to the data of the large sky surveys, such as the Sloan Digital Sky Survey (SDSS [21]), SAURON [22], WINGS [23], ATLAS3D [24], CALIFA [25], SAMI [26], MaNGA [27], etc. These surveys have provided data for thousands of galaxies permitting a more robust statistical analysis of the physical drivers behind their formation and evolution. Several SRs, such as the velocity-luminosity or Tully-Fisher relation (hereafter TF, [28, 29]), the Faber-Jackson (FJ) relation [12], the $I_e - R_e$ (hereafter Kormendy relation KR [13]), the fundamental plane of galaxies (hereafter FP, [30, 31, 4, 32, 33, 34]), the bulge mass - black hole (BH) mass relation [35], the mass-radius (MR) relation [36] are now robust for the galaxies of the nearby Universe and have now well constrained the physical laws governing the assembly of stellar systems.

On the theoretical side, despite the recent progresses, galaxy formation models are still in difficulties with some basic properties of galaxies. For instance colors, radii [37], structural bimodalities [see e.g. 38, 39], angular momentum content [40, 41], variations of the stellar initial mass function (IMF), mass-to-light ratios [42, 43, 44], central versus satellite distributions [45], and others cannot be satisfactorily matched by

the models. Some fundamental dynamical tracers of galaxy structure (e.g. the circular velocity of galaxies and stellar-to-halo mass ratio) predicted by the models are still discrepant with observations.

Another remark to keep in mind is that the technical analysis of the SRs must be considered with due caution. The observed relations often depend on a number of factors, last but not least the structural parameter definitions [46, 47], the environment that could influence the general distribution of galaxies [48], the different fitting algorithms [29, 49, 50] that provide different coefficients, redshift and peculiar motions of the galaxies in the sample used [51, 52, 53], projection effects and bandpass [54, 55, 50], the morphology of galaxies in the sample [29, 56], the stellar population content [33, 57, 58], the metallicity [59] and the statistical properties of the dark matter (DM) halos [see e.g. 36].

In general we want to stress that SRs are today universally considered convenient tools to estimate quantities such as distances and masses in an efficient way (when the data sample is large), but most importantly, they permit a much deeper understanding of galaxy structure, formation and evolution. For example Kassin et al. [60], by examining the V_{rot}/σ ratio across redshift, found that galaxies accrete baryons at different rates during evolution. At the same time, Obreschkow and Glazebrook [41] pointed out the link between the FP and FJ relations with the angular momentum (j), the stellar mass (M_s), and the bulge fraction (β) of spiral galaxies [see also 61, 62]. Lagos et al. [63], using cosmological simulations, confirmed the correlation between galaxy mass and specific angular momentum, and the evolution of the $M_s - j$ relation in passive and active galaxies, while Ferrarese et al. [64] showed that the correlation of the mass of the BHs and the bulge mass is a key element in favor of the co-evolution of the AGN with their host galaxies. Desmond and Wechsler [65] used the FP to predict the amount of DM in the central regions of elliptical galaxies, while Ouellette et al. [66] found that the tilt of the FP correlates with the DM fraction of each galaxy and Chiosi et al. [36] demonstrated that the DM halo growth function is able to shape the mass-radius relation. We will see many other examples of the utility of SRs in this review.

The utility of SRs has been recognized not only for galaxies. They are also very important to understand the central BHs in galaxies and the nature of the active galactic nuclei (AGN). The co-evolution of the central black holes and galaxies has been known for more than twenty years [see e.g. 67, 68, 69, 70, 71, 72]. Even the active nuclei have shown to obey several SRs that are useful to clarify their structure and evolution. We will therefore address in these pages several of these correlations involving the parameters that describe the properties of the central active nucleus in galaxies. This analysis will permit to conclude that, even in this context, SRs are fundamental tools to infer the physical mechanisms at work in galaxies and AGN.

In conclusion we can say that SRs are fundamental for any theory of galaxy formation and evolution. The current view is that the diversity of galaxies appears to increase rapidly with the instrumental improvements so that a good understanding of their physics requires sophisticated numerical simulations that reproduce realistic objects. The physical processes that operate together during galaxy evolution are numerous and imply that the morphological Hubble sequence is only the first approach to the complex problem of galaxy classification [19]. The SRs are the network of properties that the modern statistical tools and theoretical simulations must be able to explain and reproduce. How are their properties intertwined? How do they evolve over time? This is the challenge of future investigations.

In this work we will review some of the established SRs of galaxies and AGN, discussing our current understanding of their origin and evolution. The first six sections are dedicated to the SRs originating from the coupling of galaxies dynamics and stellar population properties. We start in Sec. 2 with the FJ relation, addressing next the TF (Sec. 3), the KR (Sec. 4), the MR relation (Sec. 5 and Sec. 6), and the FP (Sec. 7).

We have analyzed the MR relation with more details because of its cosmological implication. We go on with the color-magnitude (CM) relation (Sec. 8), the relation between the star formation (and star formation history) with the mass and initial halo density in galaxies of different morphological types (Sec. 9), the mass-metallicity relation (Sec. 10). They all provide a useful insight of the stars and gas evolutionary properties. Then, we address the correlation among the DM halos and baryonic matter properties (Sec. 11) and the angular momentum - mass relationship (Sec. 12). Finally, we enter into the AGN domain, starting with a discussion of the correlations of the black-hole masses with the galaxy host properties (Sec. 13) and the most popular correlations observed among AGN (Sec. 14 and 15). Some conclusions are finally drawn in Sec. 16.

2 THE FABER-JACKSON RELATION

The FJ relation is by far the most misunderstood correlation between galaxies parameters. Discovered by [12] in 1976, it is a correlation between the total luminosity of early-type galaxies (ETGs) L and the central velocity dispersion of their stars σ . The authors themselves did not attribute any physical significance to this relation, considering the observed trend a byproduct of the virial theorem, i.e. a translation of the correlation between mass and velocity dispersion, induced by the strong link between mass and luminosity.

The first fit on a sample of 25 ETGs gave $L \propto \sigma^4$, while further investigations provided values of the FJ parameters (slope and scatter) that depend on the magnitude range of the sample considered [73] (as in the case of the FP [55]). The slope varies from ~ 2 to ~ 5 and the scatter of the residuals (~ 0.30) correlates with the effective radius R_e (in the sense that smaller than average objects have larger velocity dispersion) and with the mass-to-light ratio [37, 74]. The correlation however extends over 8 dex in luminosity, from Globular Clusters to Galaxy Clusters. A small curvature seems to exist at $M_V \sim -21.5$ mag, separating bright and faint objects. The bright galaxies have a slope around 4-5, while the faint ones have it much closer to 2-3 [75, 76].

The FJ is not one of the orthogonal projections of the FP relation $\sigma \propto I_e^a R_e^b$ (with a scatter of ~ 0.09 in R_e). In the FJ relation the variable L include both R_e and I_e . We can better say that it is a sort of 2D version of the FP¹. The deep analysis of Nigoche-Netro et al. [77] concluded that the scatter of the FJ depends on the history of galaxies, i.e on the number and nature of the transformations that have affected the galaxies along their life times (collapse, accretion, interaction and merging). The investigations of ETGs from the ATLAS-3D survey have indeed shown that many of these galaxies possess high rotational velocities, while slow-rotating objects often present counter-rotating cores. There are multiple channels of formation, where secular processes, disk instability, mergers, and gas accretion are possible mechanisms. Star formation events are sometimes observed even in the brightest cluster galaxies (BCGs), today almost quenched, down to low redshifts [see e.g. 78, 79].

Despite this complexity there is an ample consensus on the fact that ETGs are approximately virialized object from a dynamical point of view. Since luminosity is in general a quite good tracer of stellar mass, the deviation from the expected virial slope of 2, was explained with a smooth transition of the zero-point of the relation, essentially due to a variation of the mean mass-to-light ratio. This is the same explanation given for the observed tilt of the FP (see Sec. 7).

The existence of a physical correlation between luminosity and velocity dispersion of stars has never been considered as a concrete possibility. Why should the global stars emission be aware of the mean stars velocity in a galaxy? This appears as an unphysical possibility. Recently however, D'Onofrio et al. [37] has

¹ By the way the FP was discovered by studying the residuals of the FJ relation.

opened the door to this remote possibility. The idea is that the total luminosity of galaxies is essentially the result of the stars assembly, of the SF history (SFH) and the stellar evolution. Luminosity is a non monotonic function of star's evolution. In 1973 Brosche [3] first suggested a failing of the simple SF law of Schmidt [80], based only on the gas density ρ , favoring a scenario in which the SF is a function $\sim f(\rho v^\beta)$, where v is the velocity of stars and $\beta \sim 3.6$ for most of the galaxies. Stars born in large gas aggregates have a characteristic velocity that depends on the physical condition of the galaxy during the SF event (collapse, shock, merging, etc.). For this reason the global SF might keep memory of the velocity of this gas. The SFH could therefore preserve such information, leading to a "physical" connection between L and σ .

The proof that such a physical link exists between luminosity and stellar velocity dispersion is encrypted in the appearance of some SRs. The way to demonstrate this is to write the FJ relation in this way:

$$L = L'_0 \sigma^\beta, \quad (1)$$

where L'_0 and β are now fully variable parameters that depend on the complex channel of stars assembly inside galaxies (new SF, accretion and removal events, etc.), in other words on the complex SFH we mentioned above. The connection of this empirical law (that is valid for a single galaxy and should not be confused with the fit of the whole distribution of ETGs in the FJ relation in which L_0 and β are constant) with the virial theorem is the key to understand the observed distribution of galaxies in the SRs. The MR relation, the KR relation and the FP relations are in fact perfectly reproduced when the parameters β and L'_0 change. The data of the Illustris simulation [81] used by D'Onofrio et al. [37] have shown that the values of β have an ample spectrum, going from large positive values, typical of star forming objects, to large negative values, typical of passive and quenched objects (quite often the more massive old galaxies). The peak of the distribution is observed at $\beta \sim 3$, i.e. exactly coincident with the slope of the fitted FJ relation [37].

In this new framework the slope of the classical FJ relation is mainly driven by the channel governing the star assembly inside galaxies. The bottom-up scenario of hierarchical merging gives the imprint on the slope of the FJ. Simulations indicate that this slope changes with time. The trend is from a slope equal to ~ 5 at high redshift to ~ 3 observed today. In other words there is a progressive convergence toward the value of 2 expected for the virial dynamical equilibrium. This is valid for all SRs involving mass, velocity and luminosity.

Figure 1 shows the FJ plane, the KR plane and the MR plane. The gray dots mark the observational data extracted from the WINGS database [23, 82]. Three artificial galaxies simulated by Illustris are shown with different colors marking their evolution in these planes from $z = 4$ (blue dot) to $z = 1$ (green dot) and $z = 0$ (red dot). Note how the simulation is able to follow the FJ relation, keeping small the scatter of the relation despite the variations occurring in σ and L . This happens because the relation is driven by mass. The classical FJ is essentially a relation between mass and velocity dispersion. Since galaxies are always close to the dynamical equilibrium, the variation expected in luminosity and velocity dispersion, due to SF or merging events, are never bigger than the scatter of the relation (~ 0.3 dex, that corresponds to a factor of 2). The DGs are the systems that are much distant to the virial equilibrium, probably for the strong feedback effects and SF activity still going on in many of them [36].

Note how the distribution at $z = 0$ in the KR and MR planes depends on the evolution of β . This parameter can be approximately estimated by looking at the direction of the lines connecting two redshift epochs (β is the slope of the $\log(\sigma) - \log(L)$ relation). Negative values of β in the FJ plane are those

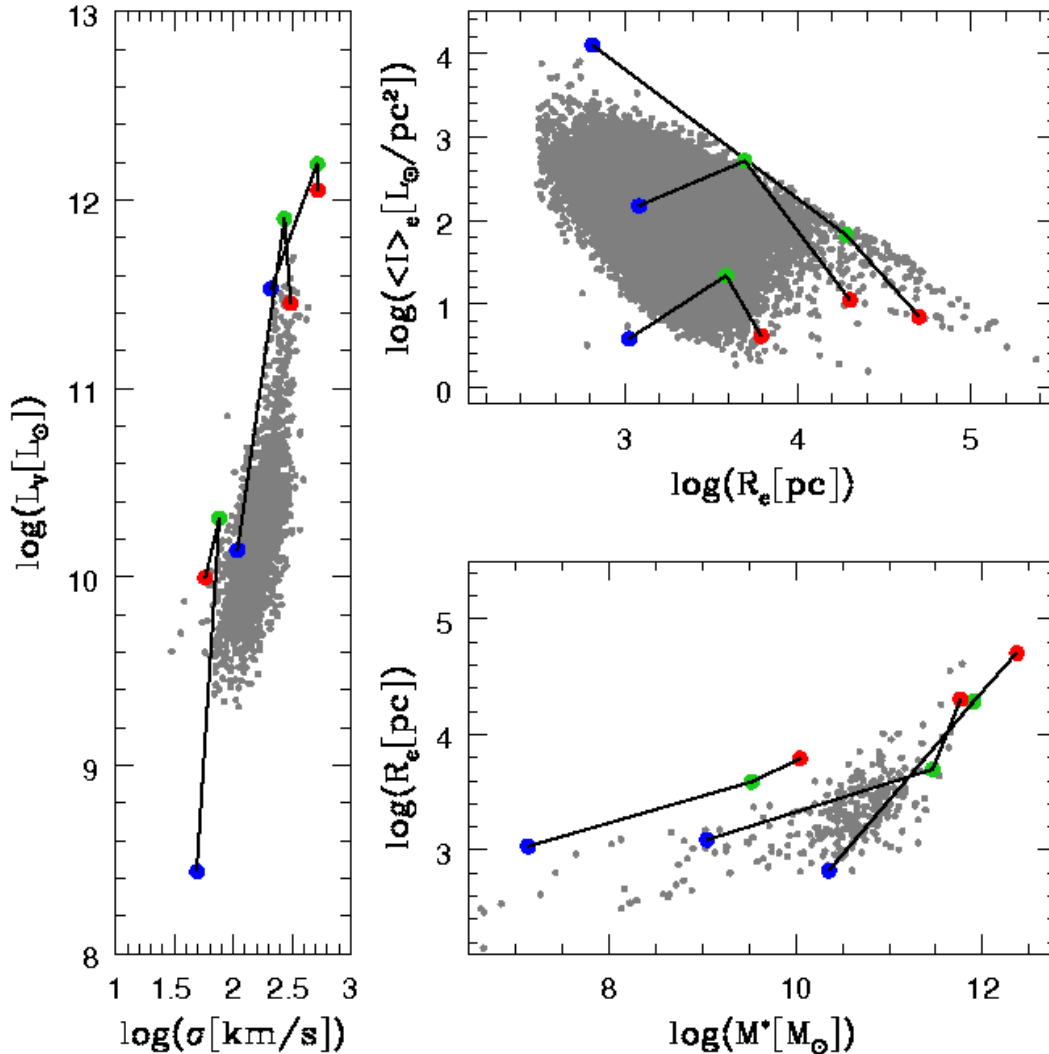


Figure 1. Left panel: the $\log(\sigma) - \log(L)$ FJ plane. The gray dots mark the observational data extracted from the WINGS database. The coloured bigger points connected by lines are three objects extracted from the Illustris simulation respectively at redshift $z = 4$ (blue dot), $z = 1$ (green dot) and $z = 0$ (red dot). The lines show the evolution of these objects across the cosmic epochs. Right upper panel: the $\log(R_e) - \log(I_e)$ KR plane. The WINGS galaxies are in gray and the coloured dots are the same objects of the left panel. Right lower panel: the $\log(M_s) - \log(R_e)$ MR plane. The symbols used are the same as before. The number of galaxies changes in each panel because masses and velocities are not available for the whole set of ETGs, in particular for the faint objects.

allowed only to quenched galaxies in passive evolution (where L decreases at nearly constant σ). As far as β becomes progressively negative the distributions in the KR and MR planes converge toward the slopes expected for virialized objects (-1 in the KR plane and 1 in the MR plane). In particular the tails observed in these two planes is that corresponding to the most massive and bright galaxies now in a quenched state of passive evolution [see Table 4 in 37, for more details]. This means that the full virialization in a galaxy can be achieved only when SF and feedback effects are stopped.

The emerging picture from the hierarchical model of galaxy assembly is that the KR and MR relations, that is the linear relations (in log units) visible when the samples contain only massive and bright ETGs,

are formed by the tails of massive and large objects appearing after $z \sim 1.5$. This is the location of the objects that today are almost quenched and passive. Their SF is over, the systems have reached a full virial configuration.

3 THE TULLY-FISHER RELATION

As we have seen for the FJ relation, the complex process of galaxy assembly has produced some regular SRs, that ultimately suggest a tight connection between the stellar component and the hosting DM halos. The Tully–Fisher relation (TF; [28]) is another example of a scaling law involving the luminosity of a galaxy (in this case of late type spiral galaxies) and the rotation velocities V of stars. The dust-corrected TF relation has the form $L \propto V^3$ in the optical band, with a slope that steepens toward redder passbands ($L \propto V^4$ in the near-infrared; [83, 84]). The variation of the slope with the passband indicate that there is a trend in color and in the stellar M/L ratio with the galaxy mass. This change constrains galaxy formation and evolution models [see e.g. 85, 86, 87].

The TF is almost linear in log units for disk galaxies with well ordered rotation, while objects with disturbed morphology and compact galaxies do not follow the main relation, exhibiting lower rotations at a given stellar mass [88, 60]. The velocity fields are affected by major merging events or tidal disruptions [89, 90, 91, 92], by accretion of external angular momentum [93, 94] and/or by disruptive feedback events [95, 96]. With spirals of the local universe the TF relation is tight [97, 98, 99]. Galaxies with rising rotation curves and those with declining rotation curve are differently distributed in the TF relation [e.g. 100].

The TF was used to measure the distance of spiral galaxies [see e.g. 101] and to test cosmological models, arguing that its slope, zero-point and tightness are set by the cosmological evolution of the galactic DM halos [102, 103, 104, 105, 106, 86]. The properties of these halos were often derived from the rotation curves of galaxies. However, the ignorance of the values of the stellar M/L ratio (the gas contribution is typically well understood and relatively small [83, 107]) determines a degeneracy: many rotation curves can be equally well fitted by models in which the central part is dominated by stellar mass or by DM [108, 109]. In order to resolve the degeneracy, some independent constraints on M/L ratios are required.

The TF relation is considered a product of the virial theorem and the almost constant mass-to-light ratio of spiral galaxies. Its origin has been discussed by Silk [e.g. 110], Mo et al. [e.g. 104]. In their semi-analytical approach, Mo et al. [104] reproduced the TF relation assuming a constant mass-to-light ratio and an empirical profile for disks and halos. Heavens and Jimenez [111] used a similar approach, including an empirical star formation model, and successfully reproduced the TF relation in four pass-bands simultaneously. However, the exponential profile and the flat rotation curves of these galaxies were not constructed as the results of simulations, but assumed a priori. Steinmetz and Navarro [112] provided the first numerical simulations within a cosmological context and explained the slope and scatter of the TF relation. They considered a volume much larger than the scale of galaxies, and some environmental effects (e.g., tidal field and infall/outflow of mass). Koda et al. [113] also reproduced the slope and scatter of the TF relation. In their approach the slope originate from the difference of mass among galaxies, while the scatter from the difference in the initial spin.

A breakthrough was the discovery that the baryonic mass better correlates with rotational velocity than luminosity [114]. The baryonic TF relation (BTF) is remarkably tight [115, 97, 116, 117, 29, 118, 119], but the exact slope still depends on the filters used [29, 99, 120].

The parametrization of the BTF gives important constraint for models of disk galaxy formation [104, 121, 86, 122]. Using a semi-analytic model, Dutton [123] predicted a minimum intrinsic scatter of ~ 0.15 dex

for the BTF while Di Cintio and Lelli [124] had a scatter of 0.17, using semi-empirical models that were able to reproduce the mass discrepancy acceleration, i.e. the ratio of total-to-baryonic mass at a given radius that anti-correlates with the acceleration due to baryons [125]. According to Bullock et al. [126] most of the scatter comes from the mass–concentration relation of DM halos well-constrained by cosmological simulations. The scatter of the BTF is therefore a key test for the Λ CDM model. The scatter is minimum when the velocity is measured in the flat part of the rotation curve well beyond the optical extent of the galaxies [97, 127], probably because such velocity is close to the virial velocity.

As remarked before, one possible application of the BTF is to constrain the properties of the DM halos. Übler et al. [128] by investigating the stellar mass and BTF relations of massive star-forming disk galaxies at redshift $z \sim 2.3$ and $z \sim 0.9$ (using the data of the KMOS3D integral field spectroscopy survey), found that the contribution of DM to the dynamical mass increases toward lower redshift. Their comparison with the local relations reveals a negative evolution of the stellar and baryonic TF zero points from $z = 0$ to $z \sim 0.9$, no evolution of the stellar TF from $z \sim 0.9$ to $z \sim 2.3$, and a positive evolution of the BTF from $z \sim 0.9$ to $z \sim 2.3$.

A useful progress came with the demonstration by Weiner et al. [129] and Kassin et al. [88] that, accounting for disordered motions (σ) and ordered rotation (V) in a new parameter $S_{0.5} = \sqrt{0.5V^2 + \sigma^2}$, it is possible to get a tight $S_{0.5}$ – M_s relation [130]. This relation is independent of the morphology of galaxies and is coincident with the FJ relation of ETGs, when σ dominates over V , and coincident with the TF when the opposite occurs. Numerical simulations seem to indicate that $S_{0.5}$ traces the potential well of the DM halos even in the case of merger events [91]. The inclusion in the TF of galaxies with disordered velocity components (often due to major mergers) has been addressed by several people [131, 132, 133, 134, 135, 136]. The scatter of the relation seems mainly due to merger events as we have seen for the FJ relation.

Galaxy morphology is another possible source of scatter being a strong function of stellar mass and the less luminous systems quite often exhibit an irregular morphology, [see e.g. 137, 138, 139]. In general disturbed galaxies are increasingly more common at low masses in the early Universe [140]. The kinematic surveys are often biased against galaxies with disturbed morphology, because their aim is to study the DM content [141]. Dwarf galaxies (DGs) show rotational signatures in both their HI and stellar components [142, 143] and when irregular galaxies, compact galaxies, and close pairs are analyzed in their kinematics the presence of peculiar velocity fields and thick disks are found [see e.g. 144, 145, 146, 135, 147] together with high star-forming dwarfs [148, 149, 150]. However, only few studies have placed large samples of these disordered systems on the TF.

In the future, it will be interesting to study the TF relation in the same perspective of the FJ, distinguishing the relation valid for a set of galaxies, which is a translation of the virial theorem (once the variations in the stellar population are taken into account), and the relation valid for single galaxies, where the luminosity and the rotational velocity are the result of the mass assembly history and of the stellar evolution. The work of D’Onofrio et al. [37] has demonstrated that it is important to look at the variations of the positions of each galaxy in the different SRs if we want to understand the origin of the observed distributions.

4 THE KORMENDY RELATION

The $I_e - R_e$ relation of ETGs (often known as KR [13]) is a projection of the FP. In this case the variables are the effective radius and the mean surface brightness inside it. It is the most easily accessible correlation of galaxies parameters even at high redshift. First discovered by Kormendy in 1977, the linear relation visible in log units between these variables, soon showed an ample curvature towards faint and dwarf

objects, suggesting the existence of two different populations of ETGs, the 'ordinary' and the 'bright', following two different relations and therefore possibly originating from two different channels of evolution [151]. The 'ordinary' family is bi-parametric ($L \propto I_e R_e^2$), its members are fainter than $M_B \sim -19$ and their radii are smaller than $R_e \sim 3$ kpc. The 'bright' family is mono-parametric (I_e depends only on R_e), it hosts only the brightest cluster galaxies (BCGs) and their members have radii exceeding $R_e = 3$ kpc. The bulges of spirals belong to the 'ordinary' family.

The curved distribution visible in the $I_e - R_e$ plane has been used (among others correlations) several times to argue for distinct formation mechanisms of dwarfs and giants ETGs [152, 153, 6, 154, 155, 156]. Many authors believe that there is a physical difference between elliptical and spheroidal galaxies. Elliptical and spheroidal galaxies exhibit different parameter correlations. Spheroidals are not low-luminosity ellipticals but rather the result of transformations induced in late-type galaxies by internal and environmental processes. Furthermore, there are possibly two distinct kinds of elliptical galaxies, whose properties differed during the last major mergers, wet or dry, according to whether cold gas dissipation and starbursts occurred or not.

The existence of two physically distinct families of ETGs has been at the center of an ample debate. Other researches that did not use the effective half light radius parameter, advocated for a continuity among the ETG population [157, 14, 158, 159]. Graham [160] explored a range of alternative radii, showing that the transition at $M_B \sim -19$ mag is likely artificial and does not imply the existence of two different types of ETGs.

The shape of the light profiles of ETGs has been also used to claim a difference between dwarfs and ordinary ETGs: dwarfs have in general exponential light profiles (similar to the disks of LTGs), while ordinary ETGs have $R^{1/n}$ Sérsic profiles [161], with $n \geq 3$. However, exponential light profiles are reproduced by the Sérsic law when $n = 1$. According to Graham [160] the curved distribution of ETGs in the KR, is likely associated to the continuous change of the Sérsic index n with the absolute magnitude (the $M_B - n$ relation [162, 163]). Along this view Graham and Guzmán [164] argued that the only magnitude of importance in the $I_e - R_e$ plane is at $M_B = -20.5$ mag, where they see a division between ETGs with Sérsic profiles and core-Sérsic profiles. This magnitude corresponds to a mass of $\sim 2 \times 10^{11} M_\odot$.

There are indeed two linear scaling relations involving the structural parameters of ETGs: the $M_B - \mu_0$ (i.e. total luminosity vs central surface brightness) and the $M_B - n$ (total luminosity vs Sérsic index). These relations do not show evident signs of curvature. The first one is a re-statement of the concentration classes introduced by Morgan [165], later quantified by the concentration index C [166, 14, 167, 168]. The second is a consequence of the first, being the Sérsic parameter a measure of the radial concentration of galaxy light. Further examples of the $M_B - n$ diagram can be found in the literature [162, 169, 170, 171, 172, 153]. The lack of curvature in these diagrams does not support the view of different formation mechanisms at work for the formation of ETGs. This debate is controversial: the original "nature" [173] (monolithic collapse) versus "nurture" (formation through mergers) [174, 175, 176] idea is still open.

Another interesting feature of the $I_e - R_e$ diagram, well visible in Fig. 2 is the presence of a zone of exclusion (ZoE). Note that there are no galaxies in the upper part of the diagram. The distribution of galaxies seems limited in the maximum surface brightness at each R_e . The slope of this line of avoidance is approximately -1 in these units, i.e. very close to the slope of the fitted KR for the brightest galaxies (~ -1.5). First noted by Bender et al. [4] in the k -space version of the FP, the ZoE was written as $k_1 + k_2 \leq 7.8$.

Recently D'Onofrio and Chiosi [76] demonstrated that the FJ relation (with L_0 and β nearly constant) is incompatible with the distribution observed in the KR plane. On the contrary the use of the modified FJ

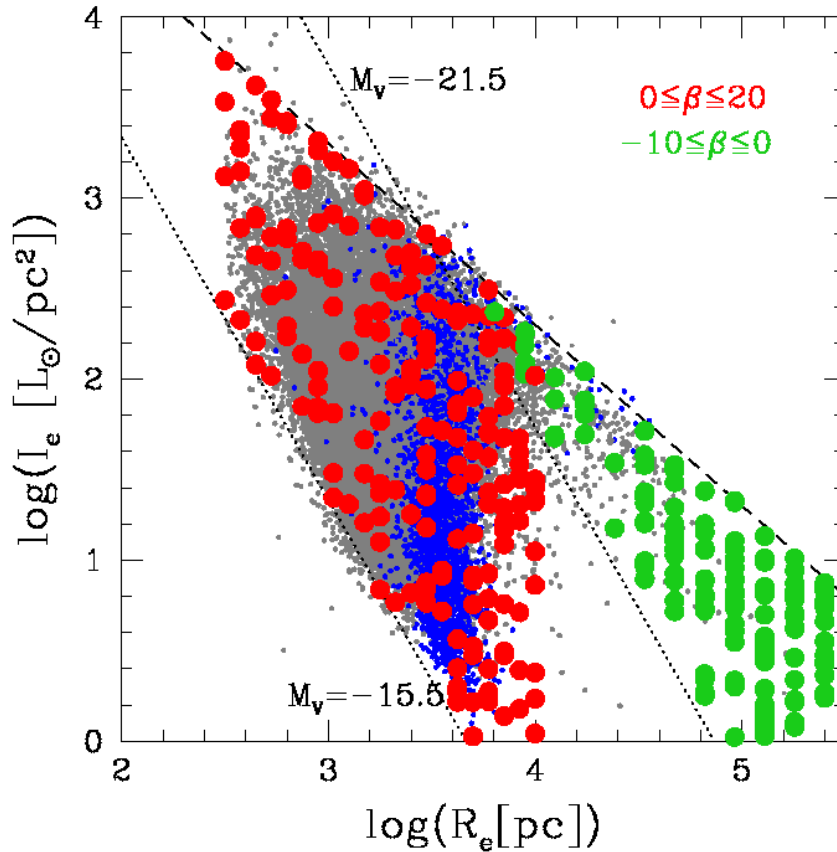


Figure 2. The KR plane. The gray dots mark the observational data of the WINGS survey. The red and green dots mark the values of I_e and R_e obtained starting from eq. 1 [see 76] using different values of β . The dashed line represents the ZoE. The dotted lines the locus of constant luminosity, respectively at $M_V = -21.5$ and $M_V = -15.5$.

relation expressed by eq. 1 is perfectly compatible with the data (see Fig. 2). This means that the parameters L'_0 and β must be variable factors depending on the mass assembly history of galaxies. Note how the complex distribution of galaxies in the $I_e - R_e$ plane is well reproduced by assuming different values of L'_0 and β . The negative values in particular are able to explain the tail formed by bright and massive objects in a quenched state of evolution.

Under this perspective the appearance of the $I_e - R_e$ plane is also connected to the mass assembly and stellar evolution history of galaxies. The tail of bright galaxies appears only at recent cosmic epochs, when some big objects start to quench their star formation and their luminosity begins to slowly decrease.

5 THE MASS-RADIUS RELATION: A PATH TOWARD VIRIAL EQUILIBRIUM

A considerable number of works have been dedicated in the past years to the MR relationship, i.e. the plot of the stellar mass of the galaxies M_s versus the effective radius R_e in log units [see e.g. 177, 178, 179, 180, 181, 182, 183, 184, 185, 186, 187, 188]. The increasing interest for the MR relation is due to the difficulty of explaining the observed distribution with the virial theorem and the various models of galaxy assembly predicted by the monolithic and hierarchical scenarios, in particular the curved shape, progressively steeper for the high masses, and the zone of exclusion (ZoE), that is, a region empty of any object on the side of the high masses (see Fig. 1 lower right panel and Fig. 3). This nontrivial distribution

is well apparent even when globular clusters (GCs) and clusters of galaxies (CGs) are added to the diagram [36].

Many papers have already emphasized that the distribution of galaxies in this plane depends on several factors, such as age [189], mass-to-light ratio [190], color, Sérsic index and velocity dispersion [see e.g. 37, 187]. The distribution of the sizes has been approximated with a log-normal function [191], noting that it is clearly different for late- and early-type galaxies. The MR relation is roughly a single power law for the bright ETGs ($M_s > 10^{10} M_\odot$), while for the LTGs and DGs the relation is significantly curved, with brighter galaxies showing a faster increase of R_e with M_s . For low-mass LTGs the trend is $R_e \propto M^{0.14}$, while for the high-mass galaxies we have $R_e \propto M^{0.39}$. The dispersion around the mean relation is high for low-mass galaxies (~ 0.5) and smaller for big objects (~ 0.3). For the ETGs the mean relation is $R_e \propto M^{0.56}$, with a slope going progressively toward 1 for galaxies more massive than $\sim 10^{10} M_\odot$. Spirals do not seem to have objects along this linear tail [37].

According to Shen et al. [191] the observed MR relation for LTGs can be attributed to the specific angular momentum (AM) of the stars, if it is similar to that of the halo and if the fraction of baryons that form stars is similar to that predicted by the standard feedback models. For ETGs, the observed MR relation is not consistent with the hypothesis that they are the remnants of major mergers, while it seems consistent with that of multiple mergers. One possibility is that the spheroids below a characteristic mass $M_s \sim 10^{10} M_\odot$ grow from disk instability and mergers, while galaxies above it from dry mergers. Gas dissipation, if present, contribute efficiently to shrink the size of the galaxies [179].

The pronounced curvature of the MR relation suggests again a dichotomy between 'bright' and 'ordinary' ETGs as in the case of the $M_B - \langle \mu \rangle_e$ diagram and the KR plane. A possible explanation invokes the role of supernova-driven winds blowing out the gas from the DGs [192, 193, 194]. This feedback effect is one of the most efficient way of puffing-up galaxies sizes. However, these studies do not take into account the gravitational binding energy of the DM halo [95], so that other mechanisms should be sought to explain the discontinuity present in these relations. The discontinuity is not seen in fact in the luminosity-metallicity relation [194, 195, 196, 197] and is only marginally visible in the $L - \sigma$ relation.

More recently D'Onofrio et al. [37] found a unique explanation for the curved shape of the MR and KR relation in combination with the almost linear trend of the $L - \sigma$ relation. They used the modified FJ relation $L = L'_0 \sigma^\beta$ introduced above that is able to reproduce the curved MR relation and $I_e - R_e$ distribution once coupled with the virial equation. In this case one gets the relation:

$$R_e = \left(\frac{1}{\frac{k_n}{G} \left(\frac{2\pi \langle I_e \rangle}{L'_0} \right)^{2/\beta}} \right)^{1/(4/\beta+1)} M^{1/(4/\beta+1)}. \quad (2)$$

and should accept the idea that the parameters L'_0 and β are variable factors for each galaxy depending on the mass assembly history, with β that can assume both positive and negative values (see Fig. 3). The advantage of this approach is that, in addition to the almost perfect reproduction of the observed SRs, it naturally predicts the existence of the ZoE as the locus of virialized and passively evolving quenched objects. Look at the red dots obtained by eq. 2. The slope of the MR progressively changes from DGs to giants, converging toward the value of 1 for the bright and massive quenched objects in full virial equilibrium.

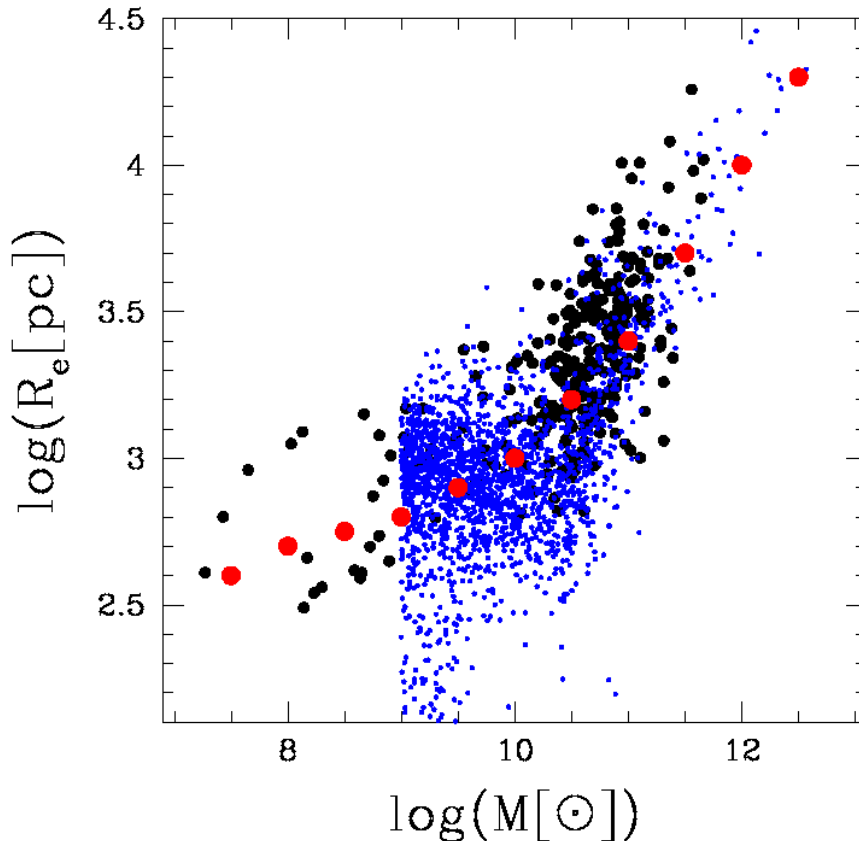


Figure 3. The MR plane. The black dots mark the observational data of the WINGS survey. The blue dots are the Illustris data of the TNG release shifted by a constant value in $\log(R_e)$ of -0.45 (simulations still provide systematically larger radii). The red dots mark the values of R_e obtained from eq. 2 (see text).

In this framework the key role of shaping the SRs is played by the merging and stripping events that play during galaxy encounters. These events may change either the luminosity and the radius of a galaxy (increasing or decreasing them). However, while luminosity rarely increases (decreases) by a factor of two (~ 0.3 in log units), the radius may change considerably (up to a factor 10). This explains why the $L - \sigma$ relation does not change its linear shape and scatter (that is approximately ~ 0.4). On the contrary in the SRs where the effective radius R_e is an explicit parameter, a strong curvature distinguishing DGs and giants, is clearly present. Sánchez Almeida [187] well showed that the MR relation changes its shape and scatter when different radii (probably much closer to the virial radius) are used instead of R_e .

When galaxy encounters result in significant stripping of stars and gas, the total luminosity of the galaxies and the velocity dispersion decrease. The same effect is induced by the quenching of SF and passive stellar evolution, producing values of β that can be negative. Notably this scenario is confirmed by numerical simulations [76]. These also predict that the MR relation evolves with the cosmic epochs, since galaxies are much more dense and smaller in size at earlier epochs. The galaxy size-luminosity relation and the MR relation were then used to argue that the compact ($R_e < 2$ kpc) massive ($M_s > 10^{11} M_\odot$) spheroidal-shaped galaxies at high-redshifts ($z \sim 2 \pm 1$) - known as “red nuggets” [198] - evolved into the large massive ellipticals in the local ($z = 1$) Universe [199, 200, 201, 202]. These massive galaxies (with stellar mass $M_s > 3 \times 10^{10} M_\odot$), evolving passively at redshifts $z \geq 1$, have average sizes smaller

by a factor of ~ 3 with respect to local ETGs with similar stellar mass. Such small sizes are expected if dissipative collapses occur.

The small objects seen at high redshift are $2 \div 6$ times more compact than local galaxies of similar stellar mass [203, 204], but observations have now established that many ETGs at high redshifts are not compact and that similar fractions of large and compact galaxies could co-exist [205, 189], with a variety of bulge-to-disk ratios [206].

From the analysis of the spectra of 62 ETGs at high redshifts Saracco et al. [204] found that compact galaxies have most of their stars formed before $z = 5$, while larger objects at fixed stellar mass are generally younger. Graham et al. [207] identified 24 “compact massive spheroids” as the bulge component of local lenticulars. These bulges have a similar distribution of size, mass, and Sérsic indices as the high- z compact massive galaxies, and comparable number densities (per unit volume) [208]. This similarity strongly suggests that the current evolutionary scenario does not explain the complete picture.

Another possibility is that the evolution of the red nuggets is driven by the growth of disks [209, 210, 211, 212, 213, 214, 215, 207, 216]. Gas accretion plays a key role for massive galaxies [217], while less massive objects accrete a small quantity of gas with time [218, 219].

The rapid stripping or ejection of baryonic matter (BM) might inflate galaxies to larger dimensions. The idea came from Biermann and Shapiro [220], who linked the formation of S0s to that of disk galaxies. Recently Ragone-Figueroa and Granato [221] explained the existence of red-nuggets with this mechanisms. The loss of BM could be triggered by quasars (QSO) and/or starburst-driven galactic winds or can be quiet for stars at the end of their evolution. In this scheme compact galaxies could transform into less massive and larger systems. Numerical models only approximately follow this scheme: the models show intense episodes of SF and significant galactic winds but, on average, the trend is toward larger masses and almost constant radii.

Guo et al. [222] and van Dokkum et al. [203] investigated the possibility that the MR relation, at least for the most massive galaxies, is linked to a systematic variation of the Sérsic index n , parameterising the surface density profiles with the redshift. According to van Dokkum et al. [203] the variation of the effective radius R_e (50% of the light) is:

$$\frac{d \log(R_e)}{d \log(M)} \approx 3.56 \log(n + 3.09) - 1.22 \quad (3)$$

which is accurate to 0.01 dex for $1 \leq n \leq 6$. This means that the radius might increase linearly with the mass if the projected density follows an exponential law, going as $M^{1.8}$ for the de Vaucouleurs profile with $n = 4$. A strong evolution in R_e is expected in all inside-out growth scenarios, unless the density profiles are close to exponential.

6 THE MR RELATION IN COSMOLOGICAL CONTEXT

A new explanation of the existence and curvature of the MR relation (thereinafter MRR) has been given recently by Chiosi et al. [36] in the cosmological context of galaxy formation and evolution. They started from the empirical hint that a unique MRR seems to connect objects from Globular Clusters (GCs) to dwarf galaxies (DGs), early type galaxies (ETGs) and Spiral Galaxies (LTGs), and finally Clusters of Galaxies (CoGs), the stellar masses M_s and radii R_e of which span about twelve and four orders of magnitude, respectively.

The data used by Chiosi et al. [36] are those of Burstein et al. [223] for GCs, galaxies in general, and CoGs, of Bernardi et al. [224] for ETGs, and of WINGS for ETGs and CoGs. The situation is visible in Fig. 4, where the pale-blue filled circles show the observational data with no distinction among the different sources. The sea-green filled circles are the Illustris models. Note that the minimum mass of the Illustris galaxies at $z = 0$ is $10^9 M_\odot$, so the comparison with the observational data should be restricted to this mass limit. The figure shows the region of the MR-plane populated by real objects of different mass, size and morphological type. Let us quickly summarize the main features of the MR-plane:

(i) The family of GCs is well detached from that of normal/giant ETGs (with mass larger than about $10^{10} M_\odot$). The region in between is populated by DGs and at the top of the distribution there are the CoGs with the largest radii and masses. The ETGs are the most numerous and the LTGs occupy more or less the same region, but are not visible in the bright tail. The relative number of objects per group is not indicative of the real number frequencies because severe selection effects are present. The best fit of the three samples of data yields linear relations with much similar slopes and zero points (they differ by 0.1 and 1.2, respectively). Therefore, one can consider them as fully equivalent and adopt the one derived from the sample of Bernardi et al. [177] as the reference case for his richness

$$\log R_e = (0.537 \pm 0.001) \log M_s - (5.26 \pm 0.01). \quad (4)$$

(ii) Extrapolating the relation for massive ETGs, eqn.(4), downward to GCs and upward to CoGs, one notes that it provides a lower limit to GCs, passes through ω Cen and M32, marks the lowest limit for the distribution of DGs, and finally reaches the region of CoGs.

(iii) There are no objects in the semi-plane for radii R_e smaller than the values fixed by relation (4), independently of mass, but for the “compact galaxies” [see 225].

6.1 The MRR of theoretical models

The situation is more complicated for galaxy models. The monolithic hydrodynamic models by Chiosi and Carraro [226, shortly indicated CC-A and CC-B] and the early-hierarchical models by Merlin et al. [227, shortly indicated M-M] provide the following MRRs:

$$\log R_e = 0.331 \log M_s - 3.644 \quad \text{CC - A} \quad (5)$$

$$\log R_e = 0.273 \log M_s - 1.994 \quad \text{CC - B} \quad (6)$$

$$\log R_e = 0.241 \log M_s - 1.750 \quad \text{M - M} \quad (7)$$

We recall that the three groups of models (identical in the input physics) are calculated with different formation redshift z_f (hence initial density): CC-A have $z_f \simeq 5$, CC-B $z_f \simeq 1$, and M-M $z_f \simeq 1 - 2$. In the MR-plane they lay on lines with similar slope but different zero point. This suggests that the slope is linked to the physical structure of the models while the zero-point is reminiscent of the initial density. Surprisingly, the slopes of the above relations are not identical to that of ETGs (eq. 4), but close to that of DGs. Furthermore, along the sequence of each group, the duration of the star formation activity is long and in a burst-like mode of low intensity in low mass galaxies and short and intense (often a single burst of activity) in the high mass ones. Remarkably, only the most massive galaxies formed in redshift interval $5 \geq z_f \geq 2$, in which star formation has ceased long ago, may fall into the region of ETGs.

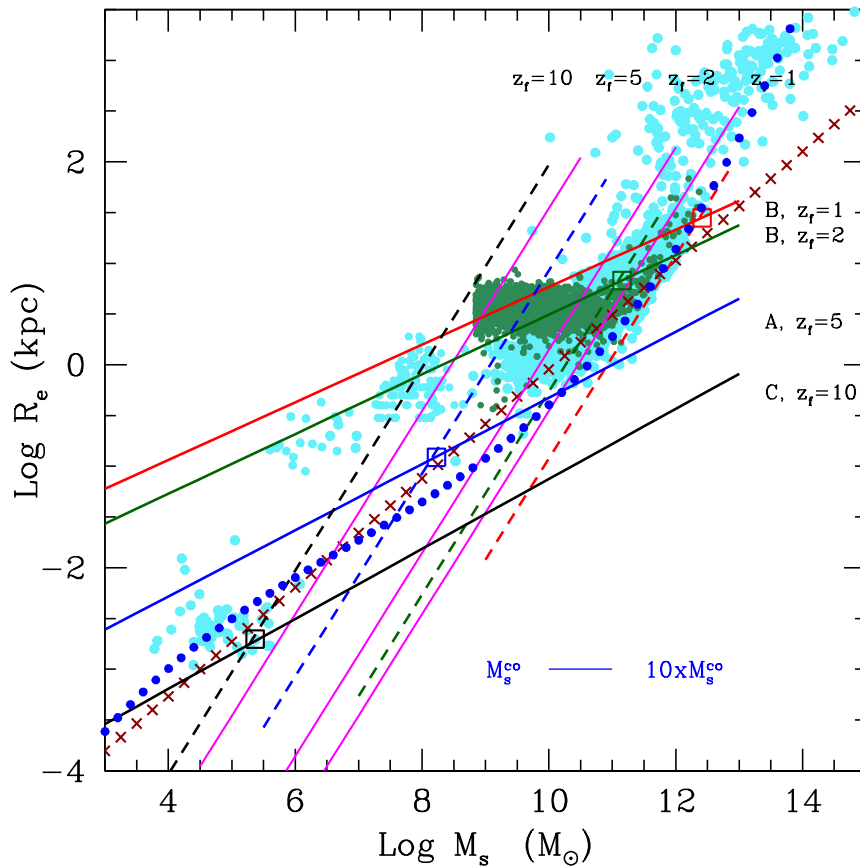


Figure 4. The Mass-Radius plane. Comparison between data and theory. Radii R_e and stellar masses M_s are in kpc and M_\odot , respectively. The pale-blue filled circles are the observational data, the sea-green filled circles the models of Illustris. The stellar masses of the observational data that refer to objects from GCs to CoGs span the range 10^4 to $10^{14} M_\odot$ while the theoretical data that are designed to represent galaxies span the mass range 10^8 to $10^{12} M_\odot$. The theoretical data overlap the observational ones for ETGs and partly also for DGs. The linear best fit of normal ETGs ($M_T \geq 10^{10} M_\odot$) given by eq.(4) is the dark-red thick crossed line that we prolonged down to the region of GCs and upwards to that of CoGs. The four solid lines labeled A ($z_f = 5$, blue), B ($z_f = 1$, red and $z_f = 2$, dark green) and C ($z_f = 10$ black) are the analytical relationships of eq. (19). They show the loci of galaxy models with different mass but constant initial density for different values of redshift of galaxy formation z_f . These lines are the best fit of the models by Chiosi and Carraro [226], Merlin et al. [227] and Chiosi et al. [225]. The magenta solid lines visualize the locus of virialized objects on the MR-plane for different values of the stellar velocity dispersion (50, 250, 500 km/s from left to right). The dashed black lines for different values of z_f are the MRRs expected for galaxies with total mass equal to $50 \times M^{CO}(z)$, the cut-off mass of the Press-Schechter at varying z_f according to relation (20). The large empty squares mark the intersections between the lines of constant initial density and the MRRs for $50 \times M^{CO}$ galaxies for equal values of the redshift. All the intersections lie very close to the relation of eqn.(4) shown by the dark-red crossed line. This is the linear interpretation of the observed MRR. Finally, the curved blue dotted line shows the expected MR relation for the baryonic component of DM halos whose mass distribution follows the cosmological HGF by Lukić et al. [228]. The curve has been extended to include the GCs and the CoGs. Note the changing slope of the MRR passing from CoGs to ETGs and GCs. Remarkably the curved line first runs very close to the large empty squares, second to linear fit of the data (crossed line), and third accounts for the observed MRR passing from GCs to CoGs (about ten orders of magnitude difference in the stellar mass). Finally, the horizontal blue line gives the interval for M_s corresponding to initial masses $M^{CO}(z) < M_T < 10 \times M^{CO}(z)$ (the percentage amounts to $\simeq 15\%$). It highlights that at each redshift the high-mass edge of the MRR has a natural width.

The Illustris hierarchical models provide similar relationships, once they are split in two groups:

$$\log R_e = 0.297 \log M_s - 2.513 \quad \text{for } \log M_s \leq 10.5, \quad (8)$$

$$\log R_e = 0.519 \log M_s - 4.492 \quad \text{for } \log M_s \geq 10.5. \quad (9)$$

The first relation holds for the vast majority of models and reminds that of normal DGs, while the second one holds for a small group of objects and is close to the case of ETGs. In the hierarchical scheme the models of the first group (in eq. 8) are the seeds of those in the second group located along the MRR of eq (9).

Finally, there is the MRR proposed by Fan et al. [229]. This is derived in the following way. Independently of the monolithic or hierarchical scheme, the seeds of galaxies are perturbations of matter made of DM and BM. These collapse when the density contrast with respect to the surrounding medium reaches a suitable value. Assuming spherical symmetry and indicating with M_T and R_T the total mass and associated radius, and making the approximation $M_T = M_D + M_B \simeq M_D$ and $R_T \simeq R_D$, the mass-radius relation for each individual galaxy is

$$R_D^3 = \left(\frac{3}{4\pi} \right) \frac{M_D}{\lambda \rho_u(z)} \rightarrow R_D \propto \frac{M_D^{1/3}}{1 + z_f} \quad (10)$$

where $\rho_u(z_f) \propto (1 + z_f)^3$ is the density of the Universe at the collapse redshift z_f , and λ the density contrast of the DM halo. This expression has a general validity, whereas λ depends on the cosmological model of the Universe, including the Λ CDM case. All details and demonstration of it can be found in Bryan and Norman [230, their Eq. 6]. The collapse increases the mean density of DM and BM so that, when a critical value of the BM density is reached, stars can form at the center of the system under suitable star formation rates. In the context of the Λ CDM cosmology, Fan et al. [229] have adapted the general relation (10) to provide an equation connecting the halo mass M_D , the stellar mass M_s , the half light (mass) radius R_e , the shape of the BM $S_S(n_S)$ related to the Sérsic profile index n_S , the velocity dispersion f_σ of the BM component with respect to that of DM, and finally the ratio $m = M_D/M_s$. The expression is

$$R_e = 0.9 \left(\frac{S_S(n_S)}{0.34} \right) \left(\frac{25}{m} \right) \left(\frac{1.5}{f_\sigma} \right)^2 \left(\frac{M_D}{10^{12} M_\odot} \right)^{1/3} \frac{4}{(1 + z_f)}. \quad (11)$$

where f_σ yields the three dimensional stellar velocity dispersion as a function of the DM velocity dispersion $\sigma_s = f_\sigma \sigma_D$ (here we adopt $f_\sigma = 1$). The typical value for $S_S(n_S)$ is 0.34. For more details see Fan et al. [229] and references therein.

The most important parameter of eq.(11) is the ratio $m = M_D/M_s$. Using the Illustris data Chiosi et al. [36] investigated how this ratio varies in the mass interval $8.5 < \log M_D < 13.5$ (masses are in M_\odot) and from $z = 0$ to $z = 4$ (see Sect. 11). They find that the following relation is good for all practical purposes

$$\log m = \log \frac{M_D}{M_s} = 0.062 \log M_D + 0.429. \quad (12)$$

The slope of the Fan et al. [229] relation, which visualizes the position on the MR-plane of systems born at the same redshift once their stars are formed, is 0.333. This is very similar to that of theoretical models, i.e. eqns. (5), (6), (7), and (8).

The most intriguing question to answer is “Why is the observational MRR for ETGs so different from the theoretical one?”

6.2 The MRR from the DM Halo Growth Function $n(M_D, z)$

The observed distribution of astrophysical objects in the MR-plane, going from GCs to galaxies of different mass and morphological type and eventually to CoGs, suggests that a unique relation could exist for all of them and that such relation likely owes its origin to the cosmological growth of DM halos. The distribution of the DM halos and their number density as a function of redshift has been the subject of several studies which culminated with the large scale numerical simulations of the Universe. We cite here one for all, the Millennium Simulation [231]. In parallel the studies of the *halo growth function*, *HGF*, as the integral of the *halo mass function*, *HMF*, appeared in literature [see for instance 228, 232, 233]. The HGF gives the number density of halos of different mass per $(\text{Mpc}/h)^3$ emerging at each epoch by all creation/destruction events and consequently yields the halos that nowadays populate the MR-plane and generate the observed galaxies. Chiosi et al. [36] adopted the HGF of Lukić et al. [228] who, using the Λ CDM cosmological model and the HMF of Warren et al. [234], derived the number density of halos $n(M_D, z)$ over ample intervals of halo masses and redshifts. Since the $n(M_D, z)$ of [228] refers to a volume of $1 (\text{Mpc}/h)^3$, before being compared with the observational data, it must be scaled by a suitable factor in order to match the volume sampled by observations. Anyway, the following characteristics of the HGF are worth being noted: (i) for each halo mass (or mass interval) the number density is small at high redshift, increases toward the present, and reach a maximum at a certain redshift. The peak is either followed by a descent (for low mass halos) or a plateau (for high mass halos). In other words, first the creation of halos outnumbers the destruction, whereas the opposite occurs in general for low mass halos after a certain redshift. (ii) At any epoch high mass halos are much less numerous than the low mass ones. This implies the existence of a cut-off mass at the high mass side. (iii) The HGF also implies that halos of different mass have a given probability of existence at any redshift [see for more details 225, 36].

Assuming a certain number density of halos N_s derived from the observational data, Chiosi et al. [36] set up the equation $n(M_D, z) = N_s$ whose solution yields the mass of the halos $M_D(z)$ as a function of the redshift and vice-versa the redshift for each halo mass. In practice for any value N_s one gets a function $M_D(z)$. To each value of M_D along this function, with the aid of eqns. 11 and 12, one can associate a value of M_s and R_e . The MRR of luminous galaxies is the result.

Notably for the N_s corresponding to 10^{-2} halos per $(\text{Mpc}/h)^3$ (roughly the volume surveyed by the SDSS, [see 36, for details]), the curve $R_e(M_s)$ falls at the edge of the observed distribution of ETGs in the MR-plane. Higher N_s would shift the curve to larger halos, the opposite for lower N_s . One can therefore draw in the MR-plane the locus of the most massive M_D and associated M_s imposed by the halo HGF. The equation $n(M_D, z) = N_s$ with $N_s = 10^{-2}$ or equivalently 10^6 halos per 10^8 Mpc^3 rewritten to derive the halo mass M_D as a function of z is

$$\log M_D = 0.0031546 z^3 - 0.006455 z^2 - 0.183 z + 13.287. \quad (13)$$

Starting from this, Chiosi et al. [36] associate M_s and R_e to each M_D for any value of the redshift. The best fit of the resulting MR relation, limited to the mass interval of normal ETGs, $9.5 \leq \log M_s \leq 12.5$ (M_s in solar units), is

$$\log R_e = 0.048562(\log M_s)^3 - 1.4329(\log M_s)^2 + 14.544(\log M_s) - 50.898. \quad (14)$$

Note that (i) the locus on the MR-plane predicted by $N_s = 10^{-2}$ halos per $(\text{Mpc}/h)^3$ nearly coincides with the observational MRR; (ii) the slope gradually changes from 0.5 to 1 going from low masses to high masses in agreement with the observational data [see 235, and references therein]; (iii) finally, eq. (14) is ultimately linked to the top end of the halo masses (and their associated baryonic objects) that might exist at each redshift. Chiosi et al. [36] named this locus the *Cosmic Galaxy Shepherd*.

The extrapolation of the Cosmic Galaxy Shepherd downward to GCs and upward to CoGs yields the relation

$$\log R_e = 0.007584[\log(m \cdot M_s)]^3 - 0.1874[\log(m \cdot M_s)]^2 + 1.908[\log(m \cdot M_s)] - 9.027 \quad (15)$$

where R_e and M_s are in the usual units and m is the ratio $m = M_D/M_s$, for which a mean value of $m = 25$ is adopted². As already said this equation represents the cut-off mass of the HDF at different redshift, however translated into the R_e vs M_s . This gives a profound physical meaning to the line splitting the MR-plane in two regions, i.e. the region where galaxies are found, and that of avoidance, the so-called Zone of Exclusion (ZoE) found by Burstein et al. [223].

Along the Cosmic Galaxy Shepherd, cut-off masses and redshift go in inverse order: low masses (and hence small radii) at high redshift and vice-versa. More precisely, halos and their luminous progeny that are born (collapse) at a certain redshift and are now located along the theoretical MRR of eqn. (11) associated to that redshift. Along each MRR only masses (both parent M_D and daughter M_s) smaller than the cut-off mass are in place, each of these with a different occurrence probability. Clearly the low mass halos are always more common than the high mass ones. We will argue that in the MR-plane, only the most massive GCs, DGs, and ETGs are expected to fall along the Cosmic Galaxy Shepherd. All other objects of lower mass, the DGs in particular, are expected to lie above this limit. This suggests that there are other physical processes concurring to shape the observed MRR. In other words, the question is “what really determines the position of each galaxy on the MR-plane?”

To answer the above question Chiosi et al. [225, 36] argue what follows. The gravitational collapse of a proto-cloud generating a luminous galaxy is surely accompanied by star formation, energy feed-back, gas cooling and heating, loss of mass and energy by winds, acquisition of mass and energy by mergers, etc. Therefore the result of all these processes taking place together may largely differ from one case to another and also differ from the ideal case of a dissipation-less collapse. For this latter [236, 237, 223] derived the relation

$$R_D \propto M_D^{0.53}. \quad (16)$$

Inside this halo a galaxy with stellar mass M_s and a half-mass radius R_e is built up over the years. Chiosi et al. [36] take the dissipation-less collapse as the reference case. Using the data of the Illustris models, they derive the following MRRs

$$\log R_e = 0.541 \log M_s - 4.702 + k_m \quad \text{for } \log M_s > 10.5 \quad (17)$$

$$\log R_e = 0.102 \log M_s - 0.017 + k_d \quad \text{for } \log M_s < 10.5 \quad (18)$$

where the constants k_m and k_d can be determined by fixing the initial conditions of the collapsing proto-halo. The slope of eq. (17) does not significantly differ from that of the dissipation-less collapse, eqn. (16) and that of the empirical MRR of ETGs, eqn.(4). Along each MRR of the theoretical manifold, the

² In Chiosi et al. [36] the same expression is written as $\log R_e = 0.007584(\log M_s)^3 - 0.1874(\log M_s)^2 + 1.908(\log M_s) - 9.027$, in which by mistake the term $(\log M_s)$ does not contain the factor m .

agreement between data and theoretical models seems to be possible only for the most massive galaxies. For smaller masses, the slope of the theoretical MRR, eqn. (18), is much flatter than the observational one (about a factor of two).

From the above considerations one could suggest that the Cosmic Galaxy Shepherd and eqn. (4) represent the locus in the MR-plane of galaxies formed by quasi dissipation-less collapses. In contrast, special conditions ought to hold for all other objects that deviate from this condition. The explanation is different for the monolithic and hierarchical scenarios:

a) In the monolithic view, in addition to star formation, galactic winds are the key ingredient to consider, in particular for low mass galaxies, because DGs show the largest deviation from the observed MRR, eq. (4) or eq. (16). The analysis of the problem made by Chiosi et al. [36] shows that: (i) the stronger the galactic wind the larger is the final R_e . Galaxies depart from the locus represented by eq. (4) and/or eq.(16) at decreasing mass and increasing galactic wind, the low mass ones having the strongest effect; (ii) the efficiency of winds tends to decrease at increasing initial density. This means that the inflating effect of galactic winds in low mass galaxies of high initial density is low and the final radius of these galaxies will be close to the value predicted by eqs. (4) and/or (16). In conclusion the flatter slope of the theoretical MRR is likely produced by galactic winds.

b) In the hierarchical scenario the situation is more entangled because both mergers and galactic winds concur to inflate a galaxy. To clarify the issue Chiosi and Carraro [226] discussed the merger between two disk galaxies calculated by Buonomo [238]. In this case an elliptical galaxy is generated with twice total mass of the component galaxies, but with stellar mass and effective radius smaller and higher, respectively, by $\Delta M_s/M_s \simeq -0.9$ and $\Delta R_e/R_e \simeq 0.5$, with respect to the case of an elliptical of the same mass generated during a monolithic collapse. The reason for that is identified in the enhancement of galactic winds caused by the interaction. More gas is lost, less stars are formed, and the resulting body is in a state of weak gravitational energy.

When does the MRR develop in the course of time and evolutionary history of galaxies? In Fig. 5 we show the R_e vs M_s distribution of the Illustris models at four cosmic epochs. At high redshifts, the distribution is clumpy and irregular. However, starting from $z \sim 1.5$ and more clearly at $z = 0$, a tail-like feature develops on the side of large masses, say for masses $\gtrsim 2 \cdot 10^{11} M_\odot$. The best fit at redshift $z = 0$, using the relationship $\log R_e = \epsilon \log M_s + \eta$ (masses and radii are in M_\odot and kpc), yields the following values: for $\log M_s > 11.3$ $\epsilon = 0.651$ and $\eta = -6.557$, while for $\log M_s < 11.3$ $\epsilon = -0.005$ and $\eta = 0.592$. What are the causes of the cloud-like and tail-like distributions? Why a cloud dominates the low mass range? Why the tail is well visible only for the high masses at low redshifts? Which is the physical meaning of this distribution? To cast light on this Chiosi et al. [36] examined the history of R_e and M_s for several individual galaxies. The main conclusion of their analysis is that mergers among objects of low and comparable mass can generate galaxies with larger masses and radii, but exceptions are possible in which either the mass or the radius or both decrease. In general the galaxies do not leave the cloud region. All this does not contradict the previous case of Buonomo [238] because the monolithic counterparts to compare with are not available. The cloud region is instead roughly coincident with the distribution of DGs of different types [see the discussion by 226]. At the same time mergers among galaxies with different masses and/or comparable masses can generate objects that shift outside the cloud producing the MR-sequence (actually they define it), the locus of which agrees with the observed distribution for ETGs [see e.g. 36, and references therein]. The stellar content of massive ETGs suggests that star formation has ceased long ago so that strong energy feed-backs are absent and the systems are close to the virial equilibrium. This implies that important mergers do not longer occur. At variance DGs are still undergoing frequent mergers, active star formation

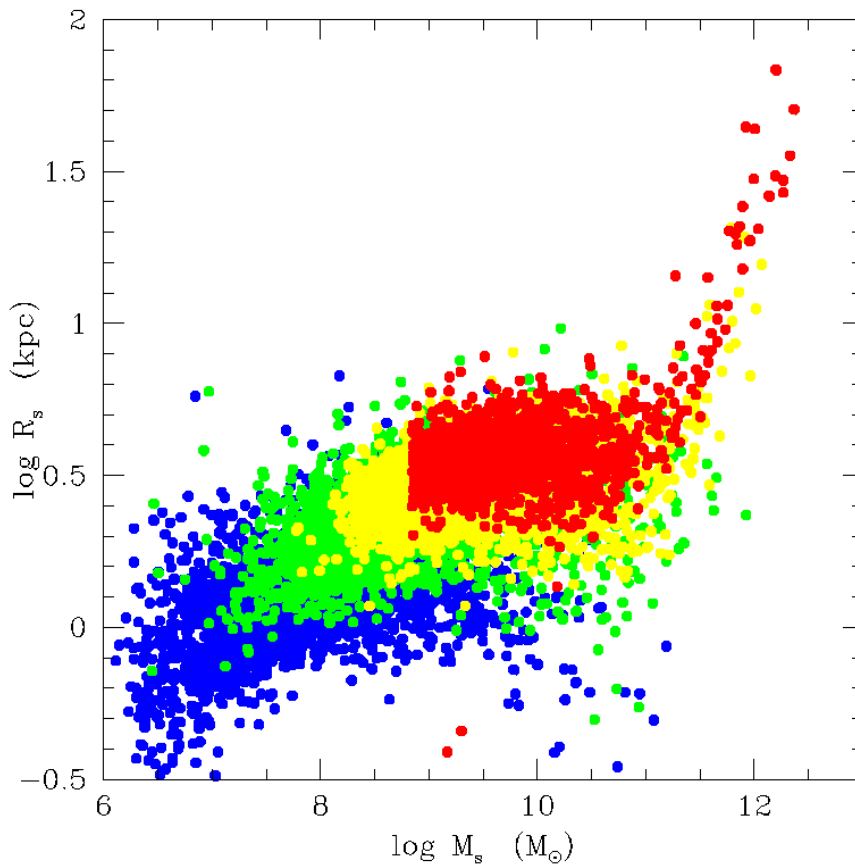


Figure 5. The stellar half-mass radius R_e plotted vs the total stellar mass M_s of galaxy models from the Illustris database at different values of the redshift, i.e. $z = 4$ (blue), $z = 2$ (green), $z = 1$ (yellow) and $z = 0$ (red).

episodes, and strong galactic winds. They cannot be therefore in this ideal condition of equilibrium and so they depart from the observed MRR. Nevertheless, there are some DGs that fall along the MRR of massive ETGs and therefore are likely in a similar dynamical and star forming condition, e.g. ω Cen and M32 [see 36, for more details].

On consideration of these premises, Chiosi et al. [36] argued that the observed distribution of ETGs, inactive DGs and GCs, represents the locus of objects that have reached the ideal situation of mechanical equilibrium and pure passive evolution. They cannot go beyond this limit. Their MRR is therefore in the boundary between the permitted and forbidden regions of the MR-plane.

6.3 Genesis of the true MRR

Putting the many tesserae of the mosaic together, the conclusion is that the observational MRR is the intersection of the theoretical manifold of the MRRs (each curve being labelled by the collapse redshift from the past to the present) with the Cosmic Galaxy Shepherd, along which objects in mechanical equilibrium and passive evolutionary state are located. To prove this statement Chiosi et al. [36] resorted to the method proposed long ago by Chiosi and Carraro [see 226], however updating it with recent theoretical and observational data. In the MR-plane of Fig.4 they draw two loci and a mass interval as a function of the initial density (redshift):

(a) The first locus is the MRR traced by models of different mass but same initial density and formation redshift. Using all models to disposal [226, 239, 240, 241, 227, 225, 36], this locus is described by the relation

$$\log R_e = [-1.172 - 0.412(1 + z_f)] + [0.244 + 0.0145(1 + z_f)] \log M_s. \quad (19)$$

This expression is robust thanks to the regular behavior of the models and the density-mass-radius relationship of eqn. (16). Relation (19) is compatible with the MRRs predicted by Fan et al. [229] and the models of Illustris by Vogelsberger et al. [81]. The cases shown in Fig. 4 are: $z_f \simeq 1$, $z_f \simeq 2$, $z \simeq 5$ and $z_f \simeq 10$.

(b) The second locus is the Cosmic Galaxy Shepherd. Among the various HGFs in literature [228, 232, 233], we adopt the HGF of Lukić et al. [228] and make use of the analytical expression for the Cosmic Galaxy Shepherd extending across the whole MR-plane given by eqn. (15). However, in order to better illustrate this issue, we present here an analytical approach based on the classical halo mass distribution of Press and Schechter [242] that is supposed to trace also the mass distribution of luminous galaxies (assuming one galaxy per halo). At each redshift, the HGF of [242] provides the relative number of galaxies per mass bin. The cut-off mass M_D^{CO} of the [242] function yields the maximum limit for the galaxy masses at each redshift. In the Press and Schechter [242] formalism, the cut-off mass varies with redshift according to:

$$M_D^{CO} = M_N \times (1 + z)^{-\frac{6}{n+3}} \quad (20)$$

The exponent n represents the slope of the power spectrum perturbations and M_N is a suitable mass scale normalization. At any redshift, most galaxies have total masses smaller than M_D^{CO} , even if higher values cannot be excluded. It can be easily shown that the fractional mass in (or the fractional number of) galaxies with mass greater than M_D^{CO} is a function of n . For $n=-1.8$, the percentage of galaxies in the interval $M_D^{CO} < M_D < 10 \times M_D^{CO}$ is about 15% while in the range $10 \times M_D^{CO} < M_D < 100 \times M_D^{CO}$ is about 1%. Therefore, at any redshift galaxy masses up to say $50 \times M_D^{CO}$ have a significant occurrence probability. Their radius is derived with the aid of the M_s vs M_D and R_e vs M_D relationships. For $M_D = \gamma M_D^{CO}$, $\gamma = 50$, and $n = -1.8$, one gets:

$$R_e = 16.9 \times 10^{-12} \times \gamma^{-0.79} \times (1 + z)^{3.96} \times M_s, \quad (21)$$

where R_e and M_s are in kpc and M_\odot . These are shown in Fig. 4 with the dotted lines labelled by the redshifts $z \simeq 1$, $\simeq 2$, $\simeq 5$ and $\simeq 10$. On the MR-plane, they give the rightmost extension of the lines of constant density and hence they identify the maximum galaxy mass. At decreasing redshift this boundary moves progressively toward higher masses. Similar results can be obtained by means of the HGFs of [228, 232, 233], the first of which is the Cosmic Galaxy Shepherd.

(c) Finally, the third locus gives the expected interval for M_s for objects with total mass M_T between M_D^{CO} and $10 \times M_D^{CO}$ as a function of redshift. Here the relation $M_s(M_T)$ has been plugged into eq. (20) for M_T^{CO} . The permitted intervals are visible in Fig. 4 by the horizontal lines labelled M_s^{CO} . The interval for M_s going from $10^{10} M_\odot$ to $10^{12} M_\odot$ is fully compatible with the redshift interval for the formation of the majority of stars in a galaxy, i.e. from 2 to 1. This is also the mass range over which at any epoch the probability for the occurrence of massive galaxies falls to a negligible value. In different words, the right-hand border of the MRR has a natural width.

In this context, the relationship for ETGs, see eqn. (4), extended to the whole mass range from GCs to CoGs should correspond to the intersection between the lines of constant initial density and the lines where

$\gamma M_T = M_T^{CO}(z)$ for equal values of the redshift (at least for all values of redshift > 1). This is what we see in Fig. 4, i.e. the straight line marked by the large empty squares. This line nearly coincides with the Cosmic Galaxy Shepherd derived from the HGF of Lukić et al. [228] that is marked by the crossed dark-red line in Fig. 4, i.e. eqs. (14) and/or (15). Finally, this line is also coincident with the locus traced by objects that underwent a dissipation-less collapse (or very close to it) and are nowadays in mechanical equilibrium and passive evolutionary state. This is mainly traced by GCs, few DGs (the large majority of DGs lie above it), ETGs, and a number of CoGs. This confirms the result by D’Onofrio et al. [37]: only passive galaxies (strongly decreasing today in their luminosity) trace the MRR with a slope varying from 0.5 to 1, the highest value being reached by galaxies that suffered the strongest luminosity decrease with the redshift, i.e. those that long ago ceased their stellar activity, i.e. the most massive ones. Spirals occupy approximately the same location of ETGs in the MR-plane, thus suggesting that their ongoing star formation is not affecting the overall situation of mechanical equilibrium. Furthermore, it is worth noting that the slope of MRR derived from the HGF is about 1 in the range of massive galaxies (say above $10^{12} M_\odot$), i.e. formally identical to the MRR derived from the virial theorem. This coincidence might suggest a dependence of the observed MRR slope from the virial condition. The true driver is instead the HGF, more precisely its fall off toward high values of the halos’ masses at any redshift. To conclude, all the objects along the MRR are in virial conditions and passive evolutionary state (all mechanical process and star formation activity are at rest).

7 THE FUNDAMENTAL PLANE

In the local universe ETGs are seen to lie along a plane, the so-called “fundamental plane” (FP, [30, 31]), connecting the surface brightness within the effective radius $\langle I_e \rangle$, the effective radius R_e , and the velocity dispersion of stars (central or within the effective radius σ_e). The intrinsic scatter around the FP is small (~ 0.05 dex) [32, 243]) and the relation appears to extend across all ETGs, DGs, GCs and CGs [244, 245].

The FP is tilted with respect to the virial prediction. The origin of the tilt has been debated for several years. The first attempts to explain it invoked a progressive change of the mass-to-light (M/L) ratio of the stellar population with galaxy luminosity, but even systematic changes of the DM fraction and the structural and dynamical non-homology of galaxies can be responsible of the observed tilt [see e.g. 246, 4, 247, 248, 33, 249].

Recently D’Onofrio et al. [250] proposed another explanation for the tilt of the FP. In their work they demonstrated that the FP can originate from the combination of the virial theorem with the modified FJ relation given by eq. 1. In this case the small scatter of the plane can be obtained if it exist a fine-tuning between the zero-points of the two relations. In other words it must exist a connection between the shape and structure of galaxies and their stellar population content [see also 251].

The FP evolves with redshift [see e.g. 252, 253, 254, 52, 255]. Beifiori et al. [256] using a sample of 19 massive red-sequence galaxies at $1.39 < z < 1.61$ observed by the K-band Multi-object Spectrograph (KMOS) Cluster Survey, find that the ZP of the FP in the B-band evolves with redshift, from 0.44 (for Coma) to -0.10 ± 0.09 , -0.19 ± 0.05 , and -0.29 ± 0.12 for clusters at $z = 1.39$, $z = 1.46$, and $z = 1.61$ respectively. Similar results are obtained by Prichard et al. [257]. The properties observed for the high redshift FP suggest an increase of the dynamical-to-stellar mass ratio by ~ 0.2 dex from $z = 2$ to the present. Consequently these data seem to indicate that the fraction of DM contained within R_e , compared to that seen in likely descendants objects at low-redshift, was increased by a factor > 4 since $z \sim 2$ [258]. The same work suggests the use of the dynamical-to-stellar mass ratio as a probe of the stellar IMF, finding that high-redshift data can constrain the IMF law.

While the debate is still open on whether the FP coefficients are constant up to $z \sim 1$ [see 259, 253, 254, 260], there is more consensus about the variation of these coefficients with the magnitude interval of the sampled population [see e.g. 55] and on the variation of the zero-point with redshift as a result of an evolving M/L [261] caused by the younger stellar population at high- z [262, 263, 264, 265, 266, 259, 267, 268, 269, 253, 270, 271] and by the structural evolution of galaxies with redshift [254, 272]. Other authors claim that there is not only a dependence of the zero point on redshift, but even the slopes of the structural relations are steeper for high redshift galaxies than for objects of the local Universe [252, 268, 273].

As discussed in the previous section, several papers have shown that a fraction of intermediate and high-redshift galaxies have smaller sizes [274, 275, 276, 277, 278, 279] and higher stellar velocity dispersions [280, 281, 282, 283, 284] compared to their local counterparts of the same mass [285, 286, 287]. Part of this difference might be attributed to environmental effects and can be observed in the FP. The environment may have a role in accelerating the size evolution in clusters with respect to the field at $z > 1.4$ [288, 289, 290, 291, 292], while in the local Universe there seems to be no significant differences between the mean galaxy sizes in different environments [58, 293]. The reason for that is not clear; is it because there is not enough time for evolution? In clusters central and satellite galaxies seem to lie on average above and below the FP, possibly for a higher and lower than average mass-to-light ratio [294].

Several studies (e.g. [295, 296]) have also suggested that the size evolution with redshift is stronger for massive galaxies ($> 10^{11} M_{\odot}$). This behaviour is consistent with the idea that high-density environments play a major role in size evolution. Galaxies in denser environments probably evolve earlier as indicated by the observed colour–density relation (e.g. [297]). It is not clear yet if the environment itself influences the size evolution, since merging events alone do not seem to explain the observed size evolution of ETGs (e.g. [198, 298]) or other growth mechanisms are at work, such as the adiabatic expansion due to mass-loss, that could indirectly lead to a correlation of size with environment (if it occurs at earlier epochs within the most massive dark matter halos). There is also the possibility of trends driven by faster quenching in high-density environments (e.g. [299]). Whatever the reason of the size evolution, the underlying correlation is likely connected to the halo mass that is strongly related to the number of satellites (e.g. [300, 301]). A full investigation of this problem requires a careful decoupling of large-scale clustering and small-scale halo occupation (e.g. [302]).

The presumed universality of the FP makes it an appropriate tool for cosmology, e.g. for the Tolman test [303, 304, 305], or to assess the evolution of M/L with z [4, 17, 262, 306, 263, 307, 308, 264]. The usefulness of the FP was recently demonstrated in the context of weak lensing magnification [309], and to map out the peculiar velocity field of galaxies [310]. These are examples of the exploitation of the FP as cosmological probe. In such applications generally one measures the observed galaxy size and predicts it using the FP. The comparisons between predictions and observations are used to get the size changes due to lensing magnification, or the line-of-sight peculiar velocities that modify the redshift and the angular diameter distance used to obtain the physical sizes.

Again we should note that hierarchical numerical simulations, like Illustris, correctly predict a tilt of the FP and an evolution of its coefficients with redshift [311].

8 THE COLOR-MAGNITUDE RELATION

The color–magnitude relation (CMR) is an important tool used to understand the physical properties of stellar systems. Its first original application started with the studies of star clusters [312, 313], followed by the analysis of our Galaxy and the Local Group [314, 315, 316] and by the analysis of the integrated light of galaxies in clusters, in particular in Virgo and Coma [317, 318, 319, 320]. The modern CCD

instrumentation have provided much richer CMRs [see e.g. 321, 322, 323, 324] allowing the study of the past history of galaxy clusters themselves [see e.g. 325, 326] up to distances of cosmological interest.

Since colors are independent of distance and are very similar for all cluster members, the CMRs have been considered good cosmological probes [327, 321], in particular when we look at the fraction of blue and red galaxies and their morphological ratios, the so-called galaxy color bimodality [328]. Both seem to be different in clusters and in the field [329, 330].

In the CMR three main loci are of interest: the first is the red sequence (first noted by [331]), a linear band throughout a broad interval of luminosities mainly occupied by evolved ETGs. The others two are the blue cloud, in which gas-rich galaxies still form stars at high rates, and the green valley in between, where a complicated interplay between gas conversion and passive evolution is at work [332].

Thanks to the large-scale surveys, magnitudes, colors, morphological types and redshifts for thousands of galaxies are now available. One example is the Galaxy Zoo, derived from the SDSS [333, 334, 335]. These data have amply confirmed the existence and the evolution of the red sequence of galaxy clusters [336, 337]. More recently, the faint end of the red sequence has been also investigated [338, 337, 339].

The theoretical analysis of the CMR is difficult because of the age–metallicity degeneracy: stars become red when age and metallicity increase [see e.g. 340, 341]. Understanding the origin of the red sequence, its slope and width has been the subject of several studies [see e.g. 342, 343, 344, 321, 345, 223, 346, 347, 348]. The general properties of the CMR have been investigated [349, 350, 351], within the classical scenario of galaxy formation and evolution with supernova-driven winds [352, 353, 354, 355, 356, 357], within semi-analytical models in the hierarchical scheme [358, 359, 360], and within N-body-Tree Smooth Particle Hydro-dynamics simulations [see e.g. 226].

The most accepted view is that the red sequence is more affected by metallicity than by age, even if the CMR has an age dispersion that increases at decreasing galaxy masses. Reproducing the slope requires a correct treatment of the chemical evolution [359, 361]. A crucial element is the knowledge of when and how the red sequence is formed. The downsizing phenomenon, discovered by spectroscopic analyses of nearby ETGs [362, 363, 75], implies that the red sequence was built over an extended period of time (~ 5 Gyr), beginning with the most massive systems [364]. Efforts to directly detect the formation of the red sequence have observed the color bimodality up to $z \sim 2$ [324, 365, 366]. The data of the legacy surveys GOODS, COSMOS, NEWFIRM, and UltraVISTA have also shown that massive quiescent galaxies ($M_s \geq 3 \times 10^{10} M_\odot$) begin to appear as early as $z = 4$ [367, 287, 368] and stop assembling by $z = 1-2$ [369, 285]. Roediger et al. [339] found that the red sequence flattens in all colors at the faint-magnitude end (starting between $-14 \leq M_g \leq -13$, around $M_s \sim 4 \times 10^7 M_\odot$), with a slope decreasing to $\sim 60\%$ or less of its value at brighter magnitudes. This could indicate that the stellar populations of faint dwarfs share similar characteristics (e.g., constant mean age) over ~ 3 mag in luminosity, suggesting that these galaxies were quenched coevally, likely via pre-processing in smaller hosts.

In recent times, large-scale numerical simulations of hierarchical galaxy formation in Λ CDM cosmogony, i.e. including DM and BM, appeared on the scene. In these simulations, much efforts have been made to include star formation, chemical enrichment, radiative cooling/heating, as well as feedback processes of different nature. With these simulations, the variation of the cosmic SF rate density (SFRD), with redshift [370, 371] has been addressed and largely explained [see e.g. 371, 372]. Some of these take into account the photometric evolution of the stellar content of galaxies, permitting the analysis of the CMR, in particular for galaxies belonging to clusters. As shown by Sciaratta et al. [326] these simulations nicely reproduce the red sequence, the green valley, and the blue cloud, the three main regions of the CMR.

The major drawback of these massive numerical simulations is their complexity, high cost in terms of time and effort, and lack of flexibility and prompt response to varying key input physics.

Since broadband optical colors are not good discriminants of stellar populations because of the age-metallicity degeneracy, attempts have been made to break the degeneracy by using stellar absorption lines indexes [373, 374]. Recent results suggest that metallicity, α -enhancement, and age vary along the mass or velocity dispersion sequence [375, 362, 363], and also vary as a function of environment [363, 376]. The general impression however, is that the age-metallicity degeneracy cannot be broken.

Finally we want to remark a notable fact: as shown by Cariddi et al. [325], galaxy clusters share with galaxies in clusters a red sequence that has a similar slope. The mean color of clusters correlates with their total absolute magnitude, in the sense that small and faint clusters are in general bluer than big and luminous clusters. This aspect of the CMR has never been addressed by dedicated studies up to now. It is interesting to note that, independently on the scale of the stellar systems, the behavior of the stellar population seems connected with the structural and dynamical properties of the system, a proof that gravity works in the same way at all scales. In general we can say that the global understanding of the CMR for clusters of galaxies is still in its infancy.

Great progresses are expected in this field with the new generation of ground and space telescopes, like ELT, JWST, etc., that will reach the faintest galaxies at high redshifts.

9 STAR FORMATION IN GALAXIES

In a galaxy's evolutionary history, SF is the starring actor. Thanks to it, gas is continuously turned into stars by a number of not yet fully understood processes, so that within the potential well of DM and BM a shining object is built that is populated by many generations of stars of different mass, age, and chemical composition. In the following we limit ourselves to mention only the most popular laws for the star formation rate that are customarily used in models of galaxy formation, leaving aside the much wider subject of the physical processes by which gas can be turned into stars. From an observational point of view, looking at the stellar populations in GCs, DGs, LTGs, and ETGs, the dominant history of SF changes a lot passing from one type to another: it is sharply peaked in one or a few initial episodes followed by quiescence in GCs, DSphs, and DEs, a series of bursts and quiescent periods in dwarf Irr, ever continuing in LTGs however showing a spatial and temporal grand design, and an initial dominant episode of high intensity and relatively long duration following by minor activity or quiescence in ETGs. Can theoretical models reproduce and physically explain this variety of behaviors that apparently is related to the mass and morphological type? To answer the question one has to assume a general law of star formation and look for the physical situations in the history of star formation can change with the morphological type of the host galaxy.

9.1 Star formation in ETGs: mass and/or initial density?

In the case of ETGs the best tool highlighting the main driver of the SF and the SFH are the NB-TSPH hydrodynamic simulations, in which the rate of star formation is usually expressed by the Schmidt [377] law

$$\frac{d\rho_s}{dt} = -\frac{d\rho_g}{dt} = c^* \frac{\rho_g^k}{t_g} \quad (22)$$

where ρ_s is the current mass density of stars, ρ_g is the current mass density of gas, t_g a characteristic time scale (typically the free-fall), k a suitable exponent (typically $k \simeq 1$), and c^* is the so-called dimensionless efficiency of star formation (typically $c^* = 0.01 \div 0.1$).

Based on simple arguments, there are at least three prerequisites for gas (likely in form of molecular clouds) to be eligible to star formation: the gas has to be in convergent motion, i.e. the velocity divergence must be negative; the gas must be gravitationally unstable, i.e. it must satisfy the Jeans condition $t_{sound} \geq t_{ff}$ (where t_{sound} is the time scale related to the local sound velocity); the gas must be cooling, i.e. it has to verify the relation $t_{cool} \ll t_{ff}$. Normally, SPH codes treat star formation simply implementing the Schmidt law in the computational language and transforming part of the gaseous particles which satisfy the three conditions above in new, collisionless particles of different mass (“stars”). The characteristic time scale is chosen to be the maximum between t_{cool} and t_{ff} time-scales, however in most situations $t_g = t_{ff}$ is also a good choice. Knowing ρ_g and ρ_s and integrating upon the current volume of the system one gets the current values of M_g and M_s . Nowadays there are numerous galaxy models whose stellar content has been calculated with the above prescription. However they differ in a number of important assumptions, chief among others the cosmological model of the Universe and the scenario in which galaxy formation and evolution is framed. In the following, for the sake of illustration we will summarize here the results of three paradigmatic cases, i.e. the pure monolithic scheme of Chiosi and Carraro [226], the early hierarchical scheme of Merlin et al. [241, 227], and the full hierarchical scheme, e.g. the Illustris case of Vogelsberger et al. [e.g. 81, and references]. It is worth recalling here that care must be paid on the link between the Schmidt and Kennicutt-Schmidt SF laws and their implications for numerical simulations [378].

The pure monolithic scheme. Chiosi and Carraro [226] highlighted the role of over-density of the initial perturbation when exceeding the threshold value. Two groups of models were analyzed according to the initial over-density: (i) models with mean initial density $\langle \rho \rangle \simeq 200 \times \rho_u(z)$ and collapse redshift $z_f = 5$ (shortly named A); (ii) models with $\langle \rho \rangle \simeq 5 \times \rho_u(z)$ and $z_f \simeq 1$ (named B). $\rho_u(z)$ is the density of the Universe at redshift z ³. Perturbations with spherical symmetry, assigned mass, mean density exceeding the critical value (and hence suitable radius) are let collapse and form stars. A MonteCarlo procedure is adopted to fix the initial coordinates and velocities of the DM and BM particles. The key result of this study is that the star formation history (rate vs. time) is found to depend on the depth of the gravitational potential well of a galaxy. The following picture can be drawn. In the case of deep gravitational potentials (such as in massive and/or dense galaxies) once star formation has started energy is injected into the gas by supernova explosions, stellar wind, etc..., but this is not enough to push the gas out of the potential well. The balance between cooling and heating is reached and the gas consumption by star formation goes to completion. Star formation cannot stop until the remaining gas is so little that any further energy injection will eventually heat it up to such high energies (temperatures) that the gravitational potential is overwhelmed. No more gas is left over and star formation is quenched. The star formation history resembles a strong unique burst of activity, a sort of monolithic star forming event, taking place over a certain amount of time, of the order of 1 to 2 Gyr. In contrast, in a galaxy of low mass and/or density and hence shallow gravitational potential, even a small star forming activity will heat up the gas above the potential well. Some of it is soon lost in galactic wind, the remaining one becomes so hot that it will take long time to cool down and to form new stars. The cycle goes on many times in a sort of repeated bursting mode of star formation taking place during long periods of times if not for ever. Out of all this we can derive what follows:

³ The cosmological parameters were $H_0 = 65 \text{ km s}^{-1} \text{ Mpc}^{-1}$, Baryonic to Dark Matter ratio 1 to 9, i.e. for $M_T = M_B + M_D$, $M_B = 0.1M_T$, $M_D = 0.9M_T$.

(i) The duration, strength, and shape of the SFR as a function of time strongly depend on the galaxy mass and the initial density: (a) Galaxies of high initial density and total mass undergo a prominent initial episode of SF followed by quiescence. (b) The same happens to high mass galaxies of low initial density, whereas the low mass galaxies experience a series of burst-like episodes up to the present. The details of their SFH are very sensitive to the value of the initial density. The typical dependence of the SFR on time for models B is shown in the left panel of Fig.6, while the right panel shows the SFR of a low mass galaxy ($M_T = 10^9 M_\odot$) for moderate variations of the initial density. Models A are not shown because their SFR is represented by a single initial spike.

(ii) The gas mass turned into stars (per unit total mass of the galaxy) is nearly constant. This means that the same engine is at work.

(iii) At increasing total mass of the galaxy the ratio between the left-over gas and the initial total BM decreases.

(iv) As a result of star formation, large amounts of gas are pushed out from the central regions to large distances. When this gas cool, part of it falls back towards the central object.

(v) In general all galaxies eject part of their gas content into the inter-galactic medium, and the percentage of the ejected material increases at decreasing galaxy masses.

The early hierarchical scheme. Merlin et al. [241, 227] using initial conditions derived from large scale cosmological simulations and abandoning the strict monolithic scheme, much improved the NB-TSPH galaxy models of Chiosi and Carraro [226]. They also adopted the Λ CDM cosmology instead of the classical CDM⁴. Without entering into detail, they cut from large scale simulations calculated with the free code COSMICS by Bertschinger1995 [379], Bertschinger [380] a spherical portion containing a proto-halos of DM and BM in cosmological proportions with the desired over-density, mass and size (the reference proto-halo with the highest mass to consider). The same is made for halos with lower mass and smaller dimensions at fixed mean density. The procedure to obtain halos with the same mass but different initial mean density is more complicated and will not reported here [see 241, 227, for the details]. These proto-halos contain a number of distinct lumps of matter that will merger together later on. The cosmological simulation provides the initial positions and velocities of all the particles in the proto-halos. The expansion of the Universe is taken into account. The proto-halos are followed through their expansion (caused by the Hubble flow), down to their collapse and aggregation into a single objects. The redshift of the collapse varies from model to model and, inside the same model, from the center to the periphery. In general the collapse occurs in the redshift interval $4 > z > 2$, it starts in the central regions and gradually moves outwards. The collapse is complete at redshift $z \simeq 2$. All models develop a stellar component. The more massive halos experience a single, intense burst of star formation (with rates $\geq 10^3 M_\odot/\text{yr}$) at the early epochs. The intermediate mass halos ($M_T \simeq 10^{11} M_\odot$) have star formation histories that strongly depend on the initial over-density, i.e. with a single or a long lasting period of activity and strong fluctuations in the rate. The small mass halos ($M_T \simeq 10^9 M_\odot$) always have fragmented star formation histories: this is the so-called “galactic breathing” phenomenon. These models are classified as *early hierarchical* because they experience repeated episodes of mass accretion at very early epochs and then evolve in isolation ever since. They confirmed the correlation between the initial properties of proto-halos and the star formation history found by Chiosi and Carraro [226]. The models have morphologies, structures and photometric properties similar to real galaxies [see 227, for all other details].

⁴ The cosmological background was the standard Λ CDM, with $H_0=70.1$ km/s/Mpc, flat geometry, $\Omega_\Lambda=0.721$, $\sigma_8=0.817$, and baryonic fraction $\simeq 0.1656$.

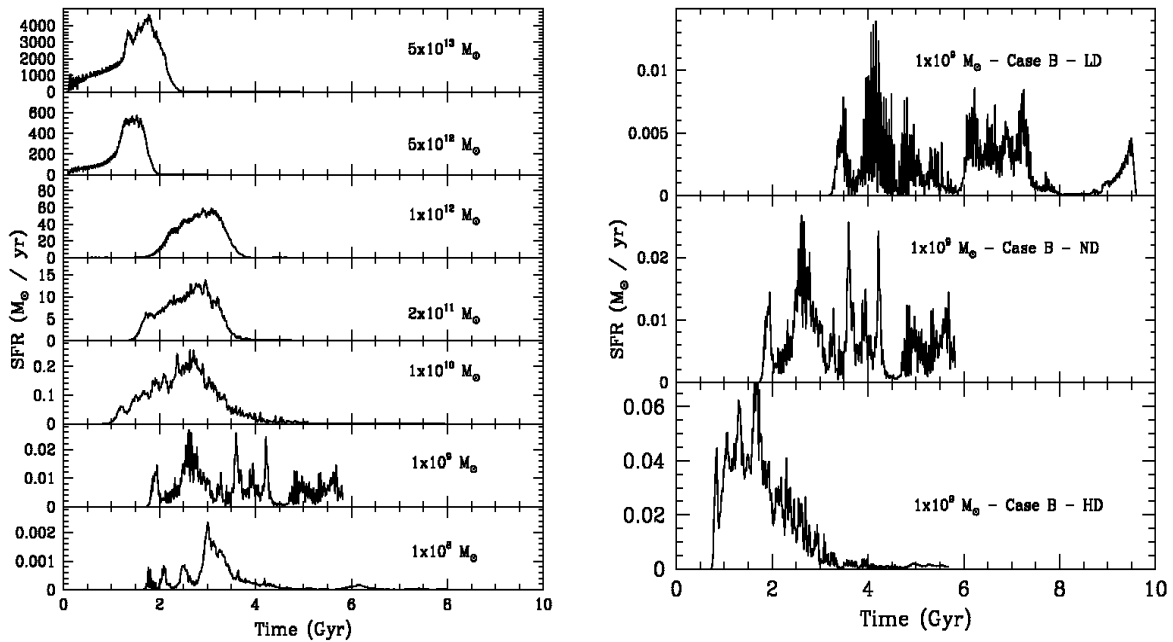


Figure 6. Left panel: The SFR as a function of time for the model galaxies of type B of [226]. Their initial conditions are rather simple and grouped according to the initial over-density: models of type A had mean initial density $\langle \rho \rangle \simeq 200 \times \rho_u(z)$, whereas models of type B had $\langle \rho \rangle \simeq 5 \times \rho_u(z)$ where $\rho_u(z)$ is the density of the Universe at redshift z . The Hubble constant was $H_0 = 65 \text{ km s}^{-1} \text{ Mpc}^{-1}$ and the redshift of the starting collapse $z_f = 5$. Only models B are shown here because they are particularly useful to highlight the effect of the mass at given initial over-density. From the bottom to the top, the SFRs refer to galaxies with $M_T = M_{DM} + M_{BM}$ from $1 \times 10^8 M_\odot$ to $5 \times 10^{13} M_\odot$. The initial baryonic and dark mass are $M_{BM} = 0.1 M_h$ and $M_{DM} = 0.9 M_h$, respectively. Right panel: the SFR of low mass type B galaxies of the same mass, but different initial over-density. The mass is $M_T = 10^9 M_\odot$. The initial over-density varies from low (LD) to intermediate (ID) to high values (HD). The figures are reproduced from Chiosi and Carraro [226].

The fully hierarchical scheme. This is the most difficult case to discuss because of mergers among galaxies of different mass, size, and age. If gas is present recurrent episodes of stronger star formation activity may occur. It is conceivable that seed galaxies prior to any encounter behave like the general scheme envisaged before and governed by the initial density and mass. Mergers among objects of similar mass would likely enhance the rate of star formation in a sort of burst of short duration and the fold the two histories together. Mergers among objects of much different mass, would simply generate a temporary perturbation on the star formation history of the most massive one, while less massive object simply loses its identity. In the hierarchical scenario, tracing the star formation history of a single galaxies is a hard task. Anyway, the observational evidence provided by the stellar content of galaxies of different mass strongly support the mass-density scheme we have described.

The general trends of the SFR described in this section agree with the picture envisaged long ago by Sandage [381], examining the SFR in galaxies of different types [see also 340, 382, 383]. This scenario has been confirmed by studies of SF histories based on absorption line indices [363], and by the recent study of Cassarà et al. [384]. A good agreement also exists with other independent numerical NB-TSPH models of galaxy formation and evolution by Kawata and Gibson [385, 386], Kobayashi [387].

9.2 The rate of star formation in disk galaxies

According to Matteucci [383] the most common parameterization of the SFR in LTGs is the Kennicutt [388] generalization of the original Schmidt [377] law, where the SFR is proportional to the gas density ρ . Kennicutt [388] suggested that the SFR can be written as:

$$SFR(t) = \nu \Sigma_g^\kappa \quad (23)$$

where Σ is the gas surface mass density, ν the efficiency of star formation (the SFR per unit mass of gas) and $\kappa = 1.4 \pm 0.15$, as deduced by the data of the star forming galaxies [see also 389]. Other parameters, such as gas temperature, viscosity and magnetic field are not considered.

Actually, the ‘‘Kennicutt law’’ was in use long before its discovery. In the mid seventies Larson [390, 391] developed the first modern hydrodynamic models of formation and structure of elliptical and spiral galaxies, showing that a rate of star formation strongly declining during the latest stages of collapse was necessary to form a massive disk in spiral galaxies. However, once the gas has settled onto the equatorial plane and built up the disk, the rate of star formation should increase to a peak value and then decline again. The duration of this phase and the height of the peak were found to depend on the position on the disk. Larson envisaged several physical mechanisms that might strongly suppress star formation during the latest stage of collapse, e.g. velocity dispersion of the gas, tidal forces exerted on the remaining gas by the already formed spheroidal component, and dependence on the cloud-cloud collision frequency. The same processes were also invoked to control the second phase of star formation. Starting from this Talbot and Arnett [392] correlated the process of star formation with the surface mass density of the gas in an already flattened disk, whose thickness is regulated by the balance between the gravitational attraction and the increase of the scale height by energy injection by short-lived stars (e.g. type II supernova explosions by massive stars). They proposed a star formation rate proportional to the surface mass density of gas. Chiosi [393] folded the Larson [391] results into the Talbot and Arnett [392] mechanism and incorporated all this into a new model for the chemical evolution of galactic disks in presence of infall. In this model the disk is described by a series of concentric rings (no mass exchange among them), whose surface mass distribution at the present time t_g is given by an exponential law of type $\Sigma(r) = \Sigma_d \exp(-r/R_d)$, where Σ_d and R_d are two scale parameters. The formation of the disk is supposed to occur by rapid infall of the gas left over by the formation of the halo and the central spheroidal component. The temporal and spatial dependence of the infall rate is given by

$$\frac{d\Sigma(r, t)}{dt} = A(r) \exp(-t/\tau) \quad (24)$$

where $A(r)$ is a suitable function to be determined. This is derived by integrating eq.(24) with respect to time and by equating it to the present day mass distribution. We obtain

$$A(r) = \Sigma_d \exp(-r/R_d) \tau^{-1} [1 - \exp(-t_g/\tau)]^{-1} \quad (25)$$

for $r_B \leq r \leq r_D$, where $r_B \simeq 2$ kpc and $r_D \simeq 20$ kpc are the typical radius of a bulge and of a disk of spiral galaxies respectively. The scale parameters Σ_d and R_d are determined by knowing the rate and the surface mass at certain position of the disk (e.g. the solar vicinity in our case). Thanks to the short time scale of the energy input from massive stars (a few million years), compared to the mass accretion time scale by infall (from hundred to thousand million years) the disk was supposed not to differ from an equilibrium state so that the Talbot and Arnett [392] formalism could be applied. Chiosi [393] and Chiosi and Matteucci [394] proposed and used the SFR:

$$\frac{d\Sigma_s(r, t)}{dt} = -\frac{d\Sigma_g(r, t)}{dt} = \tilde{\nu} \left[\frac{\Sigma(r, t)\Sigma_g(r, t)}{\Sigma(\tilde{r}, t)} \right]^{\kappa-1} \Sigma_g(r, t) \quad (26)$$

where $\Sigma_g(r, t)$ and $\Sigma_s(r, t)$, are the surface mass densities of gas, stars at the position r or and time t , respectively. The quantities $\Sigma(\tilde{r}, t)$ and $\tilde{\nu}$ are the total surface mass density at a particular distance from the galaxy center, and an efficiency parameter. They play the role of a particular radial scale controlling star formation. In the Larson's view they might be associated to the radial distance at which the central spheroidal component and the innermost regions of the disk exert their tidal effect on the residual external gas. The spatial and temporal dependence of the relation 26 in the infall model for the disk of the Milky Way and disk galaxies in general is such that at any time the SFR is strongly inhibited at distances $r > \tilde{r}$, while at any given r the SF starts small, increases to a peak value, and then declines again. This behaviour of the SFR is typical of all infall models, where because of interplay between gas accretion and consumption, the SFR starts low, reaches a peak after a time approximately equal to τ and then declines. Independently of the position, the net temporal dependence of the SFR is the time delayed exponentially declining law:

$$SFR \propto \frac{t}{\tau} \exp\left(-\frac{t}{\tau}\right). \quad (27)$$

The Schmidt law is the link between gas accretion by infall and gas consumption by star formation. Thanks to the infall model by varying τ (time scale of the galaxy formation process) one can recover all types of star formation indicated by observational data going from GCs to LTGs and ETGs. The infall scheme and companion SFR have been widely used in many studies on the subject of galactic chemical evolution [e.g. 383, for a recent review and references]. The infall galaxy model is very flexible and can be adapted to a wide range of astrophysical problems. Suffice to recall that it has been used by Bressan et al. [395] to model the spectro-photometric evolution of ETGs reduced to point mass objects, extended by Tantalo et al. [355] to the case of spherical systems made of BM and DM mimicking ETGs, adapted by Portinari and Chiosi [396] to include radial flows of gas in disk galaxies, and recently used by Chiosi et al. [397] to study the cosmic star formation rate and by Sciarratta et al. [326] to investigate the color-magnitude diagram of galaxies in general.

9.3 The Mass-SFR relation

The connection between the structure and dynamics of galaxies and their stellar population, that we have encountered addressing the FP problem, is also part of the SF problem of galaxies. Observations have in fact revealed that the SFR and the stellar mass (M_s) of active star-forming galaxies are tightly correlated ($SFR \propto M_s^{0.6}$). This trend is known as the galaxy "main sequence" (MS) [398, 399, 400, 401, 402, 403, 404, 405, 406]. Adopting different samples the MS may be different, either in slope and scatter, primarily for selection effects on the adopted SF indicator used [407]. One may select galaxies according to their mass and/or color, picking preferentially the blue cloud objects, or using the BzK color selection [408, 409, 410] or the UVJ selection [411, 403], or adopting a minimum threshold for the specific SFR ($sSFR = SFR/M_s$) [412].

The presence of a main sequence, with a scatter of 0.3 (in log units for active star-forming objects), indicates that these galaxies have a SFR that spans a factor of two. This can be explained by the self-regulating nature of the SF process, that is by the interplay between gas accretion, SF and feedback [413, 414, 415, 416, 417, 418].

The scatter however is much larger (~ 0.6) if all types of galaxies are considered. We can see it in Fig. 7. The red dots in the various panels represent the data of the WINGS database [419, 420]. The SFR in the last 20 Myrs, measured from the spectral energy distribution in more than 3000 objects of all morphological types, is plotted versus the stellar mass. The artificial data coming from the Illustris simulations are also represented for different redshift epochs: $z = 4$ (blue dots), $z = 1$ (green dots) and $z = 0$ (black dots). Before drawing any conclusion, it is worth recalling that the model galaxies of the Illustris simulation were chosen to have stellar masses above $10^9 M_\odot$ at $z = 0$. Therefore the comparison between theory (black dots) and data (red dots) in Fig 7 is possible only for $M_s \geq 10^9 M_\odot$. We note that in the common region the simulations predict the correct slope and quite a similar scatter at $z = 0$. They also predict that the slope mildly changes with redshift and that the scatter increases going to the present epoch. This limit on M_s does not exist for the samples at higher redshifts.

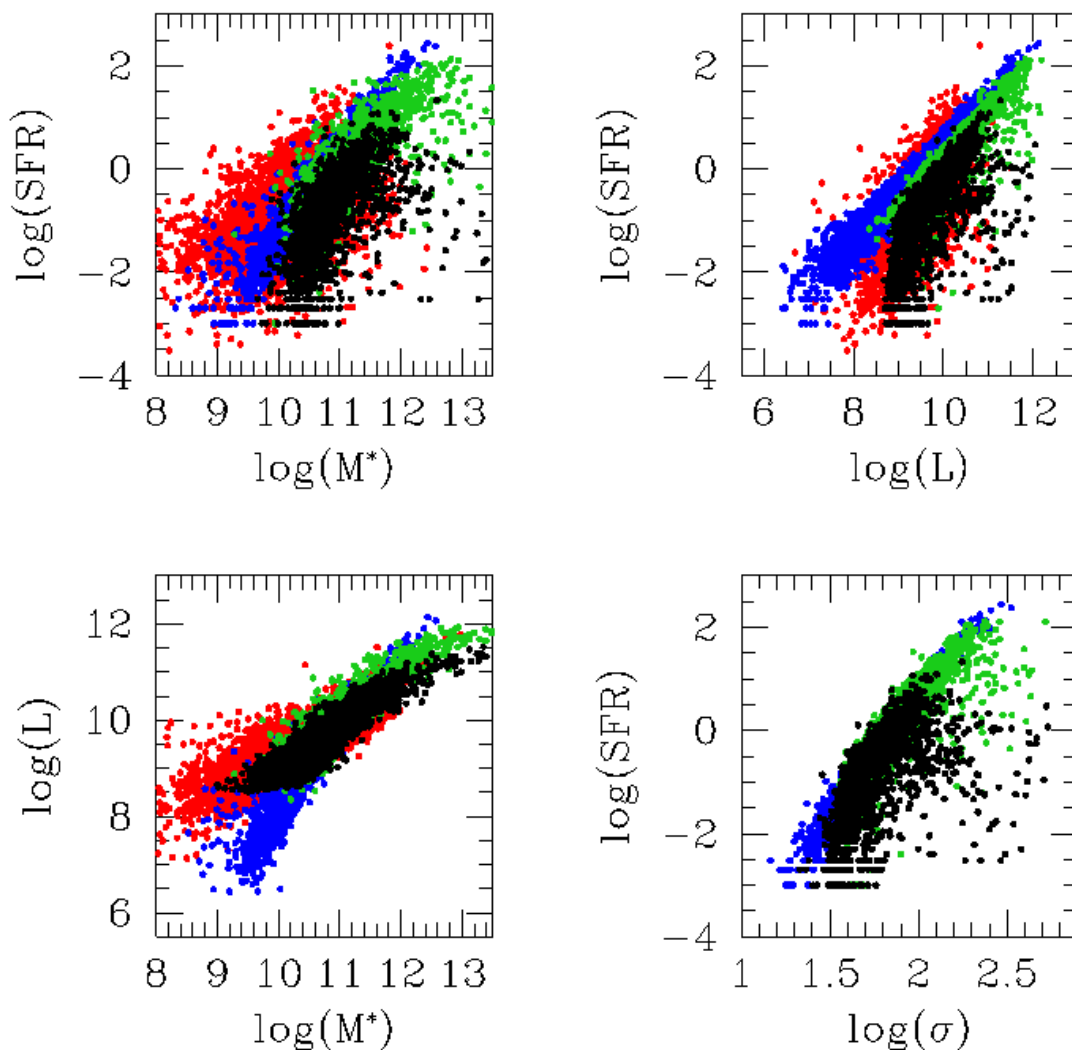


Figure 7. The correlations between M_s , L_V , SFR and σ . Mass and luminosity are in solar units, SFR in M_\odot/yr and σ in km s^{-1} . The red dots are the observational data of the WINGS survey for all morphological types [419, 420]. The blue dots are the prediction of the Illustris simulation for galaxies at $z = 4$. The green dots the prediction at $z = 1$ and the black dots the prediction at $z = 0$. Note the lack of objects with mass below $10^9 M_\odot$ at $z = 0$.

The origin of the scatter and its amount might be different for dwarf and giant galaxies [421] and can be attributed both to short-time and long-time processes, such as the competing effects of inflows and outflows, the variation of the halo mass, the variation of the SFE and the feedback effects from the active nuclei. Daddi et al. [409], Elbaz et al. [422], Noeske et al. [400] claim that the correlation is present even at redshift ~ 2 , with a nearly constant slope and a dispersion similar to that observed for galaxies in the local universe [398].

The information that one can draw from the MS is still under debate [423, 424]. There are many open questions: does the main sequence imply that the SFH of galaxies of the same stellar mass is similar? Is the MS a median “attractor-solution” [425, 233]? Is it an average sequence for a population at a certain age of the Universe [426, 427]? Do galaxies of the same mass have different SFHs on longer time-scales? What effects are most significant at different mass and time-scales?

The slope and scatter of the MS might encode such crucial information. What makes the growth of galaxies different? Which are the important time-scales of SF? Which are the systematic and stochastic effects behind the scatter? Which is the role played by the environment and by the DM in the assembly accretion history?

The MS measured at higher redshifts shows a positive correlation evolving only a bit in slope and scatter [see e.g 422, 400, 403]. This might support the idea that the link between structure and stellar population in galaxies is already in place at $z \sim 2.5$ [428].

The SFR in a galaxy depends on a variety of factors, such as the rate at which the galaxy accretes mass from the IGM, the rate of shocking and cooling of gas onto the galaxy, the details of how the inter-stellar medium (ISM) converts gas into stars, the amount of galactic fountain and outflow, etc. This complex non-linear physical mechanism is difficult to understand, in particular if one wants to discover what processes dominate, and if and how these change over time. The PCA reveals that neutral gas fraction f_{gas} , stellar mass M_s and SFR form a nearly flat 2D surface [429]. The location of the plane varies with redshift, and galaxies can move along it when f_{gas} and SFR drop with redshift. Their position along the plane is correlated with gas metallicity. This is a sort of “fundamental plane of SF” whose curvature is determined by the dependence of the SFR on gas density and metallicity.

10 THE MASS-METALLICITY RELATION

It has been known for a long time that the mean metallicity of galaxies correlates with the mass (and luminosity) [430, 431, 432, 433]. By metallicity astronomers mean the abundance of heavy elements in the gas phase of the ISM. Such relation is observed either in gas-rich and gas-poor galaxies and suggests a similar physical mechanism behind the origin of the phenomenon [434]. Recently, the data of the SDSS have permitted the analysis of the mass–metallicity (MZR) relation over a wide interval of masses and metallicities [196, 435].

All studies confirm the trend of decreasing metallicity towards lower stellar masses, but the true form of the MZR is not yet well established. This depends on the strong systematic uncertainties affecting the measurement of the metallicity. There are a variety of methods to determine the metallicity [436]. Some are based on the photoionization models for HII regions by reproducing some emission-line ratios, like $([OII]\lambda 3727 + [OIII]\lambda\lambda 4959, 5007)/H\beta$ [437] and $[NII]\lambda 6583/[OII]\lambda 3727$ [438]. Some others are based on the fits of the electronic temperature (T_e), using strong-line ratios for HII regions and galaxies, like $([OIII]\lambda 5007/H\beta)/([NII]\lambda 6583/H\alpha)$ and $[NII]\lambda 6583/H\alpha$ [439]. However, there are some problems when using these strong-line metallicity calibrations. For example, the MZR with different calibrations

have different shapes and normalization [436]. Furthermore, for high- z star-forming galaxies, these calibrations may not be valid, since their physical conditions in terms of gas density, ionization, N/O abundance, etc. might significantly be different from those in the local universe [440].

Kewley and Ellison [436] have shown that the method used to measure the oxygen abundance ($\log(O/H)$), typically assumed to trace the ISM metallicity, affects the shape and normalization of the MZR. Differences up to 0.7 dex in the abundances at fixed stellar mass, using different emission-line methods are measured. This difference is not constant with the stellar mass and can give significant differences in the shape of the MZR. Possible origins for these discrepancies are discussed in [441, 436, 442, 443, 444].

The observations are commonly explained by gas outflows that are much stronger in dwarf galaxies than in giant elliptical galaxies. The massive galaxies are able to retain the gas much longer than low-mass objects. This permits an increase of metallicity, because the new generations of stars are formed in a metal enriched environment. At the same time, low-mass objects loose their gas through galactic winds. Alternative explanations invoke a variable SF efficiency (SFE). This is larger in more massive systems, that formed most of their stars in a short time at high redshift, quickly enriching the ISM to solar or super-solar metallicities.

The MZR clearly depends on how gas accretion, SF and outflows proceed with time and therefore it contains important information about these processes. Several examples of the MZR have been published adopting samples of massive star forming galaxies at different redshifts ($0 < z < 3.5$) [see e.g. 196, 436, 445, 435, 446, 447, 448, 449, 450], while only few studies, mostly at $z \sim 0$, have extended the MZR to low mass DGs [431, 451, 452, 453, 454]. The luminosity-metallicity (LZR) relation has also been studied by several authors [431, 455, 456, 457, 458].

Recently the chemical evolution models of De Lucia et al. [459], in a hierarchical context, have also explained the observed MZR and the Tully–Fisher relation. This was possible by including feedback processes into the cosmological simulations. The drawback is that the feedback includes some free parameters, such as the efficiency or the yield, that can be chosen to match the observations.

Another difficulty of the outflow scenario is that different amounts of DM can play a key role in stopping the outflow of gas [194]. The works of Lee et al. [451] and Dalcanton [460] have for example shown that the simple outflow of the gas does not reproduce correctly the yields observed in the ISM of DGs. The large variations in the effective yields and the dispersion in the relation are difficult to understand using only superwinds or outflows, in particular for the low metallicities observed at low masses and luminosities. It seems that neither the simple infall nor the outflow models are able to reproduce the low effective yields of low-mass galaxies.

In nearby galaxies, in the $10^6 \div 10^{9.5} M_{\odot}$ range, the MZR follows a shallow power-law ($Z \propto M_s^{\alpha}$) with slope $\alpha = 0.14 \pm 0.08$. Approaching $M_s \sim 10^{9.5} M_{\odot}$ the MZR steepens significantly, showing a slope of $\alpha = 0.37 \pm 0.08$ in the $10^{9.5} \div 10^{10.5} M_{\odot}$ range. Finally a flattening towards a constant metallicity is observed at higher stellar masses because the metallicity of the most massive galaxies saturate.

The evolution with redshift of the MZR [435, 461, 462] is a tool to trace the history of chemical enrichment in the different cosmic epochs. At high redshifts the MZR has a steeper slope. The MZR at $z \sim 3.5$ seems to evolve much stronger than at lower redshifts [435]. This is an epoch of strong SF activity and metal enrichment also for massive systems. The metallicity evolution of low-mass systems seems stronger with respect to that of high-mass systems, an effect that reminds the "downsizing" of galaxies in a chemical framework. Recent results concerning the evolution with redshift of the MZR up to $z \simeq 2.7$ are those by Wuyts et al. [463]. Using the Integral Field spectroscopy they obtained data in good agreement

with the old long-slit spectra, except for the slope of the relation at $z \sim 2.3$ in the low-mass regime, where they measured a steeper slope than in previous literature results.

The ISM of galaxies can be enriched by different effects: the accretion of gas from the inter-galactic medium (IGM), the injection and mixing of metals coming from the SF, the removal of these metals when they are locked into long lived stars and stellar remnants, the ejection of these metals when galactic outflows are at work, the mixing of high and low metallicity gas in the circum-galactic medium (CGM) and the removal/re-accretion of this gas out of the halo or back in the galaxies [464, 391, 465, 466, 460, 467, 416, 468]. All these processes play an important role in shaping the evolution of galaxies.

Not surprisingly the links between the gas mass (M_g), the SFR, the stellar mass (M_s), and the metallicity Z , is evident in a number of observed correlations. The most notable examples, in addition to the MZR, are: (i) the $M_s - SFR$ correlation (dubbed the “Main Sequence”, MS [398, 400, 409, 401, 469]); (ii) the correlation $M_g - SFR$ correlation between (the so-called “Schmidt-Kennicutt”, SK, relation; [80, 470, 471, 472] that has already been discussed in previous sections.

Before leaving the subject of the mass-metallicity relation in galaxies, we would like to briefly touch upon the companion, long debated subject of the age-metallicity relation for the stellar population. Age, metallicity, stellar mass are indeed the key parameters to play with to reconstruct the past history of formation and evolution of galaxies of any type. Unfortunately, the optical colors of old populations are affected by the age-metallicity degeneracy [473, 474, 475]: it implies that the spectro-photometric properties of an unresolved stellar population can not be distinguished from those of another population three times older and with half the metal content (the so-called 3/2 degeneracy, i.e. in the space color(s)-age the axis are not each orthogonal). Many efforts have been made over the past twenty years to break the degeneracy. Worthey et al. [473] analysing some optical features of the spectrum built up the so-called Lick system of indices and found that if on one side the indices decrease the age degeneracy, on the other side the age degeneracy is still there. The Lick system has been improved [476, 477, 478], other features have been added e.g. the CaII IR triplet of [479, 480], other high resolution features have been introduced [481]. Spectral windows, in particular the mid-UV, seem to be more promising [482, 483, 484]. The overall results indicate that the UV indeed helps to better constrain the age of unresolved systems (as would be expected since the MS turn-off are much more sensitive to age than the red giant branch), but the determination of chemical composition is still better determined by the more sensitive optical features. Li et al. [485] to bypass the difficulty suggested the PCA method based on a large number of indices. The problem became even more complicated by recognizing that another parameter played an important role. i.e. the so-called α -enhancement measured by the ratio $[\alpha/Fe]$, where α is the abundance of elements like C, O Mg, Ti etc. [see 486, 487, 488, 489, 490, for a thorough discussion]. The enhancement factor adds another degree of freedom to the age-metallicity degeneracy that now becomes the age-metallicity-enhancement degeneracy. The new degeneracy has size comparable to the old one. The whole issue is still open, [see 382, for a recent review]. Despite the large uncertainties, the broad band color and line indices technique has been largely used to infer the age, metallicity and degree of *alpha*-enhancement in galaxies of different morphological type. In relation to ETGs, the most massive objects of the galaxy population and the expectation from the classical hierarchical view of galaxy formation, Jimenez et al. [491] analysed the spectra of a larger number of ETGs from the SDSS to infer the ages, metallicities and star formation histories and found clear evidence of “downsizing”, i.e. galaxies with large velocity dispersion and hence mass have older stellar populations. Most of the ETGs seem to complete their stellar content at redshift $z > 2.5$, to increase their metallicity on a rather short time scale, and to possess subsolar $[\alpha/Fe]$ ratios. This finding cannot be easily

reconciled with the hierarchical scenario while it agrees with the early hierarchical models of Merlin et al. [227]. The issue is still open.

11 RELATIONSHIPS BETWEEN DM-HALO AND BM-GUEST GALAXY

11.1 The stellar-to-halo mass ratio

The previous sections have clearly demonstrated that the observed properties of galaxies are regulated by a complex series of physical effects tightly intertwined. Last but not least is the ratio between the stellar mass in a galaxy and its dark matter component M_s/M_D (and its inverse M_D/M_s). The ratio M_s/M_D is a quantity that ultimately affects the half-luminosity radius R_e of the stellar component of a galaxy, see Sect. 6.1. The analysis of the Illustris data and the theoretical galaxy models of [226, 239, 240, 241, 227, 225] led Chiosi et al. [36] to suggest that the ratio M_s/M_D depends on the total mass of the galaxy $M_T \simeq M_D$ and the redshift z_f at which the bulk of SF occurs. This is shown by Fig. 8 for the Illustris data. For low values of the redshift (say below 0.6), the ratio smoothly decreases with mass M_D (low mass galaxies are slightly more efficient in building their stellar content); the opposite occurs for higher redshifts, where M_s/M_D increases with M_D . Chiosi et al. [36] give the following analytical expression for the ratio M_s/M_D as function of M_D and z

$$\log \frac{M_s}{M_D} = [0.218 z - 0.101] \log M_D + [0.169 z - 2.227] \quad (28)$$

where the halo mass goes from $10^4 M_\odot$ to $10^{14} M_\odot$ and the redshift from 0 to 4. The ratios M_s/M_D predicted by eq. (28) are indicated by the small black dots of Fig. 8.

Other relationships for the inverse ratio $m = M_D/M_s$ can be found in the literature [see for instance 229, 492, 493]. For $M_D \geq 10^{11} M_\odot$ Fan et al. [229] propose the relation:

$$m = \frac{M_D}{M_s} = 25 \left(\frac{M_D}{10^{12}} \right)^{0.1} \left(\frac{1+z}{4} \right)^{-0.25} \quad (29)$$

from which one derives the ratio M_s/M_D shown in Fig. 8 by the red circles. In practice there is no dependence on redshift.

Notably, the curve of Fan et al. [229] agrees with the one derived by Chiosi et al. [36] using the Illustris models for values of the redshift smaller than about 1.6 (the slope is nearly identical). Shankar et al. [492, and references there in] presented a detailed analysis of the dependence of M_s on M_D . First, they claim that for $M_D < 10^{11} M_\odot$ the relation should be

$$m = \frac{M_D}{M_s} = C M_D^{-2/3} \quad (30)$$

with C a suitable proportionality constant to be determined. Assuming equality between the values of m derived with the two above relationships (at the transition mass $M_D \geq 10^{11} M_\odot$), the proportionality constant is $\log C = 9.044$. The ratios M_D/M_s resulting by eq.(30) are shown in Fig.8 with the dark golden circles. Note that the relation of [492] agrees with that of the Illustris models for redshifts in the range from 2 to 4.

It is also worth noting that the linear extrapolation of the Fan et al. [229] relationship (red circles) in Fig. 8 to lower masses and the linear extrapolation of the Shankar et al. [492] curve (dark golden circles) to

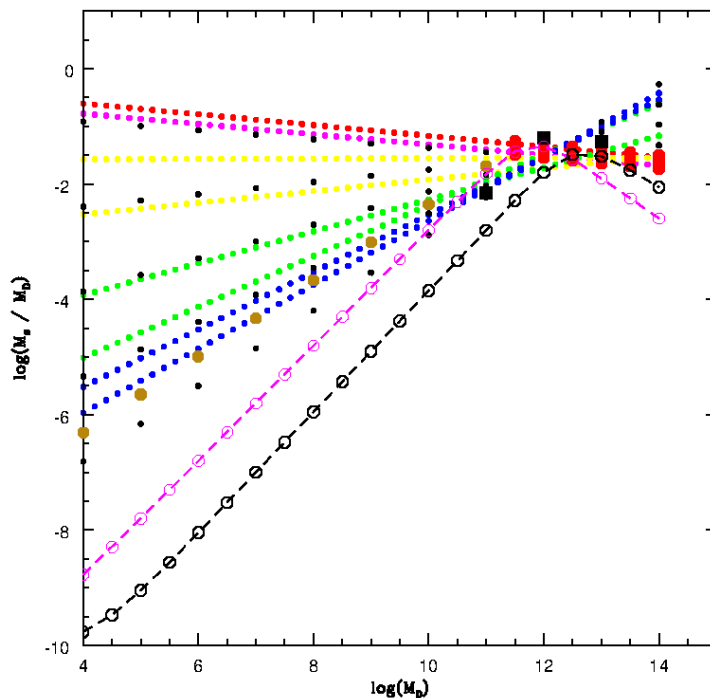


Figure 8. The relations between M_s/M_D and M_D at different redshifts for different theoretical models (all masses are in solar units). The colored dotted lines correspond to eight values of the redshift $z = 0$ and $z = 0.2$ (top, red), $z = 0.6$, $z = 1.0$ (intermediate, yellow), $z = 1.6$ and $z = 2.2$ (intermediate, green), $z = 3$ and $z = 4$ (bottom, blue). The black dots are the values resulting by eq. (28) at varying $\log M_D$ (from 4 to 14 in steps of 1) and redshift z (from 0 to 4 in steps of 1), respectively. The large red and golden circles are the combination of eq. (30) and eq. (29). The open magenta ($z = 0$) and dark-olive ($z = 3.95$) open circles are the relations M_s/M_D vs M_D at different redshifts according to Girelli et al. [493]. Note that all relations agree at $\log M_D \simeq 12$, while they badly disagree at lower values of M_D . Reproduced from Chiosi et al. [36].

higher values of the mass encompass the predictions derived from the Illustris models for all the values of the redshift.

Shankar et al. [492] derived a second analytical expression for the relation between M_s and M_D :

$$M_s = 2.3 \times 10^{10} M_\odot \frac{(M_D/3 \times 10^{11} M_\odot)^{3.1}}{1 + (M_D/3 \times 10^{11} M_\odot)^{2.2}} \quad (31)$$

for $M_D \geq 10^{11} M_\odot$. In this relation there is not an explicit dependence on the redshift. The ratios M_s/M_D predicted by eq.(31) are visible in Fig. 8 with the black filled squares. Eq. (31) predict ratios $m(M_D, z)$ that are in agreement with those from eq.(28) derived from the Illustris data, eq.(29) from Fan et al. [229], and eq.(30) only in the region around $\log(M_D) \simeq 12$ and $z \simeq 0$.

In a very recent study Girelli et al. [493] have thoroughly investigated the stellar-to-halo mass ratio of galaxies (M_s/M_D) in the mass interval $10^{11} < M_D < 10^{15}$ and redshifts from $z = 0$ to $z = 4$. They use a statistical approach to link the observed galaxy stellar mass function on the COSMOS field to the halo mass function from the Λ CDM-Dustgrain simulation and derive an empirical model to describe the variation of the stellar-to-halo mass ratio as a function of the redshift. Finally they provide analytical expressions

for the function $M_s(M_D, z)$. The relations M_s/M_D vs M_D as function of the redshift obtained with the formalism of Girelli et al. [493] are also shown in Fig. 8 (the magenta and dark-olive-green open circles joined by dashed lines of the same color). See also for a similar analysis the study of Engler et al. [494].

It is soon evident that while all studies agree on the M_s/M_D ratios for objects with halo mass in the interval $11.5 \leq \log M_D \leq 12.5$ nearly independently of the redshift, they badly disagree each other going to lower values of the halo mass. Furthermore, they also disagree with the theoretical results predicted by Illustris. The problem is open to future investigations.

11.2 Redshift evolution of DM-halos and their BM-guests

When galaxy formation started DM and BM were in cosmological proportions (i.e. $M_D = \omega M_B$ with $\omega \simeq 6$). Then the SF gradually stored more and more BM into stars.

Here, exploiting again the Illustris library of model galaxies [81] we show the relationships between the stellar mass M_s (as a proxy of the BM component) and the dark mass M_D , and that between R_e and R_D for four different values of the redshift ($z = 4, 2, 1$, and 0). They are visible in the left and right panels of Fig. 9, respectively. Masses (in M_\odot) and radii (kpc) are in log units and the color code indicates the redshift ($z = 4$, blue; $z = 2$, green; $z = 1$, yellow; $z = 0$, red).

It is clear that the efficiency of SF over the Hubble time, i.e. the transformation of gas in stars, is different in galaxies of different masses. Since $M_B < M_D$, M_s is always smaller than M_D . However, galaxies of different total mass can build stars at different efficiencies, and the ratio M_s/M_D is therefore expected to vary with M_D and redshift. In the left panel of Fig. 9, we note that M_s increases with M_D , so that low mass galaxies build up less stars than the more massive ones. The slope of the relation however decreases as the redshift goes to zero. In more detail, for redshifts $z \gtrsim 2$ and masses $M_D \simeq 10^{12} M_\odot$ the slope decreases at decreasing redshift so that more and more stars are present at given M_D . More precisely, for $z \lesssim 2$ and $M_D \leq 10^{12} M_\odot$ the above trend holds, but above this limit the opposite occurs, at a given M_D less stellar mass is present than expected. In other words, massive galaxies are less efficient builders of their stellar content. We can approximate this relation between $\log M_s$ and $\log M_D$ with the linear dependence $\log M_s = \alpha \log M_D + \beta$, where α and β may vary with the mass range and the redshift. From the linear fit we obtain: ($z=4$, $\alpha = 1.55$, $\beta = -8.19$), ($z=2$, $\alpha = 1.44$, $\beta = -6.78$), ($z=1$, $\alpha = 1.16$, $\beta = -3.37$, for $M_D < 12.0$), ($z=1$, $\alpha = 0.76$, $\beta = -2.30$, for $M_D > 12.0$), ($z=0$, $\alpha = 0.93$, $\beta = -0.43$, for $M_D < 11.5$), and ($z=0$, $\alpha = 0.79$, $\beta = -1.22$, for $M_D > 11.5$). The ratio M_s/M_D varies from 0.2 to 0.05 when the mass M_D increases from 10^7 to $10^{12} M_\odot$ with mean value $\simeq 0.10$. The overall process of star formation is not highly efficient, large amounts of gas remain unused and likely expelled into the external medium through galactic winds partially enriched in metals. Similar results are given by Merlin et al. [227, and references]. The efficiency of star formation is customarily measured by the ratio M_D/M_s as a function of M_D . This is simply given by:

$$\frac{M_D}{M_s} = 10^{-\beta} M_D^{1-\alpha} \quad (32)$$

that has already been discussed in sect. 11.

Similarly we can derive the relations: $\log R_e = \gamma \log R_D + \eta$ ($R_e = \eta R_D^\gamma$) that are shown in the right panel of Fig. 9. From the linear fit we obtain: ($z = 4$, $\gamma = 0.39$, $\eta = -8.19$), ($z = 2$, $\gamma = 0.30$, $\eta = -6.78$), ($z = 1$, $\gamma = 0.22$, $\eta = -3.37$, for $M_D < 12.0$), ($z = 1$, $\gamma = 0.22$, $\eta = -2.30$, for $M_D > 12.0$), ($z = 0$, $\gamma = 0.29$, $\eta = -0.43$, for $M_D < 11.5$), and ($z = 0$, $\gamma = 0.29$, $\eta = -1.22$, for $M_D > 11.0$).

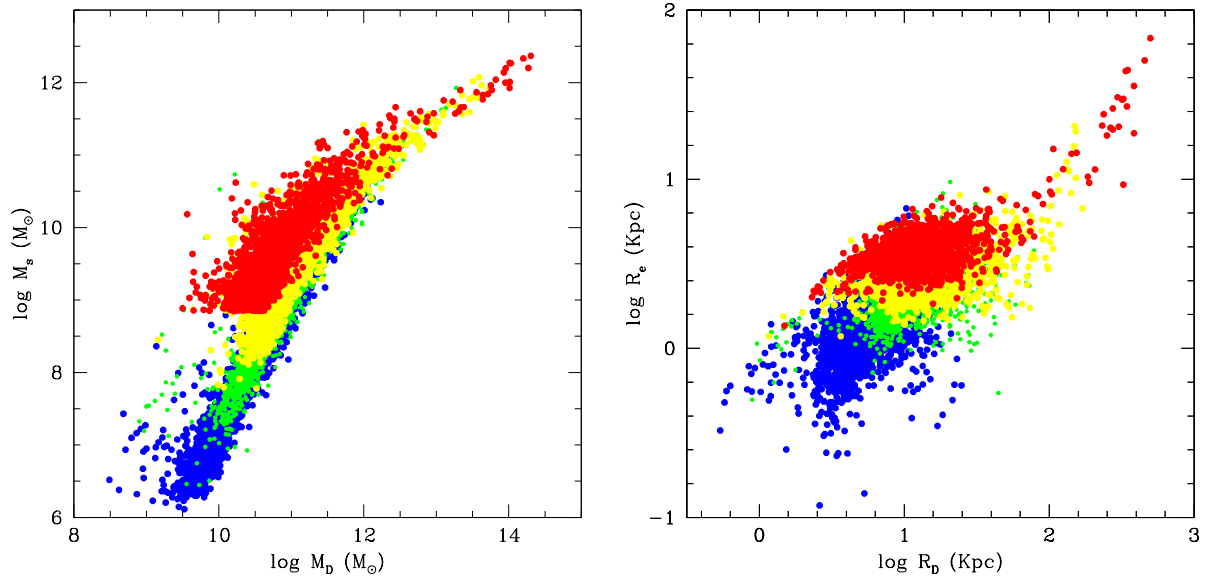


Figure 9. Left Panel: The $M_s - M_D$ relations at different redshifts ($z = 4$, blue; $z = 2$, green; $z = 1$, yellow; $z = 0$, red). Masses are in solar units. The solid lines are the best fits discussed in the text. Right Panel: the same as in the left panel but for the $R_e - R_D$ relations. Radii are in kpc.

The radius R_D is larger than R_e by a factor of 3 to 10 as the galaxy mass increases from $10^9 M_\odot$ to $10^{13} M_\odot$. The slope γ of the $R_e - R_D$ relation (in log units) first decreases by about a factor of 2, from $z = 4$ to $z = 1$, and then increases again at $z = 0$. What is important is that while at high redshifts (our $z = 4$, $z = 2$ and $z = 1$ cases) the galaxy distribution on the $R_e - R_D$ plane is a random cloud of points, at $z = 0$ a regular trend appears and R_e increases with R_D on the side of large values of R_D (largest masses). However, in the region of low radii and masses a cloud of points is still visible. The reason must be attributed to the effect of strong galactic winds and mergers among galaxies of similar mass in the hierarchical process that strongly perturb the mechanical equilibrium of these systems [see 36]. Finally, note that the ratios $M_s/M_D \simeq 0.1$ and $R_e/R_D \simeq 0.1 - 0.3$ confirm the predictions of Bertin et al. [495], Saglia et al. [496] based on analytical models for galaxies made of DM and BM.

12 THE ANGULAR MOMENTUM - MASS CORRELATION

We now turn back our attention again to the correlations observed among galaxies. First we want to explore the correlation between angular momentum J and mass M that is one of the most fundamental SRs of galaxies. It is at least as important as the SRs between rotation velocity, velocity dispersion, characteristic size, and mass. The correlation between angular momentum and mass largely determines another basic property of galaxies, i.e. the characteristic size (e.g. the half-mass radius R_h) of disk-dominated galaxies.

Operationally one defines the stellar specific angular momentum $j^* = J/M_s$ (the angular momentum per unit mass), the stellar mass M_s , and the bulge fraction $\beta^* = M_b^*/(M_d^* + M_b^*)$, where M_d and M_b are the mass of the disk and the bulge respectively. In a plot of $\log j^*$ against $\log M_s$ galaxies of different morphological types and bulge fraction β^* follow nearly parallel sequences. Over the mass range $8.9 \leq \log(M_s/M_\odot) \leq 11.8$ disks and bulges follow SRs of the form $j^* \propto M^\alpha$ with $\alpha = 0.67 \pm 0.07$. The different sequences have a maximum offset in zero-point by a factor of 8 ± 2 [497].

A similar result was obtained by Obreschkow and Glazebrook [41], who discovered a strong correlation between the baryon mass M_b , j_b , and the bulge mass fraction β , fitted by $\beta = -(0.34 \pm$

$0.03) \log(j_b M_b^{-1} / [10^{-7} \text{ kpc km s}^{-1} M_\odot^{-1}]) - (0.04 \pm 0.01)$ over a range of $0 \leq \beta \leq 0.3$ and $10^9 M_\odot < M_b < 10^{11} M_\odot$. This $M - j - \beta$ relation likely originate from the proportionality between $j M^{-1}$ and the surface density of disks.

The above picture seems to indicate that disks and spheroids are independent structures, formed by distinct physical processes: disks are likely formed by diffuse gas settling down on a flat surface within DM halos, while spheroids formed more violently by merging and collisions of cold gas clumps. In this scenario, disk-dominated galaxies are not affected by major mergers, while spheroid-dominated galaxies have properties substantially linked to stripping and merging. The interesting thing is that this relation offers a natural explanation of several classical SRs, such as the FP of spiral galaxies, the TF relation, and the MR relation. It can also be the basis for an objective classification scheme alternative to the Hubble sequence.

In CDM models, galaxies get their angular momentum in the initial phases of density perturbation growth, when the collapsing DM clouds are tidally torqued by neighboring overdensities [498, 61, 499, 500]. The classical theory of disk galaxy formation [501, 502, 503, 104] predicts that gas acquires nearly the same specific angular momentum of the host DM halo. This angular momentum sets the disk size, and largely determines the final morphology [62, 40]. The baryons increase their rotational support by falling into the potential wells of the DM halos conserving their angular momentum. To what extent the baryons preserve the angular momentum during this process is one of the key issues in our understanding of disk galaxy formation.

The angular momentum of the DM halos is often expressed with the dimensionless spin parameter $\lambda = j / \sqrt{2} R_{vir} V_{vir}$, where R_{vir} and V_{vir} are the virial radius and virial velocity of the halo, and j the specific angular momentum inside R_{vir} [126]. The spin parameter of DM within R_{vir} is found to have log-normal distribution with a median $\lambda \sim 0.04$ and rms variance of $\sigma \ln \lambda \sim 0.55$ [126, 504, 505], while BM seems to have a spin higher than the halo's average [213, 506, 507, 508, 509, 510, 511, 512]. In a set of zoom-in simulations Danovich et al. [512] have shown that λ of the cold gas grows when crossing the virial radius (see also [213]).

From the side of numerical simulations we should highlight the long suffered problem of the “angular momentum catastrophe” [513, 86]. The problem emerged from the comparison with observations of disk galaxies. While the observed disks have shown a specific angular momentum j lower by a factor of two, modelled disks appear to have radial scale-lengths smaller by a factor of 10, resembling bulges rather than disks [86]. In the last years however, simulations seem to have solved the problem by inserting an efficient stellar feedback [514, 515, 516]. For example, [517], but see also [518, 511, 519] found that supernova feedback can selectively remove low angular momentum gas via outflows, leading to disk formation more in line with observations.

In a recent paper Peng and Renzini [520] argued that the stellar angular momentum of galaxies increased by a large factor over the last ~ 10 Gyr (i.e. $z \sim 2$), starting from an epoch when the majority of galaxies acquired their ordered rotation. The size of J follows directly from the SRs of spiral galaxies, i.e. from the connection:

$$J \propto M^* R_e V_{rot} \quad (33)$$

between stellar mass, effective radius and rotational velocity. This behavior could be driven by the baryonic gas vorticity of the circum-galactic filaments that might drive the galaxy evolution. In this

framework, the gas in the filaments regulate the fluctuations in the specific SFR of galaxies, offering an explanation for the existence of the main sequence [416].

For what concern the angular momentum of galaxies at high redshift, we refer to the paper of Burkert et al. [521]. This work analyze a sample of ~ 360 massive star-forming galaxies at $z \sim 0.8-2.6$. They found a J distribution broadly consistent with the theoretical prediction for the dark matter halos, either in terms of spin parameter $\langle \lambda \rangle \sim 0.037$ and its dispersion ($\sigma_{\log \lambda} \sim 0.2$). These data support the hypothesis that on average, at high redshifts, the specific angular momentum of spirals is the same of dark matter halos ($j_d = j_{DM}$). Including the molecular gas, these authors measured a total BM to DM mass ratio of $\sim 5\%$ for halos of $\sim 10^{12} M_\odot$, which corresponds to $\sim 31\%$ of the available baryons. This means that high- z disks are strongly baryon dominated.

13 THE SCALING RELATIONS OF BLACK-HOLES AND GALAXIES

Today the idea that the history of the massive black-holes (BHs) at the center of galaxies and that of galaxies themselves is strictly entwined is widely accepted, after the discovery that the BH mass correlates with various properties of the host galaxies [522, 523, 524], such as bulge mass M_{bulge} [67], total stellar mass M_s [68], velocity dispersion σ_* [69, 70], light concentration [71], and halo circular velocity [72]. The ensuing paradigm of BH and host bulge/spheroid co-evolution is today widely accepted and supported by these well-known correlation for quiescent and almost quiescent galaxies. Unfortunately, the physical nature of this connection is still obscure [525, 526] despite intense observational efforts.

For galaxies whose nuclei are currently active, there are basic observational issues that remain open at the time of writing. The necessity to resort to type-1 AGN for studying the $M_{\text{BH}} - \sigma_*$ or M_{BH} and M_{bulge} ⁵ relations outside of the local Universe raises two overarching questions. The first one is whether the M_{BH} -bulge relations are observationally consistent with the one obtained for quiescent galaxies at very low redshift. A related issue is about the selection effects specific to the M_{BH} -bulge relation for type-1 AGN with respect to the one of non-active galaxies. The second question is whether there is a significant evolution of the M_{BH} -bulge relation with cosmic epoch.

Some general considerations are in order, before focusing on the analysis of the scaling relations and on the two main questions above. The most accurate black hole mass determinations are the ones that probe the truly central regions of a galaxy, where the gravity of the black hole is the dominant force. This occurs within a distance from the BH $r_h = GM_{\text{BH}}/(\sigma_*)^2 \approx 43 M_{\text{BH},8} \sigma_{*,100}^2$ pc, where M_{BH} is in units of 10^8 solar masses, and the σ_* of 100 km s^{-1} . The BH sphere of influence has been resolved in several nearby galaxies, presumably hosting the most massive BHs that were shining at $z \approx 2$, where the most luminous quasars are observed [527]. In the local Universe, these galaxies mostly appear as spent or almost-spent active nuclei [e.g., 527, 528]. As long as a galaxy has a central black hole, there is no such a thing as a quiescent galaxy: some nuclear activity occurs, even if at extreme low level, and detected only in the nearest cases (i.e., Sagittarius A) and under particular circumstances. We consider here weakly active sources whose Eddington ratio is too low to enter into the domain of radiative efficient accretion mode (a typical example could be M87).

13.1 Massive black holes at the center of quiescent (or weakly active) galaxies

The method employed for modelling stellar system in dynamical equilibrium is that of orbit superposition [529]. The gravitational potential is defined as the sum of the central black hole (assumed a central point whose mass is to be determined) and of the stellar mass density derived from the stellar mass-to-light ratio.

⁵ It is yet unclear which of the two relation is the most fundamental, albeit the relation σ_* with M_{BH} has been considered as the primary one in several past works. The two relations will be considered as interchangeable when the M_{BH} - bulge relation is mentioned in a generic context.

What is computed is the combination of orbits compatible with the spatially resolved stellar kinematics and photometric profiles. For the kinematically hot galaxies the early way to get the BH mass was based on the fit of the line-of-sight velocity dispersion of spherical galaxies assuming that the stellar distribution function is isotropic [530]. In more modern approaches, the fit is made over the entire line-of-sight velocity distribution [531, 532] for arbitrary galaxy models whose gravitational potential includes the effect of dark matter, and of triaxiality [533, 534]. The most general and accurate possible models, with the highest resolution of spectroscopic observations are reputed to be most accurate [523], provided that the BH sphere of influence is adequately resolved. A case in point is the estimate of the black hole mass in M87: early estimates yielded a mass $\sim 5 \times 10^9 M_\odot$ from spherical, isotropic models Young et al. [530]. More recent analyses based on stellar dynamics yielded M_{BH} in the range $\approx (6. - 6.5) \cdot 10^9 M_\odot$ [533, 535]. The stellar dynamics mass value has been spectacularly confirmed by the Event Horizon Telescopes observations that yielded $M_{\text{BH}} \approx 6.5 \pm 0.2|_{\text{stat}} \pm 0.7|_{\text{sys}} \cdot 10^9 M_\odot$ from the inference of the angular size of the black hole gravitational radius [536].

One of the most promising developments in the last years has been the increasing number of dynamical mass estimates obtained with ALMA [e.g., 537, 538, for mildly active and quiescent galaxies]. ALMA has the capability to resolve cold molecular gas kinematics on angular scales well below 1 arcsec. [539]. This is becoming instrumental to high-precision measurements of black hole masses in the “intermediate” mass domain, a previously uncharted territory. For instance, sub-parsec resolution ALMA observations revealed a black hole with mass $\sim 5 \cdot 10^5 M_\odot$ in the dwarf galaxy NGC404 [540].

Space-based long-slit spectra of optical emission lines yield a velocity cusp [541]. A striking example is provided by the radial velocity curve of NGC4374 [542]: the STIS spectra show a Keplerian swing beginning at ± 0.5 arcsec and culminating at ± 0.1 arcsec, with a radial velocity difference of $\delta v_r \approx 400 \text{ km s}^{-1}$, implying an $M_{\text{BH}} \approx (1.5_{-0.6}^{+1.1}) \cdot 10^9 M_\odot$. The main concern is that gas motions could be affected by radiation forces, shocks, turbulence, and magnetic fields, and not only by gravitation. Relatively few galaxies have been found to have regular disk-like profile suggestive of a velocity field dominated by Keplerian motion in a dynamically cold disk [523]. In addition, the Keplerian assumption is not consistent with gas flow toward low-accretion-rate SMBHs and at variance with observations of the Galactic Center [543]. For M87, both an early and a more recent analysis based on HST data suggest a black hole mass of $\approx (3 - 3.5) \cdot 10^9 M_\odot$ [544, 541, 545], and very close to the value obtained by modeling the jet boundary shape [546], but always at variance with the values obtained from stellar dynamics (Section 13.1).

13.2 Relations M_{BH} vs M_{bulge} and σ_* for quiescent galaxies

As mentioned earlier, the correlation between M_{BH} and host galaxy bulge properties – M_{bulge} and σ_* or even bulge luminosity – is now an established fact since more than 20 years [see e.g. 67, 69, 70]. Widely used forms of the relation between M_{BH} and σ_* based on sources for which there is a dynamical M_{BH} determination are the ones of McConnell et al. [547] and of Kormendy and Ho [523] for early-type galaxies. Kormendy and Ho [523] derived a power law:

$$\log(M_{\text{BH}}) \approx 8.491 \pm 0.049 + (4.384 \pm 0.287) \log \sigma_{*,200}, \quad (34)$$

where the mass is in solar units and σ_* is units of 200 km s^{-1} . For both early type and spiral galaxies McConnell and Ma [548] yield a significantly steeper slope $\gtrsim 5$, with a lower intercept for spiral galaxies, implying that M_{BH} in ETGs is about a factor 2 higher than in LTGs at a given σ_* [548]. Equivalent relations (i.e., with similar scatter, around 0.30 dex) have been defined with the bulge mass, and infrared

luminosity, usually suggesting a power-law relation between M_{BH} and M_{bulge} with an exponent ≈ 1 or larger [548, 523, 549].

There is still much ongoing research considering the linearity of the relation, its slope, and the origin of its dispersion. Theories that connect galaxy evolution and black hole growth predict the existence of a second parameter which may account for the dispersion in the $M_{\text{BH}} - \sigma_*$ correlation. Black hole - spheroid coevolution models would require that the BH mass scales with the gravitational binding energy of the spheroid host, $\sim M_{\text{bulge}}/r$ [550]. The correlation can be easily turned into bivariate relations $M_{\text{BH}} \propto M_{\text{BH}}^{0.6} \sigma_*^{1.2}$ and $\propto r_{\text{bulge}}^{0.6} \sigma_*^{2.4}$ that imply correlations between M_{BH} and σ_* and M_{bulge} consistent with the observed ones [272]. A correlation with the binding energy of the host galaxy [551, 552] implies the presence of a second parameter that may compensate for the changes in the galaxy structural parameters occurring at fixed M_{BH} . Saglia et al. [272] found significant bivariate correlations consistent with a connection between M_{BH} and binding energy and with bulge kinetic energy, although the scatter remains comparable to the one for the $M_{\text{BH}} - \sigma_*$ correlations obtained with the best dataset of M_{BH} dynamical mass measurements.

The $\log(M_{\text{BH}}) - \log(M_{s,\text{sph}})$ relation reported by [67, 553, 35, 554, 555, 68] is almost linear, but the inclusion of low-mass spheroids revealed departures from linearity. Laor [556, 557], Wandel [558] and Ryan et al. [559] obtained a much steeper power law with a slope of 1.53 ± 0.14 . The mean $M_{\text{BH}}/M_{s,\text{sph}}$ ratio is probably not a universal constant, as it drops from $\sim 0.5\%$ in bright ($M_V \sim -22$) ellipticals to $\sim 0.05\%$ in low-luminosity ($M_V \sim -18$) bulges. Salucci et al. [560] claimed that the $M_{\text{BH}} - M_{s,\text{sph}}$ relation is significantly steeper for spiral galaxies than for (massive) elliptical galaxies. Graham [561] suggested that the relation between luminosity (L) and stellar velocity dispersion (σ) for low-luminous ETGs is inconsistent with the $M_{\text{BH}} - L$ and $M_{\text{BH}} - \sigma$ relations. They prefer a broken $M_{\text{BH}} - M_{s,\text{sph}}$ power-law relation, with a near-linear slope at the high-masses and a near-quadratic slope at the low-masses. In a recent review article Graham [524] analyzed the consequences of this steeper relation, that can be rich of implications for the theories of galaxy–BH coevolution. Scott et al. [562], Graham and Scott [563] offered an interpretation for the curvature of the $M_{\text{BH}} - M_{s,\text{sph}}$ relation invoking the presence of core-Sérsic and Sérsic spheroids at the high- and low-mass ends of the distribution respectively.

The highest degree of correlation is obtained for ETGs and for bulges that follow a Sérsic - surface brightness profiles. Galaxies obeying a Sérsic photometric profile down to the resolution limits of their surface brightness profiles are believed to be the product of wet mergers, i.e., merger of gas rich galaxies that provide material to sustain accretion on the central black hole and trigger a period of sustained nuclear activity. The ensuing feedback effects (both radiative and mechanical) on the host, due to the active nucleus and to the merger-induced star formation, make it possible to couple the growth of the central black hole to the host spheroid mass [564, 565]: the feedback forces by the quasar expel so much gas to quench both star formation and stop black hole growth, ultimately accounting for the relation between M_{BH} and σ_* , and M_{BH} and M_{bulge} [566, 567].

However, the most massive elliptical galaxies often exhibit surface brightness profiles that are flatter than the extrapolation of Sérsic-like profiles. Sources showing a deficit with respect to the Sérsic profile are contributing to the scatter in the $M_{\text{BH}} - M_{\text{bulge}}$ relation [568]. Core profiles are believed to be due to dissipationless mergers of galaxies that have central black holes. N-body simulations show that merging of two galaxies with a sharp cusp may results in a merger remnant with a shallower core [569, 570, 571]. The formation of a core has been ultimately linked to a bound binary black hole system, which produces a depletion of the stellar component in the nucleus due to slingshot ejection of stars on nearly-radial orbits.

The size of the core and the starlight and mass deficits in the centers of core galaxies (i.e., the mass ejected by the binary) have been found to scale approximately with the mass of the central black hole [572, 523], in agreement with theory that predicts a mass deficit [573] to be $0.5 n M_{\text{BH}}$, with n as the number of major merger events. The luminosity deficit correlation provides an independent way to estimate M_{BH} in core ellipticals. Core radius is most strongly correlated with the black hole mass and correlates better with total galaxy luminosity than it does with velocity dispersion [574]. In addition, core scouring changes the orbit distribution. Only radial orbits allow for close passage past the galaxy center and thus only those stars can reach the vicinity of the central binary black hole. Consequently, the orbital structure in the core after core scouring is predicted to be strongly biased in favor of tangential orbits, while the ejected stars contribute to enhanced radial motions outside the core [575, 569]. For example, the orbital structure of the S0 NGC524 shows tangential anisotropy right at the SMBH radius of influence, corresponding to the core region in the photometric profile [576]. Similar results apply to the elliptical galaxy NGC1600 [577], and agree well with predictions from numerical simulations where core profiles are the result of SMBH binaries impoverishing the central nuclear regions [578].

Recent work emphasizes the presence of substructures in the $M_{\text{BH}} - \sigma_*$ relation [579]. Pseudo-bulges are associated with spiral galaxies, and studies of their photometric profiles reveal that they are disk-like with a different surface brightness profile than classical bulges [580, 581]. Pseudo-bulges are known to be offset in the $M_{\text{BH}} - \sigma_*$ relation in the sense of systematically lower M_{BH} [272]. In the case of pseudo-bulges, the growth of the central black hole may be decoupled from the growth of the host spheroid and not associated with galaxy merger, but instead with mechanisms of secular evolution not related to gravitational interaction with other galaxies; in observational terms, some studies [523] find weak M_{BH} correlations for pseudo-bulges, see, however, e.g., [549].

The most massive BHs have been detected only in the more luminous galaxies ($-22 \leq M_B \leq -18$) [522] and it is not clear yet if fainter and less massive systems host massive BHs and whether they follow the extrapolations of the SRs defined by the brightest objects. Searches for BHs in less luminous galaxies of the Local Group have produced ambiguous results, as in the case of M33 [582, 583], NGC205 [584], and M32 [585]. Some galaxies exhibit a compact stellar nucleus (with half-light radius $r_h \sim 2 - 4$ pc) in their center. This is ~ 20 times brighter than a typical globular cluster [586, 587]. In the Virgo and Fornax Clusters $\sim 25\%$ of dE galaxies contain such nuclei [588, 589, 590], but the observations with the Hubble Space Telescope revealed that these structures are far more common: about 50-80% of the less luminous galaxies contain a distinct nuclear star cluster [591, 592, 593, 594, 164, 595, 596, 597]. Nuclear star clusters are not a replacement for black holes. On the contrary low mass galaxies ($10^9 - 10^{10} M_\odot$) show a high incidence of nuclear star clusters coexisting with massive black holes [598]. However, nuclear star clusters are rare in high mass galaxies [599], suggesting that the growth of BH during activity may lead to the demise of the star cluster itself [600].

The low mass end of the relation $M_{\text{BH}} - \sigma_*$ for quiescent galaxies is still poorly sampled and of uncertain interpretation [601]. Tidal disruption events (TDEs) provide an independent methods for M_{BH} estimation. First, TDEs are luminous flares predominantly detected in quiescent galaxies (very few events have been detected in AGN, as the luminosity of the AGN obliterates the brightness increase associated with the TDE). Flares are produced by the tidal debris that fall back toward the black hole and that form an accretion ring or a disk around an otherwise inactive black hole. Second, a TDE can take only with relatively low black hole masses, $M_{\text{BH}} \lesssim 10^8 M_\odot$ for a solar-mass star [602] to avoid that the star crosses the black hole event horizon without being tidally disrupted. The central BH mass is recovered via synthetic multi-band optical light curves based on hydrodynamical simulations of polytropic tidally disrupted stars [603]. The

method is not yielding yet a good agreement with other M_{BH} estimates, as it is not clear which parameter should be correlated with M_{BH} , in a model in which the TDE luminosity is powered by fall-back accretion [602].

13.3 M_{BH} measurements in AGN

Stellar dynamical determinations for AGN has been possible only for weakly or mildly active Seyfert 1 galaxies. Presently, only $\lesssim 100$ dynamical M_{BH} measurements have been obtained by modeling stellar kinematics of quiescent and active nuclei [e.g., 523, 272]. A case in point is the intermediate Seyfert 1 galaxy NGC3327 [604] which illustrates the complexity of the nuclear regions of a mildly active AGN, even if an application of the Schwarzschild method of orbit superposition allowed for a meaningful estimate of the stellar dynamic mass $\sim 10^7 M_{\odot}$. A Population B source (see §14.2 and Fig. 12) radiating at modest Eddington ratio, NGC3227 shows a nuclear stellar distribution within a few parsecs of the central black hole affected by intense bursts of star formation occurring in its recent past. Similar considerations apply to the stellar dynamics results on MCG–6-30-15 [605]. In general, stellar populations in the closeness of the active nucleus are not easy to model, also because of the uncertain distribution of obscuring dust, even in the least active nuclei, such as NGC4258. Nonetheless the stellar dynamical and maser masses agree very well for this source [606]. A dynamical mass estimate for Cen A also agrees with the estimate derived from cold molecular H_2 gas [607, 280], suggesting that molecular gas could provide mass estimations as accurate as the ones based on stellar dynamics.

The most reliable method to probe distances within r_{h} from the black hole of galactic nuclei that are currently mildly active involves observation of H_2O masers [608, 609, 610]. The H_2O emission profile shows a radial velocity “cusp” at distances where the velocity field is governed by gravity of the black hole i.e., when $r \lesssim r_{\text{h}}$. This method is not exempt by issues that could bias the results. A maser disk with Keplerian rotation could have a non-negligible disk mass comparable to the black hole mass [611], and the effects of disk self-gravity might lead to large systematic errors in the derivation of the black hole mass [612]. Disturbed morphology and kinematics are an ubiquitous feature of maser systems especially above Eddington ratio $\lambda_{\text{Edd}} \gtrsim 0.1$ [613].

Outside of the local Universe (i.e., beyond 2.5 Mpc), VLBI observations of *mega-maser* systems can probe within the sphere of influence for BHs down to $10^6 M_{\odot}$ even at 100 Mpc [614]. *Mega-masers* are more frequently associated with active galaxies [615], and they should be more common at high redshift [614]. The exploitation of *mega-masers* is however difficult, because the maser signal of high-redshift sources is lost in noise, and major surveys have until now failed to detect a *mega-maser* in the wide majority of galaxies. Mass determinations based on the resolved maser systems are completely independent from any other method, and best suited to cross-check the estimates obtained from stellar and gas dynamics. Several H_2O masers have been detected from the circumnuclear regions of quasars also at relatively high redshift [616, 617]. The hope to go beyond modest distances rests with SKA — because of its unprecedented μJy sensitivity — and in future space based radio interferometry with μarcsec spatial resolution. Assuming Earth-space baselines of about 30,000 km, angular resolution of $2 \mu\text{-arcsec}$ would be achievable at 8 GHz [618]. This angular scale corresponds to a projected linear size of $\approx 0.02 \text{ pc}$ at $z = 2$, therefore allowing to probe within the BH sphere of influence even at the remote epochs of the “cosmic noon,” a key epoch of galaxies AGN when a population of most luminous quasars was shining bright and producing the maximum feedback on their host galaxies.

ALMA is today the most powerful tool to yield M_{BH} also for AGN [e.g., 619]. However, the CO J = 2-1 kinematics in a sample of nearby AGN reveals non circular motions in the inner kiloparsec of all

galaxies in the sample, although molecular gas and stellar kinematics show an overall agreement. The CO observations of nearby radio galaxies detect molecular disks, but also cautions about the possibility of asymmetries and disruptions due to interactions with the radio jet [620].

Several studies have employed the capabilities of STIS on board HST to study the dynamics of line emitting gas in proximity of the central black hole [621], or the sub-arcsec spatial resolution of imaging spectrometers or IFU units operating with adaptive optics [622]. The concern is that radiation forces within the inner 100 - 1000 pc of the central black hole may be affecting the dynamics of the line emitting gas even more than in the case of cold gas dynamics, especially if the AGN is radiating at high Eddington ratio [623, 624, 625, 626, 627].

Spectro-astrometry is another promising tool: the approach is based on the different photocenter position of emission lines at different velocity [628]. Whereas a relatively modest spectral resolution ($\sim 10 \text{ km s}^{-1}$) is sufficient, sub-arcsec spatial resolution is required, obviously the higher the better, achievable only from space or from ground using active optics [629]. This is the approach exploited by GRAVITY, an instrument of the Very Large Telescope Interferometer (VLTI) [630]. After first light in 2017, GRAVITY detected a spatial offset (with a resolution of 10 micro-arcseconds corresponding to about 0.03 parsecs) between the red and blue centres of the Paschen- α line of 3C273 [631]. This offset corresponds to a gradient in velocity and implies that the gas is orbiting the central supermassive BH. With the new capabilities of GRAVITY [632] and with the wave-front corrections of an adaptive optics system, it will be possible to repeat this feat in many low- z type-1 (i.e., broad line) AGN [633]. The broad line region velocity field has been spatially resolved and modelled even in NGC3783 [634] to provide an M_{BH} estimate, although this achievement will likely remain restricted to low- z Seyfert-1 nuclei for the time being.

If we exclude masers, for which BH masses can be inferred from rotation [522] and spectro-astrometry, for the vast majority of Type-1 AGN the BH masses are derived from the (presumed) virial motions of the broad line region (BLR) gas clouds orbiting in the vicinity of the central compact object. If the motion in the emitting gas is in virial equilibrium, we can write the central black hole mass M_{BH} as:

$$M_{\text{BH}} = \frac{r_{\text{BLR}} \delta v_{\text{K}}^2}{G}. \quad (35)$$

Here δv_{K} is the virial velocity module, r_{BLR} the radius of the BLR, G the gravitational constant. Eq. 35 can be useful if we can relate δv_{K} to the observed velocity dispersion, represented here either by the dispersion σ or by the FWHM of a suitable broad emission line:

$$M_{\text{BH}} = f_{\text{S}} \frac{r_{\text{BLR}} \text{FWHM}^2}{G} \quad (36)$$

via the structure factor (a.k.a. form or virial factor) whose definition is given by:

$$\delta v_{\text{K}}^2 = f_{\text{S}} \text{FWHM}^2. \quad (37)$$

Mildly ionized gas dynamics i.e., gas motions within the broad line regions of type-1 AGN, is the basis of the estimate of the M_{BH} for large samples of quasars up to the highest z , following Eq. 36. In addition to a measure of the virial broadening provided by the emission line width, a measure of the line emitting gas distance from the central black hole is needed. Under the assumption that the main source of line emission is provided by photoionization [635], the distance is measured by the time lag of the emission lines with

respect to continuum variations [636]: $r_{\text{BLR}} \approx c\tau$, where τ is the time delay. Recent observations measure τ as a function of wavelength across the line profile in an attempt to resolve the velocity field of the emitting region [637, 638]. The ”reverberation mapping” technique has been described in several reviews that also include a critical discussion of the technique shortcomings [639, 640, 641]. The r_{BLR} estimates have been carried out mainly for the HI Balmer line $H\beta$ for ~ 100 type-1 AGN, recently supplemented by the monitoring of the SDSS Reverberation Mapping Project that yielded data for 144 quasars [642]. The reverberation mapping determinations of r_{BLR} offer a sort of primary step over which a correlation between r_{BLR} and luminosity is built (Section 13.4), in turn instrumental to the determination of the M_{BH} in large samples of quasars (Sect. 13.5).

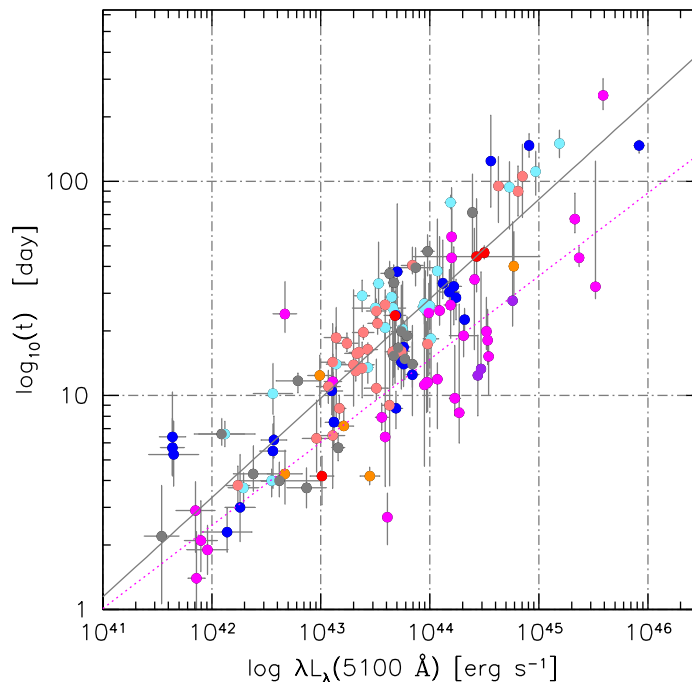


Figure 10. The radius-luminosity relation, expressed as the relation between the time lag derived from reverberation mapping and the optical luminosity. Data are from [643], and include, in addition to the sources of [644] also the xA sources monitored in dedicated campaigns [645, 646]. Sources are color coded according to the spectral types identified along the quasar main sequence: B1⁺⁺ (red), B1⁺ (orange), B1 (rose), B2 (grey), A1 (aquamarine), A2 (blue), A3 (magenta), A4 (purple), and roughly correspond to a sequence of increasing Eddington ratio. The grey line traces an unweighted least square fit for the full sample, the dotted magenta line refers to an unweighted lsq but for sources radiating at extreme Eddington ratios (A3 and A4) only.

13.4 The Radius - Luminosity relation

A correlation between radius of the emitting regions and continuum luminosity is expected on the basis of the spectral similarity of quasars. Even if this is an oversimplification, we observe always the same lines, and their relative intensities change only within a limited range, also in response to continuum variation. The ionization parameter should remain roughly constant, implying that $r \propto L^a$, with an exponent a at any rate close to 0.5 [647, 644]. The scaling relation has been derived from spectroscopic monitoring of emission lines (mostly the HI Balmer line $H\beta$) that yield the time delay τ of the emission line response

to continuum variations [636, 648]. A sufficient number of sources is available for a correlation analysis since the early 2000s [647]. The consideration of various aspects (host galaxy subtraction and removal of the line narrow component believed to be emitted in a different region) and the increase of the number of monitored sources has led to a standard $r - L$ relation with an exponent consistent with 0.5 within the uncertainties [649, 650, 651, 644]. However, the $r - L$ relation suffers of significant scatter because it was derived neglecting the diversity of type-1 quasars organized by the quasar Main Sequence (MS, see below), and is biased in favour of sources radiating at relatively low Eddington ratio. It is not difficult to account for this preferential selection: such sources are relatively low accretors and therefore more prone to variability associated with an unsteady accretion flow. Recent work [645, 643] has shown that sources that radiate at high L/L_{Edd} significantly deviate from the correlation of [644]: their radius is shorter than the one expected on the basis of their luminosity. Including high Eddington ratio sources in the correlation creates a cluster of data points that increases the scatter in the correlation. Fig. 10 shows that the relation for sources radiating at the highest value of the Eddington ratio is significantly offset from the one of other spectral type along the quasar main sequence discussed in Sect. 14.2. Linear combination with the dimensionless accretion rate (i.e., the mass accretion rate normalized by the Eddington accretion rate) or Eddington ratio leads to a significant reduction of the scatter [643, 652].

13.5 Scaling laws for AGN black hole mass estimates

The virial theorem can be conveniently rewritten as $\log M_{\text{BH}} = \alpha \log L + \beta \log \text{FWHM} + \gamma$, where $\beta = 2$. The luminosity term comes from the use of the radius — luminosity relation, $r - L^a$. Several different scaling laws based on this expression have been defined for the width of different lines, and for different continuum and line luminosity as well. The most widely used has been perhaps the one formulated by Vestergaard and Peterson [653] for $\text{H}\beta$ and continuum luminosity at 5100 Å.

The main underlying assumptions in the use of the virial theorem are that the broadening is due to Doppler effect because of the line emitting gas, and that the velocity field is such that the emitting gas remains gravitationally bound to the black hole. Early UV and optical inter-line shift analysis provided evidence that not all the line emitting gas is bound to the black hole [654, 655, 656, 657, 658]. The emerging scenario is that outflows are ubiquitous in AGN, they occur under a wide range of physical conditions, and are detected in almost every band of the electromagnetic spectrum and on a wide range of spatial scales, from few gravitational radii to tens of kpc (e.g., [659, 660, 661, 662, 663, 664, 665]).

For $z > 4$, M_{BH} estimates historically rely on the $\text{CIV}\lambda 1549$ high-ionization line, and the highest- z sources appear almost always high-accretors [666, 667]. The source of concern is that high-ionization lines such as $\text{CIV}\lambda 1549$ are subject to a considerable broadening and blueshifts associated with outflow motions already at low redshift [668, 669, 670, 671]. Overestimates of the virial broadening by a factor as large as 5 – 10 [672, 673, 674, 675] for SMBHs at high z may pose a spurious challenge to concordance cosmology [676] and lead to erroneous inferences on the properties of the seed BHs believed to be fledgling precursors of massive BHs. The solution is either to carry out $\text{H}\beta$ observations at high redshift (a feat that is becoming easier as more NIR spectrometers are being installed at the focus of large telescopes) or to use a surrogate line whose profile is also virially broadened. The $\text{AlIII}\lambda 1860$ and $\text{CIII}\lambda 1909$ lines could be much robust estimator of the BH mass. These lines, in a blend at 1900 Å, can be easily observed with optical spectrometers up to redshift $z \approx 4$. Similar considerations apply to the use of $\text{MgII}\lambda 2800$ [677, 678] which however can be observed only up to $z \approx 2.5$ without the use of NIR spectrometers. Another approach has been to apply corrections to the $\text{CIV}\lambda 1549$ line width [679, 680], although such corrections, to be effective, require the knowledge of the quasar rest frame, that remains poorly known from rest-frame UV observations only. Shen and Liu [678] propose scaling laws in which the virial assumption

is released that is, with $\beta \neq 2$. For CIV $\lambda 1549$, this means correcting for effect associated with the emission component due to an outflow, that overbroadens (and shifts) the line. The scaling law introduced by Park et al. [681] follows this approach assuming $\gamma = 0.5$, that is, a FWHM dependence that is much weaker than the one of the virial law. The scaling law suggested by Park et al. [681] applied to a high luminosity sample properly corrects for the overbroadening of the CIV $\lambda 1549$ line profiles of high Eddington ratio sources of a high-luminosity sample, but overcorrects the width in case of sources radiating at modest Eddington ratios, yielding a large deviation from the H β -derived M_{BH} values [680].

13.5.1 The virial factor: orientation and radiation effects

The application of Eq. 36 requires the knowledge of the f_{S} , a quantity of $\mathcal{O} \sim 1$ but that can be significantly different from source to source. The presence of a rotating accretion disk and a spin axis for the central black hole guarantees that axial, and not spherical symmetry, is satisfied for AGN [682, 683]. Accordingly, unification schemes distinguish between sources that are observed with the line of sight oriented not very far from the disk axis, and sources that are seen almost edge-on, for which the observation of the BLR is precluded by obscuration (type-2 AGN). Leaving apart obscured sources, there is a considerable range of orientation angles (from 0 to 45 - 60) that are possible for type-1 AGN. The effect of orientation can be quantified by assuming that the line broadening is due to an isotropic component + a flattened component whose velocity field projection along the line of sight is $\propto 1/\sin \theta$ [684, 685, 686, 675]. Even with this assumption, it is not known how to connect the viewing angle of the black hole + accretion disk system and the parameters measured on the optical and UV spectra. Only in a few special cases this feat has been possible. In such cases the viewing angle is constrained by data unrelated to the spectra, such as the radio morphology or the jet beaming [687, 686, 688]. The dependence on orientation can be overcome by spectropolarimetric measurements: if the emission line light is scattered by an equatorial scatterer, then the width of the polarized line flux should be related to the velocity field as measured by an observer in the equatorial plane of the accretion disk, i.e., as if the viewing angle were $\theta = 90$ from the disk axis, de facto removing the orientation effect. Spectropolarimetric measurements allowed for the estimate of the black hole mass in a few tens of type-1 AGN [689, 690, 691, 692]. The technique requires large-aperture telescopes even for nearby, bright AGN, whose polarization is notoriously low ($\lesssim 1\%$; Sniegowska et al. 2021, in preparation).

A parameterization of the virial product dependent on the Balmer H β line has been suggested [675] in the form $f_{\text{BLR}} \propto \text{FWHM}^{-1.17}$ and exploited in several works [693, 694]. This relation is however especially risky in samples covering a wide range of luminosity, since it is not accounting for the increase in line width expected with increasing mass, if line broadening is predominantly virial (Sect. 15). In addition, orientation is not the only variable affecting f_{S} . Radiation forces act on gas motions and make the f_{S} dependent on Eddington ratio [e.g., 695, 696]. The effect can be as large as a factor ≈ 2 and, perhaps more importantly, the efficiency of radiation forces is dependent on the gas column density, leading to the preferential expulsion of gas of lower column density [695]. Recent attempts to derive the f_{S} from dynamical models still do not consider the role of radiation pressure on the gas motion [697, 698, 699, 700]. In addition, there are basic difficulties in modelling the BLR. One of the main issues is whether there are indeed gas clouds or whether the broad lines are emitted directly by a continuum-illuminated accretion disk [701, 702]. If clouds are indeed present, the mechanism of confinement is unclear, although confinement by an external magnetic field is favored [703, 704, 705, 706, 707]. The quasar main sequence discussed in Sect. 14.2 provides a focus for these questions, but the physical processes of line emitting gas dynamics have not yet been contextualized for different accretion modes (Sect. 14.3).

The virial factor f_S has been estimated by scaling the *virial product* $r_{\text{BLR}}\delta v^2$ to the $M_{\text{BH}} - \sigma_*$ for quiescent galaxies obtaining an average $f_S \approx 5.5$ if the velocity dispersion of the broad emission line is used (≈ 2.3 from the FWHM). This approach provides a test of consistency for the reverberation mapping technique [549] within a factor 2-3 uncertainty. In principle, the f_S uncertainties could be reduced, if a careful separation of different morphological types and of different accretion modes is carried out. For instance, the technique applied to NLSy1s yields $f_S \approx 1.1$ (for FWHM; [708]); Du and Wang [643] show that sources accreting at high rates do not obey the Bentz et al. [644] relation.

13.6 M_{BH} vs M_{bulge} and σ_* for AGN and its consistency with quiescent galaxies at low- z

There is a general consensus that most galaxies host a massive BHs that went through phases of activity. This latter had a role in the BH growth and in the regulation of the SF activity of the host galaxy by means of wind/jet driven feedback mechanisms [709, 710, 711]. The theoretical models show that an AGN and its host may coevolve [525, 712], leading to characteristics (such as the $M_{s,\text{sph}}/M_s$ ratio and/or the central stellar velocity dispersion σ) related to black hole mass (M_{BH}).

An early answer to the question “do galaxies hosting an AGN share the same $M_{\text{BH}} - M_{\text{bulge}}$ correlation of normal galaxies?” was affirmative: AGN have the same BH-bulge relation as ordinary (inactive) galaxies [713]. Fast forward twenty years, there is not yet an established view. A most recent work, based on state of the art surface photometry, and spatially-resolved kinematics to measure σ_* , find that correlations between M_{BH} and host galaxy properties hold for AGN within the limits of an intrinsic scatter 0.2 - 0.4 dex, and are consistent with the ones of quiescent galaxies [549].

Recent works also point toward a complex scenario involving selection biases [714] and a better appreciation of the active galaxies diversity. We may represent the distribution of objects in the $M_{\text{BH}} - M_{\text{bulge}}$ (or σ_*) diagram by the bivariate distribution function of bulge mass M_{bulge} and M_{BH} $\Psi(M_{\text{BH}}, M_{\text{bulge}})$. The Ψ distribution can be factorized as $\Psi = \gamma(M_{\text{BH}} | M_{\text{bulge}})\phi(M_{\text{bulge}})$ where $\phi(M_{\text{bulge}})$ is the spheroid mass function and γ represents the $M_{\text{BH}} - M_{\text{bulge}}$ correlation i.e., the probability of having the black hole mass M_{BH} for a given M_{bulge} . A correct evaluation of $\gamma(M_{\text{BH}} | M_{\text{bulge}})$ relies on: (1) the knowledge of $\phi(M_{\text{bulge}})$, which is not a trivial task to achieve even in the local Universe, and needs a separate consideration of purely spheroidal (i.e., diskless) galaxies and galaxies with pseudo-bulges or with a bulge/disk system; (2) the absence of biases affecting $\gamma(M_{\text{BH}} | M_{\text{bulge}})$.

Both the determinations of M_{BH} and bulge parameters are challenging, when derived from conventional optical and NIR measurements. At present, black hole masses for type-1 AGN are more frequently derived through the so-called, single epoch “virial broadening” estimation i.e., through the measurement of the radial velocity broadening term that appears squared in Eq. 36 from single epoch spectra. In practice, it is the measurement of the FWHM or σ^6 of broad emission lines [e.g. 684, 653]. To obtain M_{BH} , an estimate of the radius r_{BLR} is also needed, and a rather poorly-defined scaling law of r_{BLR} vs luminosity is applied.

The bulge estimates in AGN samples are hampered by the luminous source associated with the active nucleus, which may well outshine the entire galaxy. The M_{bulge} has been frequently computed from the host galaxy luminosity [715, 716, 717, 718, 719, 720, 721, 722]. However, type-1 AGN remain offset from inactive galaxies in the $M_{\text{BH}} - L_{\text{bulge}}$ relation: AGN have more luminous bulges at a given black hole mass [723, 549]. There are evidences that the $M_{\text{BH}} - L_{\text{bulge}}$ relations defined by quiescent BH samples differs from that defined by the galaxies in the SDSS [724]. Interestingly, the offset is larger for AGN of larger Eddington ratio [725]. This suggests that the central regions of galaxies hosting an AGN have in general

⁶ Not to be confused with σ_* .

lower mass-to-light ratios than inactive galaxies, most likely for the presence of a young stellar population in the bulge of active systems [726].

The σ_* has been measured either directly i.e., from the width of absorption lines associated with the stellar component of the host galaxies [727, 728, 729] or by using the widths of narrow emission lines a proxy of the stellar velocity dispersion [730, 731, 732]. The latter approach is fraught from systematic effects. In the case of quasars and AGN radiating at moderate and high Eddington ratio, the [OIII] λ 5007 broadening is strongly affected by non-virial motions [623, 640, 733, 734, 735].

More reliable results for dynamical mass measurements of the host galaxy from spatially-resolved images have been obtained with adaptive optics [736]. CO emission profiles have been used to estimate dynamical masses for individual objects since the early 2000s [737] even at fairly high redshift, and nowadays ALMA is rapidly adding to the available dynamical mass measurements for the host galaxy [e.g., 738, 739], considering that the velocity field of the molecular gas is often regular and consistent with rotation. State-of-the-art surface photometry of the AGN host galaxies in the NIR achieve decomposition in spheroid, disk and bar component, as most of the host of nearby Seyfert galaxies are of morphological type Sa/SBa. As mentioned, a most recent work didn't detect significant differences in the scaling with M_{BH} and σ_* between active and non-active galactic nuclei [740, 549], and didn't find difference between pseudo and classical bulges or barred and non-barred galaxies in the $M_{\text{BH}} - M_{\text{bulge}}$ relation [549], although this result is still controversial [741, 742]. In addition, γ is still computed with the single epoch technique, without consideration of the diversity in accretion structure (and hence virial factor) that is expected in type-1 AGN samples. For type-1 active nuclei radiating at Eddington ratio above 0.01, the geometry and structure of the emitting region are affected by the accretion mode, which in turns affects the expression of the virial factor that is dependent on kinematics, geometry, and viewing angle [685, 674, 675, 743, 744]. A study separately considering sources in different accretion modes and the statistical bias introduced by orientation effects is not available has yet.

Keeping the attention focused on γ , the radius of influence r_h is of the order of parsecs, and insufficient resolution may prevent reliable BH mass estimates or forces to target only the largest BHs [745, 746], leading to a selection effect that yields an increase in the $M_{\text{BH}} - \sigma$ relation for quiescent galaxies by a factor of a few [747, 744]. AGN will on average host more massive BHs than in the volume-limited case [748], determining a Malmquist bias towards more massive BHs at a given spheroid mass, shifting γ upwards and causing an offset in the zero-point of the $M_{\text{BH}} - M_{\text{bulge}}$ relation. There are competing effects: the fraction of active galaxies among SMBHs varies considerably with mass (high-mass BHs are likely less active than low-mass BHs [714]). The strength of the bias depends on the limit in luminosity, the shape of the distribution function of spheroids, the scatter of the $M_{\text{BH}} - M_{\text{bulge}}$ relation, and the Eddington ratios. If, as mentioned, the active fraction decreases as the BH mass increases, then for a given spheroid mass it will be more probable to find small-masses BHs in an AGN sample, causing a bias towards lower $M_{\text{BH}}/M_{\text{bulge}}$ ratios, and a change in the slope of the relation.

The low- M_{BH} end of the correlation is especially problematic, as it is for quiescent galaxies. Narrow-line Seyfert 1s nuclei (NLSy1s, low- z type-1 AGN several of which are accreting at high rate, [749]), often hosted in dwarf high surface brightness galaxies [750] and in barred spirals [751, 752], possess under-massive BHs [753, 754]. NLSy1 nuclei often reside in disk-dominated galaxies with pseudo-bulges [755, 756, 757, 758, 759, 760]. These types of bulges are more closely associated with the evolution of disks and may be typical of systems that did not experience a minor or major merger capable to lead to a real bulge development. Several studies found that disk-dominated galaxies deviate from the $M_{\text{BH}} - M_{\text{bulge}}$ correlation, and, if considered as a distinct class, may not follow a $M_{\text{BH}} - M_{\text{bulge}}$ correlation

[741, 761, 579]. However, if one applies a correction for the disk component, and considers only the bulge, the AGN in the low black hole mass ranges $M_{\text{BH}} \lesssim 10^8 M_{\odot}$ might follow a relation consistent with the local $M_{\text{BH}}-M_{\text{bulge}}$ correlation [762, 763]. At any rate, the relation between M_{BH} and σ_* or M_{bulge} should be taken with special care in particular in the lower M_{BH} range. Relatively few objects are unobscured type-1 AGN. Chandra observations are detecting a wealth of black holes in star-forming galaxies, in the range between $10^6 - 10^7 M_{\odot}$, even at high z [764, 765, 766]. They are low mass by supermassive black hole mass standards, and most likely still growing in an obscure phase. It is not known how they would be located in the $M_{\text{BH}}-M_{\text{bulge}}$ plane. These elusive AGN are potential targets for JWST [767].

13.7 Over-massive and under-massive black holes

At the time of its discovery, the luminous quasar HE0450-2958 appeared as an oddity: a quasar without a host galaxy! [768]. Understandably enough, the source attracted a lot of interest, and perhaps even a revival of the non-cosmological interpretation of quasar redshifts [769, 770, 771]. HE0450-2958 appears hosted by a galaxy much fainter than that inferred from the correlation between BH mass and bulge luminosity [772]. In the case of quiescent galaxies, compact dwarf galaxies whose BH has a mass reaching even 15% of the total galaxy mass [773, 774, 775] are observed. A possible explanation is that their outer parts may have been stripped by repeated encounters with other galaxies and produced an ultra-compact dwarf galaxy. The EAGLE cosmological and hydrodynamical simulations suggest that these kind of objects are outliers resulting from the combination of stellar tidal stripping and the early formation epoch, that led to a rapid BH growth at high redshift, with the first mechanism being the most relevant for 2/3 of these sources [776]. However, the disk/bulge decomposition is a delicate procedure. A careful reanalysis of the most striking cases, Mrk1216, NGC1277, NGC1271, and NGC1332, suggests that a proper re-evaluation of the disk size with an ensuing increase in spheroid mass will bring these sources in better agreement with the $M_{\text{BH}}-M_{\text{bulge}}$ relation [777]. The case of HE0450-2958 has not been fully explained to-date. Past works have considered intriguing lines of evidence suggesting high L/L_{Edd} and BAL outflow [778, 779]. However HE0450-2958, that appears as a mini-BAL from a FOS spectrum, shows modest optical FeII emission, and a spectrum similar to the one of PG1211+143 [778]. According to the main sequence trends (see §14.2), the object should not be highly accreting [749, 780]. It is also unlikely that HE0450-2958 is a recoiling black hole ejected by a companion galaxy at about 7 kpc of projected linear distance, on the ground of the strong narrow line emission of [OIII] $\lambda\lambda 4959, 5007$ [778]. HE0450-2958 does not appear as an extraordinary powerful quasar. The upper limits on the host galaxy luminosity are not very constraining, so that this object could be well within the limits set by the scatter in the $M_{\text{bulge}}-M_{\text{BH}}$ correlation [772].

However, recoiling black holes — provided that they are the active member of the binary, as suggested by numerical simulations [781] — may systematically lower M_{BH} and ultimately increase the scatter of the observed BH–host galaxy bulge relation due to ejected BHs [782]. Recoiling BHs have lower masses than their stationary counterparts, but the deficit in mass depends on kick speed and merger remnant properties [783]. The effect is of an overall downward shift in the normalization and an increase of the scatter in the $M_{\text{BH}}-M_{\text{bulge}}$ relation: the offset between the stationary and the recoiling BH population can reach $\delta \log g \approx 0.4$ dex, if the rotational velocity of the secondary BH is close to its escape velocity. The amplitude of the downward offset depends on the recoil velocity as well as on the accretion history of the stationary black hole, and can be lower, yielding a $\delta \log \phi \approx 0.2$ dex. This scenario is not as yet contextualized: a large fraction of type-1 AGN shows evidence that they do not host a sub-parsec binary black hole with a significant mass ratio between the secondary and the primary (say $q \gtrsim 0.1$). Conclusive evidences in favor of such binary systems are very rare at the time of writing.

13.8 Evolution of the $M_{\text{BH}}-M_{\text{bulge}}$ relation

Active galactic nuclei and quiescent bulge-dominant galaxies do not show strong evidence of evolution in the $M_{\text{BH}} - M_{\text{bulge}}$ relation up to $z \sim 0.6 - 1$ [732, 784, 785]. At higher redshift, there is an increasing evidence of evolution, in the sense of high- z SMBHs that are overmassive at a given bulge mass than expected from the local scaling relation [786, 787]. Between redshift 1 and 2, Merloni et al. [788] suggested a significant increase of the $M_{\text{BH}}/M_{\text{Bulge}}$ ratio ($\propto (1+z)^{0.68}$). Studies at even higher redshift used the velocity dispersion of the gas as a proxy of the stellar velocity dispersion and dynamical mass measurement from inclined disk models [789]. They suggest over-massive black holes [721] with respect to the local scaling law. The most recent results confirm that quasars host galaxies are under massive relative to M_{BH} , and detect a large difference, even by an order of magnitude, with systems at redshift in between 1.4 and 2.6 residing off the local scaling relation. Several quasar host galaxies have been resolved in their [C II] emission on a few kpc scale at redshift ≈ 6 . Even in this case, the dynamical mass estimates for the host galaxies give masses more than an order of magnitude below the values expected from the local scaling relation [787], in agreement with the results for galaxies at $z \approx 7$ derived from cosmological hydrodynamical simulations [790].

The evolution of the $M_{\text{BH}} - M_{\text{bulge}}$ relation with the cosmic epochs can be interpreted in several ways: the most straightforward is that of a rapid growth of SMBHs at high redshift [791]. Also a variation of structural properties of AGN hosts remains possible [792, 793]: elliptical galaxies are not really monolithic spheroids, but have undergone significant late-time dissipation-less assembly. There are intriguing caveats with the interpretation of a rapid black hole growth. First, very massive seed black holes need to be formed at $z \approx 20$ to account for masses $\sim 10^9 M_{\odot}$ observed at redshift $z \gtrsim 4$ ([794, 795], and references therein). Second, BH masses (unlike the masses of galaxies!) can only increase with cosmic epoch. If the merger-driven hierarchical scenario that implies the parallel growth of bulges and BHs is taken literally, the larger $M_{\text{BH}}/M_{\text{Bulge}}$ ratio at high z means that mergers affect more bulge than BH masses (at cosmic epochs associated with $z \gtrsim 1$), an implication consistent with the anti-hierarchical growth and downsizing of the nuclear activity at low- z [796]. If pseudo-bulges follow the same M_{BH} scaling relations as that of classical bulges [e.g., 549], hierarchical growth might not be the only mechanism that drives the relation between $M_{\text{BH}} - M_{\text{bulge}}$: in spiral galaxies, secular evolution might lead to a parallel growth of bulge and central black hole. Clearly, this issue should be analysed in connection to ongoing star formation properties of the pseudo-bulge hosts [797]. Host and black hole properties are different for different masses, and the relation between galaxy color and black hole mass is different for the red and blue sequence quiescent galaxies, suggesting different channels of black hole growth for the two sequences [798].

In conclusion, AGN with “coreless” elliptical/bulge-dominated hosts may straightforwardly follow a relation similar to the one of normal galaxies. In other words, the $M_{\text{BH}}-M_{\text{bulge}}$ relation may strictly holds for massive evolved systems, also if the nucleus is active, in a form that is as yet indistinguishable from the one of quiescent galaxies. It remains to be tested whether these sources could be mainly AGN accreting at relatively low rate and radiating at modest Eddington ratios (Population B, Section 14.2). Significant deviations may be associated with disk dominance, but a careful assessment of the relative disk and bulge contribution might bring the system with the over-massive BHs in agreement with the established relation [740, 797]. The local NLSy1s – all of which are Population A (Section 14.2), with a significant fraction of high accretors – are instead believed to be with black holes under massive with respect to their host masses. In this respect they are different from the high- z quasars with over-massive black holes. However, the observational properties of low- z AGN accreting at relatively high rate can still be regarded as typical of very high z quasars, when massive bulges were not yet formed, as originally

suggested by Mathur [799], Sulentic et al. [800]. The analogy is based on the optical, UV, and X-ray AGN spectroscopic properties that are mainly governed by the Eddington ratio. In addition, modest masses of low- z quasars can grow by a factor ~ 10 on time scales shorter than timescale of the cosmic evolution of quasar accretion rates, and therefore bring under massive BHs in line with the $M_{\text{BH}} - M_{\text{bulge}}$ relation [801].

14 THE FUNDAMENTAL PLANE OF AGN AND THE TYPE-1 AGN MAIN SEQUENCE

Some general considerations are in order when restricting the attention to the nuclei of galaxies. First, the central engine of nuclear activity is contained within a few parsec from its prime mover, the accreting massive black hole. Several scaling laws that are widely applied in the study of galaxies are not considered in the study of AGN: the Kormendy relation loses its meaning in the context of a system that is observed without spatial extension. Or, they might connect different physical bodies: when we speak about the $r - L$ relation for AGN, r is the radius of the line emitting region, and L is the luminosity of the AGN. The two parameters do not refer to cospatial entities. Similar consideration apply to the $M_{\text{BH}} - r$, or the $M_{\text{BH}} - L$, or the $M_{\text{BH}} - \text{metallicity}$ relations.

The virial equation (Eq. 36) is yielding the same FWHM for the same r/M_{BH} ; what matters is the radius in units of gravitational radii, a dimensionless quantity. A smaller mass can give the same line width of a larger mass provided that r scales with M_{BH} . This is why we need an estimate of the linear size r to recover a value of M_{BH} in physical units. This scale invariance is obviously not applicable to radiative phenomena: the flux reaching a distance r will decrease with the inverse of the square of r on a *dimensional* scale. The BLR radius r_{BLR} subtends such a small angle that has not been directly resolved if not in the last few year thanks to the GRAVITY instrument [802, 634]. The foundations of any AGN diagnostics therefore rest on the scale invariance of gravitational forces, and on electromagnetic phenomena instead lacking such scale invariance. These considerations can be translated in mathematical terms to provide at least a self-similar framework that includes the fundamental plane of black holes, the modelization of jets [803] and the quasar main sequence (MS).

14.1 The fundamental plane of black hole activity

The fundamental plane of black hole activity can be written as a correlation between black hole mass, X-ray and radio luminosity. The correlation defines a plane in the space of parameters defined by the mass and the radio and X-ray luminosities. In its original formulation, the fundamental plane was written as [804]:

$$\log L_{\text{R}} = (0.60 \pm 0.11) \log L_{\text{X}} + (0.78_{-0.09}^{+0.11}) \log M_{\text{BH}} + 7.33_{-4.07}^{+4.05}. \quad (38)$$

The scatter is large, implying that a fourth variable might be involved, for instance black hole spin [805]. The salient point is however that the relation holds over a huge range of black hole masses, from a few times solar (i.e., from the domain of the so-called micro-quasars) to the largest black hole masses detected in the Universe $\sim 10^{10} M_{\odot}$ [e.g., 806, 807].⁷ It is remarkable that also stellar-mass black holes exhibit relativistic jets, as spectacularly demonstrated by the relatively recent discovery of superluminal motion in a Galactic black hole candidate by Mirabel and Rodríguez [812]. The self-similarity expressed in Eq. 38 allows for an invariant jet model and a simple relation between M_{BH} and radio power [803]. The self-similarity notwithstanding, there is a non-linear relation between BH mass and radio power, with $P_{\nu} \propto$

⁷ As stressed by Sulentic et al. [808, 809, 673], M_{BH} much in excess of $\sim 10^{10} M_{\odot}$ are unrealistic and probably the results of the use of a high-ionisation line affected by wind kinematics as a virial broadening estimator (VBE). This makes the primary black hole of OJ287 [810] as the most massive active black hole known to-date, with a mass of $\approx 1.8 \cdot 10^{10} M_{\odot}$, second to the black hole of Holm 15A, the central galaxy of galaxy cluster Abell 85, with $\approx 4 \cdot 10^{10} M_{\odot}$ [811].

$M_{\text{BH}}^{1.3-1.4}$, implying that the radio emission normalized to the bolometric luminosity should be much higher for AGN than for microquasars. In the framework of the model of Heinz and Sunyaev [803], flat spectrum synchrotron jet emission is produced by an inefficient accretion mode. The fundamental plane of black hole activity refers to sources accreting at very low rate (dimensionless accretion rate $\dot{m} \lesssim 0.01$), and radiating below a few hundredths of their Eddington luminosity.

14.2 The quasar Main Sequence

The quasar main sequence is, in many way, analogous to the FP for black holes in a different accretion mode sustained by higher $\dot{m} \sim 0.01 - 1$. The formulation is rather different, and follows a different discovery path based on the statistical analysis of sources that are predominantly radio-quiet. The quasar main sequence (MS) is defined from the first Eigenvector (E1) that was originally identified by a PCA of about 80 Palomar-Green (PG) quasars and associated with an anti-correlation between the strength of optical FeII emission measured from the prominence of the emission blend centered at $\lambda 4570 \text{ \AA}$ (FeII $\lambda 4570$) with respect to H β ($R_{\text{FeII}} = I(\text{FeII}\lambda 4570)/I(\text{H}\beta)$) and FWHM of H β [813]. The E1 MS has withstood the test of time [Fig. 11, 814, 815, 816, 817, 818, 819], and the main optical trend shown in Fig. 11 has been confirmed by samples of more than two order of magnitude larger in size than the original one [819]. The importance of FeII stems from its extensive emission from UV to the IR that can dominate the thermal balance of the low-ionization BLR. The FWHM(H β) is associated with the velocity field in the low-ionization BLR, most likely predominantly virialized [820]. These two parameters are related to the physical conditions and to the dynamics of the emitting regions, that are in turn influenced by the accretion mode of the central black hole, and its evolutionary stage.

Trends associated with the MS have been extended to the radio [821, 819, 822, 823], FIR [824, 823], IR, [825, 826, 827], UV [828, 829, 830, 809, 831, 832, 833, 834] and X-ray domain [835, 836, 837], and to optical variability as well [838, 839]. Table 1 of Fraix-Burnet et al. [801] provides a detailed list of the various parameters that have been measured in the various frequency domains. A summary description of the trends and a justification for the two quasar populations are also provided by several authors [840, 841, 842]. A nonlinear decay curve provides a quantitative description of the main sequence in the FWHM — R_{FeII} plane [843].

The distribution of the data in the plane R_{FeII} –FWHM(H β) makes it expedient to define spectral types [Fig. 12, 844, 819]. This provides the considerable advantage that a composite spectrum within each bin could be representative of objects in similar physical conditions. In alternative, a prototype object can be defined for each spectral type and used to analyze systematic changes along the quasar MS. It is also expedient to distinguish between two populations: Population A made of sources with FWHM(H β) $\leq 4,000 \text{ km s}^{-1}$ and Population B (broader) with FWHM(H β) $> 4,000 \text{ km s}^{-1}$. Extreme Population A are quasars with $R_{\text{FeII}} \gtrsim 1$ and extreme Pop. B with undetectable FeII emission and the broadest Balmer lines (extreme FWHM H β can reach $\sim 15,000 - 20,000 \text{ km s}^{-1}$ [845, 846, 847]). Basically, Population B includes sources termed as “disk dominated”, where radiation forces exert a modest influence on the overall dynamics of the gas [833], while Population A is made of quasars radiating at relatively high Eddington ratio $L/L_{\text{Edd}} \gtrsim 0.2$, for which radiation forces are able to maintain a wind that leads to easily identified systematic wavelength displacements toward the blue with respect to the quasar rest frame in the high-ionization emission lines [654, 656, 657, 848, 668, 669]. The extreme of Population A identifies the class of “strong FeII emitters” [849, 850]. FeII emission overwhelming H β line emission ($R_{\text{FeII}} \gtrsim 1$) implies extreme Eddington ratio ($L/L_{\text{Edd}} \sim 1$, [749]) and possibly super-Eddington accretion rate [851, 780, 852, 780, 853, 854].

However, along the entire MS, the BLR gas emitting the low-ionization lines belong to predominantly virialized systems [820]. The main asymmetries in the low-ionization line profiles can be explained in the context of a dynamical system whose velocity field is predominantly Keplerian. The single peaked, symmetric and unshifted profile typical of Population A has been traditionally explained as due to an extended disk [702], and the same explanation apparently remains valid in the case of extreme Pop. A AGN that are characterised by extreme high-ionisation blueshifts [658, 673, 855, 856, 664, 669]. The high $\text{CIV}\lambda 1549/\text{H}\beta$ intensity ratio of the blueshifted emission [857] makes it possible that the $\text{H}\beta$ profile remains almost symmetric and can be easily symmetrized by applying a small correction [858]. In general, the distinguish feature of Pop. B sources, a redward asymmetric profile, can be explained by the sum of a disk contribution and emission from a larger distance [859, 860]. Reverberation mapping studies of lines from different ionic species has provided evidence of “ionization stratification” and velocity-resolved reverberation mapping of sources with asymmetric $\text{H}\beta$ basically confirms the scenario of a Keplerian velocity field [861, 637]. The red-ward asymmetry has been interpreted as due to gravitational and transverse redshift [862, 688] or by gas clouds infalling toward the central black hole [863]. At the extreme end of Pop. B sources, the profiles are often very broad and double peaked, accounted for by a bare Keplerian disk model with mild relativistic effects [864, 847]. So, all along the quasar MS the low-ionization lines (at variance with the high-ionization emission) appear to be predominantly associated with a bound, Keplerian dynamical system [701, 865].

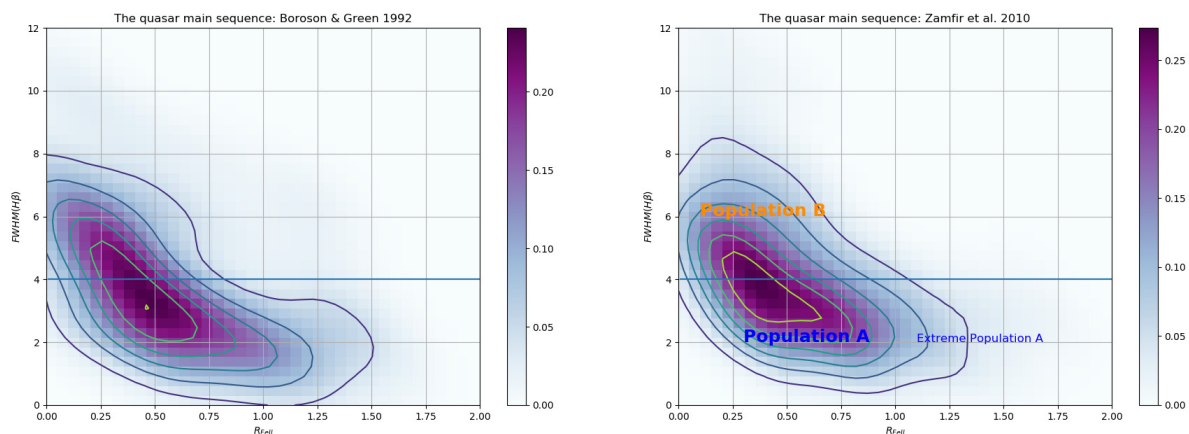


Figure 11. The quasar main sequence as defined from the original paper by [813] based on 88 quasars (left) and the one based on the SDSS sample of 310 low- z quasars by Zamfir et al. [815]. The color shading from cyan to navy blue is proportional to the number density as a function of the FeII prominence parameter and of the FWHM of $\text{H}\beta$, and therefore to the source occupation in the parameter plane.

Many studies still distinguish between the NLSy1s ($\text{FWHM H}\beta \lesssim 2000 \text{ km s}^{-1}$) and the rest of type-1 AGNs [e.g., 735], and consider NLSy1s an independent class. There is a general consensus that the limit at 2000 km s^{-1} , albeit of historical importance, has no special meaning. The main reason to extend the limit from 2000 to 4000 km s^{-1} is that several properties of NLSy1s are consistent with the ones of “the rest of Population A” in the range $2000 \text{ km s}^{-1} \lesssim \text{FWHM}(\text{H}\beta) \lesssim 4000 \text{ km s}^{-1}$. The change — in low redshift samples $z \lesssim 1$ — occurs around 4000 km s^{-1} , not 2000 km s^{-1} [735]. On the converse Population A and B can be distinguished on the basis of the Balmer line profiles, and because of the amplitude of the systematic blueshift of the high-ionization lines with respect to the quasar rest frame. Composite $\text{H}\beta$

profiles of spectral types along the MS are consistent with a Lorentzian for both NLSy1s and the rest of Population A. Other parameters (CIV λ 1549 centroid, R_{FeII}) also span the same ranges in NLSy1s and the rest of Population A.

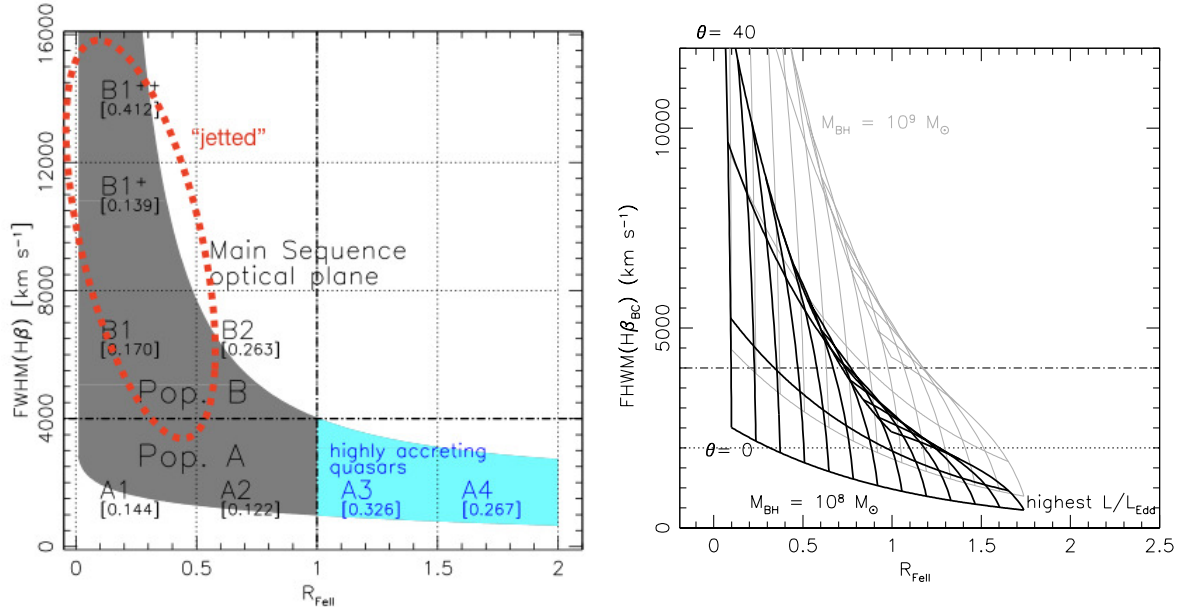


Figure 12. The optical plane of the quasar main sequence with the occupation accounted for by the combined effect of Eddington ratio and orientation, as claimed by [819]. The two grids were computed for $M_{\text{BH}} = 10^8 M_{\odot}$ and $10^9 M_{\odot}$ (grey), for several values of L/L_{Edd} and for viewing angle θ between 0 and 40 degrees, following the toy model described in the text and in more detail in Ref. [866]. In the left panel, the labels identify the areas of Population A and B (respectively below and above the FWHM limit at 4000 km s^{-1}), and of extreme Population A ($R_{\text{FeII}} \gtrsim 1$).

The governing accretion parameter accounting for the MS trends is most likely the Eddington ratio, which is related to the mass accretion rate by a monotonic albeit non-linear relation [867, 868, 869]. This explanation — originally suggested by Boroson & Green [813] — has also withstood the test of time [870, 871, 815, 872, 873, 819, 852, 874, 853], even if several key pieces needed to connect L/L_{Edd} to the observed parameters remain poorly understood to date. The evidence of a correlation between R_{FeII} and L/L_{Edd} is still made murky by the strong effect of orientation on the line broadening, affecting M_{BH} and L/L_{Edd} computations with both random and systematic errors [680]. Sun and Shen [852] provided evidence of this based on the stellar velocity dispersion of the host spheroid (a proxy for M_{BH}) anti-correlation with R_{FeII} , implying that L/L_{Edd} increases with FeII. Recent approaches include a careful analysis of the role of metallicity and of density and ionization trends [853, 854], and confirm L/L_{Edd} as the main physical parameter governing the MS “horizontal branch” along the R_{FeII} axis.

A toy scheme can explain in a qualitative way the occupation of the MS plane under the assumptions that Eddington ratio, mass and an aspect angle θ (i.e., the angle between the line-of-sight and the accretion disk axis) are the parameters setting the location of quasar along the MS [870, 866]. If the BLR radius follows a scaling power-law with luminosity ($r \propto L^a$, Kaspi et al. [647], Bentz et al. [644]), under the standard

virial assumption, then

$$\text{FWHM} \propto f_S(\theta)^{-\frac{1}{2}} \left(\frac{L}{M_{\text{BH}}} \right)^{-\frac{a}{2}} M_{\text{BH}}^{\frac{1-a}{2}} \propto f_S^{-\frac{1}{2}} L^{\frac{1-a}{2}} \left(\frac{L}{M_{\text{BH}}} \right)^{-\frac{1}{2}}. \quad (39)$$

We can also write R_{FeII} as a function of (L/L_{Edd}) and θ , that needs to be established either empirically or theoretically. For illustrative purposes, we consider the “fundamental plane of accreting BHs” that relates L/L_{Edd} to R_{FeII} [780, 694], ignoring other relevant factors, such as systematic differences in line shapes and in chemical composition along the MS [854, 831], and we assume that R_{FeII} depends on θ following a limb-darkening law [870, 875].

As expected, the right panel of Fig. 12 shows that θ predominantly affects FWHM $\text{H}\beta$ and L/L_{Edd} predominantly (but not exclusively) affects R_{FeII} . Under the assumptions of the toy scheme the FWHM limit at 4000 km s^{-1} should include mainly sources with $L/L_{\text{Edd}} \gtrsim 0.1 - 0.2$. Sources at lower L/L_{Edd} are expected to be rare because they should be observed almost pole-on (for example, core-dominated radio-loud quasars whose viewing angle θ is relatively small [870, 822]), and the probability of observing a randomly oriented source at an angle θ between the symmetry axis and the line of sight is $P(\theta) \propto \sin \theta$. Even if such sources are expected to be rare, their number increases in flux-limited samples for a Malmquist bias, due to a continuum enhancement via relativistic beaming. We can say that separating Pop. A and B at 4000 km s^{-1} makes sense for low z samples and that, also by a fortunate occurrence, Pop. A includes mostly relatively high L/L_{Edd} sources.

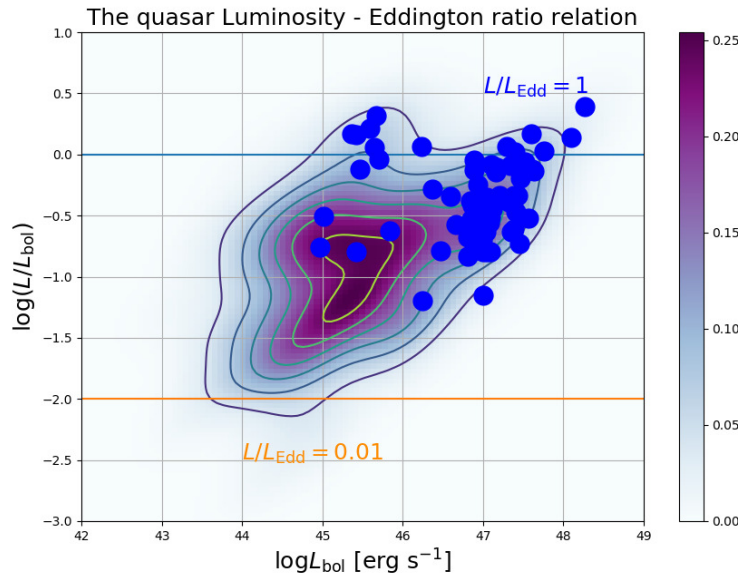


Figure 13. The relation between Eddington ratio L/L_{Edd} and bolometric luminosity for the sample described in Fig. 11, second panel. Quasars occupy the range 0.01 — 1, but only above Eddington ratio ≈ 0.1 large shifts are observed, as shown by the distribution of the blue data points, which represent quasars with the largest $[\text{OIII}]\lambda\lambda 4959, 5007$ blueshift.

The bolometric luminosity L can be estimated from optical or UV luminosities.⁸ The diagram L/L_{Edd} vs. bolometric luminosity (Fig. 13) also provides a strong rationale for the existence of two populations: only above a threshold of $L/L_{\text{Edd}} \approx 0.1$ large shifts are observed. Data points whose high-ionization lines are strongly blue shifted with respect to the rest frame are superimposed on the distribution of Fig. 13, and are clearly seen for $L/L_{\text{Edd}} \gtrsim 0.1$ only. This corresponds to the population A and B of [800], of wind and disk-dominated quasars [833], and population 1 and 2 of Collin et al. [685]. The data of Fig. 13 refer to sources with large blueshift in $[\text{OIII}]\lambda\lambda 4959, 5007$, but an equivalent behaviour is observed also for the blueshift of $\text{CIV}\lambda 1549$. At the same time, Fig. 13 (and Fig. 15 as well) show the effect of a strong bias typically affecting quasar studies over a broad range of redshifts: at high z we detect only the high luminosity sources that corresponds to relatively high L/L_{Edd} .

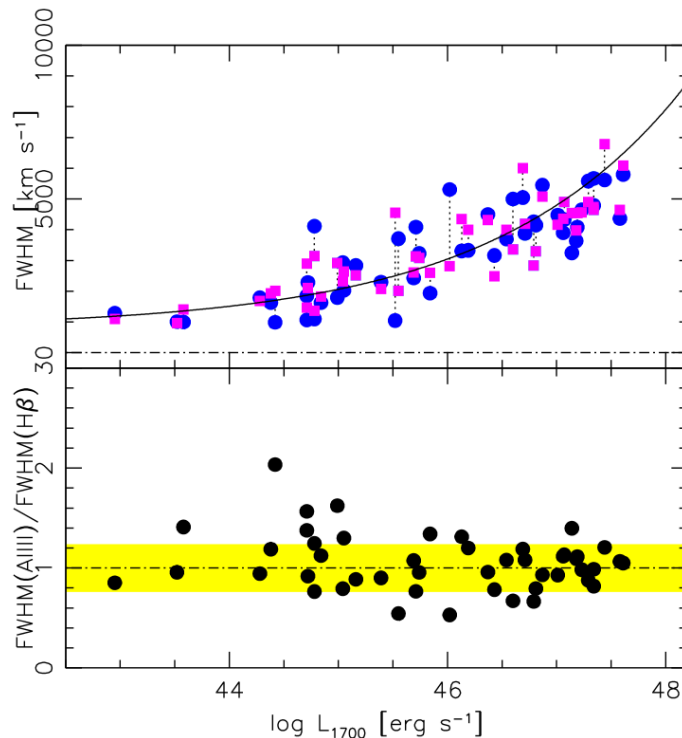


Figure 14. The relation between FWHM of $\text{H}\beta$ (blue) and $\text{AlIII}\lambda 1860$ (magenta) and their FWHM ratio (bottom panel), and bolometric luminosity. The filled line represent the trend $\text{FWHM} \propto L^{1/4}$, with arbitrary normalization. The yellow band defines the uncertainty range in the ratio $\text{FWHM AlIII}\lambda 1860 / \text{FWHM H}\beta$.

Fig. 11 refers to low- z ($z \lesssim 1$) samples. A complete mapping of the MS at high L is still missing (we consider high-luminosity quasars those with bolometric $\log L \gtrsim 47$ [erg/s]): the $\text{H}\beta$ spectral range is therefore accessible only with IR spectrometers to observe the $\text{H}\beta$ spectral regions of high-luminosity quasars that are very rare at $z \lesssim 1$. A significant progress is expected in the next years, since IR spectral observations covering $\text{H}\beta$ of high- z and high- L quasars are becoming widespread. A systematic increase in BH mass M_{BH} has a corresponding increase in FWHM. If $a = 0.5$, the FWHM grows with $M_{\text{BH}}^{0.25}$,

⁸ There is as yet no consolidated way to compute bolometric corrections, and ideally the bolometric correction should be computed from the spectral energy distribution (SED) of each individual quasar [876], or at least for each spectral type along the quasar main sequence [877]. Bolometric corrections can be also computed from theoretical considerations on the emission properties of the accretion disk [878, 879]. The simplest, and most widely used approach to compute the bolometric correction is to multiply the monochromatic luminosity by a constant scale factor that is obviously frequency-dependent and roughly 10 for λL_λ at 5000 Å, and $\approx 2 - 3$ for the UV wavelengths where the strongest lines are observed [880, 881, 882].

i.e. a factor of 10 for $\log L$, passing from 44 (relatively low luminosity) to 48 (very luminous quasars). The trend may not be detectable in low- z flux limited samples, but becomes appreciable if quasars over a wide interval in L are considered. At high M_{BH} , the MS becomes displaced toward higher FWHM values; the displacement probably accounts for the wedge-shaped appearance of the MS when large samples of quasars are considered [819]. If we consider a limiting Eddington ratio ($L/L_{\text{Edd}} \sim 0.1 - 0.2$) as a physical criterion for the distinction between Pop. A and B, then the separation based on the FWHM becomes luminosity dependent. According to the toy scheme, the FWHM of $\text{H}\beta$ (or of any other virialized line) should be $\propto (L/L_{\text{Edd}})^{-\frac{1}{2}} \times L^{\frac{1-a}{2}}$. Fig. 14 shows that the $\propto L^{0.25}$ for the width of a low- and an intermediate ionisation line. The maximum L/L_{Edd} should correspond to the minimum FWHM, expected to increase with luminosity as $\propto L^{0.25}$. If the FWHM is plotted against the luminosity, a trend-line nicely envelops the lower FWHM end of the data point distribution [883].

14.3 The BH mass – luminosity relation

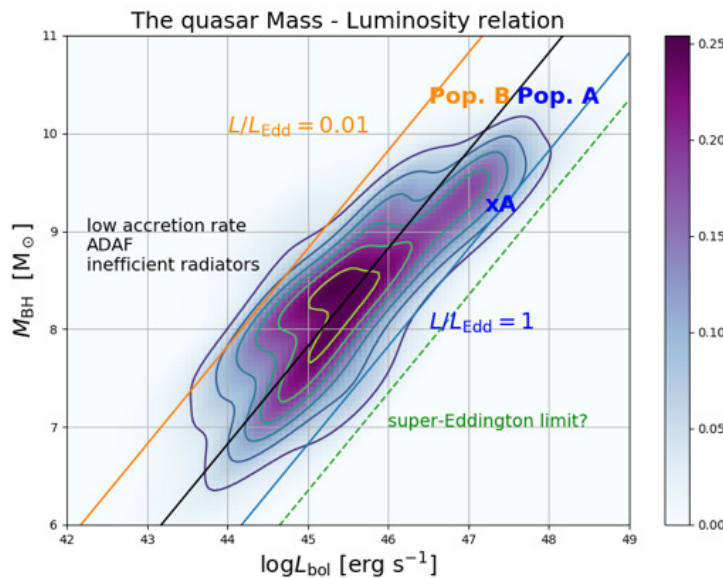


Figure 15. Mass-luminosity relation for a sample of ≈ 330 AGNs, made of 280 low- z quasars from [884] and high-luminosity 50 HE quasars of the sample described by Sulentic et al. [808]. The diagonal lines trace the lower $\sim 0.01 \cdot L/L_{\text{Edd}}$ and $\sim 1.00 \cdot L/L_{\text{Edd}}$. The wide majority of AGN is included within these limits.

Joining the fundamental plane and the main sequence trends for AGN, four main regimes can be isolated (c.f. [885]) where the physics of the inner accretion and ejection is expected to change. Observationally, they range from low-luminosity AGN at extremely low accretion rates ($\dot{m} \lesssim 0.01$) and Population B quasars radiating at rates $0.01 \lesssim L/L_{\text{Edd}} \lesssim 0.1 - 0.2$, to Population A sources with $L/L_{\text{Edd}} \gtrsim 0.1 - 0.2$, and extreme Population A sources radiating close or somewhat above the Eddington limit ($L/L_{\text{Edd}} \gtrsim 1$). There is a close formal analogy between the FP of accreting black hole and the MS. Eq. 38 can be rewritten as an implicit relation between L/L_{Edd} and M_{BH} . Similarly the MS is a sequence in the plane FWHM $\text{H}\beta - R_{\text{FeII}}$ that can be translated into a relation between L/L_{Edd} ($\propto R_{\text{FeII}}$) and M_{BH} ($\propto \text{FWHM}$). The relations of the MS are, as in the case of the FP, self-similar over 9 order of magnitude in M_{BH} [886]. Radiation driven winds appear to dominate in the high-ionization line emission in Population A and especially extreme Pop. A, reflecting the importance of the balance between radiation and gravitation

forces expressed by L/L_{Edd} in the accretion processes of AGN [887, 857], whereas the black hole mass is the ultimate parameter governing the energetics [669].

The M_{BH} —luminosity relation can be constructed for large quasars samples once the M_{BH} has been computed (Fig. 15). Fig. 15 shows that the distribution of quasars in the plane $M_{\text{BH}} - L$ is constrained within two well-defined diagonal lines, corresponding the $L/L_{\text{Edd}} \approx 0.01$ and $L/L_{\text{Edd}} \approx 1$. The empty area at the top left corner is due to inefficient radiators accreting at very low rate [888], which are most often not type-1 quasars and are difficult to detect; the bottom right area is associated with sources that should be super Eddington radiators. Such sources are not expected to exist; $L/L_{\text{Edd}} \approx a \text{ few}$ could be a physical limit for highly super-Eddington accretion [867, 869].

15 A TULLY-FISHER LAW FOR QUASARS

Strong FeII emitters have attracted attention since long, but they have been linked to a particular accretion state only recently [749, 889]. The simple selection criterion $R_{\text{FeII}} > 1.0$ used for the identification of xA sources from optical data, corresponds to an equally-simple selection with UV criteria [749]. In addition, the distinguishing features of the UV composite spectrum of Martinez-Aldama et al. [890] reveals that the spectrum of xA sources can be recognized by a simple visual inspection.

Extreme Population A sources account for $\sim 10\%$ of quasars in low- z , optically selected sample FeII in Pop. A. Lines have low equivalent width: some xAs are weak lined quasars [$W(\text{CIV}\lambda 1549) \leq 10 \text{ \AA}$, WLQ 891], whereas WLQs can be considered as the extreme of Pop. A [856]. The CIII] $\lambda 1909$ emission almost disappears. In the plane $\log U - \log n_{\text{H}}$ defined by CLOUDY simulations, UV line intensity ratio converge toward extreme values for density (high, $n_{\text{H}} > 10^{12} - 10^{13} \text{ cm}^3$) [892, 893], ionization (low, ionization parameter $U \sim 10^{-3} - 10^{-2.5}$). Extreme values of metallicity are also derived from the intensity ratios CIV/AIII, CIV/HeII, AIII/SiIII [892, 890, 831], most likely above 10 — 20 times solar or with abundances anomalies that might selectively increase aluminum or silicon, or both.

xA quasars radiate at extreme L/L_{Edd} along the MS. The L/L_{Edd} dispersion has been found to be small [749]. This result is consistent with accretion disk theory that predicts low radiative efficiency at high accretion rate and that L/L_{Edd} converges toward a limiting value [867, 894, 869]. Another important fact is the self similarity of the spectra selected by the R_{FeII} criterion: the low-ionization lines become broader with increasing luminosity according to Eq. 39, but the relative intensity ratios (and so the overall appearance of the spectrum) remains basically unchanged, although some redshift and luminosity effects are expected. Accretion disk theory predicts that at high accretion rate a geometrically thick, advection dominated disk should develop [894, 869]. The innermost part of the disk is puffed up by radiation pressure, while the outermost one remains geometrically thin. The effect on the BLR structure can be addressed by two dimensional reverberation mapping and by careful modelling of the coupling between dynamical and physical conditions [895, 698, 896]. However, this change from the standard thin disk provides two key elements for the BLR structure: the existence of a collimated cone-like region, where the high ionization outflows might be produced, and the shadowing of the outer disk where low-ionization emission lines form [897]. The low-ionization emitting region may therefore remain shadowed from the intense radiation field that is associated with the continuum observed if the line of sight is not too far from the polar axis, and the velocity field stays unperturbed.

15.1 A relation between luminosity and velocity dispersion for quasars

Three conditions are satisfied for xA quasars: (1) constant Eddington ratio L/L_{Edd} , close to Eddington limit; (2) The assumption of virial motions of the low-ionization BLR, so that the black hole mass M_{BH}

can be expressed by the virial relation (Eq. 36); (3) spectral invariance: for extreme Population A, the ionization parameter U can be written as $U = Q(H)/4\pi r_{\text{BLR}}^2 n_{\text{H}} c \propto L/r_{\text{BLR}}^2 n_{\text{H}}$ [875], where $Q(H)$ is the number of hydrogen ionizing photons. U has to be approximately constant, otherwise we would observe a significant change in the spectral appearance. The three constraints make it possible to derive a relation between line width (the FWHM of the $\text{H}\beta$ broad component is expressed in units of 1000 km s^{-1}) and luminosity:

$$L(\text{FWHM}) = \mathcal{L}_0 \cdot (\text{FWHM})_{1000}^4 \text{ erg s}^{-1} \quad (40)$$

where \mathcal{L}_0 depends on the square of L/L_{Edd} , the ionizing range of the spectral energy distribution, and a parameter directly derived from the UV spectra, the product density times ionization parameter that has been scaled to the typical value $10^{9.6} \text{ cm}^{-3}$ [898, 899, 892]. Until now, the FWHM of $\text{H}\beta$ broad component and of $\text{AlIII}\lambda 1860$ have been adopted as VBEs [900, 901, 902]. Equation (40) implies that a simple measurement of the FWHM of a low-ionization line yields a z -independent estimate of the accretion luminosity [749, c.f. [903]].

The virial luminosity equation is conceptually equivalent to the Tully-Fisher and the early formulation of the Faber Jackson laws for ETGs [12, 28]. Recent works proposed the “virial luminosity” could provide suitable distance indicators because several emission properties appear to be extreme and stable with luminosity scaling with black hole mass at a fixed ratio [904, 905, 851]. The virial equation has been applied to $x\text{A}$ quasars only ($L/L_{\text{Edd}} \sim 1$), although in principle could be useful for all quasars with known L/L_{Edd} , provided a suitable emission line broadened by virial motions is used for the luminosity computation. At present, the virial equation can be considered for *all* $x\text{A}$ quasars distributed over a wide range of luminosity and redshift, where conventional cosmological distance indicators are not available [906, 901, 902].

16 CONCLUSIONS

In this work we have reviewed only a small part of the big efforts done up to now on the SRs of galaxies and AGN. We have not addressed for example the correlations that are observed in the X-ray and radio domain, as well as many correlations involving the line emissions visible in the spectra.

It should be now clear that SRs are used continuously in every research area. The aims are different, going from the estimation of masses and distances, or peculiar velocities, or simply to check the output of theories, or to extract from them some useful indications about the physical mechanisms shaping the structure and evolution of galaxies and AGN.

The clear message emerging from this vast panorama of connections between structural, dynamical, gas and stellar population and halo parameters, is that galaxies are very complex objects formed through different channels, that include merging of sub-units, inflows, shocks, collapses, etc., as some of the most influent processes at work. In addition, it is also clear that galaxies vary their properties across the cosmic time, changing their morphology and physical characteristics. The simple Hubble morphological classification is therefore only a first naive tentative of summarizing such complexity that today are leading astrophysicists to adopt new specific strategies to classify galaxies, describe their properties, and highlight the amount of diversity across the cosmic epochs, but always keeping in mind the necessity of looking at the most important parameters that are able to trace the evolution of galaxies.

This new way of working is now facing the need of sophisticated numerical simulations and new statistical tools able to tackle the big astronomical number of data, exploring different classification schemes and strategies and group galaxies according to their similar evolutionary paths.

The multivariate partitioning analyses appear to be one of the most appropriate techniques. The Principal component analysis is one of these tools [907, 908], but it is not a clustering tool. Many new attempts have used multivariate clustering methods [see e.g. 909, 910, 911, 912, 913, 914, 915]. These sophisticated statistical tools are now used in different areas of astrophysics and are giving encouraging results, in particular for the problem of the identification of the galaxy ancestors and the processes more active in the transformation of galaxies [19].

In conclusion we can say that the world of SRs is big and complex. A lot of efforts are still necessary to organize such complexity, identify the key relationships having a real physical role for galaxies and AGN and understand the profound implications behind their intrinsic nature. Possibly the future high- z observations will add new information that will help the clarification of many long-standing open problems.

ABBREVIATIONS AND ACRONYMS USED IN THE TEXT

Table 1. Abbreviations and acronyms used in the text

N	Symbols	Meaning	N	Symbols	Meaning
1	AGN	Active Galactic Nuclei	25	JWST	James Webb Space Telescope
2	ALMA	Atacama Large Millimeter Array	26		
3	BTF	Baryonic Tully-Fisher	27	LTGs	Late Type Galaxies
4	BM	Baryonic Matter	28	LZR	Luminosity-Metallicity Relation
5	BH	Black Hole	29	MR	Mass -Radius
6	BLR	Broad-Line Region	30	MRR	Mass-Radius Relation
7	CoGs	Clusters of Galaxies	31	MS	Main Sequence
8	CGM	Circum-Galactic Medium	32	MZR	Mass-Metallicity Relation
9	CMR	Color-Magnitude Diagram	33	NIR	Near Infra-Red
10	DEs	Dwarf Elliptical galaxies	34	NLSy1	Narrow Line Seyfert 1
11	DGs	Dwarf Galaxies	35	PCA	Principal Component Analysis
12	DSphs	Dwarf Spheroidal Galaxies	36	SED	Spectral Energy Distribution
13	DM	Dark Matter	37	SF	Star Formation
14	EAGLE	Evolution and Assembly of	38	SFH	Star Formation History
15		Galaxies and their Environments	39	SFR	Star Formation Rate
16	ETGs	Early Type Galaxies	40	SKA	Square Kilometer Array
17	FIR	Far Infra-Red	41	SMBHs	
18	FJ	Faber - Jackson	42	SRs	Scale Relations
19	FP	Fundamental Plane	43	TF	Tully- Fisher
20	FOS	Fiber Optic Switch	44	VBE	
21	FWHM	Full Width at Half Maximum	45	VLBI	Very Long Baseline Interferometry
22	IGM	Inter-Galactic Medium	46	VLT	Very large Telescope Interferometry
23	IMF	Initial Mass Function	47	WLQ	Weak-Lined Quasars
24	ISM	Inter-Stellar Medium	48	ZoE	Zone of Exclusion

AUTHOR CONTRIBUTIONS

All the authors contributed equally to this work.

ACKNOWLEDGMENTS

MD want to thank Frontiers for the assistance in the production of the Research Topic.

REFERENCES

- [1] Hubble EP. *Realm of the Nebulae* (1936).
- [2] de Vaucouleurs G. Classification of galaxies by form, luminosity and color. Name1 E, Name2 E, editors, *IAU Symp. n. 15* (The name of the publisher) (1962), 3–21.
- [3] Brosche P. The Manifold of Galaxies. Galaxies with known Dynamical Parameters. *Astronomy and Astrophysics* **23** (1973) 259–268.
- [4] Bender R, Burstein D, Faber SM. Dynamically Hot Galaxies. I. Structural Properties. *The Astrophysical Journal* **399** (1992) 462. doi:10.1086/171940.
- [5] Cappellari M, Emsellem E, Krajnović D, McDermid RM, Serra P, Alatalo K, et al. The ATLAS^{3D} project - VII. A new look at the morphology of nearby galaxies: the kinematic morphology-density relation. *Mon. Not. R. Astron. Soc.* **416** (2011) 1680–1696. doi:10.1111/j.1365-2966.2011.18600.x.
- [6] Kormendy J, Bender R. A Revised Parallel-sequence Morphological Classification of Galaxies: Structure and Formation of S0 and Spheroidal Galaxies. *The Astrophysical Journal Suppl.* **198** (2012) 2. doi:10.1088/0067-0049/198/1/2.

- [7] Sandage, A, Freeman, KC, Stokes, NR. The intrinsic flattening of e, so, and spiral galaxies as related to galaxy formation and evolution. *The Astrophysical Journal* **160** (1970) 831–844. doi:10.3389/fnins.2013.12345.
- [8] Brosche P. A Model for the Early Evolution of Galaxies. *Astronomy and Astrophysics* **6** (1970) 240–253.
- [9] Searle L, Sargent WLW, Bagnuolo WG. The History of Star Formation and the Colors of Late-Type Galaxies. *The Astrophysical Journal* **179** (1973) 427–438. doi:10.1086/151882.
- [10] King IR. Stellar Populations in Galaxies. *Publications of the Astronomical Society of the Pacific* **83** (1971) 377. doi:10.1086/129146.
- [11] Fish RA. A Mass-Potential Relationship in Elliptical Galaxies and Some Inferences Concerning the Formation and Evolution of Galaxies. *The Astrophysical Journal* **139** (1964) 284. doi:10.1086/147753.
- [12] Faber SM, Jackson RE. Velocity dispersions and mass-to-light ratios for elliptical galaxies. *ApJ* **204** (1976) 668–683. doi:10.1086/154215.
- [13] Kormendy J. Brightness distributions in compact and normal galaxies. II. Structure parameters of the spheroidal component. *The Astrophysical Journal* **218** (1977) 333–346. doi:10.1086/155687.
- [14] Binggeli B, Sandage A, Tarenghi M. Studies of the Virgo Cluster. I. Photometry of 109 galaxies near the cluster center to serve as standards. *The Astronomical Journal* **89** (1984) 64–82. doi:10.1086/113484.
- [15] Sandage A. Absolute Magnitudes of E and S0 Galaxies in the Virgo and Coma Clusters as a Function of $U - B$ Color. *The Astrophysical Journal* **176** (1972) 21. doi:10.1086/151606.
- [16] Terlevich R, Davies RL, Faber SM, Burstein D. The metallicities, velocity dispersions and true shapes of ellipticalgalaxies. *Mon. Not. R. Astron. Soc.* **196** (1981) 381–395. doi:10.1093/mnras/196.2.381.
- [17] Guzman, R, Lucey, JR, Bower, RG. The fundamental relations of elliptical galaxies. *Mon. Not. R. Astron. Soc.* **265** (1993) 731–746.
- [18] Disney MJ, Romano JD, Garcia-Appadoo DA, West AA, Dalcanton JJ, Cortese L. Galaxies appear simpler than expected. *Nature* **455** (2008) 1082–1084. doi:10.1038/nature07366.
- [19] Fraix-Burnet D, D'Onofrio M, Marziani P. Maximum parsimony analysis of the effect of the environment on the evolution of galaxies. *Astronomy and Astrophysics* **630** (2019) A63. doi:10.1051/0004-6361/201935604.
- [20] Sandage, A. The Classification of Galaxies: Early History and Ongoing Developments. *Ann. Rev. Astron. Astrophys.* **43** (2005) 581–624. doi:10.1146/annurev.astro.43.112904.104839.
- [21] Abazajian K, Adelman-McCarthy J, Agüeros M, Allam S, et al. The First Data Release of the Sloan Digital Sky Survey. *The Astronomical Journal* **126** (2003) 2081–2086. doi:10.1086/378165.
- [22] Bacon R, Copin Y, Monnet G, Miller BW, Allington-Smith JR, Bureau M, et al. The SAURON project - I. The panoramic integral-field spectrograph. *Mon. Not. R. Astron. Soc.* **326** (2001) 23–35. doi:10.1046/j.1365-8711.2001.04612.x.
- [23] Fasano G, Marmo C, Varela J, D'Onofrio M, Poggianti BM, Moles M, et al. WINGS: a Wide-field Nearby Galaxy-cluster Survey. I. Optical imaging. *Astronomy and Astrophysics* **445** (2006) 805–817. doi:10.1051/0004-6361:20053816.
- [24] Cappellari M, Emsellem E, Krajnović D, McDermid RM, Scott N, Verdoes Kleijn GA, et al. The ATLAS^{3D} project - I. A volume-limited sample of 260 nearby early-type galaxies: science goals and selection criteria. *Mon. Not. R. Astron. Soc.* **413** (2011) 813–836. doi:10.1111/j.1365-2966.2010.18174.x.

- [25] Sánchez SF, Kennicutt RC, Gil de Paz A, van de Ven G, Vílchez JM, Wisotzki L, et al. CALIFA, the Calar Alto Legacy Integral Field Area survey. I. Survey presentation. *AAp* **538** (2012) A8. doi:10.1051/0004-6361/201117353.
- [26] Croom SM, Lawrence JS, Bland-Hawthorn J, Bryant JJ, Fogarty L, Richards S, et al. The Sydney-AAO Multi-object Integral field spectrograph. *Mon. Not. R. Astron. Soc.* **421** (2012) 872–893. doi:10.1111/j.1365-2966.2011.20365.x.
- [27] Bundy K. MaNGA: Mapping Nearby Galaxies at Apache Point Observatory. *American Astronomical Society Meeting Abstracts #225* (2015), *American Astronomical Society Meeting Abstracts*, vol. 225, 143.29.
- [28] Tully RB, Fisher JR. Reprint of 1977A&A....54..661T. A new method of determining distance to galaxies. *Astronomy and Astrophysics* **500** (1977) 105–117.
- [29] Courteau S, Dutton AA, van den Bosch FC, MacArthur LA, Dekel A, McIntosh DH, et al. Scaling Relations of Spiral Galaxies. *The Astrophysical Journal* **671** (2007) 203–225. doi:10.1086/522193.
- [30] Djorgovski S, Davis M. Fundamental Properties of Elliptical Galaxies. *The Astrophysical Journal* **313** (1987) 59. doi:10.1086/164948.
- [31] Dressler A, Lynden-Bell D, Burstein D, Davies RL, Faber SM, Terlevich R, et al. Spectroscopy and Photometry of Elliptical Galaxies. I. New Distance Estimator. *The Astrophysical Journal* **313** (1987) 42. doi:10.1086/164947.
- [32] Bernardi M, Sheth RK, Annis J, Burles S, Eisenstein DJ, Finkbeiner DP, et al. Early-Type Galaxies in the Sloan Digital Sky Survey. III. The Fundamental Plane. *The Astronomical Journal* **125** (2003) 1866–1881. doi:10.1086/367794.
- [33] Cappellari M, Bacon R, Bureau M, Damen MC, Davies RL, de Zeeuw PT, et al. The SAURON project - IV. The mass-to-light ratio, the virial mass estimator and the Fundamental Plane of elliptical and lenticular galaxies. *Mon. Not. R. Astron. Soc.* **366** (2006) 1126–1150. doi:10.1111/j.1365-2966.2005.09981.x.
- [34] La Barbera F, Busarello G, Merluzzi P, de la Rosa IG, Coppola G, Haines CP. The SDSS-UKIDSS Fundamental Plane of Early-Type Galaxies. *The Astrophysical Journal* **689** (2008) 913–918. doi:10.1086/592769.
- [35] Magorrian J, Tremaine S, Richstone D, Bender R, Bower G, Dressler A, et al. The Demography of Massive Dark Objects in Galaxy Centers. *The Astronomical Journal* **115** (1998) 2285–2305. doi:10.1086/300353.
- [36] Chiosi C, D'Onofrio M, Merlin E, Piovan L, Marziani P. The parallelism between galaxy clusters and early-type galaxies: III. The Mass-Radius Relationship. *arXiv e-prints* (2019) arXiv:1908.08808.
- [37] D'Onofrio M, Chiosi C, Sciarratta M, Marziani P. The parallelism between galaxy clusters and early-type galaxies. II. Clues on the origin of the scaling relations. *Astronomy and Astrophysics* **641** (2020) A94. doi:10.1051/0004-6361/202038221.
- [38] Dekel A, Birnboim Y. Galaxy bimodality due to cold flows and shock heating. *Mon. Not. R. Astron. Soc.* **368** (2006) 2–20. doi:10.1111/j.1365-2966.2006.10145.x.
- [39] McDonald M, Courteau S, Tully RB. Bulge-disc decompositions and structural bimodality of Ursa Major cluster spiral galaxies. *Mon. Not. R. Astron. Soc.* **393** (2009) 628–640. doi:10.1111/j.1365-2966.2008.14239.x.
- [40] Fall SM, Romanowsky AJ. Angular Momentum and Galaxy Formation Revisited: Effects of Variable Mass-to-light Ratios. *The Astrophysical Journal Lett.* **769** (2013) L26. doi:10.1088/2041-8205/769/2/L26.

- [41] Obreschkow D, Glazebrook K. Fundamental Mass-Spin-Morphology Relation Of Spiral Galaxies. *The Astrophysical Journal* **784** (2014) 26. doi:10.1088/0004-637X/784/1/26.
- [42] Dutton AA, Conroy C, van den Bosch FC, Simard L, Mendel JT, Courteau S, et al. Dark halo response and the stellar initial mass function in early-type and late-type galaxies. *Mon. Not. R. Astron. Soc.* **416** (2011) 322–345. doi:10.1111/j.1365-2966.2011.19038.x.
- [43] Cappellari M, McDermid RM, Alatalo K, Blitz L, Bois M, Bournaud F, et al. Systematic variation of the stellar initial mass function in early-type galaxies. *Nature* **484** (2012) 485–488. doi:10.1038/nature10972.
- [44] Smith RJ. Variations in the initial mass function in early-type galaxies: a critical comparison between dynamical and spectroscopic results. *Mon. Not. R. Astron. Soc.* **443** (2014) L69–L73. doi:10.1093/mnras/lu082.
- [45] Rodríguez-Puebla A, Avila-Reese V, Yang X, Foucaud S, Drory N, Jing YP. The Stellar-to-Halo Mass Relation of Local Galaxies Segregates by Color. *The Astrophysical Journal* **799** (2015) 130. doi:10.1088/0004-637X/799/2/130.
- [46] Courteau S. Deep r-Band Photometry for Northern Spiral Galaxies. *The Astrophysical Journal Suppl.* **103** (1996) 363. doi:10.1086/192281.
- [47] Courteau S. Optical Rotation Curves and Linewidths for Tully-Fisher Applications. *The Astronomical Journal* **114** (1997) 2402. doi:10.1086/118656.
- [48] Mocz P, Green A, Malacari M, Glazebrook K. The Tully-Fisher relation for 25 000 Sloan Digital Sky Survey galaxies as a function of environment. *Mon. Not. R. Astron. Soc.* **425** (2012) 296–310. doi:10.1111/j.1365-2966.2012.21458.x.
- [49] Avila-Reese V, Zavala J, Firmani C, Hernández-Toledo HM. On the Baryonic, Stellar, and Luminous Scaling Relations of Disk Galaxies. *The Astronomical Journal* **136** (2008) 1340–1360. doi:10.1088/0004-6256/136/3/1340.
- [50] Hall M, Courteau S, Dutton AA, McDonald M, Zhu Y. An investigation of Sloan Digital Sky Survey imaging data and multiband scaling relations of spiral galaxies. *Mon. Not. R. Astron. Soc.* **425** (2012) 2741–2765. doi:10.1111/j.1365-2966.2012.21290.x.
- [51] Willick JA, Courteau S, Faber SM, Burstein D, Dekel A, Strauss MA. Homogeneous Velocity-Distance Data for Peculiar Velocity Analysis. III. The Mark III Catalog of Galaxy Peculiar Velocities. *Astrophysical Journal Suppl.* **109** (1997) 333–366. doi:10.1086/312983.
- [52] Fernández Lorenzo M, Cepa J, Bongiovanni A, Pérez García AM, Ederoclite A, Lara-López MA, et al. Evolution of the fundamental plane of $0.2 < z < 1.2$ early-type galaxies in the EGS. *Astronomy and Astrophysics* **526** (2011) A72. doi:10.1051/0004-6361/201015368.
- [53] Miller SH, Bundy K, Sullivan M, Ellis RS, Treu T. The Assembly History of Disk Galaxies. I. The Tully-Fisher Relation to $z \sim 1.3$ from Deep Exposures with DEIMOS. *The Astrophysical Journal* **741** (2011) 115. doi:10.1088/0004-637X/741/2/115.
- [54] Aaronson M, Bothun G, Mould J, Huchra J, Schommer RA, Cornell ME. A Distance Scale from the Infrared Magnitude/ $H\alpha$ Velocity-Width Relation. V. Distance Moduli to 10 Galaxy Clusters, and Positive Detection of Bulk Supercluster Motion toward the Microwave Anisotropy. *The Astrophysical Journal* **302** (1986) 536. doi:10.1086/164014.
- [55] D'Onofrio M, Fasano G, Varela J, Bettoni D, Moles M, Kjærgaard P, et al. The Fundamental Plane of Early-Type Galaxies in Nearby Clusters from the WINGS Database. *The Astrophysical Journal* **685** (2008) 875–896. doi:10.1086/591143.
- [56] Tollerud EJ, Bullock JS, Graves GJ, Wolf J. From Galaxy Clusters to Ultra-faint Dwarf Spheroidals: A Fundamental Curve Connecting Dispersion-supported Galaxies to Their Dark Matter Halos. *The*

- Astrophysical Journal* **726** (2011) 108. doi:10.1088/0004-637X/726/2/108.
- [57] Falcón-Barroso J, van de Ven G, Peletier RF, Bureau M, Jeong H, Bacon R, et al. The SAURON project - XIX. Optical and near-infrared scaling relations of nearby elliptical, lenticular and Sa galaxies. *Mon. Not. R. Astron. Soc.* **417** (2011) 1787–1816. doi:10.1111/j.1365-2966.2011.19372.x.
- [58] Cappellari M. Effect of Environment on Galaxies' Mass-Size Distribution: Unveiling the Transition from outside-in to inside-out Evolution. *The Astrophysical Journal Lett.* **778** (2013) L2. doi:10.1088/2041-8205/778/1/L2.
- [59] Woo J, Courteau S, Dekel A. Scaling relations and the fundamental line of the local group dwarf galaxies. *Mon. Not. R. Astron. Soc.* **390** (2008) 1453–1469. doi:10.1111/j.1365-2966.2008.13770.x.
- [60] Kassin SA, Weiner BJ, Faber SM, Gardner JP, Willmer CNA, Coil AL, et al. The Epoch of Disk Settling: $z \sim 1$ to Now. *The Astrophysical Journal* **758** (2012) 106. doi:10.1088/0004-637X/758/2/106.
- [61] Peebles PJE. Origin of the Angular Momentum of Galaxies. *The Astrophysical Journal* **155** (1969) 393. doi:10.1086/149876.
- [62] Fall SM. Galaxy formation - Some comparisons between theory and observation. Athanassoula E, editor, *Internal Kinematics and Dynamics of Galaxies* (1983), *IAU Symposium*, vol. 100, 391–398.
- [63] Lagos CdP, Theuns T, Stevens ARH, Cortese L, Padilla ND, Davis TA, et al. Angular momentum evolution of galaxies in EAGLE. *Mon. Not. R. Astron. Soc.* **464** (2017) 3850–3870. doi:10.1093/mnras/stw2610.
- [64] Ferrarese L, Côté P, Dalla Bontà E, Peng EW, Merritt D, Jordán A, et al. A Fundamental Relation between Compact Stellar Nuclei, Supermassive Black Holes, and Their Host Galaxies. *The Astrophysical Journal Lett.* **644** (2006) L21–L24. doi:10.1086/505388.
- [65] Desmond H, Wechsler RH. The Faber-Jackson relation and Fundamental Plane from halo abundance matching. *Mon. Not. R. Astron. Soc.* **465** (2017) 820–833. doi:10.1093/mnras/stw2804.
- [66] Ouellette NNQ, Courteau S, Holtzman JA, Dutton AA, Cappellari M, Dalcanton JJ, et al. The Spectroscopy and H-band Imaging of Virgo Cluster Galaxies (SHIVir) Survey: Scaling Relations and the Stellar-to-total Mass Relation. *The Astrophysical Journal* **843** (2017) 74. doi:10.3847/1538-4357/aa74b1.
- [67] Kormendy J, Richstone D. Inward Bound—The Search For Supermassive Black Holes In Galactic Nuclei. *Ann. Rev. Astron. Astrophys.* **33** (1995) 581. doi:10.1146/annurev.aa.33.090195.003053.
- [68] Häring N, Rix HW. On the Black Hole Mass-Bulge Mass Relation. *The Astrophysical Journal Lett.* **604** (2004) L89–L92. doi:10.1086/383567.
- [69] Ferrarese L, Merritt D. A Fundamental Relation between Supermassive Black Holes and Their Host Galaxies. *The Astrophysical Journal Lett.* **539** (2000) L9–L12. doi:10.1086/312838.
- [70] Gebhardt K, Bender R, Bower G, Dressler A, Faber SM, Filippenko AV, et al. A Relationship between Nuclear Black Hole Mass and Galaxy Velocity Dispersion. *The Astrophysical Journal Lett.* **539** (2000) L13–L16. doi:10.1086/312840.
- [71] Graham AW, Erwin P, Caon N, Trujillo I. A Correlation between Galaxy Light Concentration and Supermassive Black Hole Mass. *The Astrophysical Journal Lett.* **563** (2001) L11–L14. doi:10.1086/338500.
- [72] Ferrarese L. Beyond the Bulge: A Fundamental Relation between Supermassive Black Holes and Dark Matter Halos. *The Astrophysical Journal* **578** (2002) 90–97. doi:10.1086/342308.
- [73] Nigoche-Netro A, Aguerri JAL, Lagos P, Ruelas-Mayorga A, Sánchez LJ, Machado A. The Faber-Jackson relation for early-type galaxies: dependence on the magnitude range. *Astronomy and Astrophysics* **516** (2010) A96. doi:10.1051/0004-6361/200912719.

- [74] Cappellari M, McDermid RM, Alatalo K, Blitz L, Bois M, Bournaud F, et al. The ATLAS^{3D} project - XX. Mass-size and mass- σ distributions of early-type galaxies: bulge fraction drives kinematics, mass-to-light ratio, molecular gas fraction and stellar initial mass function. *Mon. Not. R. Astron. Soc.* **432** (2013) 1862–1893. doi:10.1093/mnras/stt644.
- [75] Choi J, Conroy C, Moustakas J, Graves GJ, Holden BP, Brodwin M, et al. The Assembly Histories of Quiescent Galaxies since $z = 0.7$ from Absorption Line Spectroscopy. *The Astrophysical Journal* **792** (2014) 95. doi:10.1088/0004-637X/792/2/95.
- [76] D’Onofrio M, Chiosi C. A tomography of the $\log(\langle I \rangle_e) - \log(R_e)$ plane. *arXiv e-prints* (2020) arXiv:2011.07315.
- [77] Nigoche-Netro A, Aguerri JAL, Lagos P, Ruelas-Mayorga A, Sánchez LJ, Muñoz-Tuñón C, et al. The intrinsic dispersion in the Faber-Jackson relation for early-type galaxies as function of the mass and redshift. *Astronomy and Astrophysics* **534** (2011) A61. doi:10.1051/0004-6361/201016360.
- [78] Liu FS, Mao S, Meng XM. Star formation activities in early-type brightest cluster galaxies. *Mon. Not. R. Astron. Soc.* **423** (2012) 422–436. doi:10.1111/j.1365-2966.2012.20886.x.
- [79] Oliva-Altamirano P, Brough S, Jimmy KV Tran, Couch WJ, McDermid RM, Lidman C, et al. The accretion histories of brightest cluster galaxies from their stellar population gradients. *Mon. Not. R. Astron. Soc.* **449** (2015) 3347–3359. doi:10.1093/mnras/stv475.
- [80] Schmidt M. The Rate of Star Formation. *The Astrophysical Journal* **129** (1959) 243. doi:10.1086/146614.
- [81] Vogelsberger M, Genel S, Springel V, Torrey P, Sijacki D, Xu D, et al. Properties of galaxies reproduced by a hydrodynamic simulation. *Nature* **509** (2014) 177–182. doi:10.1038/nature13316.
- [82] Moretti A, Poggianti BM, Fasano G, Bettoni D, D’Onofrio M, Fritz J, et al. WINGS Data Release: a database of galaxies in nearby clusters. *Astronomy and Astrophysics* **564** (2014) A138. doi:10.1051/0004-6361/201323098.
- [83] Verheijen MAW. *The Ursa Major Cluster of Galaxies: TF-relations and dark matter*. Ph.D. thesis, - (1997).
- [84] Tully RB, Pierce MJ, Huang JS, Saunders W, Verheijen MAW, Witchalls PL. Global Extinction in Spiral Galaxies. *The Astronomical Journal* **115** (1998) 2264–2272. doi:10.1086/300379.
- [85] Cole S, Lacey CG, Baugh CM, Frenk CS. Hierarchical galaxy formation. *Mon. Not. R. Astron. Soc.* **319** (2000) 168–204. doi:10.1046/j.1365-8711.2000.03879.x.
- [86] Navarro JF, Steinmetz M. Dark Halo and Disk Galaxy Scaling Laws in Hierarchical Universes. *The Astrophysical Journal* **538** (2000) 477–488. doi:10.1086/309175.
- [87] van den Bosch FC. Constraints on Galaxy Formation from the Tully-Fisher Relation. Combes F, Mamon GA, Charmandaris V, editors, *Dynamics of Galaxies: from the Early Universe to the Present* (2000), *Astronomical Society of the Pacific Conference Series*, vol. 197, 179.
- [88] Kassin SA, Weiner BJ, Faber SM, Koo DC, Lotz JM, Diemand J, et al. The Stellar Mass Tully-Fisher Relation to $z = 1.2$ from AEGIS. *The Astrophysical Journal Lett.* **660** (2007) L35–L38. doi:10.1086/517932.
- [89] Rampazzo R, Plana H, Amram P, Bagarotto S, Boulesteix J, Rosado M. Two-dimensional warm gas kinematics in interacting galaxy systems. *Mon. Not. R. Astron. Soc.* **356** (2005) 1177–1190. doi:10.1111/j.1365-2966.2004.08549.x.
- [90] Kronberger T, Kapferer W, Schindler S, Ziegler BL. 2D velocity fields of simulated interacting disc galaxies. *Astronomy and Astrophysics* **473** (2007) 761–770. doi:10.1051/0004-6361:20077696.
- [91] Covington MD, Kassin SA, Dutton AA, Weiner BJ, Cox TJ, Jonsson P, et al. Evolution of the Stellar Mass Tully-Fisher Relation in Disk Galaxy Merger Simulations. *The Astrophysical Journal* **710**

- (2010) 279–288. doi:10.1088/0004-637X/710/1/279.
- [92] De Rossi ME, Tissera PB, Pedrosa SE. Fingerprints of the hierarchical building-up of the structure on the gas kinematics of galaxies. *Astronomy and Astrophysics* **546** (2012) A52. doi:10.1051/0004-6361/201118409.
- [93] Brooks AM, Governato F, Quinn T, Brook CB, Wadsley J. The Role of Cold Flows in the Assembly of Galaxy Disks. *The Astrophysical Journal* **694** (2009) 396–410. doi:10.1088/0004-637X/694/1/396.
- [94] Elmegreen BG, Burkert A. Accretion-Driven Turbulence and the Transition to Global Instability in Young Galaxy Disks. *The Astrophysical Journal* **712** (2010) 294–302. doi:10.1088/0004-637X/712/1/294.
- [95] Mac Low MM, Ferrara A. Starburst-driven Mass Loss from Dwarf Galaxies: Efficiency and Metal Ejection. *The Astrophysical Journal* **513** (1999) 142–155. doi:10.1086/306832.
- [96] Lehnert MD, Nesvadba NPH, Le Tiran L, Di Matteo P, van Driel W, Douglas LS, et al. Physical Conditions in the Interstellar Medium of Intensely Star-Forming Galaxies at Redshift-2. *The Astrophysical Journal* **699** (2009) 1660–1678. doi:10.1088/0004-637X/699/2/1660.
- [97] Verheijen MAW. The Ursa Major Cluster of Galaxies. V. H I Rotation Curve Shapes and the Tully-Fisher Relations. *The Astrophysical Journal* **563** (2001) 694–715. doi:10.1086/323887.
- [98] Bekeraïté S, Walcher CJ, Falcón-Barroso J, Garcia Lorenzo B, Lyubenova M, Sánchez SF, et al. Space density distribution of galaxies in the absolute magnitude - rotation velocity plane: a volume-complete Tully-Fisher relation from CALIFA stellar kinematics. *Astronomy and Astrophysics* **593** (2016) A114. doi:10.1051/0004-6361/201527405.
- [99] Ponomareva AA, Verheijen MAW, Peletier RF, Bosma A. The multiwavelength Tully-Fisher relation with spatially resolved H I kinematics. *Mon. Not. R. Astron. Soc.* **469** (2017) 2387–2400. doi:10.1093/mnras/stx1018.
- [100] Persic M, Salucci P, Stel F. The universal rotation curve of spiral galaxies — I. The dark matter connection. *Mon. Not. R. Astron. Soc.* **281** (1996) 27–47. doi:10.1093/mnras/278.1.27.
- [101] Giovanelli R, Haynes MP, da Costa LN, Freudling W, Salzer JJ, Wegner G. The Tully-Fisher Relation and H_0 . *The Astrophysical Journal Lett.* **477** (1997) L1–L4. doi:10.1086/310521.
- [102] Cole S, Aragon-Salamanca A, Frenk CS, Navarro JF, Zepf SE. A recipe for galaxy formation. *Mon. Not. R. Astron. Soc.* **271** (1994) 781–806. doi:10.1093/mnras/271.4.781.
- [103] Eisenstein DJ, Loeb A. Can the Tully-Fisher Relation Be the Result of Initial Conditions? *The Astrophysical Journal* **459** (1996) 432. doi:10.1086/176905.
- [104] Mo HJ, Mao S, White SDM. The formation of galactic discs. *Mon. Not. R. Astron. Soc.* **295** (1998) 319–336. doi:10.1046/j.1365-8711.1998.01227.x.
- [105] Avila-Reese V, Firmani C, Hernández X. On the Formation and Evolution of Disk Galaxies: Cosmological Initial Conditions and the Gravitational Collapse. *The Astrophysical Journal* **505** (1998) 37–49. doi:10.1086/306136.
- [106] Courteau S, Rix HW. Maximal Disks and the Tully-Fisher Relation. *The Astrophysical Journal* **513** (1999) 561–571. doi:10.1086/306872.
- [107] Swaters RA, Madore BF, Trewella M. High-Resolution Rotation Curves of Low Surface Brightness Galaxies. *The Astrophysical Journal Lett.* **531** (2000) L107–L110. doi:10.1086/312540.
- [108] van Albada TS, Bahcall JN, Begeman K, Sancisi R. Distribution of dark matter in the spiral galaxy NGC 3198. *The Astrophysical Journal* **295** (1985) 305–313. doi:10.1086/163375.
- [109] Swaters R. Dark Matter in Late-type Dwarf Galaxies. Merritt DR, Valluri M, Sellwood JA, editors, *Galaxy Dynamics - A Rutgers Symposium* (1999), *Astronomical Society of the Pacific Conference Series*, vol. 182, 369.

- [110] Silk J. Feedback, Disk Self-Regulation, and Galaxy Formation. *ApJ* **481** (1997) 703–709. doi:10.1086/304073.
- [111] Heavens AF, Jimenez R. The role of star formation in the Tully-Fisher law. *MNRAS* **305** (1999) 770–774. doi:10.1046/j.1365-8711.1999.02448.x.
- [112] Steinmetz M, Navarro JF. The Cosmological Origin of the Tully-Fisher Relation. *ApJ* **513** (1999) 555–560. doi:10.1086/306904.
- [113] Koda J, Sofue Y, Wada K. On the Origin of the Tully-Fisher Relation. *ApJ* **532** (2000) 214–220. doi:10.1086/308579.
- [114] McGaugh SS, Schombert JM, Bothun GD, de Blok WJG. The Baryonic Tully-Fisher Relation. *The Astrophysical Journal Lett.* **533** (2000) L99–L102. doi:10.1086/312628.
- [115] Bell EF, de Jong RS. Stellar Mass-to-Light Ratios and the Tully-Fisher Relation. *The Astrophysical Journal* **550** (2001) 212–229. doi:10.1086/319728.
- [116] Pizagno J, Prada F, Weinberg DH, Rix HW, Harbeck D, Grebel EK, et al. Dark Matter and Stellar Mass in the Luminous Regions of Disk Galaxies. *The Astrophysical Journal* **633** (2005) 844–856. doi:10.1086/491614.
- [117] Kassin SA, de Jong RS, Weiner BJ. Dark and Baryonic Matter in Bright Spiral Galaxies. II. Radial Distributions for 34 Galaxies. *The Astrophysical Journal* **643** (2006) 804–824. doi:10.1086/502959.
- [118] Masters KL, Springob CM, Huchra JP. 2MTF. I. The Tully-Fisher Relation in the Two Micron All Sky Survey J, H, and K Bands. *The Astronomical Journal* **135** (2008) 1738–1748. doi:10.1088/0004-6256/135/5/1738.
- [119] Reyes R, Mandelbaum R, Gunn JE, Pizagno J, Lackner CN. Calibrated Tully-Fisher relations for improved estimates of disc rotation velocities. *Mon. Not. R. Astron. Soc.* **417** (2011) 2347–2386. doi:10.1111/j.1365-2966.2011.19415.x.
- [120] Schulz E. Scaling Relations of Mass, Velocity, and Radius for Disk Galaxies. *The Astrophysical Journal* **836** (2017) 151. doi:10.3847/1538-4357/aa5b88.
- [121] Somerville RS, Primack JR. Semi-analytic modelling of galaxy formation: the local Universe. *Mon. Not. R. Astron. Soc.* **310** (1999) 1087–1110. doi:10.1046/j.1365-8711.1999.03032.x.
- [122] Dutton AA, van den Bosch FC, Dekel A, Courteau S. A Revised Model for the Formation of Disk Galaxies: Low Spin and Dark Halo Expansion. *The Astrophysical Journal* **654** (2007) 27–52. doi:10.1086/509314.
- [123] Dutton AA. The baryonic Tully-Fisher relation and galactic outflows. *Mon. Not. R. Astron. Soc.* **424** (2012) 3123–3128. doi:10.1111/j.1365-2966.2012.21469.x.
- [124] Di Cintio A, Lelli F. The mass discrepancy acceleration relation in a Λ CDM context. *Mon. Not. R. Astron. Soc.* **456** (2016) L127–L131. doi:10.1093/mnras/rlv185.
- [125] McGaugh SS. The Mass Discrepancy-Acceleration Relation: Disk Mass and the Dark Matter Distribution. *The Astrophysical Journal* **609** (2004) 652–666. doi:10.1086/421338.
- [126] Bullock JS, Dekel A, Kolatt TS, Primack JR, Somerville RS. Strong Evolution in the Luminosity-Velocity Relation at $Z \lesssim 1$? *The Astrophysical Journal* **550** (2001) 21–25. doi:10.1086/319738.
- [127] Noordermeer E, Verheijen MAW. The high-mass end of the Tully-Fisher relation. *Mon. Not. R. Astron. Soc.* **381** (2007) 1463–1472. doi:10.1111/j.1365-2966.2007.12369.x.
- [128] Übler H, Förster Schreiber NM, Genzel R, Wisnioski E, Wuyts S, Lang P, et al. The Evolution of the Tully-Fisher Relation between $z \sim 2.3$ and $z \sim 0.9$ with KMOS^{3D}. *ApJ* **842** (2017) 121. doi:10.3847/1538-4357/aa7558.
- [129] Weiner BJ, Willmer CNA, Faber SM, Harker J, Kassin SA, Phillips AC, et al. A Survey of Galaxy Kinematics to $z \sim 1$ in the TKRS/GOODS-N Field. II. Evolution in the Tully-Fisher Relation. *The*

- Astrophysical Journal* **653** (2006) 1049–1069. doi:10.1086/508922.
- [130] Aquino-Ortíz E, Valenzuela O, Sánchez SF, Hernández-Toledo H, Ávila-Reese V, van de Ven G, et al. Kinematic scaling relations of CALIFA galaxies: A dynamical mass proxy for galaxies across the Hubble sequence. *Mon. Not. R. Astron. Soc.* **479** (2018) 2133–2146. doi:10.1093/mnras/sty1522.
- [131] Lemoine-Busserolle M, Lamareille F. 2D kinematics and physical properties of $1.0 < z < 1.5$ star-forming galaxies. *Mon. Not. R. Astron. Soc.* **402** (2010) 2291–2307. doi:10.1111/j.1365-2966.2009.16082.x.
- [132] Puech M, Hammer F, Flores H, Delgado-Serrano R, Rodrigues M, Yang Y. The baryonic content and Tully-Fisher relation at $z \sim 0.6$. *Astronomy and Astrophysics* **510** (2010) A68. doi:10.1051/0004-6361/200912081.
- [133] Catinella B, Kauffmann G, Schiminovich D, Lemonias J, Scannapieco C, Wang J, et al. The GALEX Arecibo SDSS Survey - IV. Baryonic mass-velocity-size relations of massive galaxies. *Mon. Not. R. Astron. Soc.* **420** (2012) 1959–1976. doi:10.1111/j.1365-2966.2011.20012.x.
- [134] Vergani D, Epinat B, Contini T, Tasca L, Tresse L, Amram P, et al. MASSIV: Mass Assembly Survey with SINFONI in VVDS. IV. Fundamental relations of star-forming galaxies at $1 < z < 1.6$. *Astronomy and Astrophysics* **546** (2012) A118. doi:10.1051/0004-6361/201118453.
- [135] Cortese L, Fogarty LMR, Ho IT, Bekki K, Bland-Hawthorn J, Colless M, et al. The SAMI Galaxy Survey: Toward a Unified Dynamical Scaling Relation for Galaxies of All Types. *The Astrophysical Journal Lett.* **795** (2014) L37. doi:10.1088/2041-8205/795/2/L37.
- [136] Wisnioski E, Förster Schreiber NM, Wuyts S, Wuyts E, Bandara K, Wilman D, et al. The KMOS^{3D} Survey: Design, First Results, and the Evolution of Galaxy Kinematics from $0.7 < z < 2.7$. *The Astrophysical Journal* **799** (2015) 209. doi:10.1088/0004-637X/799/2/209.
- [137] Roberts MS, Haynes MP. Physical Parameters along the Hubble Sequence. *Ann. Rev. Astron. Astrophys.* **32** (1994) 115–152. doi:10.1146/annurev.aa.32.090194.000555.
- [138] Bothwell MS, Kennicutt RC, Lee JC. On the interstellar medium and star formation demographics of galaxies in the local universe. *Mon. Not. R. Astron. Soc.* **400** (2009) 154–167. doi:10.1111/j.1365-2966.2009.15471.x.
- [139] Mahajan S, Drinkwater MJ, Driver S, Kelvin LS, Hopkins AM, Baldry I, et al. Galaxy And Mass Assembly (GAMA): the unimodal nature of the dwarf galaxy population. *Mon. Not. R. Astron. Soc.* **446** (2015) 2967–2984. doi:10.1093/mnras/stu2009.
- [140] Mortlock A, Conselice CJ, Hartley WG, Ownsworth JR, Lani C, Bluck AFL, et al. The redshift and mass dependence on the formation of the Hubble sequence at $z < 1$ from CANDELS/UDS. *Mon. Not. R. Astron. Soc.* **433** (2013) 1185–1201. doi:10.1093/mnras/stt793.
- [141] Bershady MA, Verheijen MAW, Swaters RA, Andersen DR, Westfall KB, Martinsson T. The DiskMass Survey. I. Overview. *The Astrophysical Journal* **716** (2010) 198–233. doi:10.1088/0004-637X/716/1/198.
- [142] Swaters RA, van Albada TS, van der Hulst JM, Sancisi R. The Westerbork HI survey of spiral and irregular galaxies. I. HI imaging of late-type dwarf galaxies. *Astronomy and Astrophysics* **390** (2002) 829–861. doi:10.1051/0004-6361:20011755.
- [143] McConnachie AW. The Observed Properties of Dwarf Galaxies in and around the Local Group. *The Astronomical Journal* **144** (2012) 4. doi:10.1088/0004-6256/144/1/4.
- [144] Barton EJ, Geller MJ, Bromley BC, van Zee L, Kenyon SJ. The Tully-Fisher Relation as a Measure of Luminosity Evolution: A Low-Redshift Baseline for Evolving Galaxies. *The Astronomical Journal* **121** (2001) 625–648. doi:10.1086/318759.

- [145] Kannappan SJ, Fabricant DG, Franx M. Physical Sources of Scatter in the Tully-Fisher Relation. *The Astronomical Journal* **123** (2002) 2358–2386. doi:10.1086/339972.
- [146] Vaduvescu O, McCall ML, Richer MG, Fingerhut RL. Infrared Properties of Star-forming Dwarf Galaxies. I. Dwarf Irregular Galaxies in the Local Volume. *The Astronomical Journal* **130** (2005) 1593–1626. doi:10.1086/444498.
- [147] Kirby EN, Bullock JS, Boylan-Kolchin M, Kaplinghat M, Cohen JG. The dynamics of isolated Local Group galaxies. *Mon. Not. R. Astron. Soc.* **439** (2014) 1015–1027. doi:10.1093/mnras/stu025.
- [148] van Zee L, Skillman ED, Salzer JJ. Neutral Gas Distributions and Kinematics of Five Blue Compact Dwarf Galaxies. *The Astronomical Journal* **116** (1998) 1186–1204. doi:10.1086/300510.
- [149] Cannon JM, Dohm-Palmer RC, Skillman ED, Bomans DJ, Cote S, Miller BW. Extended Star Formation in the Dwarf Starburst/W-R Galaxy NGC 625. Lamers HJGLM, Smith LJ, Nota A, editors, *The Formation and Evolution of Massive Young Star Clusters* (2004), *Astronomical Society of the Pacific Conference Series*, vol. 322, 207.
- [150] Lelli F, Verheijen M, Fraternali F. The triggering of starbursts in low-mass galaxies. *Mon. Not. R. Astron. Soc.* **445** (2014) 1694–1712. doi:10.1093/mnras/stu1804.
- [151] Capaccioli M, Caon N, D'Onofrio M. Families of galaxies in the μ_e - R_e plane. *Mon. Not. R. Astron. Soc.* **259** (1992) 323–327. doi:10.1093/mnras/259.2.323.
- [152] Capaccioli M, Caon N, D'Onofrio M. The $(\log r_e, \mu_e)$ Plane of Hot Stellar Systems. *European Southern Observatory Conference and Workshop Proceedings* (1993), *European Southern Observatory Conference and Workshop Proceedings*, vol. 45, 43.
- [153] Kormendy J, Fisher DB, Cornell ME, Bender R. Structure and Formation of Elliptical and Spheroidal Galaxies. *The Astrophysical Journal Suppl.* **182** (2009) 216–309. doi:10.1088/0067-0049/182/1/216.
- [154] Tolstoy E, Hill V, Tosi M. Star-Formation Histories, Abundances, and Kinematics of Dwarf Galaxies in the Local Group. *Ann. Rev. Astron. Astrophys.* **47** (2009) 371–425. doi:10.1146/annurev-astro-082708-101650.
- [155] Somerville RS, Davé R. Physical Models of Galaxy Formation in a Cosmological Framework. *Ann. Rev. Astron. Astrophys.* **53** (2015) 51–113. doi:10.1146/annurev-astro-082812-140951.
- [156] Kormendy J. *Elliptical Galaxies and Bulges of Disc Galaxies: Summary of Progress and Outstanding Issues*, *Astrophysics and Space Science Library*, vol. 418 (2016), 431. doi:10.1007/978-3-319-19378-6_16.
- [157] Caldwell N. Structure and stellar content of dwarf elliptical galaxies. *The Astronomical Journal* **88** (1983) 804–812. doi:10.1086/113367.
- [158] Bothun GD, Mould JR, Caldwell N, MacGillivray HT. Comparative photometric parameters of dwarf irregular and elliptical galaxies in the Virgo cluster : two different classes of dwarf galaxies ? *The Astronomical Journal* **92** (1986) 1007–1019. doi:10.1086/114231.
- [159] Caldwell N, Bothun GD. Dwarf Elliptical Galaxies in the Fornax Cluster. II. Their Structure and Stellar Populations. *The Astronomical Journal* **94** (1987) 1126. doi:10.1086/114550.
- [160] Graham AW. R_e . I. Understanding galaxy sizes, associated luminosity densities, and the artificial division of the early-type galaxy population. *Pub. of the Astron. Soc. of Australia* **36** (2019) e035. doi:10.1017/pasa.2019.23.
- [161] Sersic JL. *Atlas de Galaxias Australes* (1968).
- [162] Caon N, Capaccioli M, D'Onofrio M. On the shape of the light profiles of early-type galaxies. *Mon. Not. R. Astron. Soc.* **265** (1993) 1013–1021. doi:10.1093/mnras/265.4.1013.
- [163] D'Onofrio M, Capaccioli M, Caon N. On the shape of the light profiles of early-type galaxies - II. The (D_n/A_e) - μ_e diagram. *Mon. Not. R. Astron. Soc.* **271** (1994) 523–529. doi:10.1093/mnras/

271.3.523.

- [164] Graham AW, Guzmán R. HST Photometry of Dwarf Elliptical Galaxies in Coma, and an Explanation for the Alleged Structural Dichotomy between Dwarf and Bright Elliptical Galaxies. *The Astronomical Journal* **125** (2003) 2936–2950. doi:10.1086/374992.
- [165] Morgan WW. A Preliminary Classification of the Forms of Galaxies According to Their Stellar Population. *Pub. of the Astron. Soc. of Pacific* **70** (1958) 364. doi:10.1086/127243.
- [166] Fraser CW. Concentration indices of galaxies. *The Observatory* **92** (1972) 51–54.
- [167] Kent SM. CCD surface photometry of field galaxies. II. Bulge/disk decompositions. *The Astrophysical Journal Suppl.* **59** (1985) 115–159. doi:10.1086/191066.
- [168] Ichikawa SI, Wakamatsu KI, Okamura S. Surface Photometry of Dwarf Elliptical Galaxies in the Virgo Cluster. *The Astrophysical Journal Suppl.* **60** (1986) 475. doi:10.1086/191094.
- [169] Young CK, Currie MJ. A new extragalactic distance indicator based on the surface brightness profiles of dwarf elliptical galaxies. *Mon. Not. R. Astron. Soc.* **268** (1994) L11–L15. doi:10.1093/mnras/268.1.L11.
- [170] Graham A, Lauer TR, Colless M, Postman M. Brightest Cluster Galaxy Profile Shapes. *The Astrophysical Journal* **465** (1996) 534. doi:10.1086/177440.
- [171] Jerjen H, Binggeli B, Freeman KC. Surface BR Photometry of Newly Discovered Dwarf Elliptical Galaxies in the Nearby Sculptor and Centaurus A Groups. *The Astronomical Journal* **119** (2000) 593–608. doi:10.1086/301216.
- [172] Ferrarese L, Côté P, Jordán A, Peng EW, Blakeslee JP, Piatek S, et al. The ACS Virgo Cluster Survey. VI. Isophotal Analysis and the Structure of Early-Type Galaxies. *The Astrophysical Journal Suppl.* **164** (2006) 334–434. doi:10.1086/501350.
- [173] Eggen OJ, Lynden-Bell D, Sandage AR. Evidence from the motions of old stars that the Galaxy collapsed. *The Astrophysical Journal* **136** (1962) 748. doi:10.1086/147433.
- [174] Toomre A, Toomre J. Galactic Bridges and Tails. *The Astrophysical Journal* **178** (1972) 623–666. doi:10.1086/151823.
- [175] Searle L, Zinn R. Composition of halo clusters and the formation of the galactic halo. *The Astrophysical Journal* **225** (1978) 357–379. doi:10.1086/156499.
- [176] Schweizer F. Colliding and Merging Galaxies. *Science* **231** (1986) 227–234. doi:10.1126/science.231.4735.227.
- [177] Bernardi M, Roche N, Shankar F, Sheth RK. Evidence of major dry mergers at $M^* > 2 \times 10^{11} M_{\odot}$ from curvature in early-type galaxy scaling relations? *Mon. Not. R. Astron. Soc.* **412** (2011) L6–L10. doi:10.1111/j.1745-3933.2010.00982.x.
- [178] Graham AW. How Non-Linear Scaling Relations Unify Dwarf and Giant Elliptical Galaxies. Koleva M, Prugniel P, Vauglin I, editors, *EAS Publications Series* (2011), *EAS Publications Series*, vol. 48, 231–236. doi:10.1051/eas/1148052.
- [179] Shankar F, Marulli F, Bernardi M, Mei S, Meert A, Vikram V. Size evolution of spheroids in a hierarchical Universe. *Mon. Not. R. Astron. Soc.* **428** (2013) 109–128. doi:10.1093/mnras/sts001.
- [180] Graham AW. *Elliptical and Disk Galaxy Structure and Modern Scaling Laws*, vol. 6 (2013), 91. doi:10.1007/978-94-007-5609-0_2.
- [181] Bernardi M, Meert A, Vikram V, Huertas-Company M, Mei S, Shankar F, et al. Systematic effects on the size-luminosity relations of early- and late-type galaxies: dependence on model fitting and morphology. *Mon. Not. R. Astron. Soc.* **443** (2014) 874–897. doi:10.1093/mnras/stu1106.
- [182] Agertz O, Kravtsov AV. The Impact of Stellar Feedback on the Structure, Size, and Morphology of Galaxies in Milky-Way-sized Dark Matter Halos. *The Astrophysical Journal* **824** (2016) 79.

doi:10.3847/0004-637X/824/2/79.

- [183] Kuchner U, Ziegler B, Verdugo M, Bamford S, Häußler B. The effects of the cluster environment on the galaxy mass-size relation in MACS J1206.2-0847. *Astronomy and Astrophysics* **604** (2017) A54. doi:10.1051/0004-6361/201630252.
- [184] Huang KH, Fall SM, Ferguson HC, van der Wel A, Grogin N, Koekemoer A, et al. Relations between the Sizes of Galaxies and Their Dark Matter Halos at Redshifts $0 < z < 3$. *The Astrophysical Journal* **838** (2017) 6. doi:10.3847/1538-4357/aa62a6.
- [185] Somerville RS, Behroozi P, Pandya V, Dekel A, Faber SM, Fontana A, et al. The relationship between galaxy and dark matter halo size from $z \sim 3$ to the present. *Mon. Not. R. Astron. Soc.* **473** (2018) 2714–2736. doi:10.1093/mnras/stx2040.
- [186] Genel S, Nelson D, Pillepich A, Springel V, Pakmor R, Weinberger R, et al. The size evolution of star-forming and quenched galaxies in the IllustrisTNG simulation. *Mon. Not. R. Astron. Soc.* **474** (2018) 3976–3996. doi:10.1093/mnras/stx3078.
- [187] Sánchez Almeida J. Analysis of the galaxy size versus stellar mass relation. *Mon. Not. R. Astron. Soc.* **495** (2020) 78–89. doi:10.1093/mnras/staa1108.
- [188] Terrazas BA, Bell EF, Pillepich A, Nelson D, Somerville RS, Genel S, et al. The relationship between black hole mass and galaxy properties: examining the black hole feedback model in IllustrisTNG. *Mon. Not. R. Astron. Soc.* **493** (2020) 1888–1906. doi:10.1093/mnras/staa374.
- [189] Valentinuzzi T, Fritz J, Poggianti BM, Cava A, Bettoni D, Fasano G, et al. Superdense Massive Galaxies in Wings Local Clusters. *The Astrophysical Journal* **712** (2010) 226–237. doi:10.1088/0004-637X/712/1/226.
- [190] Cappellari M. Dynamical Mass Determinations and Scaling Relations of Early-Type Galaxies. Cappellari M, Courteau S, editors, *Galaxy Masses as Constraints of Formation Models* (2015), vol. 311, 20–30. doi:10.1017/S1743921315003324.
- [191] Shen S, Mo HJ, White SDM, Blanton MR, Kauffmann G, Voges W, et al. The size distribution of galaxies in the Sloan Digital Sky Survey. *Mon. Not. R. Astron.* **343** (2003) 978–994. doi:10.1046/j.1365-8711.2003.06740.x.
- [192] Mathews WG, Baker JC. Galactic Winds. *The Astrophysical Journal* **170** (1971) 241. doi:10.1086/151208.
- [193] Saito M. Note: On the Formation of Dwarf Spheroidal Galaxies. *Publications of the Astronomical Society of Japan* **31** (1979) 193–198.
- [194] Dekel A, Silk J. The Origin of Dwarf Galaxies, Cold Dark Matter, and Biased Galaxy Formation. *The Astrophysical Journal* **303** (1986) 39. doi:10.1086/164050.
- [195] Mateo ML. Dwarf Galaxies of the Local Group. *Ann. Rev. Astron. Astrophys.* **36** (1998) 435–506. doi:10.1146/annurev.astro.36.1.435.
- [196] Tremonti CA, Heckman TM, Kauffmann G, Brinchmann J, Charlot S, White SDM, et al. The Origin of the Mass-Metallicity Relation: Insights from 53,000 Star-forming Galaxies in the Sloan Digital Sky Survey. *The Astrophysical Journal* **613** (2004) 898–913. doi:10.1086/423264.
- [197] Veilleux S, Cecil G, Bland-Hawthorn J. Galactic Winds. *Ann. Rev. Astron. Astrophys.* **43** (2005) 769–826. doi:10.1146/annurev.astro.43.072103.150610.
- [198] Damjanov I, McCarthy PJ, Abraham RG, Glazebrook K, Yan H, Mentuch E, et al. Red Nuggets at $z \sim 1.5$: Compact Passive Galaxies and the Formation of the Kormendy Relation. *The Astrophysical Journal* **695** (2009) 101–115. doi:10.1088/0004-637X/695/1/101.
- [199] Daddi E, Renzini A, Pirzkal N, Cimatti A, Malhotra S, Stiavelli M, et al. Passively Evolving Early-Type Galaxies at $1.4 < z < 2.5$ in the Hubble Ultra Deep Field. *The Astrophysical Journal* **626**

- (2005) 680–697. doi:10.1086/430104.
- [200] Kriek M, van Dokkum PG, Franx M, Quadri R, Gawiser E, Herrera D, et al. Spectroscopic Identification of Massive Galaxies at $z \sim 2.3$ with Strongly Suppressed Star Formation. *The Astrophysical Journal Lett.* **649** (2006) L71–L74. doi:10.1086/508371.
- [201] Trujillo I, Feulner G, Goranova Y, Hopp U, Longhetti M, Saracco P, et al. Extremely compact massive galaxies at $z \sim 1.4$. *Mon. Not. R. Astron. Soc.* **373** (2006) L36–L40. doi:10.1111/j.1745-3933.2006.00238.x.
- [202] van Dokkum PG, Franx M, Kriek M, Holden B, Illingworth GD, Magee D, et al. Confirmation of the Remarkable Compactness of Massive Quiescent Galaxies at $z \sim 2.3$: Early-Type Galaxies Did not Form in a Simple Monolithic Collapse. *The Astrophysical Journal Lett.* **677** (2008) L5. doi:10.1086/587874.
- [203] van Dokkum PG, Whitaker KE, Brammer G, Franx M, Kriek M, Labbé I, et al. The Growth of Massive Galaxies Since $z = 2$. *The Astrophysical Journal* **709** (2010) 1018–1041. doi:10.1088/0004-637X/709/2/1018.
- [204] Saracco P, Longhetti M, Gargiulo A. Constraining the star formation and the assembly histories of normal and compact early-type galaxies at $1 < z < 2$. *Mon. Not. R. Astron. Soc.* **412** (2011) 2707–2716. doi:10.1111/j.1365-2966.2010.18098.x.
- [205] Mancini C, Matute I, Cimatti A, Daddi E, Dickinson M, Rodighiero G, et al. Searching for massive galaxies at $z \geq 3.5$ in GOODS-North. *Astronomy and Astrophysics* **500** (2009) 705–723. doi:10.1051/0004-6361/200810630.
- [206] van der Wel A, Rix HW, Wuyts S, McGrath EJ, Koekemoer AM, Bell EF, et al. The Majority of Compact Massive Galaxies at $z \sim 2$ are Disk Dominated. *The Astrophysical Journal* **730** (2011) 38. doi:10.1088/0004-637X/730/1/38.
- [207] Graham AW, Dullo BT, Savorgnan GAD. Hiding in Plain Sight: An Abundance of Compact Massive Spheroids in the Local Universe. *The Astrophysical Journal* **804** (2015) 32. doi:10.1088/0004-637X/804/1/32.
- [208] de la Rosa IG, La Barbera F, Ferreras I, Sánchez Almeida J, Dalla Vecchia C, Martínez-Valpuesta I, et al. The fate of high-redshift massive compact galaxies. *Mon. Not. R. Astron. Soc.* **457** (2016) 1916–1930. doi:10.1093/mnras/stw130.
- [209] Caldwell N. The ages of the disks of the S0 galaxies. *The Astrophysical Journal* **268** (1983) 90–101. doi:10.1086/160932.
- [210] Morganti R, de Zeeuw PT, Oosterloo TA, McDermid RM, Krajnović D, Cappellari M, et al. Neutral hydrogen in nearby elliptical and lenticular galaxies: the continuing formation of early-type galaxies. *Mon. Not. R. Astron. Soc.* **371** (2006) 157–169. doi:10.1111/j.1365-2966.2006.10681.x.
- [211] Sancisi R, Fraternali F, Oosterloo T, van der Hulst T. Cold gas accretion in galaxies. *The Astronomy and Astrophysics Review* **15** (2008) 189–223. doi:10.1007/s00159-008-0010-0.
- [212] Stewart KR, Bullock JS, Wechsler RH, Maller AH. Gas-rich Mergers in LCDM: Disk Survivability and the Baryonic Assembly of Galaxies. *The Astrophysical Journal* **702** (2009) 307–317. doi:10.1088/0004-637X/702/1/307.
- [213] Pichon C, Pogosyan D, Kimm T, Slyz A, Devriendt J, Dubois Y. Rigging dark haloes: why is hierarchical galaxy formation consistent with the inside-out build-up of thin discs? *Mon. Not. R. Astron. Soc.* **418** (2011) 2493–2507. doi:10.1111/j.1365-2966.2011.19640.x.
- [214] Moffett AJ, Kannappan SJ, Baker AJ, Laine S. Extended Ultraviolet Disks and Ultraviolet-bright Disks in Low-mass E/S0 Galaxies. *The Astrophysical Journal* **745** (2012) 34. doi:10.1088/0004-637X/745/1/34.

- [215] Stark DV, Kannappan SJ, Wei LH, Baker AJ, Leroy AK, Eckert KD, et al. The Fueling Diagram: Linking Galaxy Molecular-to-atomic Gas Ratios to Interactions and Accretion. *The Astrophysical Journal* **769** (2013) 82. doi:10.1088/0004-637X/769/1/82.
- [216] Kleiner D, Pimblet KA, Jones DH, Koribalski BS, Serra P. Evidence for H I replenishment in massive galaxies through gas accretion from the cosmic web. *Mon. Not. R. Astron. Soc.* **466** (2017) 4692–4710. doi:10.1093/mnras/stw3328.
- [217] Feldmann R, Hopkins PF, Quataert E, Faucher-Giguère CA, Kereš D. The formation of massive, quiescent galaxies at cosmic noon. *Mon. Not. R. Astron. Soc.* **458** (2016) L14–L18. doi:10.1093/mnras/slw014.
- [218] Cowie LL, Songaila A, Hu EM, Cohen JG. New Insight on Galaxy Formation and Evolution From Keck Spectroscopy of the Hawaii Deep Fields. *The Astronomical Journal* **112** (1996) 839. doi:10.1086/118058.
- [219] Graham AW, Janz J, Penny SJ, Chilingarian IV, Ciambur BC, Forbes DA, et al. Implications for the Origin of Early-type Dwarf Galaxies: A Detailed Look at the Isolated Rotating Early-type Dwarf Galaxy LEDA 2108986 (CG 611), Ramifications for the Fundamental Plane's $\{S\}$ - $\{K\}$ Kinematic Scaling, and the Spin-Ellipticity Diagram. *The Astrophysical Journal* **840** (2017) 68. doi:10.3847/1538-4357/aa6e56.
- [220] Biermann P, Shapiro SL. Puffing up flat galaxies by rapid stripping and the formation of S0 galaxies. *The Astrophysical Journal Lett.* **230** (1979) L33–L35. doi:10.1086/182956.
- [221] Ragone-Figueroa C, Granato GL. Puffing up early-type galaxies by baryonic mass loss: numerical experiments. *Mon. Not. R. Astron. Soc.* **414** (2011) 3690–3698. doi:10.1111/j.1365-2966.2011.18670.x.
- [222] Guo Y, McIntosh DH, Mo HJ, Katz N, Van Den Bosch FC, Weinberg M, et al. Structural properties of central galaxies in groups and clusters. *Mon. Not. R. Astron. Soc.* **398** (2009) 1129–1149. doi:10.1111/j.1365-2966.2009.15223.x.
- [223] Burstein D, Bender R, Faber S, Nolthenius R. Global Relationships Among the Physical Properties of Stellar Systems. *The Astronomical Journal* **114** (1997) 1365. doi:10.1086/118570.
- [224] Bernardi M, Shankar F, Hyde JB, Mei S, Marulli F, Sheth RK. Galaxy luminosities, stellar masses, sizes, velocity dispersions as a function of morphological type. *Mon. Not. R. Astron. Soc.* **404** (2010) 2087–2122. doi:10.1111/j.1365-2966.2010.16425.x.
- [225] Chiosi C, Merlin E, Piovan L. The Origin of the Mass-Radius Relation of Early-Type Galaxies. *arXiv e-prints* (2012).
- [226] Chiosi C, Carraro G. Formation and evolution of elliptical galaxies. *Mon. Not. R. Astron. Soc.* **335** (2002) 335–357. doi:10.1046/j.1365-8711.2002.05590.x.
- [227] Merlin E, Chiosi C, Piovan L, Grassi T, Buonomo U, La Barbera F. Formation and evolution of early-type galaxies - III. Dependence of the star formation history on the total mass and initial overdensity. *Mon. Not. R. Astron. Soc.* **427** (2012) 1530–1554. doi:10.1111/j.1365-2966.2012.21965.x.
- [228] Lukić Z, Heitmann K, Habib S, Bashinsky S, Ricker PM. The Halo Mass Function: High-Redshift Evolution and Universality. *The Astrophysical Journal* **671** (2007) 1160–1181. doi:10.1086/523083.
- [229] Fan L, Lapi A, Bressan A, Bernardi M, De Zotti G, Danese L. Cosmic Evolution of Size and Velocity Dispersion for Early-type Galaxies. *The Astrophysical Journal* **718** (2010) 1460–1475. doi:10.1088/0004-637X/718/2/1460.
- [230] Bryan GL, Norman ML. Statistical Properties of X-Ray Clusters: Analytic and Numerical Comparisons. *The Astrophysical Journal* **495** (1998) 80. doi:10.1086/305262.

- [231] Springel V, White SDM, Jenkins A, Frenk CS, Yoshida N, Gao L, et al. Simulations of the formation, evolution and clustering of galaxies and quasars. *Nature* **435** (2005) 629–636. doi:10.1038/nature03597.
- [232] Angulo RE, Springel V, White SDM, Jenkins A, Baugh CM, Frenk CS. Scaling relations for galaxy clusters in the Millennium-XXL simulation. *Mon. Not. R. Astron. Soc.* **426** (2012) 2046–2062. doi:10.1111/j.1365-2966.2012.21830.x.
- [233] Behroozi PS, Wechsler RH, Wu HY, Busha MT, Klypin AA, Primack JR. Gravitationally Consistent Halo Catalogs and Merger Trees for Precision Cosmology. *The Astrophysical Journal* **763** (2013) 18. doi:10.1088/0004-637X/763/1/18.
- [234] Warren S, Lawrence A, Almaini O, Cirasuolo M, Foucaud S, Hambly N, et al. Early Science Results from the UKIDSS ESO Public Survey. *The Messenger* **126** (2006) 7–10.
- [235] van Dokkum PG, Whitaker KE, Brammer G, Franx M, Kriek M, Labbé I, et al. The Growth of Massive Galaxies Since $z = 2$. *The Astrophysical Journal* **709** (2010) 1018–1041. doi:10.1088/0004-637X/709/2/1018.
- [236] Gott JR III, Rees MJ. A theory of galaxy formation and clustering. *Astronomy and Astrophysics* **45** (1975) 365–376.
- [237] Faber SM. Galaxy Formation and Cosmology. G Setti & L Van Hove, editor, *Large-Scale Structure of the Universe* (1984), 187.
- [238] Buonomo F. *Formation and Evolution of Early Type Galaxies in the Hierarchical Scheme with NB-TSPH simulations*. Ph.D. thesis, Astronomy Department, Padova University, Vicolo Osservatorio 2, 35122 Padova, Italy (2000).
- [239] Merlin E, Chiosi C. Formation and evolution of early-type galaxies. II. Models with quasi-cosmological initial conditions. *Astronomy and Astrophysics* **457** (2006) 437–453. doi:10.1051/0004-6361:20054486.
- [240] Merlin E, Chiosi C. Simulating the formation and evolution of galaxies: multi-phase description of the interstellar medium, star formation, and energy feedback. *Astronomy and Astrophysics* **473** (2007) 733–745. doi:10.1051/0004-6361:20077465.
- [241] Merlin E, Buonomo U, Grassi T, Piovan L, Chiosi C. EvoL: the new Padova Tree-SPH parallel code for cosmological simulations. I. Basic code: gravity and hydrodynamics. *Astronomy and Astrophysics* **513** (2010) A36. doi:10.1051/0004-6361/200913514.
- [242] Press WH, Schechter P. Formation of Galaxies and Clusters of Galaxies by Self-Similar Gravitational Condensation. *The Astrophysical Journal* **187** (1974) 425–438. doi:10.1086/152650.
- [243] Saulder C, Mieske S, Zeilinger WW, Chilingarian I. Calibrating the fundamental plane with SDSS DR8 data. *Astronomy and Astrophysics* **557** (2013) A21. doi:10.1051/0004-6361/201321466.
- [244] Misgeld I, Hilker M. Families of dynamically hot stellar systems over 10 orders of magnitude in mass. *Mon. Not. R. Astron. Soc.* **414** (2011) 3699–3710. doi:10.1111/j.1365-2966.2011.18669.x.
- [245] D'Onofrio M, Bettoni D, Bindoni D, Cava A, Fasano G, Marziani P, et al. The fundamental plane of clusters of galaxies. *Astronomische Nachrichten* **334** (2013) 373. doi:10.1002/asna.201211860.
- [246] Ciotti L. Stellar systems following the $R1/m$ luminosity law. *Astronomy and Astrophysics* **249** (1991) 99–106.
- [247] Renzini A, Ciotti L. Transverse Dissections of the Fundamental Planes of Elliptical Galaxies and Clusters of Galaxies. *The Astrophysical Journal Lett.* **416** (1993) L49. doi:10.1086/187068.
- [248] Jorgensen I, Franx M, Kjaergaard P. The Fundamental Plane for cluster E and S0 galaxies. *Mon. Not. R. Astron. Soc.* **280** (1996) 167–185. doi:10.1093/mnras/280.1.167.

- [249] D'Onofrio M, Fasano G, Moretti A, Marziani P, Bindoni D, Fritz J, et al. The hybrid solution for the Fundamental Plane. *Mon. Not. R. Astron. Soc.* **435** (2013) 45–63. doi:10.1093/mnras/stt1278.
- [250] D'Onofrio M, Cariddi S, Chiosi C, Chiosi E, Marziani P. On the Origin of the Fundamental Plane and Faber-Jackson Relations: Implications for the Star Formation Problem. *The Astrophysical Journal* **838** (2017) 163. doi:10.3847/1538-4357/aa6540.
- [251] D'Onofrio M, Valentinuzzi T, Fasano G, Moretti A, Bettoni D, Poggianti B, et al. On the Connection Between Shape and Stellar Population in Early-type Galaxies. *The Astrophysical Journal Lett.* **727** (2011) L6. doi:10.1088/2041-8205/727/1/L6.
- [252] Treu T, Ellis RS, Liao TX, van Dokkum PG, Tozzi P, Coil A, et al. The Assembly History of Field Spheroidals: Evolution of Mass-to-Light Ratios and Signatures of Recent Star Formation. *The Astrophysical Journal* **633** (2005) 174–197. doi:10.1086/444585.
- [253] Holden BP, van der Wel A, Kelson DD, Franx M, Illingworth GD. M/L_B and Color Evolution for a Deep Sample of M^{sstarf} Cluster Galaxies at $z \sim 1$: The Formation Epoch and the Tilt of the Fundamental Plane. *The Astrophysical Journal* **724** (2010) 714–729. doi:10.1088/0004-637X/724/1/714.
- [254] Saglia RP, Sánchez-Blázquez P, Bender R, Simard L, Desai V, Aragón-Salamanca A, et al. The fundamental plane of EDisCS galaxies. The effect of size evolution. *Astronomy and Astrophysics* **524** (2010) A6. doi:10.1051/0004-6361/201014703.
- [255] van de Sande J, Kriek M, Franx M, Bezanson R, van Dokkum PG. The Fundamental Plane of Massive Quiescent Galaxies Out to $z \sim 2$. *The Astrophysical Journal* **793** (2014) L31. doi:10.1088/2041-8205/793/2/L31.
- [256] Beifiori A, Mendel JT, Chan JCC, Saglia RP, Bender R, Cappellari M, et al. The KMOS Cluster Survey (KCS). I. The Fundamental Plane and the Formation Ages of Cluster Galaxies at Redshift 1.4 $\leq z \leq 1.6$. *ApJ* **846** (2017) 120. doi:10.3847/1538-4357/aa8368.
- [257] Prichard LJ, Davies RL, Beifiori A, Chan JCC, Cappellari M, Houghton RCW, et al. The KMOS Cluster Survey (KCS). III. Fundamental Plane of Cluster Galaxies at $z \simeq 1.80$ in JKCS 041. *ApJ* **850** (2017) 203. doi:10.3847/1538-4357/aa96a6.
- [258] Mendel JT, Beifiori A, Saglia RP, Bender R, Brammer GB, Chan J, et al. The Kinematics of Massive Quiescent Galaxies at 1.4 $\leq z \leq 2.1$: Dark Matter Fractions, IMF Variation, and the Relation to Local Early-type Galaxies. *ApJ* **899** (2020) 87. doi:10.3847/1538-4357/ab9ffc.
- [259] di Serego Alighieri S, Vernet J, Cimatti A, Lanzoni B, Cassata P, Ciotti L, et al. The evolution of early-type galaxies at $z \sim 1$ from the K20 survey. *Astronomy and Astrophysics* **442** (2005) 125–136. doi:10.1051/0004-6361:20053168.
- [260] Jorgensen I, Chiboucas K. Stellar Populations and Evolution of Early-type Cluster Galaxies: Constraints from Optical Imaging and Spectroscopy of $z = 0.5-0.9$ Galaxy Clusters. *The Astronomical Journal* **145** (2013) 77. doi:10.1088/0004-6256/145/3/77.
- [261] Faber SM, Dressler A, Davies RL, Burstein D, Lynden Bell D, Terlevich R, et al. Global Scaling Relations for Elliptical Galaxies and Implications for Formation. Faber SM, editor, *Nearly Normal Galaxies. From the Planck Time to the Present* (1987), 175.
- [262] van Dokkum PG, Franx M. The Fundamental Plane in CL 0024 at $z = 0.4$: implications for the evolution of the mass-to-light ratio. *Mon. Not. R. Astron. Soc.* **281** (1996) 985–1000. doi:10.1093/mnras/281.3.985.
- [263] Bender R, Saglia RP, Ziegler B, Belloni P, Greggio L, Hopp U, et al. Exploring Cluster Elliptical Galaxies as Cosmological Standard Rods. *The Astrophysical Journal* **493** (1998) 529–535. doi:10.1086/305166.

- [264] Kelson DD, Illingworth GD, van Dokkum PG, Franx M. The Evolution of Early-Type Galaxies in Distant Clusters. III. M/L_V Ratios in the $z=0.33$ Cluster CL 1358+62. *The Astrophysical Journal* **531** (2000) 184–199. doi:10.1086/308440.
- [265] Gebhardt K, Faber SM, Koo DC, Im M, Simard L, Illingworth GD, et al. The DEEP Groth Strip Survey. IX. Evolution of the Fundamental Plane of Field Galaxies. *The Astrophysical Journal* **597** (2003) 239–262. doi:10.1086/378401.
- [266] Wuyts S, van Dokkum PG, Kelson DD, Franx M, Illingworth GD. The Detailed Fundamental Plane of Two High-Redshift Clusters: MS 2053-04 at $z=0.58$ and MS 1054-03 at $z=0.83$. *The Astrophysical Journal* **605** (2004) 677–688. doi:10.1086/381746.
- [267] Holden BP, van der Wel A, Franx M, Illingworth GD, Blakeslee JP, van Dokkum P, et al. The Fundamental Plane of Cluster Elliptical Galaxies at $z=1.25$. *The Astrophysical Journal Lett.* **620** (2005) L83–L86. doi:10.1086/428663.
- [268] Jorgensen I, Chiboucas K, Flint K, Bergmann M, Barr J, Davies R. The Fundamental Plane for $z = 0.8-0.9$ Cluster Galaxies. *ApJL* **639** (2006) L9–L12. doi:10.1086/501348.
- [269] van Dokkum PG, van der Marel RP. The Star Formation Epoch of the Most Massive Early-Type Galaxies. *The Astrophysical Journal* **655** (2007) 30–50. doi:10.1086/509633.
- [270] Toft S, Gallazzi A, Zirm A, Wold M, Zibetti S, Grillo C, et al. Deep Absorption Line Studies of Quiescent Galaxies at $z \sim 2$: The Dynamical-mass-Size Relation and First Constraints on the Fundamental Plane. *The Astrophysical Journal* **754** (2012) 3. doi:10.1088/0004-637X/754/1/3.
- [271] Bezanson R, van Dokkum PG, van de Sande J, Franx M, Leja J, Kriek M. Tight Correlations between Massive Galaxy Structural Properties and Dynamics: The Mass Fundamental Plane was in Place by $z \sim 2$. *The Astrophysical Journal Lett.* **779** (2013) L21. doi:10.1088/2041-8205/779/2/L21.
- [272] Saglia RP, Opitsch M, Erwin P, Thomas J, Beifiori A, Fabricius M, et al. The SINFONI Black Hole Survey: The Black Hole Fundamental Plane Revisited and the Paths of (Co)evolution of Supermassive Black Holes and Bulges. *ApJ* **818** (2016) 47. doi:10.3847/0004-637X/818/1/47.
- [273] Fritz A, Jorgensen I, Schiavon RP, Chiboucas K. The evolution of cluster early-type galaxies over the past 8 Gyr. *Astronomische Nachrichten* **330** (2009) 931. doi:10.1002/asna.200911266.
- [274] Trujillo I, Förster Schreiber NM, Rudnick G, Barden M, Franx M, Rix H, et al. Size Evolution of Galaxies Since $Z \sim 3$: COMBINING SDSS, GEMS and FIRES. *Astrophysics and Space Science Proceedings* **3** (2007) 481. doi:10.1007/978-1-4020-5573-7_83.
- [275] Newman S, Genzel R. Compact, Dispersion-dominated, Star-forming Galaxies at $z \sim 2$. *American Astronomical Society Meeting Abstracts #219* (2012), *American Astronomical Society Meeting Abstracts*, vol. 219, 441.19.
- [276] Houghton RCW, Davies RL, Dalla Bontà E, Masters R. Data and two-dimensional scaling relations for galaxies in Abell 1689: a hint of size evolution at $z \sim 0.2$. *Mon. Not. R. Astron. Soc.* **423** (2012) 256–283. doi:10.1111/j.1365-2966.2012.20842.x.
- [277] van der Wel A, Franx M, van Dokkum PG, Skelton RE, Momcheva IG, Whitaker KE, et al. 3D-HST+CANDELS: The Evolution of the Galaxy Size-Mass Distribution since $z = 3$. *The Astrophysical Journal* **788** (2014) 28. doi:10.1088/0004-637X/788/1/28.
- [278] Beifiori A, Thomas D, Maraston C, Steele O, Masters KL, Pforr J, et al. Redshift Evolution of the Dynamical Properties of Massive Galaxies from SDSS-III/BOSS. *The Astrophysical Journal* **789** (2014) 92. doi:10.1088/0004-637X/789/2/92.
- [279] Chan JCC, Beifiori A, Mendel JT, Saglia RP, Bender R, Fossati M, et al. Sizes, colour gradients and resolved stellar mass distributions for the massive cluster galaxies in XMMUJ2235-2557 at $z = 1.39$. *Mon. Not. R. Astron. Soc.* **458** (2016) 3181–3209. doi:10.1093/mnras/stw502.

- [280] Cappellari M, di Serego Alighieri S, Cimatti A, Daddi E, Renzini A, Kurk JD, et al. Dynamical Masses of Early-Type Galaxies at $z \sim 2$: Are they Truly Superdense? *The Astrophysical Journal Lett.* **704** (2009) L34–L39. doi:10.1088/0004-637X/704/1/L34.
- [281] Cenarro AJ, Trujillo I. Mild Velocity Dispersion Evolution of Spheroid-Like Massive Galaxies Since $z \sim 2$. *The Astrophysical Journal Lett.* **696** (2009) L43–L47. doi:10.1088/0004-637X/696/1/L43.
- [282] van Dokkum PG, Kriek M, Franx M. A high stellar velocity dispersion for a compact massive galaxy at redshift $z = 2.186$. *Nature* **460** (2009) 717–719. doi:10.1038/nature08220.
- [283] van de Sande J, Kriek M, Franx M, van Dokkum PG, Bezanson R, Bouwens RJ, et al. Stellar Kinematics of $z \sim 2$ Galaxies and the Inside-out Growth of Quiescent Galaxies. *The Astrophysical Journal* **771** (2013) 85. doi:10.1088/0004-637X/771/2/85.
- [284] Belli S, Newman AB, Ellis RS. Velocity Dispersions and Dynamical Masses for a Large Sample of Quiescent Galaxies at $z \lesssim 1$: Improved Measures of the Growth in Mass and Size. *The Astrophysical Journal* **783** (2014) 117. doi:10.1088/0004-637X/783/2/117.
- [285] Brammer GB, Whitaker KE, van Dokkum PG, Marchesini D, Franx M, Kriek M, et al. The Number Density and Mass Density of Star-forming and Quiescent Galaxies at $0.4 \lesssim z \lesssim 2.2$. *The Astrophysical Journal* **739** (2011) 24. doi:10.1088/0004-637X/739/1/24.
- [286] Patel S, Van Dokkum PG, Franx M, Quadri R, Muzzin A, Marchesini D, et al. HST/WFC3 Confirmation of the Inside-Out Growth of Massive Galaxies at $0 \lesssim z \lesssim 2$ and Identification of Their Star Forming Progenitors at $z \sim 3$. *American Astronomical Society Meeting Abstracts #221* (2013), *American Astronomical Society Meeting Abstracts*, vol. 221, 129.05.
- [287] Muzzin A, Marchesini D, Stefanon M, Franx M, McCracken HJ, Milvang-Jensen B, et al. The Evolution of the Stellar Mass Functions of Star-forming and Quiescent Galaxies to $z = 4$ from the COSMOS/UltraVISTA Survey. *The Astrophysical Journal* **777** (2013) 18. doi:10.1088/0004-637X/777/1/18.
- [288] Lani C, Almaini O, Hartley WG, Mortlock A, Häußler B, Chuter RW, et al. Evidence for a correlation between the sizes of quiescent galaxies and local environment to $z \sim 2$. *Mon. Not. R. Astron. Soc.* **435** (2013) 207–221. doi:10.1093/mnras/stt1275.
- [289] Strazzullo V, Gobat R, Daddi E, Onodera M, Carollo M, Dickinson M, et al. Galaxy Evolution in Overdense Environments at High Redshift: Passive Early-type Galaxies in a Cluster at $z \sim 2$. *The Astrophysical Journal* **772** (2013) 118. doi:10.1088/0004-637X/772/2/118.
- [290] Delaye L, Huertas-Company M, Mei S, Lidman C, Licitra R, Newman A, et al. Larger sizes of massive quiescent early-type galaxies in clusters than in the field at $0.8 \lesssim z \lesssim 1.5$. *Mon. Not. R. Astron. Soc.* **441** (2014) 203–223. doi:10.1093/mnras/stu496.
- [291] Saracco P, Casati A, Gargiulo A, Longhetti M, Lonoce I, Tamburri S, et al. Scaling relations of cluster elliptical galaxies at $z \sim 1.3$. Distinguishing luminosity and structural evolution. *Astronomy and Astrophysics* **567** (2014) A94. doi:10.1051/0004-6361/201423495.
- [292] Newman AB, Ellis RS, Andreon S, Treu T, Raichoor A, Trinchieri G. Spectroscopic Confirmation of the Rich $z = 1.80$ Galaxy Cluster JKCS 041 using the WFC3 Grism: Environmental Trends in the Ages and Structure of Quiescent Galaxies. *The Astrophysical Journal* **788** (2014) 51. doi:10.1088/0004-637X/788/1/51.
- [293] Huertas-Company M, Shankar F, Mei S, Bernardi M, Aguerri JAL, Meert A, et al. No Evidence for a Dependence of the Mass-Size Relation of Early-type Galaxies on Environment in the Local Universe. *The Astrophysical Journal* **779** (2013) 29. doi:10.1088/0004-637X/779/1/29.
- [294] Joachimi B, Singh S, Mandelbaum R. Detection of spatial correlations of Fundamental Plane residuals, and cosmological implications. *Mon. Not. R. Astron. Soc.* **454** (2015) 478–488. doi:10.

- 1093/mnras/stv1962.
- [295] Franx M, van Dokkum PG, Förster Schreiber NM, Wuyts S, Labbé I, Toft S. Structure and Star Formation in Galaxies out to $z = 3$: Evidence for Surface Density Dependent Evolution and Upsizing. *ApJ* **688** (2008) 770–788. doi:10.1086/592431.
- [296] Cimatti A, Nipoti C, Cassata P. Fast evolving size of early-type galaxies at $z \lesssim 2$ and the role of dissipationless (dry) merging. *MNRAS* **422** (2012) L62–L66. doi:10.1111/j.1745-3933.2012.01237.x.
- [297] Chuter RW, Almaini O, Hartley WG, McLure RJ, Dunlop JS, Foucaud S, et al. Galaxy environments in the UKIDSS Ultra Deep Survey. *MNRAS* **413** (2011) 1678–1686. doi:10.1111/j.1365-2966.2011.18241.x.
- [298] Nipoti C, Treu T, Leauthaud A, Bundy K, Newman AB, Auger MW. Size and velocity-dispersion evolution of early-type galaxies in a Λ cold dark matter universe. *MNRAS* **422** (2012) 1714–1731. doi:10.1111/j.1365-2966.2012.20749.x.
- [299] Cassata P, Giavalisco M, Williams CC, Guo Y, Lee B, Renzini A, et al. Constraining the Assembly of Normal and Compact Passively Evolving Galaxies from Redshift $z = 3$ to the Present with CANDELS. *ApJ* **775** (2013) 106. doi:10.1088/0004-637X/775/2/106.
- [300] Skibba RA, Sheth RK. A halo model of galaxy colours and clustering in the Sloan Digital Sky Survey. *MNRAS* **392** (2009) 1080–1091. doi:10.1111/j.1365-2966.2008.14007.x.
- [301] Muldrew SI, Croton DJ, Skibba RA, Pearce FR, Ann HB, Baldry IK, et al. Measures of galaxy environment - I. What is 'environment'? *MNRAS* **419** (2012) 2670–2682. doi:10.1111/j.1365-2966.2011.19922.x.
- [302] Hartley WG, Almaini O, Mortlock A, Conselice CJ, Grützbauch R, Simpson C, et al. Studying the emergence of the red sequence through galaxy clustering: host halo masses at $z \lesssim 2$. *MNRAS* **431** (2013) 3045–3059. doi:10.1093/mnras/stt383.
- [303] Kjaergaard P, Jorgensen I, Moles M. The Fundamental Plane and the Surface Brightness Test for the Expansion of the Universe. *The Astrophysical Journal* **418** (1993) 617. doi:10.1086/173421.
- [304] Pahre MA, Djorgovski SG, de Carvalho RR. A Tolman Surface Brightness Test for Universal Expansion and the Evolution of Elliptical Galaxies in Distant Clusters. *The Astrophysical Journal Lett.* **456** (1996) L79. doi:10.1086/309872.
- [305] Moles M, Campos A, Kjaergaard P, Fasano G, Bettoni D. On the Use of Scaling Relations for the Tolman Test. *The Astrophysical Journal Lett.* **495** (1998) L31–L34. doi:10.1086/311208.
- [306] Kelson DD, van Dokkum PG, Franx M, Illingworth GD, Fabricant D. Evolution of Early-Type Galaxies in Distant Clusters: The Fundamental Plane from Hubble Space Telescope Imaging and Keck Spectroscopy. *The Astrophysical Journal Lett.* **478** (1997) L13–L16. doi:10.1086/310545.
- [307] Ziegler BL, Saglia RP, Bender R, Belloni P, Greggio L, Seitz S. Probing early-type galaxy evolution with the Kormendy relation. *Astronomy and Astrophysics* **346** (1999) 13–32.
- [308] Jorgensen I, Franx M, Hjorth J, van Dokkum PG. The evolution of cluster E and S0 galaxies measured from the Fundamental Plane. *Mon. Not. R. Astron. Soc.* **308** (1999) 833–853. doi:10.1046/j.1365-8711.1999.02761.x.
- [309] Huff EM, Graves GJ. Magnificent Magnification: Exploiting the Other Half of the Lensing Signal. *The Astrophysical Journal Lett.* **780** (2014) L16. doi:10.1088/2041-8205/780/2/L16.
- [310] Springob CM, Magoulas C, Colless M, Mould J, Erdoğdu P, Jones DH, et al. The 6dF Galaxy Survey: peculiar velocity field and cosmography. *Mon. Not. R. Astron. Soc.* **445** (2014) 2677–2697. doi:10.1093/mnras/stu1743.
- [311] Lu S, Xu D, Wang Y, Mao S, Ge J, Springel V, et al. Redshift evolution of the Fundamental Plane relation in the IllustrisTNG simulation. *Mon. Not. R. Astron. Soc.* **492** (2020) 5930–5939.

doi:10.1093/mnras/staa173.

- [312] Hertzsprung E. Über die Sterne der Unterabteilungen c und ac nach der Spektralklassifikation von Antonia C. Maury. *Astronomische Nachrichten* **179** (1909) 373. doi:10.1002/asna.19081792402.
- [313] Russell HN. Relations Between the Spectra and Other Characteristics of the Stars. *Popular Astronomy* **22** (1914) 275–294.
- [314] Baade W. The Resolution of Messier 32, NGC 205, and the Central Region of the Andromeda Nebula. *The Astrophysical Journal* **100** (1944) 137. doi:10.1086/144650.
- [315] Sandage A. Observational Approach to Evolution. II. a Computed Luminosity Function for K0-K2 Stars from $M_{\{v\}} = +5$ to $M_{\{v\}} = -4.5$. *The Astrophysical Journal* **125** (1957) 435. doi:10.1086/146319.
- [316] Blaauw A. Empirical data and position in the Hertzsprung-Russell diagram for O and B-type stars. Greenstein JL, editor, *The Hertzsprung-Russell Diagram* (1959), vol. 10, 105.
- [317] Chester C, Roberts MS. Properties of Galaxies: color-magnitude diagram. *The Astronomical Journal* **69** (1964) 635. doi:10.1086/109339.
- [318] Chiosi C. On the colour magnitude diagram of galaxies. *Memorie della Società Astronomica Italiana* **38** (1967) 3.
- [319] Visvanathan N, Sandage A. The color - absolute magnitude relation for E and S0 galaxies. I. Calibration and tests for universality using Virgo and eight other nearby clusters. *The Astrophysical Journal* **216** (1977) 214–226. doi:10.1086/155464.
- [320] Sandage A, Visvanathan N. The color - absolute magnitude relation for E and S0 galaxies. II. New colors, magnitudes, and types for 405 galaxies. *The Astrophysical Journal* **223** (1978) 707–729. doi:10.1086/156305.
- [321] Bower RG, Lucey JR, Ellis RS. Precision photometry of early-type galaxies in the Coma and Virgo clusters : a test of the universality of the colour-magnitude relation - I. The data. *Mon. Not. R. Astron. Soc.* **254** (1992) 589–600. doi:10.1093/mnras/254.4.589.
- [322] Kodama T, Arimoto N, Barger AJ, Arag'on-Salamanca A. Evolution of the colour-magnitude relation of early-type galaxies in distant clusters. *Astronomy and Astrophysics* **334** (1998) 99–109.
- [323] Terlevich AI, Caldwell N, Bower RG. The colour-magnitude relation for galaxies in the Coma cluster. *Mon. Not. R. Astron. Soc.* **326** (2001) 1547–1562. doi:10.1111/j.1365-2966.2001.04702.x.
- [324] Bell EF, Wolf C, Meisenheimer K, Rix HW, Borch A, Dye S, et al. Nearly 5000 Distant Early-Type Galaxies in COMBO-17: A Red Sequence and Its Evolution since $z=1$. *The Astrophysical Journal* **608** (2004) 752–767. doi:10.1086/420778.
- [325] Cariddi S, D'Onofrio M, Fasano G, Poggianti BM, Moretti A, Gullieuszik M, et al. Characterization of Omega-WINGS galaxy clusters. I. Stellar light and mass profiles. *Astronomy and Astrophysics* **609** (2018) A133. doi:10.1051/0004-6361/201731605.
- [326] Sciarratta M, Chiosi C, D'Onofrio M, Cariddi S. Cosmological Interpretation of the Color-Magnitude Diagrams of Galaxy Clusters. *The Astrophysical Journal* **870** (2019) 70. doi:10.3847/1538-4357/aaf00d.
- [327] Tully RB, Mould JR, Aaronson M. A color-magnitude relation for spiral galaxies. *The Astrophysical Journal* **257** (1982) 527–537. doi:10.1086/160009.
- [328] Baldry IK, Glazebrook K, Brinkmann J, Ivezić Ž, Lupton RH, Nichol RC, et al. Quantifying the Bimodal Color-Magnitude Distribution of Galaxies. *The Astrophysical Journal* **600** (2004) 681–694. doi:10.1086/380092.
- [329] Butcher H, Oemler J A. The evolution of galaxies in clusters. II. The galaxy content of nearby clusters. *The Astrophysical Journal* **226** (1978) 559–565. doi:10.1086/156640.

- [330] Dressler A. Galaxy morphology in rich clusters: implications for the formation and evolution of galaxies. *The Astrophysical Journal* **236** (1980) 351–365. doi:10.1086/157753.
- [331] de Vaucouleurs G. Integrated Colors of Bright Galaxies in the u, b, V System. *The Astrophysical Journal Suppl.* **5** (1961) 233. doi:10.1086/190056.
- [332] Menci N, Fontana A, Giallongo E, Salimbeni S. Bimodal Color Distribution in Hierarchical Galaxy Formation. *The Astrophysical Journal* **632** (2005) 49–57. doi:10.1086/432788.
- [333] Blanton MR, Brinkmann J, Csabai I, Doi M, Eisenstein D, Fukugita M, et al. Estimating Fixed-Frame Galaxy Magnitudes in the Sloan Digital Sky Survey. *The Astronomical Journal* **125** (2003) 2348–2360. doi:10.1086/342935.
- [334] Lintott CJ, Schawinski K, Slosar A, Land K, Bamford S, Thomas D, et al. Galaxy Zoo: morphologies derived from visual inspection of galaxies from the Sloan Digital Sky Survey. *Mon. Not. R. Astron. Soc.* **389** (2008) 1179–1189. doi:10.1111/j.1365-2966.2008.13689.x.
- [335] Wong OI, Schawinski K, Kaviraj S, Masters KL, Nichol RC, Lintott C, et al. Galaxy Zoo: building the low-mass end of the red sequence with local post-starburst galaxies. *Mon. Not. R. Astron. Soc.* **420** (2012) 1684–1692. doi:10.1111/j.1365-2966.2011.20159.x.
- [336] Stott JP, Pimblett KA, Edge AC, Smith GP, Wardlow JL. The evolution of the red sequence slope in massive galaxy clusters. *Mon. Not. R. Astron. Soc.* **394** (2009) 2098–2108. doi:10.1111/j.1365-2966.2009.14477.x.
- [337] Head JTCG, Lucey JR, Hudson MJ, Smith RJ. Dissecting the red sequence: the bulge and disc colours of early-type galaxies in the Coma cluster. *Mon. Not. R. Astron. Soc.* **440** (2014) 1690–1711. doi:10.1093/mnras/stu325.
- [338] Boselli A, Gavazzi G. On the origin of the faint-end of the red sequence in high-density environments. *The Astronomy and Astrophysics Review* **22** (2014) 74. doi:10.1007/s00159-014-0074-y.
- [339] Roediger JC, Ferrarese L, Côté P, MacArthur LA, Sánchez-Janssen R, Blakeslee JP, et al. The Next Generation Virgo Cluster Survey (NGVS). XXIV. The Red Sequence to $\sim 10^6 L_{\odot}$ and Comparisons with Galaxy Formation Models. *The Astrophysical Journal* **836** (2017) 120. doi:10.3847/1538-4357/836/1/120.
- [340] Tinsley BM. Evolution of the Stars and Gas in Galaxies. *Fundamentals of Cosmic Physics* **5** (1980) 287–388.
- [341] Silk J, Mamon GA. The current status of galaxy formation. *Research in Astronomy and Astrophysics* **12** (2012) 917–946. doi:10.1088/1674-4527/12/8/004.
- [342] Baum WA. Population Inferences from Star Counts, Surface Brightness and Colors. *Publications of the Astronomical Society of the Pacific* **71** (1959) 106–117. doi:10.1086/127346.
- [343] Faber SM. The Chemical Composition of Old Stellar Populations. Tinsley BM, Larson DC Richard B Gehret, editors, *Evolution of Galaxies and Stellar Populations* (1977), 157.
- [344] Dressler A. Internal kinematics of galaxies in clusters. I. Velocity dispersions for elliptical galaxies in Coma and Virgo. *The Astrophysical Journal* **281** (1984) 512–524. doi:10.1086/162124.
- [345] Burstein D, Bender R, Faber SM, Nolthenius R. Towards understanding the physical properties of stellar systems. *Astrophysical Letters and Communications* **31** (1995) 95.
- [346] Gallazzi A, Charlot S, Brinchmann J, White SDM. Ages and metallicities of early-type galaxies in the Sloan Digital Sky Survey: new insight into the physical origin of the colour-magnitude and the $Mg_2-\sigma_V$ relations. *Mon. Not. R. Astron. Soc.* **370** (2006) 1106–1124. doi:10.1111/j.1365-2966.2006.10548.x.
- [347] Menci N, Rosati P, Gobat R, Strazzullo V, Rettura A, Mei S, et al. The Red Sequence of High-Redshift Clusters: A Comparison with Cosmological Galaxy Formation Models. *The Astrophysical*

- Journal* **685** (2008) 863–874. doi:10.1086/591016.
- [348] Valentinuzzi T, Poggianti BM, Fasano G, D'Onofrio M, Moretti A, Ramella M, et al. The red-sequence of 72 WINGS local galaxy clusters. *Astronomy and Astrophysics* **536** (2011) A34. doi:10.1051/0004-6361/201117522.
- [349] Gladders MD, López-Cruz O, Yee HKC, Kodama T. The Slope of the Cluster Elliptical Red Sequence: A Probe of Cluster Evolution. *The Astrophysical Journal* **501** (1998) 571–577. doi:10.1086/305858.
- [350] Tran KVH. A Keck Spectroscopic Study of MS-1054-03 ($z=0.83$): Forming the Red Sequence. Metcalfe N, Shanks T, editors, *Cosmic Frontiers* (2007), *Astronomical Society of the Pacific Conference Series*, vol. 379, 348.
- [351] Mei S, Holden BP, Blakeslee JP, Ford HC, Franx M, Homeier NL, et al. Evolution of the Color-Magnitude Relation in Galaxy Clusters at $z \sim 1$ from the ACS Intermediate Redshift Cluster Survey. *The Astrophysical Journal* **690** (2009) 42–68. doi:10.1088/0004-637X/690/1/42.
- [352] Larson RB. Effects of supernovae on the early evolution of galaxies. *Mon. Not. R. Astron. Soc.* **169** (1974) 229–246. doi:10.1093/mnras/169.2.229.
- [353] Arimoto N, Yoshii Y. Chemical and photometric properties of a galactic wind model for elliptical galaxies. *Astronomy and Astrophysics* **173** (1987) 23–38.
- [354] Tantalo R, Chiosi C, Bressan A, Fagotto F. Spectro-photometric evolution of elliptical galaxies. II. Models with infall. *Astronomy and Astrophysics* **311** (1996) 361–383.
- [355] Tantalo R, Chiosi C, Bressan A, Marigo P, Portinari L. Spectro-photometric evolution of elliptical galaxies. III. Infall models with gradients in mass density and star formation. *Astronomy and Astrophysics* **335** (1998) 823–846.
- [356] Kodama T, Arimoto N. Origin of the colour-magnitude relation of elliptical galaxies. *Astronomy and Astrophysics* **320** (1997) 41–53.
- [357] Chiosi C, Bressan A, Portinari L, Tantalo R. A new scenario of galaxy evolution under a universal Initial Mass Function. *Astronomy and Astrophysics* **339** (1998) 355–381.
- [358] White SDM, Frenk CS. Galaxy Formation through Hierarchical Clustering. *The Astrophysical Journal* **379** (1991) 52. doi:10.1086/170483.
- [359] Kauffmann G. The age of elliptical galaxies and bulges in a merger model. *Mon. Not. R. Astron. Soc.* **281** (1996) 487–492. doi:10.1093/mnras/281.2.487.
- [360] Kauffmann G, Charlot S. The K-band luminosity function at $z=1$: a powerful constraint on galaxy formation theory. *Mon. Not. R. Astron. Soc.* **297** (1998) L23–L28. doi:10.1046/j.1365-8711.1998.01708.x.
- [361] Nelson D, Pillepich A, Springel V, Weinberger R, Hernquist L, Pakmor R, et al. First results from the IllustrisTNG simulations: the galaxy colour bimodality. *Mon. Not. R. Astron. Soc.* **475** (2018) 624–647. doi:10.1093/mnras/stx3040.
- [362] Nelan JE, Smith RJ, Hudson MJ, Wegner GA, Lucey JR, Moore SAW, et al. NOAO Fundamental Plane Survey. II. Age and Metallicity along the Red Sequence from Line-Strength Data. *The Astrophysical Journal* **632** (2005) 137–156. doi:10.1086/431962.
- [363] Thomas D, Maraston C, Bender R, Mendes de Oliveira C. The Epochs of Early-Type Galaxy Formation as a Function of Environment. *The Astrophysical Journal* **621** (2005) 673–694. doi:10.1086/426932.
- [364] Tanaka M, Kodama T, Arimoto N, Okamura S, Umetsu K, Shimasaku K, et al. The build-up of the colour-magnitude relation as a function of environment. *Mon. Not. R. Astron. Soc.* **362** (2005) 268–288. doi:10.1111/j.1365-2966.2005.09300.x.

- [365] Willmer CNA, Faber SM, Koo DC, Weiner BJ, Newman JA, Coil AL, et al. The Deep Evolutionary Exploratory Probe 2 Galaxy Redshift Survey: The Galaxy Luminosity Function to $z \sim 1$. *The Astrophysical Journal* **647** (2006) 853–873. doi:10.1086/505455.
- [366] Cassata P, Cimatti A, Kurk J, Rodighiero G, Pozzetti L, Bolzonella M, et al. GMASS ultradeep spectroscopy of galaxies at $z \sim 2$. III. The emergence of the color bimodality at $z \sim 2$. *Astronomy and Astrophysics* **483** (2008) L39–L42. doi:10.1051/0004-6361/200809881.
- [367] Fontana A, Santini P, Grazian A, Pentericci L, Fiore F, Castellano M, et al. The fraction of quiescent massive galaxies in the early Universe. *Astronomy and Astrophysics* **501** (2009) 15–20. doi:10.1051/0004-6361/200911650.
- [368] Marchesini D, Muzzin A, Stefanon M, Franx M, Brammer GG, Marsan CZ, et al. The Progenitors of Local Ultra-massive Galaxies Across Cosmic Time: From Dusty Star-bursting to Quiescent Stellar Populations. *The Astrophysical Journal* **794** (2014) 65. doi:10.1088/0004-637X/794/1/65.
- [369] Ilbert O, Salvato M, Le Flocc'h E, Aussel H, Capak P, McCracken HJ, et al. Galaxy Stellar Mass Assembly Between $0.2 < z < 2$ from the S-COSMOS Survey. *The Astrophysical Journal* **709** (2010) 644–663. doi:10.1088/0004-637X/709/2/644.
- [370] Madau P, Dickinson M. Cosmic Star-Formation History. *Ann. Rev. Astron. Astrophys.* **52** (2014) 415–486. doi:10.1146/annurev-astro-081811-125615.
- [371] Katsianis A, Tescari E, Blanc G, Sargent M. The evolution of the star formation rate function and cosmic star formation rate density of galaxies at $z \sim 1-4$. *Mon. Not. R. Astron. Soc.* **464** (2017) 4977–4994. doi:10.1093/mnras/stw2680.
- [372] Pillepich A, Nelson D, Hernquist L, Springel V, Pakmor R, Torrey P, et al. First results from the IllustrisTNG simulations: the stellar mass content of groups and clusters of galaxies. *Mon. Not. R. Astron. Soc.* **475** (2018) 648–675. doi:10.1093/mnras/stx3112.
- [373] Worthey G. Comprehensive Stellar Population Models and the Disentanglement of Age and Metallicity Effects. *The Astrophysical Journal Suppl.* **95** (1994) 107. doi:10.1086/192096.
- [374] Thomas D, Maraston C. The impact of α /Fe enhanced stellar evolutionary tracks on the ages of elliptical galaxies. *Astronomy and Astrophysics* **401** (2003) 429–432. doi:10.1051/0004-6361:20030153.
- [375] Caldwell N, Rose JA, Concannon KD. Star Formation Histories of Early-Type Galaxies. I. Higher Order Balmer Lines as Age Indicators. *The Astronomical Journal* **125** (2003) 2891–2926. doi:10.1086/375308.
- [376] Smith RJ, Hudson MJ, Lucey JR, Nelan JE, Wegner GA. The NOAO Fundamental Plane Survey - III. Variations in the stellar populations of red-sequence galaxies from the cluster core to the virial radius. *Mon. Not. R. Astron. Soc.* **369** (2006) 1419–1436. doi:10.1111/j.1365-2966.2006.10393.x.
- [377] Schmidt M. The Rate of Star Formation. *The Astrophysical Journal* **129** (1959) 243. doi:10.1086/146614.
- [378] Schaye J, Dalla Vecchia C. On the relation between the Schmidt and Kennicutt-Schmidt star formation laws and its implications for numerical simulations. *Mon. Not. R. Astron. Soc.* **383** (2008) 1210–1222. doi:10.1111/j.1365-2966.2007.12639.x.
- [379] Bertschinger 1995 E. COSMICS: Cosmological Initial Conditions and Microwave Anisotropy Codes. *arXiv e-prints* (1995) astro-ph/9506070.
- [380] Bertschinger E. Simulations of Structure Formation in the Universe. *AnnRevAap* **36** (1998) 599–654. doi:10.1146/annurev.astro.36.1.599.
- [381] Sandage A. Star formation rates, galaxy morphology, and the Hubble sequence. *Astronomy and Astrophysics* **161** (1986) 89–101.

- [382] Chiosi C, Merlin E, Piovan L, Tantalo R. Monolithic View of Galaxy Formation and Evolution. *Galaxies* **2** (2014) 300–381. doi:10.3390/galaxies2030300.
- [383] Matteucci F. Introduction to Galactic Chemical Evolution. *Journal of Physics Conference Series* (2016), *Journal of Physics Conference Series*, vol. 703, 012004. doi:10.1088/1742-6596/703/1/012004.
- [384] Cassarà LP, Maccagni D, Garilli B, Scodreggio M, Thomas R, Le Fèvre O, et al. Effect of the star formation histories on the $SFR - M^*$ relation at $z \geq 2$. *Astronomy and Astrophysics* **593** (2016) A9. doi:10.1051/0004-6361/201526505.
- [385] Kawata D, Gibson BK. GCD+: a new chemodynamical approach to modelling supernovae and chemical enrichment in elliptical galaxies. *Mon. Not. R. Astron. Soc.* **340** (2003) 908–922. doi:10.1046/j.1365-8711.2003.06356.x.
- [386] Kawata D, Gibson BK. Multiwavelength cosmological simulations of elliptical galaxies. *Mon. Not. R. Astron. Soc.* **346** (2003) 135–152. doi:10.1046/j.1365-2966.2003.07080.x.
- [387] Kobayashi C. GRAPE-SPH chemodynamical simulation of elliptical galaxies - II. Scaling relations and the fundamental plane. *Mon. Not. R. Astron. Soc.* **361** (2005) 1216–1226. doi:10.1111/j.1365-2966.2005.09248.x.
- [388] Kennicutt J Robert C. The Global Schmidt Law in Star-forming Galaxies. *The Astrophysical Journal* **498** (1998) 541–552. doi:10.1086/305588.
- [389] Kennicutt J Robert C. Star Formation in Galaxies Along the Hubble Sequence. *Ann. Rev. Astron. Astrophys.* **36** (1998) 189–232. doi:10.1146/annurev.astro.36.1.189.
- [390] Larson RB. Models for the formation of elliptical galaxies. *Mon. Not. R. Astron. Soc.* **173** (1975) 671–699.
- [391] Larson RB. Models for the formation of disc galaxies. *Mon. Not. R. Astron. Soc.* **176** (1976) 31–52. doi:10.1093/mnras/176.1.31.
- [392] Talbot J R J, Arnett WD. The evolution of galaxies. IV. Highly flattened disks. *The Astrophysical Journal* **197** (1975) 551–570. doi:10.1086/153543.
- [393] Chiosi C. Chemical evolution of the galactic disk: the inflow problem. *Astronomy and Astrophysics* **83** (1980) 206–216.
- [394] Chiosi C, Matteucci F. Gradients of chemical composition in the galactic disk. *Mem. Soc. Astron. It.* **51** (1980) 107–115.
- [395] Bressan A, Chiosi C, Fagotto F. Spectrophotometric Evolution of Elliptical Galaxies. I. Ultraviolet Excess and Color-Magnitude-Redshift Relations. *ApJS* **94** (1994) 63. doi:10.1086/192073.
- [396] Portinari L, Chiosi C. On radial gas flows, the Galactic Bar and chemical evolution in the Galactic Disc. *AAp* **355** (2000) 929–948.
- [397] Chiosi C, Sciaratta M, D'Onofrio M, Chiosi E, Brotto F, De Michele R, et al. Cosmic Star Formation: A Simple Model of the SFRD(z). *ApJ* **851** (2017) 44. doi:10.3847/1538-4357/aa99d5.
- [398] Brinchmann J, Charlot S, White SDM, Tremonti C, Kauffmann G, Heckman T, et al. The physical properties of star-forming galaxies in the low-redshift Universe. *Mon. Not. R. Astron. Soc.* **351** (2004) 1151–1179. doi:10.1111/j.1365-2966.2004.07881.x.
- [399] Salim S, Rich RM, Charlot S, Brinchmann J, Johnson BD, Schiminovich D, et al. UV Star Formation Rates in the Local Universe. *The Astrophysical Journal Suppl.* **173** (2007) 267–292. doi:10.1086/519218.
- [400] Noeske KG, Weiner BJ, Faber SM, Papovich C, Koo DC, Somerville RS, et al. Star Formation in AEGIS Field Galaxies since $z=1.1$: The Dominance of Gradually Declining Star Formation, and the Main Sequence of Star-forming Galaxies. *The Astrophysical Journal Lett.* **660** (2007) L43–L46.

doi:10.1086/517926.

- [401] Elbaz D, Dickinson M, Hwang HS, Díaz-Santos T, Magdis G, Magnelli B, et al. GOODS-Herschel: an infrared main sequence for star-forming galaxies. *Astronomy and Astrophysics* **533** (2011) A119. doi:10.1051/0004-6361/201117239.
- [402] Salim S, Fang JJ, Rich RM, Faber SM, Thilker DA. Galaxy-scale Star Formation on the Red Sequence: The Continued Growth of S0s and the Quiescence of Ellipticals. *The Astrophysical Journal* **755** (2012) 105. doi:10.1088/0004-637X/755/2/105.
- [403] Whitaker KE, van Dokkum PG, Brammer G, Franx M. The Star Formation Mass Sequence Out to $z = 2.5$. *The Astrophysical Journal Lett.* **754** (2012) L29. doi:10.1088/2041-8205/754/2/L29.
- [404] Rodighiero G, Renzini A, Daddi E, Baronchelli I, Berta S, Cresci G, et al. A multiwavelength consensus on the main sequence of star-forming galaxies at $z \sim 2$. *Mon. Not. R. Astron. Soc.* **443** (2014) 19–30. doi:10.1093/mnras/stu1110.
- [405] Speagle JS, Steinhardt CL, Capak PL, Silverman JD. A Highly Consistent Framework for the Evolution of the Star-Forming “Main Sequence” from $z \sim 0$ –6. *The Astrophysical Journal Suppl.* **214** (2014) 15. doi:10.1088/0067-0049/214/2/15.
- [406] Schreiber C, Pannella M, Elbaz D, Béthermin M, Inami H, Dickinson M, et al. The Herschel view of the dominant mode of galaxy growth from $z = 4$ to the present day. *Astronomy and Astrophysics* **575** (2015) A74. doi:10.1051/0004-6361/201425017.
- [407] Popesso P, Concas A, Morselli L, Schreiber C, Rodighiero G, Cresci G, et al. The main sequence of star-forming galaxies - I. The local relation and its bending. *Mon. Not. R. Astron. Soc.* **483** (2019) 3213–3226. doi:10.1093/mnras/sty3210.
- [408] Daddi E, Cimatti A, Renzini A, Fontana A, Mignoli M, Pozzetti L, et al. A New Photometric Technique for the Joint Selection of Star-forming and Passive Galaxies at $1.4 < z < 2.5$. *The Astrophysical Journal* **617** (2004) 746–764. doi:10.1086/425569.
- [409] Daddi E, Dickinson M, Morrison G, Chary R, Cimatti A, Elbaz D, et al. Multiwavelength Study of Massive Galaxies at $z \sim 2$. I. Star Formation and Galaxy Growth. *The Astrophysical Journal* **670** (2007) 156–172. doi:10.1086/521818.
- [410] Pannella M, Carilli CL, Daddi E, McCracken HJ, Owen FN, Renzini A, et al. Star Formation and Dust Obscuration at $z \approx 2$: Galaxies at the Dawn of Downsizing. *The Astrophysical Journal Lett.* **698** (2009) L116–L120. doi:10.1088/0004-637X/698/2/L116.
- [411] Williams RJ, Quadri RF, Franx M, van Dokkum P, Labbé I. Detection of Quiescent Galaxies in a Bicolor Sequence from $Z = 0$ –2. *The Astrophysical Journal* **691** (2009) 1879–1895. doi:10.1088/0004-637X/691/2/1879.
- [412] Karim A, Schinnerer E, Martínez-Sansigre A, Sargent MT, van der Wel A, Rix HW, et al. The Star Formation History of Mass-selected Galaxies in the COSMOS Field. *The Astrophysical Journal* **730** (2011) 61. doi:10.1088/0004-637X/730/2/61.
- [413] Schaye J, Dalla Vecchia C, Booth CM, Wiersma RPC, Theuns T, Haas MR, et al. The physics driving the cosmic star formation history. *Mon. Not. R. Astron. Soc.* **402** (2010) 1536–1560. doi:10.1111/j.1365-2966.2009.16029.x.
- [414] Davé R, Oppenheimer BD, Finlator K. Galaxy evolution in cosmological simulations with outflows - I. Stellar masses and star formation rates. *Mon. Not. R. Astron. Soc.* **415** (2011) 11–31. doi:10.1111/j.1365-2966.2011.18680.x.
- [415] Haas MR, Schaye J, Booth CM, Dalla Vecchia C, Springel V, Theuns T, et al. Physical properties of simulated galaxy populations at $z = 2$ - I. Effect of metal-line cooling and feedback from star formation and AGN. *Mon. Not. R. Astron. Soc.* **435** (2013) 2931–2954. doi:10.1093/mnras/stt1487.

- [416] Lilly SJ, Carollo CM, Pipino A, Renzini A, Peng Y. Gas Regulation of Galaxies: The Evolution of the Cosmic Specific Star Formation Rate, the Metallicity-Mass-Star-formation Rate Relation, and the Stellar Content of Halos. *ApJ* **772** (2013) 119. doi:10.1088/0004-637X/772/2/119.
- [417] Tacchella S, Dekel A, Carollo CM, Ceverino D, DeGraf C, Lapiner S, et al. The confinement of star-forming galaxies into a main sequence through episodes of gas compaction, depletion and replenishment. *Mon. Not. R. Astron. Soc.* **457** (2016) 2790–2813. doi:10.1093/mnras/stw131.
- [418] Rodríguez-Puebla A, Primack JR, Behroozi P, Faber SM. Is main-sequence galaxy star formation controlled by halo mass accretion? *Mon. Not. R. Astron. Soc.* **455** (2016) 2592–2606. doi:10.1093/mnras/stv2513.
- [419] Fritz J, Poggianti BM, Bettoni D, Cava A, Couch WJ, D'Onofrio M, et al. A spectrophotometric model applied to cluster galaxies: the WINGS dataset. *Astronomy and Astrophysics* **470** (2007) 137–152. doi:10.1051/0004-6361:20077097.
- [420] Fritz J, Poggianti BM, Cava A, Valentinuzzi T, Moretti A, Bettoni D, et al. WINGS-SPE II: A catalog of stellar ages and star formation histories, stellar masses and dust extinction values for local clusters galaxies. *Astronomy and Astrophysics* **526** (2011) A45. doi:10.1051/0004-6361/201015214.
- [421] Matthee J, Schaye J. The origin of scatter in the star formation rate-stellar mass relation. *Mon. Not. R. Astron. Soc.* **484** (2019) 915–932. doi:10.1093/mnras/stz030.
- [422] Elbaz D, Daddi E, Le Borgne D, Dickinson M, Alexander DM, Chary RR, et al. The reversal of the star formation-density relation in the distant universe. *Astronomy and Astrophysics* **468** (2007) 33–48. doi:10.1051/0004-6361:20077525.
- [423] Kelson DD. Decoding the Star-Forming Main Sequence or: How I Learned to Stop Worrying and Love the Central Limit Theorem. *arXiv e-prints* (2014) arXiv:1406.5191.
- [424] Abramson LE, Gladders MD, Dressler A, Oemler J Augustus, Poggianti B, Vulcani B. Matching the Evolution of the Stellar Mass Function Using Log-Normal Star Formation Histories. *The Astrophysical Journal Lett.* **801** (2015) L12. doi:10.1088/2041-8205/801/1/L12.
- [425] Peng Yj, Lilly SJ, Kovač K, Bolzonella M, Pozzetti L, Renzini A, et al. Mass and Environment as Drivers of Galaxy Evolution in SDSS and zCOSMOS and the Origin of the Schechter Function. *The Astrophysical Journal* **721** (2010) 193–221. doi:10.1088/0004-637X/721/1/193.
- [426] Gladders MD, Oemler A, Dressler A, Poggianti B, Vulcani B, Abramson L. The IMACS Cluster Building Survey. IV. The Log-normal Star Formation History of Galaxies. *The Astrophysical Journal* **770** (2013) 64. doi:10.1088/0004-637X/770/1/64.
- [427] Abramson LE, Gladders MD, Dressler A, Oemler J Augustus, Poggianti B, Vulcani B. Return to [Log-]Normalcy: Rethinking Quenching, The Star Formation Main Sequence, and Perhaps Much More. *The Astrophysical Journal* **832** (2016) 7. doi:10.3847/0004-637X/832/1/7.
- [428] Wuyts S, Förster Schreiber NM, van der Wel A, Magnelli B, Guo Y, Genzel R, et al. Galaxy Structure and Mode of Star Formation in the SFR-Mass Plane from $z \sim 2.5$ to $z \sim 0.1$. *The Astrophysical Journal* **742** (2011) 96. doi:10.1088/0004-637X/742/2/96.
- [429] Lagos CdP, Theuns T, Schaye J, Furlong M, Bower RG, Schaller M, et al. The Fundamental Plane of star formation in galaxies revealed by the EAGLE hydrodynamical simulations. *Mon. not. R. Astron. Soc.* **459** (2016) 2632–2650. doi:10.1093/mnras/stw717.
- [430] Faber SM. Variations in Spectral-Energy Distributions and Absorption-Line Strengths among Elliptical Galaxies. *The Astrophysical Journal* **179** (1973) 731–754. doi:10.1086/151912.
- [431] Lequeux J, Peimbert M, Rayo JF, Serrano A, Torres-Peimbert S. Reprint of 1979A&A....80..155L. Chemical composition and evolution of irregular and blue compact galaxies. *Astronomy and Astrophysics* **500** (1979) 145–156.

- [432] Skillman ED, Kennicutt RC, Hodge PW. Oxygen Abundances in Nearby Dwarf Irregular Galaxies. *The Astrophysical Journal* **347** (1989) 875. doi:10.1086/168178.
- [433] Brodie JP, Huchra JP. Extragalactic Globular Clusters. III. Metallicity Comparisons and Anomalies. *The Astrophysical Journal* **379** (1991) 157. doi:10.1086/170492.
- [434] Zaritsky D, Kennicutt J Robert C, Huchra JP. H II Regions and the Abundance Properties of Spiral Galaxies. *The Astrophysical Journal* **420** (1994) 87. doi:10.1086/173544.
- [435] Maiolino R, Nagao T, Grazian A, Cocchia F, Marconi A, Mannucci F, et al. AMAZE. I. The evolution of the mass-metallicity relation at $z \lesssim 3$. *Astronomy and Astrophysics* **488** (2008) 463–479. doi:10.1051/0004-6361:200809678.
- [436] Kewley LJ, Ellison SL. Metallicity Calibrations and the Mass-Metallicity Relation for Star-forming Galaxies. *The Astrophysical Journal* **681** (2008) 1183–1204. doi:10.1086/587500.
- [437] Kobulnicky HA, Kewley LJ. Metallicities of $0.3 \lesssim z \lesssim 1.0$ Galaxies in the GOODS-North Field. *The Astrophysical Journal* **617** (2004) 240–261. doi:10.1086/425299.
- [438] Kewley LJ, Dopita MA. Using Strong Lines to Estimate Abundances in Extragalactic H II Regions and Starburst Galaxies. *The Astrophysical Journal Suppl.* **142** (2002) 35–52. doi:10.1086/341326.
- [439] Pettini M, Pagel BEJ. [OIII]/[NII] as an abundance indicator at high redshift. *Mon. Not. R. Astron. Soc.* **348** (2004) L59–L63. doi:10.1111/j.1365-2966.2004.07591.x.
- [440] Ly C, Malkan MA, Rigby JR, Nagao T. The Metal Abundances across Cosmic Time (MACT) Survey. II. Evolution of the Mass-metallicity Relation over 8 Billion Years, Using [OIII]4363AA-based Metallicities. *The Astrophysical Journal* **828** (2016) 67. doi:10.3847/0004-637X/828/2/67.
- [441] Stasińska G, Schaerer D, Leitherer C. The evolution of emission lines in HII galaxies as a probe of interaction between stellar and interstellar component. *Astrophysics and Space Science* **281** (2002) 335–336. doi:10.1023/A:1019574425717.
- [442] López-Sánchez ÁR, Dopita MA, Kewley LJ, Zahid HJ, Nicholls DC, Scharwächter J. Eliminating error in the chemical abundance scale for extragalactic H II regions. *Mon. Not. R. Astron. Soc.* **426** (2012) 2630–2651. doi:10.1111/j.1365-2966.2012.21145.x.
- [443] Blanc GA, Kewley L, Vogt FPA, Dopita MA. IZI: Inferring the Gas Phase Metallicity (Z) and Ionization Parameter (q) of Ionized Nebulae Using Bayesian Statistics. *The Astrophysical Journal* **798** (2015) 99. doi:10.1088/0004-637X/798/2/99.
- [444] Bresolin F, Kudritzki RP, Urbaneja MA, Gieren W, Ho IT, Pietrzyński G. Young Stars and Ionized Nebulae in M83: Comparing Chemical Abundances at High Metallicity. *The Astrophysical Journal* **830** (2016) 64. doi:10.3847/0004-637X/830/2/64.
- [445] Erb DK, Shapley AE, Pettini M, Steidel CC, Reddy NA, Adelberger KL. The Mass-Metallicity Relation at $z \sim 2$. *The Astrophysical Journal* **644** (2006) 813–828. doi:10.1086/503623.
- [446] Zahid HJ, Kewley LJ, Bresolin F. The Mass-Metallicity and Luminosity-Metallicity Relations from DEEP2 at $z \sim 0.8$. *The Astrophysical Journal* **730** (2011) 137. doi:10.1088/0004-637X/730/2/137.
- [447] Henry A, Scarlata C, Domínguez A, Malkan M, Martin CL, Siana B, et al. Low Masses and High Redshifts: The Evolution of the Mass-Metallicity Relation. *The Astrophysical Journal* **776** (2013) L27. doi:10.1088/2041-8205/776/2/L27.
- [448] Maier C, Lilly SJ, Ziegler BL, Contini T, Pérez Montero E, Peng Y, et al. The Mass-Metallicity and Fundamental Metallicity Relations at $z \lesssim 2$ Using Very Large Telescope and Subaru Near-infrared Spectroscopy of zCOSMOS Galaxies. *The Astrophysical Journal* **792** (2014) 3. doi:10.1088/0004-637X/792/1/3.
- [449] Steidel CC, Rudie GC, Strom AL, Pettini M, Reddy NA, Shapley AE, et al. Strong Nebular Line Ratios in the Spectra of $z \sim 2$ -3 Star Forming Galaxies: First Results from KBSS-MOSFIRE. *The*

- Astrophysical Journal* **795** (2014) 165. doi:10.1088/0004-637X/795/2/165.
- [450] Sanders RL, Shapley AE, Kriek M, Reddy NA, Freeman WR, Coil AL, et al. The MOSDEF Survey: Mass, Metallicity, and Star-formation Rate at $z \sim 2.3$. *The Astrophysical Journal* **799** (2015) 138. doi:10.1088/0004-637X/799/2/138.
- [451] Lee H, Skillman ED, Cannon JM, Jackson DC, Gehrz RD, Polomski EF, et al. On Extending the Mass-Metallicity Relation of Galaxies by 2.5 Decades in Stellar Mass. *The Astrophysical Journal* **647** (2006) 970–983. doi:10.1086/505573.
- [452] Vaduvescu O, McCall ML, Richer MG. Chemical Properties of Star-Forming Dwarf Galaxies. *The Astronomical Journal* **134** (2007) 604–616. doi:10.1086/518865.
- [453] Zahid HJ, Bresolin F, Kewley LJ, Coil AL, Davé R. The Metallicities of Low Stellar Mass Galaxies and the Scatter in the Mass-Metallicity Relation. *The Astrophysical Journal* **750** (2012) 120. doi:10.1088/0004-637X/750/2/120.
- [454] Andrews BH, Martini P. The Mass-Metallicity Relation with the Direct Method on Stacked Spectra of SDSS Galaxies. *The Astrophysical Journal* **765** (2013) 140. doi:10.1088/0004-637X/765/2/140.
- [455] Richer MG, McCall ML. Oxygen Abundances in Diffuse Ellipticals and the Metallicity-Luminosity Relations for Dwarf Galaxies. *The Astrophysical Journal* **445** (1995) 642. doi:10.1086/175727.
- [456] Melbourne J, Salzer JJ. Metal Abundances of KISS Galaxies. I. Coarse Metal Abundances and the Metallicity-Luminosity Relation. *The Astronomical Journal* **123** (2002) 2302–2311. doi:10.1086/339834.
- [457] Salzer JJ, Lee JC, Melbourne J, Hinz JL, Alonso-Herrero A, Jangren A. Metal Abundances of KISS Galaxies. IV. Galaxian Luminosity-Metallicity Relations in the Optical and Near-Infrared. *The Astrophysical Journal* **624** (2005) 661–679. doi:10.1086/429386.
- [458] Sweet SM, Drinkwater MJ, Meurer G, Bekki K, Dopita MA, Kilborn V, et al. Choirs H I Galaxy Groups: The Metallicity of Dwarf Galaxies. *The Astrophysical Journal* **782** (2014) 35. doi:10.1088/0004-637X/782/1/35.
- [459] De Lucia G, Kauffmann G, White SDM. Chemical enrichment of the intracluster and intergalactic medium in a hierarchical galaxy formation model. *Mon. Not. R. Astron. Soc.* **349** (2004) 1101–1116. doi:10.1111/j.1365-2966.2004.07584.x.
- [460] Dalcanton JJ. The Metallicity of Galaxy Disks: Infall versus Outflow. *The Astrophysical Journal* **658** (2007) 941–959. doi:10.1086/508913.
- [461] Yuan TT, Kewley LJ, Richard J. The Metallicity Evolution of Star-forming Galaxies from Redshift 0 to 3: Combining Magnitude-limited Survey with Gravitational Lensing. *The Astrophysical Journal* **763** (2013) 9. doi:10.1088/0004-637X/763/1/9.
- [462] Zahid HJ, Dima GI, Kudritzki RP, Kewley LJ, Geller MJ, Hwang HS, et al. The Universal Relation of Galactic Chemical Evolution: The Origin of the Mass-Metallicity Relation. *The Astrophysical Journal* **791** (2014) 130. doi:10.1088/0004-637X/791/2/130.
- [463] Wuyts E, Wisnioski E, Fossati M, Förster Schreiber NM, Genzel R, Davies R, et al. The Evolution of Metallicity and Metallicity Gradients from $z = 2.7$ to 0.6 with KMOS^{3D}. *ApJ* **827** (2016) 74. doi:10.3847/0004-637X/827/1/74.
- [464] Lynden-Bell D. The chemical evolution of galaxies. *Vistas in Astronomy* **19** (1975) 299–316. doi:10.1016/0083-6656(75)90005-7.
- [465] Lacey CG, Fall SM. Chemical evolution of the galactic disk with radial gas flows. *The Astrophysical Journal* **290** (1985) 154–170. doi:10.1086/162970.
- [466] Edmunds MG. General Constraints on the Effect of Gas Flows in the Chemical Evolution of Galaxies. *Mon. Not. R. Astron. Soc.* **246** (1990) 678.

- [467] Oppenheimer BD, Davé R, Kereš D, Fardal M, Katz N, Kollmeier JA, et al. Feedback and recycled wind accretion: assembling the $z = 0$ galaxy mass function. *Mon. Not. R. Astron. Soc.* **406** (2010) 2325–2338. doi:10.1111/j.1365-2966.2010.16872.x.
- [468] Ma X, Hopkins PF, Faucher-Giguère CA, Zolman N, Muratov AL, Kereš D, et al. The origin and evolution of the galaxy mass-metallicity relation. *Mon. Not. R. Astron. Soc.* **456** (2016) 2140–2156. doi:10.1093/mnras/stv2659.
- [469] Renzini A, Peng Yj. An Objective Definition for the Main Sequence of Star-forming Galaxies. *The Astrophysical Journal Lett.* **801** (2015) L29. doi:10.1088/2041-8205/801/2/L29.
- [470] Kennicutt J Robert C. The Global Schmidt Law in Star-forming Galaxies. *The Astrophysical Journal* **498** (1998) 541–552. doi:10.1086/305588.
- [471] Bigiel F, Leroy A, Walter F, Brinks E, de Blok WJG, Madore B, et al. The Star Formation Law in Nearby Galaxies on Sub-Kpc Scales. *The Astronomical Journal* **136** (2008) 2846–2871. doi:10.1088/0004-6256/136/6/2846.
- [472] Leroy AK, Bolatto A, Bot C, Engelbracht CW, Gordon K, Israel FP, et al. The Structure of a Low-metallicity Giant Molecular Cloud Complex. *The Astrophysical Journal* **702** (2009) 352–367. doi:10.1088/0004-637X/702/1/352.
- [473] Worthey G, Faber SM, Gonzalez JJ, Burstein D. Old Stellar Populations. V. Absorption Feature Indices for the Complete Lick/IDS Sample of Stars. *ApJS* **94** (1994) 687. doi:10.1086/192087.
- [474] Worthey G. Comprehensive Stellar Population Models and the Disentanglement of Age and Metallicity Effects. *ApJS* **95** (1994) 107. doi:10.1086/192096.
- [475] Worthey G. The Age-Metallicity Degeneracy. Hubeny I, Heap S, Cornett R, editors, *Spectrophotometric Dating of Stars and Galaxies* (1999), *Astronomical Society of the Pacific Conference Series*, vol. 192, 283.
- [476] Trager SC, Faber SM, Worthey G, González JJ. The Stellar Population Histories of Local Early-Type Galaxies. I. Population Parameters. *AJ* **119** (2000) 1645–1676. doi:10.1086/301299.
- [477] Trager SC, Faber SM, Worthey G, González JJ. The Stellar Population Histories of Early-Type Galaxies. II. Controlling Parameters of the Stellar Populations. *AJ* **120** (2000) 165–188. doi:10.1086/301442.
- [478] Vazdekis A, Sánchez-Blázquez P, Falcón-Barroso J, Cenarro AJ, Beasley MA, Cardiel N, et al. Evolutionary stellar population synthesis with MILES - I. The base models and a new line index system. *MNRAS* **404** (2010) 1639–1671. doi:10.1111/j.1365-2966.2010.16407.x.
- [479] Cenarro AJ, Cardiel N, Gorgas J, Peletier RF, Vazdekis A, Prada F. Empirical calibration of the near-infrared Ca ii triplet - I. The stellar library and index definition. *MNRAS* **326** (2001) 959–980. doi:10.1046/j.1365-8711.2001.04688.x.
- [480] Cenarro AJ, Gorgas J, Cardiel N, Pedraz S, Peletier RF, Vazdekis A. Empirical calibration of the near-infrared Ca ii triplet - II. The stellar atmospheric parameters. *MNRAS* **326** (2001) 981–994. doi:10.1046/j.1365-8711.2001.04689.x.
- [481] Rodríguez-Merino LH, Mayya YD, Coelho PRT, Bruzual G, Charlot S, Carrasco E, et al. High-resolution Spectral Line Indices Useful for the Analysis of Stellar Populations. *ApJL* **889** (2020) L31. doi:10.3847/2041-8213/ab6d64.
- [482] Yi SK. Uncertainties of Synthetic Integrated Colors as Age Indicators. *ApJ* **582** (2003) 202–214. doi:10.1086/344640.
- [483] Dorman B, O'Connell RW, Rood RT. Age and Abundance Discrimination in Old Stellar Populations Using Mid-Ultraviolet Colors. *ApJ* **591** (2003) 878–890. doi:10.1086/375413.

- [484] Kaviraj S, Rey SC, Rich RM, Yoon SJ, Yi SK. Better age estimation using ultraviolet-optical colours: breaking the age-metallicity degeneracy. *MNRAS* **381** (2007) L74–L78. doi:10.1111/j.1745-3933.2007.00370.x.
- [485] Li Z, Han Z, Zhang F. Potential of colors for determining age and metallicity of stellar populations. *AAp* **464** (2007) 853–857. doi:10.1051/0004-6361:20066337.
- [486] Tantalò R, Chiosi C, Bressan A. Ages and metallicities in elliptical galaxies from the H β , [Fe I] , and Mg $_2$ diagnostics. *AAp* **333** (1998) 419–432.
- [487] Tantalò R. Measuring age, metallicity and abundance ratios from absorption line indices. *Mem. Soc. It. Fisica* **75** (2004) 202.
- [488] Tantalò R, Chiosi C. Measuring age, metallicity and abundance ratios from absorption-line indices. *MNRAS* **353** (2004) 917–940. doi:10.1111/j.1365-2966.2004.08123.x.
- [489] Tantalò R, Chiosi C. Star formation history in early-type galaxies - I. The line absorption indices diagnostics. *MNRAS* **353** (2004) 405–421. doi:10.1111/j.1365-2966.2004.08070.x.
- [490] Tantalò R, Chiosi C, Piovan L. New response functions for absorption-line indices from high-resolution spectra. *AAp* **462** (2007) 481–494. doi:10.1051/0004-6361:20053774.
- [491] Jimenez R, Bernardi M, Haiman Z, Panter B, Heavens AF. The Ages, Metallicities, and Star Formation Histories of Early-Type Galaxies in the SDSS. *ApJ* **669** (2007) 947–951. doi:10.1086/521323.
- [492] Shankar F, Lapi A, Salucci P, De Zotti G, Danese L. New Relationships between Galaxy Properties and Host Halo Mass, and the Role of Feedbacks in Galaxy Formation. *The Astrophysical Journal* **643** (2006) 14–25. doi:10.1086/502794.
- [493] Girelli G, Pozzetti L, Bolzonella M, Giocoli C, Marulli F, Baldi M. The stellar-to-halo mass relation over the past 12 Gyr. I. Standard Λ CDM model. *Astronomy and Astrophysics* **634** (2020) A135. doi:10.1051/0004-6361/201936329.
- [494] Engler C, Pillepich A, Joshi GD, Nelson D, Pasquali A, Grebel EK, et al. The Distinct Stellar-to-Halo Mass Relations of Satellite and Central Galaxies: Insights from the IllustrisTNG Simulations. *arXiv e-prints* (2020) arXiv:2002.11119.
- [495] Bertin G, Saglia RP, Stiavelli M. Elliptical galaxies with dark matter. I - Self-consistent models. II - Optimal luminous-dark matter decomposition for a sample of bright objects. *The Astrophysical Journal* **384** (1992) 423–447. doi:10.1086/170884.
- [496] Saglia RP, Bertin G, Stiavelli M. Elliptical Galaxies with Dark Matter. II. Optimal Luminous–Dark Matter Decomposition for a Sample of Bright Objects. *The Astrophysical Journal* **384** (1992) 433. doi:10.1086/170885.
- [497] Fall SM, Romanowsky AJ. Angular Momentum and Galaxy Formation Revisited: Scaling Relations for Disks and Bulges. *The Astrophysical Journal* **868** (2018) 133. doi:10.3847/1538-4357/aab27.
- [498] Hoyle F. The Origin of the Rotations of the Galaxies. *Problems of Cosmical Aerodynamics* (1951), 195.
- [499] Doroshkevich AG. Spatial structure of perturbations and origin of galactic rotation in fluctuation theory. *Astrophysics* **6** (1970) 320–330. doi:10.1007/BF01001625.
- [500] White SDM. Angular momentum growth in protogalaxies. *The Astrophysical Journal* **286** (1984) 38–41. doi:10.1086/162573.
- [501] Fall SM, Efstathiou G. Formation and rotation of disc galaxies with haloes. *Mon. Not. R. Astron. Soc.* **193** (1980) 189–206. doi:10.1093/mnras/193.2.189.
- [502] Ryden BS, Gunn JE. Galaxy Formation by Gravitational Collapse. *The Astrophysical Journal* **318** (1987) 15. doi:10.1086/165349.

- [503] Dalcanton JJ, Spergel DN, Summers FJ. The Formation of Disk Galaxies. *The Astrophysical Journal* **482** (1997) 659–676. doi:10.1086/304182.
- [504] Vitvitska M, Klypin AA, Kravtsov AV, Wechsler RH, Primack JR, Bullock JS. The Origin of Angular Momentum in Dark Matter Halos. *The Astrophysical Journal* **581** (2002) 799–809. doi:10.1086/344361.
- [505] Bett P, Eke V, Frenk CS, Jenkins A, Okamoto T. The angular momentum of cold dark matter haloes with and without baryons. *Mon. Not. R. Astron. Soc.* **404** (2010) 1137–1156. doi:10.1111/j.1365-2966.2010.16368.x.
- [506] Kimm T, Devriendt J, Slyz A, Pichon C, Kassin SA, Dubois Y. The angular momentum of baryons and dark matter halos revisited. *arXiv e-prints* (2011) arXiv:1106.0538.
- [507] Tillson H, Miller L, Devriendt J. The environment and redshift dependence of accretion on to dark matter haloes and subhaloes. *Mon. Not. R. Astron. Soc.* **417** (2011) 666–680. doi:10.1111/j.1365-2966.2011.19311.x.
- [508] Danovich M, Dekel A, Hahn O, Teyssier R. Coplanar streams, pancakes and angular-momentum exchange in high-*z* disc galaxies. *Mon. Not. R. Astron. Soc.* **422** (2012) 1732–1749. doi:10.1111/j.1365-2966.2012.20751.x.
- [509] Codis S, Pichon C, Devriendt J, Slyz A, Pogosyan D, Dubois Y, et al. Connecting the cosmic web to the spin of dark haloes: implications for galaxy formation. *Mon. Not. R. Astron. Soc.* **427** (2012) 3320–3336. doi:10.1111/j.1365-2966.2012.21636.x.
- [510] Stewart KR, Brooks AM, Bullock JS, Maller AH, Diemand J, Wadsley J, et al. Angular Momentum Acquisition in Galaxy Halos. *The Astrophysical Journal* **769** (2013) 74. doi:10.1088/0004-637X/769/1/74.
- [511] Übler H, Naab T, Oser L, Aumer M, Sales LV, White SDM. Why stellar feedback promotes disc formation in simulated galaxies. *Mon. Not. R. Astron. Soc.* **443** (2014) 2092–2111. doi:10.1093/mnras/stu1275.
- [512] Danovich M, Dekel A, Hahn O, Ceverino D, Primack J. Four phases of angular-momentum buildup in high-*z* galaxies: from cosmic-web streams through an extended ring to disc and bulge. *Mon. Not. R. Astron. Soc.* **449** (2015) 2087–2111. doi:10.1093/mnras/stv270.
- [513] Navarro JF, White SDM. Simulations of dissipative galaxy formation in hierarchically clustering universes-2. Dynamics of the baryonic component in galactic haloes. *Mon. Not. R. Astron. Soc.* **267** (1994) 401–412. doi:10.1093/mnras/267.2.401.
- [514] Scannapieco C, Tissera PB, White SDM, Springel V. Effects of supernova feedback on the formation of galaxy discs. *Mon. Not. R. Astron. Soc.* **389** (2008) 1137–1149. doi:10.1111/j.1365-2966.2008.13678.x.
- [515] Zavala J, Okamoto T, Frenk CS. Bulges versus discs: the evolution of angular momentum in cosmological simulations of galaxy formation. *Mon. Not. R. Astron. Soc.* **387** (2008) 364–370. doi:10.1111/j.1365-2966.2008.13243.x.
- [516] Sales LV, Navarro JF, Schaye J, Dalla Vecchia C, Springel V, Booth CM. Feedback and the structure of simulated galaxies at redshift $z=2$. *Mon. Not. R. Astron. Soc.* **409** (2010) 1541–1556. doi:10.1111/j.1365-2966.2010.17391.x.
- [517] Brook CB, Governato F, Roškar R, Stinson G, Brooks AM, Wadsley J, et al. Hierarchical formation of bulgeless galaxies: why outflows have low angular momentum. *Mon. Not. R. Astron. Soc.* **415** (2011) 1051–1060. doi:10.1111/j.1365-2966.2011.18545.x.
- [518] Brook CB, Stinson G, Gibson BK, Roškar R, Wadsley J, Quinn T. Hierarchical formation of bulgeless galaxies - II. Redistribution of angular momentum via galactic fountains. *Mon. Not. R. Astron. Soc.*

- 419 (2012) 771–779. doi:10.1111/j.1365-2966.2011.19740.x.
- [519] Christensen CR, Brooks AM, Fisher DB, Governato F, McCleary J, Quinn TR, et al. Simulating disc galaxy bulges that are consistent with observed scaling relations. *Mon. Not. R. Astron. Soc.* **440** (2014) L51–L55. doi:10.1093/mnras/slu020.
- [520] Peng Yj, Renzini A. Disc growth and quenching. *MNRAS* **491** (2020) L51–L55. doi:10.1093/mnras/slz163.
- [521] Burkert A, Förster Schreiber NM, Genzel R, Lang P, Tacconi LJ, Wisnioski E, et al. The Angular Momentum Distribution and Baryon Content of Star-forming Galaxies at $z \sim 1-3$. *ApJ* **826** (2016) 214. doi:10.3847/0004-637X/826/2/214.
- [522] Ferrarese L, Ford H. Supermassive Black Holes in Galactic Nuclei: Past, Present and Future Research. *Space Science Reviews* **116** (2005) 523–624. doi:10.1007/s11214-005-3947-6.
- [523] Kormendy J, Ho LC. Coevolution (Or Not) of Supermassive Black Holes and Host Galaxies. *Ann. Rev. Astron. Soc.* **51** (2013) 511–653. doi:10.1146/annurev-astro-082708-101811.
- [524] Graham AW. *Galaxy Bulges and Their Massive Black Holes: A Review*, vol. 418 (2016), 263. doi:10.1007/978-3-319-19378-6_11.
- [525] Silk J, Rees MJ. Quasars and galaxy formation. *Astronomy and Astrophysics* **331** (1998) L1–L4.
- [526] Shapiro SL. Spin, Accretion, and the Cosmological Growth of Supermassive Black Holes. *The Astrophysical Journal* **620** (2005) 59–68. doi:10.1086/427065.
- [527] Lynden-Bell D. Galactic Nuclei as Collapsed Old Quasars. *Nat* **223** (1969) 690–694. doi:10.1038/223690a0.
- [528] King A, Nealon R. Supermassive black hole demographics: evading $M - \sigma$. *MNRAS* **487** (2019) 4827–4831. doi:10.1093/mnras/stz1569.
- [529] Schwarzschild M. A numerical model for a triaxial stellar system in dynamical equilibrium. *ApJ* **232** (1979) 236–247. doi:10.1086/157282.
- [530] Young PJ, Westphal JA, Kristian J, Wilson CP, Landauer FP. Evidence for a supermassive object in the nucleus of the galaxy M87 from SIT and CCD area photometry. *The Astrophysical Journal* **221** (1978) 721–730. doi:10.1086/156076.
- [531] Rix HW, de Zeeuw PT, Cretton N, van der Marel RP, Carollo CM. Dynamical Modeling of Velocity Profiles: The Dark Halo around the Elliptical Galaxy NGC 2434. *The Astrophysical Journal* **488** (1997) 702–719. doi:10.1086/304733.
- [532] Gebhardt K, Lauer TR, Pinkney J, Bender R, Richstone D, Aller M, et al. The Black Hole Mass and Extreme Orbital Structure in NGC 1399. *The Astrophysical Journal* **671** (2007) 1321–1328. doi:10.1086/522938.
- [533] Gebhardt K, Thomas J. The Black Hole Mass, Stellar Mass-to-Light Ratio, and Dark Halo in M87. *ApJ* **700** (2009) 1690–1701. doi:10.1088/0004-637X/700/2/1690.
- [534] van den Bosch RCE, van de Ven G, Verolme EK, Cappellari M, de Zeeuw PT. Triaxial orbit based galaxy models with an application to the (apparent) decoupled core galaxy NGC 4365. *MNRAS* **385** (2008) 647–666. doi:10.1111/j.1365-2966.2008.12874.x.
- [535] Gebhardt K, Adams J, Richstone D, Lauer TR, Faber SM, Gültekin K, et al. The Black Hole Mass in M87 from Gemini/NIFS Adaptive Optics Observations. *ApJ* **729** (2011) 119. doi:10.1088/0004-637X/729/2/119.
- [536] Event Horizon Telescope Collaboration, Akiyama K, Alberdi A, Alef W, Asada K, Azulay R, et al. First M87 Event Horizon Telescope Results. I. The Shadow of the Supermassive Black Hole. *ApJL* **875** (2019) L1. doi:10.3847/2041-8213/ab0ec7.

- [537] Barth AJ, Boizelle BD, Darling J, Baker AJ, Buote DA, Ho LC, et al. Measurement of the Black Hole Mass in NGC 1332 from ALMA Observations at 0.044 arcsecond Resolution. *ApJL* **822** (2016) L28. doi:10.3847/2041-8205/822/2/L28.
- [538] Boizelle BD, Barth AJ, Walsh JL, Buote DA, Baker AJ, Darling J, et al. A Precision Measurement of the Mass of the Black Hole in NGC 3258 from High-resolution ALMA Observations of Its Circumnuclear Disk. *ApJ* **881** (2019) 10. doi:10.3847/1538-4357/ab2a0a.
- [539] Wootten A, Thompson AR. The Atacama Large Millimeter/Submillimeter Array. *IEEE Proceedings* **97** (2009) 1463–1471. doi:10.1109/JPROC.2009.2020572.
- [540] Davis TA, Nguyen DD, Seth AC, Greene JE, Nyland K, Barth AJ, et al. Revealing the intermediate-mass black hole at the heart of the dwarf galaxy NGC 404 with sub-parsec resolution ALMA observations. *MNRAS* **496** (2020) 4061–4078. doi:10.1093/mnras/staa1567.
- [541] Macchetto F, Marconi A, Axon DJ, Capetti A, Sparks W, Crane P. The Supermassive Black Hole of M87 and the Kinematics of Its Associated Gaseous Disk. *ApJ* **489** (1997) 579–+. doi:10.1086/304823.
- [542] Bower GA, Green RF, Danks A, Gull T, Heap S, Hutchings J, et al. Kinematics of the Nuclear Ionized Gas in the Radio Galaxy M84 (NGC 4374). *ApJL* **492** (1998) L111–L114. doi:10.1086/311109.
- [543] Jeter B, Broderick AE, McNamara BR. Impact of Accretion Flow Dynamics on Gas-dynamical Black Hole Mass Estimates. *ApJ* **882** (2019) 82. doi:10.3847/1538-4357/ab3221.
- [544] Harms RJ, Ford HC, Tsvetanov ZI, Hartig GF, Dressel LL, Kriss GA, et al. HST FOS Spectroscopy of M87: Evidence for a Disk of Ionized Gas around a Massive Black Hole. *The Astrophysical Journal Lett.* **435** (1994) L35. doi:10.1086/187588.
- [545] Walsh JL, Barth AJ, Ho LC, Sarzi M. The M87 Black Hole Mass from Gas-dynamical Models of Space Telescope Imaging Spectrograph Observations. *ApJ* **770** (2013) 86. doi:10.1088/0004-637X/770/2/86.
- [546] Nokhrina EE, Gurvits LI, Beskin VS, Nakamura M, Asada K, Hada K. M87 black hole mass and spin estimate through the position of the jet boundary shape break. *Mon. Not. R. Astron. Soc.* **489** (2019) 1197–1205. doi:10.1093/mnras/stz2116.
- [547] McConnell NJ, Ma CP, Gebhardt K, Wright SA, Murphy JD, Lauer TR, et al. Two ten-billion-solar-mass black holes at the centres of giant elliptical galaxies. *Nat* **480** (2011) 215–218. doi:10.1038/nature10636.
- [548] McConnell NJ, Ma CP. Revisiting the Scaling Relations of Black Hole Masses and Host Galaxy Properties. *ApJ* **764** (2013) 184. doi:10.1088/0004-637X/764/2/184.
- [549] Bennert VN, Treu T, Ding X, Stomberg I, Birrer S, Snyder T, et al. A local baseline of the black hole mass scaling relations for active galaxies. IV. Correlations between M_{BH} and host galaxy σ , stellar mass, and luminosity. *arXiv e-prints* (2021) arXiv:2101.10355.
- [550] Hopkins PF, Hernquist L, Cox TJ, Robertson B, Krause E. A Theoretical Interpretation of the Black Hole Fundamental Plane. *ApJ* **669** (2007) 45–66. doi:10.1086/521590.
- [551] Barway S, Kembhavi A. A Supermassive Black Hole Fundamental Plane for Ellipticals. *ApJL* **662** (2007) L67–L70. doi:10.1086/519560.
- [552] Aller MC, Richstone DO. Host Galaxy Bulge Predictors of Supermassive Black Hole Mass. *ApJ* **665** (2007) 120–156. doi:10.1086/519298.
- [553] Franceschini A, Vercellone S, Fabian AC. Supermassive Black Holes in Early-Type Galaxies: Relationship with Radio Emission and Constraints on the Black Hole Mass Function. *Mon. Not. R. Astron. Soc.* **297** (1998) 817–824. doi:10.1046/j.1365-8711.1998.01534.x.

- [554] McLure RJ, Dunlop JS. On the black hole-bulge mass relation in active and inactive galaxies. *Mon. Not. R. Astron. Soc.* **331** (2002) 795–804. doi:10.1046/j.1365-8711.2002.05236.x.
- [555] Marconi A, Hunt LK. The Relation between Black Hole Mass, Bulge Mass, and Near-Infrared Luminosity. *The Astrophysical Journal Lett.* **589** (2003) L21–L24. doi:10.1086/375804.
- [556] Laor A. On Quasar Masses and Quasar Host Galaxies. *The Astrophysical Journal Lett.* **505** (1998) L83–L86. doi:10.1086/311619.
- [557] Laor A. On the Linearity of the Black Hole-Bulge Mass Relation in Active and in Nearby Galaxies. *The Astrophysical Journal* **553** (2001) 677–682. doi:10.1086/320989.
- [558] Wandel A. The Black Hole-to-Bulge Mass Relation in Active Galactic Nuclei. *The Astrophysical Journal Lett.* **519** (1999) L39–L42. doi:10.1086/312106.
- [559] Ryan CJ, De Robertis MM, Virani S, Laor A, Dawson PC. The Central Engines of Narrow-Line Seyfert 1 Galaxies. *The Astrophysical Journal* **654** (2007) 799–813. doi:10.1086/509313.
- [560] Salucci P, Ratnam C, Monaco P, Danese L. The masses of black holes in the nuclei of spirals. *Mon. Not. R. Astron. Soc.* **317** (2000) 488–496. doi:10.1046/j.1365-8711.2000.03622.x.
- [561] Graham AW. Breaking the Law: The M_{bh} - $M_{spheroid}$ Relations for Core-Sérsic and Sérsic Galaxies. *The Astrophysical Journal* **746** (2012) 113. doi:10.1088/0004-637X/746/1/113.
- [562] Scott N, Graham AW, Schombert J. The Supermassive Black Hole Mass-Spheroid Stellar Mass Relation for Sérsic and Core-Sérsic Galaxies. *The Astrophysical Journal* **768** (2013) 76. doi:10.1088/0004-637X/768/1/76.
- [563] Graham AW, Scott N. The M_{BH} - $L_{spheroid}$ Relation at High and Low Masses, the Quadratic Growth of Black Holes, and Intermediate-mass Black Hole Candidates. *The Astrophysical Journal* **764** (2013) 151. doi:10.1088/0004-637X/764/2/151.
- [564] Zubovas K, King A. Clearing Out a Galaxy. *ApJL* **745** (2012) L34. doi:10.1088/2041-8205/745/2/L34.
- [565] King A, Pounds K. Powerful Outflows and Feedback from Active Galactic Nuclei. *AnnRevAAp* **53** (2015) 115–154. doi:10.1146/annurev-astro-082214-122316.
- [566] Di Matteo T, Springel V, Hernquist L. Energy input from quasars regulates the growth and activity of black holes and their host galaxies. *Nat* **433** (2005) 604–607. doi:10.1038/nature03335.
- [567] Robertson B, Cox TJ, Hernquist L, Franx M, Hopkins PF, Martini P, et al. The Fundamental Scaling Relations of Elliptical Galaxies. *ApJ* **641** (2006) 21–40. doi:10.1086/500360.
- [568] Kormendy J, Bender R. Correlations between Supermassive Black Holes, Velocity Dispersions, and Mass Deficits in Elliptical Galaxies with Cores. *ApJL* **691** (2009) L142–L146. doi:10.1088/0004-637X/691/2/L142.
- [569] Milosavljević M, Merritt D. Formation of Galactic Nuclei. *ApJ* **563** (2001) 34–62. doi:10.1086/323830.
- [570] Kulkarni G, Loeb A. Formation of galactic nuclei with multiple supermassive black holes at high redshifts. *MNRAS* **422** (2012) 1306–1323. doi:10.1111/j.1365-2966.2012.20699.x.
- [571] Bortolas E, Gualandris A, Dotti M, Spera M, Mapelli M. Brownian motion of massive black hole binaries and the final parsec problem. *MNRAS* **461** (2016) 1023–1031. doi:10.1093/mnras/stw1372.
- [572] Graham AW. Core Depletion from Coalescing Supermassive Black Holes. *ApJL* **613** (2004) L33–L36. doi:10.1086/424928.
- [573] Merritt D. Mass Deficits, Stalling Radii, and the Merger Histories of Elliptical Galaxies. *ApJ* **648** (2006) 976–986. doi:10.1086/506139.
- [574] Rusli SP, Erwin P, Saglia RP, Thomas J, Fabricius M, Bender R, et al. Depleted Galaxy Cores and Dynamical Black Hole Masses. *AJ* **146** (2013) 160. doi:10.1088/0004-6256/146/6/160.

- [575] Quinlan GD, Hernquist L. The dynamical evolution of massive black hole binaries — II. Self-consistent N-body integrations. *New Astr.* **2** (1997) 533–554. doi:10.1016/S1384-1076(97)00039-0.
- [576] Krajnović D, McDermid RM, Cappellari M, Davies RL. Determination of masses of the central black holes in NGC 524 and 2549 using laser guide star adaptive optics. *MNRAS* **399** (2009) 1839–1857. doi:10.1111/j.1365-2966.2009.15415.x.
- [577] Thomas J, Ma CP, McConnell NJ, Greene JE, Blakeslee JP, Janish R. A 17-billion-solar-mass black hole in a group galaxy with a diffuse core. *Nat* **532** (2016) 340–342. doi:10.1038/nature17197.
- [578] Rantala A, Johansson PH, Naab T, Thomas J, Frigo M. The Formation of Extremely Diffuse Galaxy Cores by Merging Supermassive Black Holes. *ApJ* **864** (2018) 113. doi:10.3847/1538-4357/aada47.
- [579] Sahu N, Graham AW, Davis BL. Defining the (Black Hole)-Spheroid Connection with the Discovery of Morphology-dependent Substructure in the M_{BH} - n_{sph} and M_{BH} - $R_{e,sph}$ Diagrams: New Tests for Advanced Theories and Realistic Simulations. *ApJ* **903** (2020) 97. doi:10.3847/1538-4357/abb675.
- [580] Kormendy J, Kennicutt J Robert C. Secular Evolution and the Formation of Pseudobulges in Disk Galaxies. *AnnRevAap* **42** (2004) 603–683. doi:10.1146/annurev.astro.42.053102.134024.
- [581] Kormendy J, Bender R. A Revised Parallel-sequence Morphological Classification of Galaxies: Structure and Formation of S0 and Spheroidal Galaxies. *ApJS* **198** (2012) 2. doi:10.1088/0067-0049/198/1/2.
- [582] Merritt D, Ferrarese L, Joseph CL. No Supermassive Black Hole in M33? *Science* **293** (2001) 1116–1119. doi:10.1126/science.1063896.
- [583] Gebhardt K, Lauer TR, Kormendy J, Pinkney J, Bower GA, Green R, et al. M33: A Galaxy with No Supermassive Black Hole. *The Astronomical Journal* **122** (2001) 2469–2476. doi:10.1086/323481.
- [584] Valluri M, Merritt D, Emsellem E. Difficulties with Recovering the Masses of Supermassive Black Holes from Stellar Kinematical Data. *The Astrophysical Journal* **602** (2004) 66–92. doi:10.1086/380896.
- [585] Verolme EK, Cappellari M, Copin Y, van der Marel RP, Bacon R, Bureau M, et al. A SAURON study of M32: measuring the intrinsic flattening and the central black hole mass. *Mon. Not. R. Astron. Soc.* **335** (2002) 517–525. doi:10.1046/j.1365-8711.2002.05664.x.
- [586] Kormendy J, McClure RD. The Nucleus of M33. *The Astronomical Journal* **105** (1993) 1793. doi:10.1086/116555.
- [587] Butler DJ, Martínez-Delgado D. On the Stellar Populations in NGC 185 and NGC 205 and the Nuclear Star Cluster in NGC 205 from Hubble Space Telescope Observations. *The Astronomical Journal* **129** (2005) 2217–2231. doi:10.1086/429524.
- [588] Binggeli B, Sandage A, Tammann GA. Studies of the Virgo cluster. II. A catalog of 2096 galaxies in the Virgo cluster area. *The Astronomical Journal* **90** (1985) 1681–1758. doi:10.1086/113874.
- [589] Ferguson HC. Population Studies in Groups and Clusters of Galaxies. II. A Catalog of Galaxies in the Central 3.5 Degrees of the Fornax Cluster. *The Astronomical Journal* **98** (1989) 367. doi:10.1086/115152.
- [590] Binggeli B, Cameron LM. Dwarf galaxies in the Virgo cluster. I. The systematic photometric properties of early-type dwarfs. *Astronomy and Astrophysics* **252** (1991) 27.
- [591] Carollo CM, Stiavelli M, Mack J. Spiral Galaxies with WFPC2. II. The Nuclear Properties of 40 Objects. *The Astronomical Journal* **116** (1998) 68–84. doi:10.1086/300407.
- [592] Matthews LD, Gallagher I John S, Krist JE, Watson AM, Burrows CJ, Griffiths RE, et al. WFPC2 Observations of Compact Star Cluster Nuclei in Low-Luminosity Spiral Galaxies. *The Astronomical Journal* **118** (1999) 208–235. doi:10.1086/300909.

- [593] Böker T, Laine S, van der Marel RP, Sarzi M, Rix HW, Ho LC, et al. A Hubble Space Telescope Census of Nuclear Star Clusters in Late-Type Spiral Galaxies. I. Observations and Image Analysis. *The Astronomical Journal* **123** (2002) 1389–1410. doi:10.1086/339025.
- [594] Balcells M, Graham AW, Domínguez-Palmero L, Peletier RF. Galactic Bulges from Hubble Space Telescope Near-Infrared Camera Multi-Object Spectrometer Observations: The Lack of $r^{1/4}$ Bulges. *The Astrophysical Journal Lett.* **582** (2003) L79–L82. doi:10.1086/367783.
- [595] Lotz JM, Miller BW, Ferguson HC. The Colors of Dwarf Elliptical Galaxy Globular Cluster Systems, Nuclei, and Stellar Halos. *The Astrophysical Journal* **613** (2004) 262–278. doi:10.1086/422871.
- [596] Grant NI, Kuipers JA, Phillipps S. Nucleated dwarf elliptical galaxies in the Virgo cluster. *Mon. Not. R. Astron. Soc.* **363** (2005) 1019–1030. doi:10.1111/j.1365-2966.2005.09518.x.
- [597] Côté P, Piatek S, Ferrarese L, Jordán A, Merritt D, Peng EW, et al. The ACS Virgo Cluster Survey. VIII. The Nuclei of Early-Type Galaxies. *The Astrophysical Journal Suppl.* **165** (2006) 57–94. doi:10.1086/504042.
- [598] Greene JE, Strader J, Ho LC. Intermediate-Mass Black Holes. *AnnRevAap* **58** (2020) 257–312. doi:10.1146/annurev-astro-032620-021835.
- [599] Graham AW, Spitler LR. Quantifying the coexistence of massive black holes and dense nuclear star clusters. *MNRAS* **397** (2009) 2148–2162. doi:10.1111/j.1365-2966.2009.15118.x.
- [600] Antonini F, Gieles M, Gualandris A. Black hole growth through hierarchical black hole mergers in dense star clusters: implications for gravitational wave detections. *MNRAS* **486** (2019) 5008–5021. doi:10.1093/mnras/stz1149.
- [601] Graham AW, Scott N. The (Black Hole)-bulge Mass Scaling Relation at Low Masses. *ApJ* **798** (2015) 54. doi:10.1088/0004-637X/798/1/54.
- [602] Gezari S. Tidal Disruption Events. *arXiv e-prints* (2021) arXiv:2104.14580.
- [603] Mockler B, Guillochon J, Ramirez-Ruiz E. Weighing Black Holes Using Tidal Disruption Events. *ApJ* **872** (2019) 151. doi:10.3847/1538-4357/ab010f.
- [604] Davies RI, Thomas J, Genzel R, Müller Sánchez F, Tacconi LJ, Sternberg A, et al. The Star-forming Torus and Stellar Dynamical Black Hole Mass in the Seyfert 1 Nucleus of NGC 3227. *ApJ* **646** (2006) 754–773. doi:10.1086/504963.
- [605] Raimundo SI, Davies RI, Gandhi P, Fabian AC, Canning REA, Ivanov VD. The black hole and central stellar population of MCG-6-30-15. *MNRAS* **431** (2013) 2294–2306. doi:10.1093/mnras/stt327.
- [606] Siopis C, Gebhardt K, Lauer TR, Kormendy J, Pinkney J, Richstone D, et al. A Stellar Dynamical Measurement of the Black Hole Mass in the Maser Galaxy NGC 4258. *ApJ* **693** (2009) 946–969. doi:10.1088/0004-637X/693/1/946.
- [607] Neumayer N, Cappellari M, Reunanen J, Rix HW, van der Werf PP, de Zeeuw PT, et al. The Central Parsecs of Centaurus A: High-excitation Gas, a Molecular Disk, and the Mass of the Black Hole. *ApJ* **671** (2007) 1329–1344. doi:10.1086/523039.
- [608] Miyoshi M, Moran J, Herrnstein J, Greenhill L, Nakai N, Diamond P, et al. Evidence for a black hole from high rotation velocities in a sub-parsec region of NGC4258. *Nat* **373** (1995) 127–129. doi:10.1038/373127a0.
- [609] Herrnstein JR, Moran JM, Greenhill LJ, Trotter AS. The Geometry of and Mass Accretion Rate through the Maser Accretion Disk in NGC 4258. *ApJ* **629** (2005) 719–738. doi:10.1086/431421.
- [610] Greene JE, Peng CY, Kim M, Kuo CY, Braatz JA, Violette Impellizzeri CM, et al. Precise Black Hole Masses from Megamaser Disks: Black Hole-Bulge Relations at Low Mass. *ApJ* **721** (2010) 26–45. doi:10.1088/0004-637X/721/1/26.

- [611] Huré JM, Hersant F, Surville C, Nakai N, Jacq T. AGN disks and black holes on the weighting scales. *AAp* **530** (2011) A145. doi:10.1051/0004-6361/201015062.
- [612] Kuo CY, Reid MJ, Braatz JA, Gao F, Impellizzeri CMV, Chien WT. On Estimating the Mass of Keplerian Accretion Disks in H₂O Maser Galaxies. *ApJ* **859** (2018) 172. doi:10.3847/1538-4357/aabff1.
- [613] Kuo CY, Braatz JA, Impellizzeri CMV, Gao F, Pesce D, Reid MJ, et al. The Megamaser Cosmology Project - XII. VLBI imaging of H₂O maser emission in three active galaxies and the effect of AGN winds on disc dynamics. *MNRAS* **498** (2020) 1609–1627. doi:10.1093/mnras/staa2260.
- [614] van den Bosch RCE, Greene JE, Braatz JA, Constantin A, Kuo CY. TOWARD PRECISION SUPERMASSIVE BLACK HOLE MASSES USING MEGAMASER DISKS. *The Astrophysical Journal* **819** (2016) 11. doi:10.3847/0004-637x/819/1/11.
- [615] Constantin A. Linking the Supermassive Black Hole Growth with the Megamaser Emission. *Journal of Physics Conference Series* (2012), *Journal of Physics Conference Series*, vol. 372, 012047. doi:10.1088/1742-6596/372/1/012047.
- [616] Stacey HR, Lafontaine A, McKean JP. Smoke on the water: CO and H₂O in a circumnuclear disc around a quasar at redshift 2.64. *MNRAS* **493** (2020) 5290–5300. doi:10.1093/mnras/staa494.
- [617] Broome M, Impellizzeri V, Ivison R, Messias H. Hunting for High-Redshift Water Masers: Searching for Circumnuclear Megamasers Using the VLA. *American Astronomical Society Meeting Abstracts #233* (2019), *American Astronomical Society Meeting Abstracts*, vol. 233, 454.13.
- [618] Taylor AR. The Square Kilometre Array. Jin WJ, Platais I, Perryman MAC, editors, *A Giant Step: from Milli- to Micro-arcsecond Astrometry* (2008), vol. 248, 164–169. doi:10.1017/S1743921308018954.
- [619] Onishi K, Iguchi S, Sheth K, Kohno K. A Measurement of the Black Hole Mass in NGC 1097 Using ALMA. *ApJ* **806** (2015) 39. doi:10.1088/0004-637X/806/1/39.
- [620] Ruffa I, Davis TA, Prandoni I, Laing RA, Paladino R, Parma P, et al. The AGN fuelling/feedback cycle in nearby radio galaxies - II. Kinematics of the molecular gas. *MNRAS* **489** (2019) 3739–3757. doi:10.1093/mnras/stz2368.
- [621] Pastorini G, Marconi A, Capetti A, Axon DJ, Alonso-Herrero A, Atkinson J, et al. Supermassive black holes in the Sbc spiral galaxies NGC 3310, NGC 4303 and NGC 4258. *AAp* **469** (2007) 405–423. doi:10.1051/0004-6361:20066784.
- [622] Hicks EKS, Malkan MA. Circumnuclear Gas in Seyfert 1 Galaxies: Morphology, Kinematics, and Direct Measurement of Black Hole Masses. *ApJS* **174** (2008) 31–73. doi:10.1086/521650.
- [623] Zamanov R, Marziani P, Sulentic JW, Calvani M, Dultzin-Hacyan D, Bachev R. Kinematic Linkage between the Broad- and Narrow-Line-emitting Gas in Active Galactic Nuclei. *ApJL* **576** (2002) L9–L13. doi:10.1086/342783.
- [624] Xu D, Komossa S. New insights into AGNs with low-mass black holes and high accretion rates: the case of narrow-line Seyfert 1 galaxies. *Science China Physics, Mechanics, and Astronomy* **53** (2010) 216–219. doi:10.1007/s11433-010-0060-y.
- [625] Marziani P, Sulentic JW, Stirpe GM, Dultzin D, Del Olmo A, Martínez-Carballo MA. Blue outliers among intermediate redshift quasars. *ApSpSci* **361** (2016) 3. doi:10.1007/s10509-015-2590-2.
- [626] Schmidt EO, Oio GA, Ferreira D, Vega L, Weidmann W. Asymmetric emission of the [OIII]λ5007 profile in narrow-line Seyfert 1 galaxies. *AAp* **615** (2018) A13. doi:10.1051/0004-6361/201731557.
- [627] Berton M, Foschini L, Ciroi S, Cracco V, La Mura G, Di Mille F, et al. [O III] line properties in two samples of radio-emitting narrow-line Seyfert 1 galaxies. *AAp* **591** (2016) A88. doi:10.1051/0004-6361/201527056.

- [628] Gnerucci A, Marconi A, Capetti A, Axon DJ, Robinson A, Neumayer N. Spectroastrometry of rotating gas disks for the detection of supermassive black holes in galactic nuclei. II. Application to the galaxy Centaurus A (NGC 5128). *AAp* **536** (2011) A86. doi:10.1051/0004-6361/201117388.
- [629] Gravity Collaboration, Abuter R, Amorim A, Bauböck M, Berger JP, Bonnet H, et al. Improved GRAVITY astrometric accuracy from modeling optical aberrations. *AAp* **647** (2021) A59. doi:10.1051/0004-6361/202040208.
- [630] Gravity Collaboration, Abuter R, Accardo M, Amorim A, Anugu N, Ávila G, et al. First light for GRAVITY: Phase referencing optical interferometry for the Very Large Telescope Interferometer. *AAp* **602** (2017) A94. doi:10.1051/0004-6361/201730838.
- [631] Gravity Collaboration, Sturm E, Dexter J, Pfuhl O, Stock MR, Davies RI, et al. Spatially resolved rotation of the broad-line region of a quasar at sub-parsec scale. *Nat* **563** (2018) 657–660. doi:10.1038/s41586-018-0731-9.
- [632] Gravity Collaboration, Abuter R, Accardo M, Amorim A, Anugu N, Ávila G, et al. First light for GRAVITY: Phase referencing optical interferometry for the Very Large Telescope Interferometer. *AAp* **602** (2017) A94. doi:10.1051/0004-6361/201730838.
- [633] Bosco F, Hennawi JF, Stern J, Pott JU. Spatially Resolving the Kinematics of the $\lesssim 100 \mu\text{as}$ Quasar Broad-line Region Using Spectroastrometry II. The First Tentative Detection in a Luminous Quasar at $z = 2.3$. *arXiv e-prints* (2021) arXiv:2106.15900.
- [634] GRAVITY Collaboration, Amorim A, Bauböck M, Brandner W, Bolzer M, Clénet Y, et al. The central parsec of NGC 3783: a rotating broad emission line region, asymmetric hot dust structure, and compact coronal line region. *arXiv e-prints* (2021) arXiv:2102.00068.
- [635] Shuder JM. Emission-line-continuum correlations in active galactic nuclei. *ApJ* **244** (1981) 12–18. doi:10.1086/158678.
- [636] Peterson BM. Reverberation mapping of active galactic nuclei. *PASP* **105** (1993) 247–268. doi:10.1086/133140.
- [637] Brotherton MS, Du P, Xiao M, Bao DW, Zhao B, McLane JN, et al. Monitoring AGNs with $H\beta$ Asymmetry. II. Reverberation Mapping of Three Seyfert Galaxies Historically Displaying $H\beta$ Profiles with Changing Asymmetry: Mrk 79, NGC 3227, and Mrk 841. *ApJ* **905** (2020) 77. doi:10.3847/1538-4357/abc2d2.
- [638] Williams PR, Treu T, Dahle H, Valenti S, Abramson L, Barth AJ, et al. The Black Hole Mass of the $z = 2.805$ Multiply Imaged Quasar SDSS J2222+2745 from Velocity-resolved Time Lags of the C IV Emission Line. *ApJ* **911** (2021) 64. doi:10.3847/1538-4357/abe943.
- [639] Horne K, Peterson BM, Collier SJ, Netzer H. Observational Requirements for High-Fidelity Reverberation Mapping. *PASP* **116** (2004) 465–476. doi:10.1086/420755.
- [640] Marziani P, Dultzin-Hacyan D, Sulentic JW. Accretion onto Supermassive Black Holes in Quasars: Learning from Optical/UV Observations. Kreitler PV, editor, *New Developments in Black Hole Research* (Nova Press, New York) (2006), 123.
- [641] Peterson BM. Measuring the Masses of Supermassive Black Holes. *SpScieRev* **183** (2014) 253–275. doi:10.1007/s11214-013-9987-4.
- [642] Li J, Shen Y, Horne K, Brandt WN, Greene JE, Grier CJ, et al. The Sloan Digital Sky Survey Reverberation Mapping Project: Composite Lags at $z \leq 1$. *ApJ* **846** (2017) 79. doi:10.3847/1538-4357/aa845d.
- [643] Du P, Wang JM. The Radius-Luminosity Relationship Depends on Optical Spectra in Active Galactic Nuclei. *ApJ* **886** (2019) 42. doi:10.3847/1538-4357/ab4908.

- [644] Bentz MC, Denney KD, Grier CJ, Barth AJ, Peterson BM, Vestergaard M, et al. The Low-luminosity End of the Radius-Luminosity Relationship for Active Galactic Nuclei. *ApJ* **767** (2013) 149. doi:10.1088/0004-637X/767/2/149.
- [645] Du P, Lu KX, Hu C, Qiu J, Li YR, Huang YK, et al. Supermassive Black Holes with High Accretion Rates in Active Galactic Nuclei. VI. Velocity-resolved Reverberation Mapping of the H β Line. *ApJ* **820** (2016) 27. doi:10.3847/0004-637X/820/1/27.
- [646] Du P, Zhang ZX, Wang K, Huang YK, Zhang Y, Lu KX, et al. Supermassive Black Holes with High Accretion Rates in Active Galactic Nuclei. IX. 10 New Observations of Reverberation Mapping and Shortened H β Lags. *ApJ* **856** (2018) 6. doi:10.3847/1538-4357/aaae6b.
- [647] Kaspi S, Smith PS, Netzer H, Maoz D, Jannuzi BT, Giveon U. Reverberation Measurements for 17 Quasars and the Size-Mass-Luminosity Relations in Active Galactic Nuclei. *ApJ* **533** (2000) 631–649. doi:10.1086/308704.
- [648] Peterson BM. Space Telescope and Optical Reverberation Mapping Project: A Leap Forward in Reverberation Mapping. *IAU Symposium* (2017), *IAU Symposium*, vol. 324, 215–218. doi:10.1017/S1743921316012680.
- [649] Bentz MC, Peterson BM, Pogge RW, Vestergaard M, Onken CA. The Radius-Luminosity Relationship for Active Galactic Nuclei: The Effect of Host-Galaxy Starlight on Luminosity Measurements. *ApJ* **644** (2006) 133–142. doi:10.1086/503537.
- [650] Bentz MC, Peterson BM, Netzer H, Pogge RW, Vestergaard M. The Radius-Luminosity Relationship for Active Galactic Nuclei: The Effect of Host-Galaxy Starlight on Luminosity Measurements. II. The Full Sample of Reverberation-Mapped AGNs. *ApJ* **697** (2009) 160–181. doi:10.1088/0004-637X/697/1/160.
- [651] Bentz MC, Walsh JL, Barth AJ, Yoshii Y, Woo JH, Wang X, et al. The Lick AGN Monitoring Project: Reverberation Mapping of Optical Hydrogen and Helium Recombination Lines. *ApJ* **716** (2010) 993–1011. doi:10.1088/0004-637X/716/2/993.
- [652] Martínez-Aldama ML, Zajaček M, Czerny B, Panda S. Scatter Analysis along the Multidimensional Radius-Luminosity Relations for Reverberation-mapped Mg II Sources. *ApJ* **903** (2020) 86. doi:10.3847/1538-4357/abb6f8.
- [653] Vestergaard M, Peterson BM. Determining Central Black Hole Masses in Distant Active Galaxies and Quasars. II. Improved Optical and UV Scaling Relationships. *ApJ* **641** (2006) 689–709. doi:10.1086/500572.
- [654] Gaskell CM. A redshift difference between high and low ionization emission-line regions in QSOs - Evidence for radial motions. *ApJ* **263** (1982) 79–86. doi:10.1086/160481.
- [655] Tytler D, Fan XM. Systematic QSO emission-line velocity shifts and new unbiased redshifts. *ApJS* **79** (1992) 1–36. doi:10.1086/1916142.
- [656] Brotherton MS, Wills BJ, Steidel CC, Sargent WLW. Statistics of QSO broad emission-line profiles. 2: The C IV wavelength 1549, C III) wavelength 1909, and MG II wavelength 2798 lines. *ApJ* **423** (1994) 131–142. doi:10.1086/173171.
- [657] Marziani P, Sulentic JW, Dultzin-Hacyan D, Calvani M, Moles M. Comparative Analysis of the High- and Low-Ionization Lines in the Broad-Line Region of Active Galactic Nuclei. *ApJS* **104** (1996) 37–+. doi:10.1086/192291.
- [658] Leighly KM, Moore JR. Hubble Space Telescope STIS Ultraviolet Spectral Evidence of Outflow in Extreme Narrow-Line Seyfert 1 Galaxies. I. Data and Analysis. *ApJ* **611** (2004) 107–124. doi:10.1086/422088.

- [659] Capetti A, Axon DJ, Macchetto F, Sparks WB, Boksenberg A. Radio Outflows and the Origin of the Narrow-Line Region in Seyfert Galaxies. *ApJ* **469** (1996) 554. doi:10.1086/177804.
- [660] Colbert EJM, Baum SA, O'Dea CP, Veilleux S. Large-Scale Outflows in Edge-on Seyfert Galaxies. III. Kiloparsec-Scale Soft X-Ray Emission. *ApJ* **496** (1998) 786–796. doi:10.1086/305417.
- [661] Everett JE. Outflows from AGNs: a brief overview of observations and models. *ApSpSci* **311** (2007) 269–273. doi:10.1007/s10509-007-9536-2.
- [662] Carniani S, Marconi A, Maiolino R, Balmaverde B, Brusa M, Cano-Díaz M, et al. Ionised outflows in $z \sim 2.4$ quasar host galaxies. *AAP* **580** (2015) A102. doi:10.1051/0004-6361/201526557.
- [663] Cresci G, Marconi A, Zibetti S, Risaliti G, Carniani S, Mannucci F, et al. The MAGNUM survey: positive feedback in the nuclear region of NGC 5643 suggested by MUSE. *AAP* **582** (2015) A63. doi:10.1051/0004-6361/201526581.
- [664] Bischetti M, Piconcelli E, Vietri G, Bongiorno A, Fiore F, Sani E, et al. The WISSH quasars project. I. Powerful ionised outflows in hyper-luminous quasars. *AAP* **598** (2017) A122. doi:10.1051/0004-6361/201629301.
- [665] Komossa S, Xu DW, Wagner AY. Extreme gaseous outflows in radio-loud narrow-line Seyfert 1 galaxies. *MNRAS* **477** (2018) 5115–5126. doi:10.1093/mnras/sty901.
- [666] Bañados E, Venemans BP, Mazzucchelli C, Farina EP, Walter F, Wang F, et al. An 800-million-solar-mass black hole in a significantly neutral Universe at a redshift of 7.5. *Nat* **553** (2018) 473–476. doi:10.1038/nature25180.
- [667] Nardini E, Lusso E, Risaliti G, Bisogni S, Civano F, Elvis M, et al. The most luminous blue quasars at $3.0 < z < 3.3$. I. A tale of two X-ray populations. *AAP* **632** (2019) A109. doi:10.1051/0004-6361/201936911.
- [668] Coatman L, Hewett PC, Banerji M, Richards GT. C iv emission-line properties and systematic trends in quasar black hole mass estimates. *MNRAS* **461** (2016) 647–665. doi:10.1093/mnras/stw1360.
- [669] Sulentic JW, del Olmo A, Marziani P, Martínez-Carballo MA, D'Onofrio M, Dultzin D, et al. What does CIV λ 1549 tell us about the physical driver of the Eigenvector quasar sequence? *AAP* **608** (2017) A122. doi:10.1051/0004-6361/201630309.
- [670] Marinello M, Rodríguez-Ardila A, Marziani P, Sigut A, Pradhan A. Panchromatic properties of the extreme Fe II emitter PHL 1092. *MNRAS* **494** (2020) 4187–4202. doi:10.1093/mnras/staa934.
- [671] Marinello M, Overzier RA, Röttgering HJA, Kurk JD, De Breuck C, Vernet J, et al. VLT/SINFONI study of black hole growth in high-redshift radio-loud quasars from the CARLA survey. *MNRAS* **492** (2020) 1991–2016. doi:10.1093/mnras/stz3333.
- [672] Netzer H, Lira P, Trakhtenbrot B, Shemmer O, Cury I. Black Hole Mass and Growth Rate at High Redshift. *ApJ* **671** (2007) 1256–1263. doi:10.1086/523035.
- [673] Sulentic JW, Bachev R, Marziani P, Negrete CA, Dultzin D. C IV λ 1549 as an Eigenvector 1 Parameter for Active Galactic Nuclei. *ApJ* **666** (2007) 757–777. doi:10.1086/519916.
- [674] Mejía-Restrepo JE, Trakhtenbrot B, Lira P, Netzer H, Capellupo DM. Active galactic nuclei at $z \sim 1.5$: II. Black Hole Mass estimation by means of broad emission lines. *MNRAS* **460** (2016).
- [675] Mejía-Restrepo JE, Lira P, Netzer H, Trakhtenbrot B, Capellupo DM. The effect of nuclear gas distribution on the mass determination of supermassive black holes. *Nature Astronomy* **2** (2018) 63–68. doi:10.1038/s41550-017-0305-z.
- [676] Trakhtenbrot B, Urry CM, Civano F, Rosario DJ, Elvis M, Schawinski K, et al. An over-massive black hole in a typical star-forming galaxy, 2 billion years after the Big Bang. *Science* **349** (2015) 168–171. doi:10.1126/science.aaa4506.

- [677] Trakhtenbrot B, Netzer H. Black hole growth to $z = 2$ - I. Improved virial methods for measuring M_{BH} and L/L_{Edd} . *MNRAS* **427** (2012) 3081–3102. doi:10.1111/j.1365-2966.2012.22056.x.
- [678] Shen Y, Liu X. Comparing Single-epoch Virial Black Hole Mass Estimators for Luminous Quasars. *ApJ* **753** (2012) 125. doi:10.1088/0004-637X/753/2/125.
- [679] Coatman L, Hewett PC, Banerji M, Richards GT, Hennawi JF, Prochaska JX. Correcting C IV-based virial black hole masses. *MNRAS* **465** (2017) 2120–2142. doi:10.1093/mnras/stw2797.
- [680] Marziani P, del Olmo A, Martínez-Carballo MA, Martínez-Aldama ML, Stirpe GM, Negrete CA, et al. Black hole mass estimates in quasars. A comparative analysis of high- and low-ionization lines. *AAP* **627** (2019) A88. doi:10.1051/0004-6361/201935265.
- [681] Park D, Woo JH, Denney KD, Shin J. Calibrating C-IV-based Black Hole Mass Estimators. *ApJ* **770** (2013) 87. doi:10.1088/0004-637X/770/2/87.
- [682] Antonucci R. Unified models for active galactic nuclei and quasars. *AnnRevAap* **31** (1993) 473–521. doi:10.1146/annurev.aa.31.090193.002353.
- [683] Urry CM, Padovani P. Unified Schemes for Radio-Loud Active Galactic Nuclei. *PASP* **107** (1995) 803. doi:10.1086/133630.
- [684] McLure RJ, Jarvis MJ. Measuring the black hole masses of high-redshift quasars. *MNRAS* **337** (2002) 109–116. doi:10.1046/j.1365-8711.2002.05871.x.
- [685] Collin S, Kawaguchi T, Peterson BM, Vestergaard M. Systematic effects in measurement of black hole masses by emission-line reverberation of active galactic nuclei: Eddington ratio and inclination. *A&Ap* **456** (2006) 75–90. doi:10.1051/0004-6361:20064878.
- [686] Decarli R, Dotti M, Treves A. Geometry and inclination of the broad-line region in blazars. *MNRAS* **413** (2011) 39–46. doi:10.1111/j.1365-2966.2010.18102.x.
- [687] Wills BJ, Browne IWA. Relativistic beaming and quasar emission lines. *ApJ* **302** (1986) 56–63. doi:10.1086/163973.
- [688] Punsly B, Marziani P, Berton M, Kharb P. The Extreme Red Excess in Blazar Ultraviolet Broad Emission Lines. *ApJ* **903** (2020) 44. doi:10.3847/1538-4357/abb950.
- [689] Savić D, Goosmann R, Popović LČ, Marin F, Afanasiev VL. AGN black hole mass estimates using polarization in broad emission lines. *AAP* **614** (2018) A120. doi:10.1051/0004-6361/201732220.
- [690] Afanasiev VL, Popović LČ, Shapovalova AI. Spectropolarimetry of Seyfert 1 galaxies with equatorial scattering: black hole masses and broad-line region characteristics. *MNRAS* **482** (2019) 4985–4999. doi:10.1093/mnras/sty2995.
- [691] Savić D., Popović LČ, Shablovinskaya E, Afanasiev VL. Estimating supermassive black hole masses in active galactic nuclei using polarization of broad Mg II, H α , and H β lines. *MNRAS* **497** (2020) 3047–3054. doi:10.1093/mnras/staa2039.
- [692] Capetti A, Laor A, Baldi RD, Robinson A, Marconi A. Spectropolarimetry of low redshift quasars: origin of the polarization and implications for black hole mass estimates. *MNRAS* **502** (2021) 5086–5103. doi:10.1093/mnras/stab279.
- [693] Martínez-Aldama ML, Czerny B, Kawka D, Karas V, Panda S, Zajaček M, et al. Can Reverberation-measured Quasars Be Used for Cosmology? *ApJ* **883** (2019) 170. doi:10.3847/1538-4357/ab3728.
- [694] Bon N, Marziani P, Bon E, Negrete CA, Dultzin D, del Olmo A, et al. Selection of highly-accreting quasars. Spectral properties of Fe II_{opt} emitters not belonging to extreme Population A. *AAP* **635** (2020) A151. doi:10.1051/0004-6361/201936773.
- [695] Netzer H, Marziani P. The Effect of Radiation Pressure on Emission-line Profiles and Black Hole Mass Determination in Active Galactic Nuclei. *ApJ* **724** (2010) 318–328. doi:10.1088/0004-637X/724/1/318.

- [696] Khajenabi F. On the dynamics of clouds in the broad-line region of AGNs with an ADAF atmosphere. *MNRAS* **446** (2015) 1848–1854. doi:10.1093/mnras/stu2193.
- [697] Pancoast A, Brewer BJ, Treu T. Modelling reverberation mapping data - I. Improved geometric and dynamical models and comparison with cross-correlation results. *MNRAS* **445** (2014) 3055–3072. doi:10.1093/mnras/stu1809.
- [698] Pancoast A, Brewer BJ, Treu T, Park D, Barth AJ, Bentz MC, et al. Modelling reverberation mapping data - II. Dynamical modelling of the Lick AGN Monitoring Project 2008 data set. *MNRAS* **445** (2014) 3073–3091. doi:10.1093/mnras/stu1419.
- [699] Pancoast A, Barth AJ, Horne K, Treu T, Brewer BJ, Bennert VN, et al. Stability of the Broad-line Region Geometry and Dynamics in Arp 151 Over Seven Years. *ApJ* **856** (2018) 108. doi:10.3847/1538-4357/aab3c6.
- [700] Williams PR, Pancoast A, Treu T, Brewer BJ, Peterson BM, Barth AJ, et al. Space Telescope and Optical Reverberation Mapping Project. XII. Broad-line Region Modeling of NGC 5548. *ApJ* **902** (2020) 74. doi:10.3847/1538-4357/abbad7.
- [701] Collin-Souffrin S, Dyson JE, McDowell JC, Perry JJ. The environment of active galactic nuclei. I - A two-component broad emission line model. *MNRAS* **232** (1988) 539–550.
- [702] Dumont AM, Collin-Souffrin S. Line and Continuum Emission from the Outer Regions of Accretion Discs in Active Galactic Nuclei - Part IV - Line Emission. *AAp* **229** (1990) 313–+.
- [703] Rees MJ. Magnetic confinement of broad-line clouds in active galactic nuclei. *MNRAS* **228** (1987) 47P–50. doi:10.1093/mnras/228.1.47P.
- [704] Bottorff MC, Ferland GJ. Magnetic confinement, magnetohydrodynamic waves and smooth line profiles in active galactic nuclei. *MNRAS* **316** (2000) 103–106. doi:10.1046/j.1365-8711.2000.03465.x.
- [705] Chelouche D, Netzer H. Radiation pressure acceleration by X-rays in active galactic nuclei. *MNRAS* **326** (2001) 916–926. doi:10.1046/j.1365-8711.2001.04586.x.
- [706] Shadmehri M. On the orbital motion of cold clouds in broad-line regions. *MNRAS* **451** (2015) 3671–3678. doi:10.1093/mnras/stv1212.
- [707] Esser J, Pott JU, Landt H, Vacca WD. Analyzing temporal variations of AGN emission line profiles in the context of (dusty) cloud structure formation in the broad line region. *AAp* **621** (2019) A46. doi:10.1051/0004-6361/201834291.
- [708] Woo JH, Yoon Y, Park S, Park D, Kim SC. The Black Hole Mass-Stellar Velocity Dispersion Relation of Narrow-line Seyfert 1 Galaxies. *ApJ* **801** (2015) 38. doi:10.1088/0004-637X/801/1/38.
- [709] Shankar F, Bernardi M, Haiman Z. The Evolution of the $M_{BH}-\sigma$ Relation Inferred from the Age Distribution of Local Early-Type Galaxies and Active Galactic Nuclei Evolution. *The Astrophysical Journal* **694** (2009) 867–878. doi:10.1088/0004-637X/694/2/867.
- [710] Shankar F, Weinberg DH, Miralda-Escudé J. Self-Consistent Models of the AGN and Black Hole Populations: Duty Cycles, Accretion Rates, and the Mean Radiative Efficiency. *The Astrophysical Journal* **690** (2009) 20–41. doi:10.1088/0004-637X/690/1/20.
- [711] Alexander DM, Hickox RC. What drives the growth of black holes? *New Astronomy Review* **56** (2012) 93–121. doi:10.1016/j.newar.2011.11.003.
- [712] Granato GL, De Zotti G, Silva L, Bressan A, Danese L. A Physical Model for the Coevolution of QSOs and Their Spheroidal Hosts. *The Astrophysical Journal* **600** (2004) 580–594. doi:10.1086/379875.
- [713] Wandel A. Black Holes of Active and Quiescent Galaxies. I. The Black Hole-Bulge Relation Revisited. *ApJ* **565** (2002) 762–772. doi:10.1086/338134.

- [714] Schulze A, Wisotzki L. Selection effects in the black hole-bulge relation and its evolution. *AAP* **535** (2011) A87. doi:10.1051/0004-6361/201117564.
- [715] Peng CY, Impey CD, Ho LC, Barton EJ, Rix HW. Probing the Coevolution of Supermassive Black Holes and Quasar Host Galaxies. *ApJ* **640** (2006) 114–125. doi:10.1086/499930.
- [716] Peng CY, Impey CD, Rix HW, Kochanek CS, Keeton CR, Falco EE, et al. Probing the Coevolution of Supermassive Black Holes and Galaxies Using Gravitationally Lensed Quasar Hosts. *ApJ* **649** (2006) 616–634. doi:10.1086/506266.
- [717] Treu T, Woo JH, Malkan MA, Blandford RD. Cosmic Evolution of Black Holes and Spheroids. II. Scaling Relations at $z=0.36$. *ApJ* **667** (2007) 117–130. doi:10.1086/520633.
- [718] McLeod KK, Bechtold J. Host Galaxies of $z = 4$ Quasars. *ApJ* **704** (2009) 415–438. doi:10.1088/0004-637X/704/1/415.
- [719] Decarli R, Falomo R, Treves A, Kotilainen JK, Labita M, Scarpa R. The quasar MBH-Mhost relation through cosmic time - I. Data set and black hole masses. *MNRAS* **402** (2010) 2441–2452. doi:10.1111/j.1365-2966.2009.16048.x.
- [720] Bennert VN, Treu T, Woo JH, Malkan MA, Le Bris A, Auger MW, et al. Cosmic Evolution of Black Holes and Spheroids. IV. The $M_{BH}-L_{sph}$ Relation. *ApJ* **708** (2010) 1507–1527. doi:10.1088/0004-637X/708/2/1507.
- [721] Targett TA, Dunlop JS, McLure RJ, Best PN, Cirasuolo M, Almaini O. A near-infrared morphological comparison of high-redshift submillimetre and radio galaxies: massive star-forming discs versus relaxed spheroids. *MNRAS* **412** (2011) 295–317. doi:10.1111/j.1365-2966.2010.17905.x.
- [722] Schramm M, Wisotzki L, Jahnke K. Host galaxies of bright high redshift quasars: luminosities and colours. *AAP* **478** (2008) 311–319. doi:10.1051/0004-6361:20077319.
- [723] Nelson CH, Green RF, Bower G, Gebhardt K, Weistrop D. The Relationship Between Black Hole Mass and Velocity Dispersion in Seyfert 1 Galaxies. *ApJ* **615** (2004) 652–661. doi:10.1086/424657.
- [724] Bernardi M, Sheth RK, Tundo E, Hyde JB. Selection Bias in the $M_{\bullet}-\sigma$ and $M_{\bullet}-L$ Correlations and Its Consequences. *The Astrophysical Journal* **660** (2007) 267–275. doi:10.1086/512719.
- [725] Barth AJ, Son S, Kim M, Ho LC. A Hubble Snapshot Survey of AGN Host Galaxies from the Swift-BAT Sample. *American Astronomical Society Meeting Abstracts* (2021), *American Astronomical Society Meeting Abstracts*, vol. 53, 308.03.
- [726] Kim M, Ho LC. Evidence for a Young Stellar Population in Nearby Type 1 Active Galaxies. *ApJ* **876** (2019) 35. doi:10.3847/1538-4357/ab11cf.
- [727] Woo JH, Treu T, Malkan MA, Blandford RD. Cosmic Evolution of Black Holes and Spheroids. I. The $M_{BH}-\sigma$ Relation at $z = 0.36$. *ApJ* **645** (2006) 900–919. doi:10.1086/504586.
- [728] Woo JH, Treu T, Malkan MA, Blandford RD. Cosmic Evolution of Black Holes and Spheroids. III. The $M_{BH}-\sigma_{*}$ Relation in the Last Six Billion Years. *ApJ* **681** (2008) 925–930. doi:10.1086/588804.
- [729] Shen Y, Greene JE, Strauss MA, Richards GT, Schneider DP. Biases in Virial Black Hole Masses: An SDSS Perspective. *ApJ* **680** (2008) 169–190. doi:10.1086/587475.
- [730] Shields GA, Gebhardt K, Salviander S, Wills BJ, Xie B, Brotherton MS, et al. The Black Hole-Bulge Relationship in Quasars. *ApJ* **583** (2003) 124–133. doi:10.1086/345348.
- [731] Shields GA, Menezes KL, Massart CA, Vanden Bout P. The Black Hole-Bulge Relationship for QSOs at High Redshift. *ApJ* **641** (2006) 683–688. doi:10.1086/500542.
- [732] Salviander S, Shields GA, Gebhardt K, Bonning EW. The Black Hole Mass-Galaxy Bulge Relationship for QSOs in the Sloan Digital Sky Survey Data Release 3. *ApJ* **662** (2007) 131–144. doi:10.1086/513086.

- [733] Mathur S. Host galaxies of NLS1s. Foschini L, Colpi M, Gallo L, Grupe D, Komossa S, Leighly K, et al., editors, *Narrow-Line Seyfert 1 Galaxies and their Place in the Universe* (2011), 35.
- [734] Marziani P, Sulentic JW. Estimating black hole masses in quasars using broad optical and UV emission lines. *NARev* **56** (2012) 49–63. doi:10.1016/j.newar.2011.09.001.
- [735] Cracco V, Ciroi S, Berton M, Di Mille F, Foschini L, La Mura G, et al. A spectroscopic analysis of a sample of narrow-line Seyfert 1 galaxies selected from the Sloan Digital Sky Survey. *MNRAS* **462** (2016) 1256–1280. doi:10.1093/mnras/stw1689.
- [736] Inskip KJ, Jahnke K, Rix HW, van de Ven G. Resolving the Dynamical Mass of a $z \sim 1.3$ Quasi-stellar Object Host Galaxy Using SINFONI and Laser Guide Star Assisted Adaptive Optics. *ApJ* **739** (2011) 90. doi:10.1088/0004-637X/739/2/90.
- [737] Walter F, Bertoldi F, Carilli C, Cox P, Lo KY, Neri R, et al. Molecular gas in the host galaxy of a quasar at redshift $z = 6.42$. *Nat* **424** (2003) 406–408. doi:10.1038/nature01821.
- [738] Tan QH, Gao Y, Kohno K, Xia XY, Omont A, Hao CN, et al. Resolving the Interstellar Medium in Ultraluminous Infrared QSO Hosts with ALMA. *ApJ* **887** (2019) 24. doi:10.3847/1538-4357/ab50be.
- [739] Molina, J, Wang, R, Shangguan, J, et al. Compact Molecular Gas Distribution in Quasar Host Galaxies. *arXiv e-prints* (2021) arXiv:2101.00764.
- [740] Caglar T, Burtscher L, Brandl B, Brinchmann J, Davies RI, Hicks EKS, et al. LLAMA: The $M_{BH}-\sigma_*$ relation of the most luminous local AGNs. *Aap* **634** (2020) A114. doi:10.1051/0004-6361/201936321.
- [741] Kormendy J, Bender R, Cornell ME. Supermassive black holes do not correlate with galaxy disks or pseudobulges. *Nat* **469** (2011) 374–376. doi:10.1038/nature09694.
- [742] Ho LC, Kim M. The black hole mass scale of classical and pseudo bulges in active galaxies. *The Astrophysical Journal* **789** (2014) 17. doi:10.1088/0004-637x/789/1/17.
- [743] Park D, Kelly BC, Woo JH, Treu T. Recalibration of the Virial Factor and $M_{BH}-\sigma_*$ Relation for Local Active Galaxies. *ApJS* **203** (2012) 6. doi:10.1088/0067-0049/203/1/6.
- [744] Shankar F, Bernardi M, Richardson K, Marsden C, Sheth RK, Allevato V, et al. Black hole scaling relations of active and quiescent galaxies: Addressing selection effects and constraining virial factors. *MNRAS* **485** (2019) 1278–1292. doi:10.1093/mnras/stz376.
- [745] Gültekin K, Richstone DO, Gebhardt K, Lauer TR, Tremaine S, Aller MC, et al. The $M-\sigma$ and $M-L$ Relations in Galactic Bulges, and Determinations of Their Intrinsic Scatter. *ApJ* **698** (2009) 198–221. doi:10.1088/0004-637X/698/1/198.
- [746] Gültekin K, Tremaine S, Loeb A, Richstone DO. Observational Selection Effects and the $M-\sigma$ Relation. *ApJ* **738** (2011) 17. doi:10.1088/0004-637X/738/1/17.
- [747] Shankar F, Bernardi M, Sheth RK, Ferrarese L, Graham AW, Savorgnan G, et al. Selection bias in dynamically measured supermassive black hole samples: its consequences and the quest for the most fundamental relation. *MNRAS* **460** (2016) 3119–3142. doi:10.1093/mnras/stw678.
- [748] Lauer TR, Tremaine S, Richstone D, Faber SM. Selection Bias in Observing the Cosmological Evolution of the $M_\bullet-\sigma$ and $M_\bullet-L$ Relationships. *ApJ* **670** (2007) 249–260. doi:10.1086/522083.
- [749] Marziani P, Sulentic JW. Highly accreting quasars: sample definition and possible cosmological implications. *MNRAS* **442** (2014) 1211–1229. doi:10.1093/mnras/stu951.
- [750] Krongold Y, Dultzin-Hacyan D, Marziani P. Host Galaxies and Circumgalactic Environment of “Narrow Line” Seyfert 1 Nuclei. *AJ* **121** (2001) 702–709. doi:10.1086/318768.
- [751] Crenshaw DM, Kraemer SB, Gabel JR. The Host Galaxies of Narrow-Line Seyfert 1 Galaxies: Evidence for Bar-Driven Fueling. *AJ* **126** (2003) 1690–1698. doi:10.1086/377625.

- [752] Ohta K, Aoki K, Kawaguchi T, Kiuchi G. A Bar Fuels a Supermassive Black Hole?: Host Galaxies of Narrow-Line Seyfert 1 Galaxies. *ApJS* **169** (2007) 1–20. doi:10.1086/510204.
- [753] Mathur S, Kuraszekiewicz J, Czerny B. Evolution of active galaxies: black-hole mass-bulge relations for narrow line objects. *New Astronomy* **6** (2001) 321–329. doi:10.1016/S1384-1076(01)00058-6.
- [754] Chao LH, Bian WH, Huang KL. The relation between the Black hole mass and the Bulge mass for low redshift AGNs. Part I: Ground-based observations. *Advances in Space Research* **42** (2008) 544–549. doi:10.1016/j.asr.2007.11.012.
- [755] Orban de Xivry G, Davies R, Schartmann M, Komossa S, Marconi A, Hicks E, et al. The role of secular evolution in the black hole growth of narrow-line Seyfert 1 galaxies. *MNRAS* **417** (2011) 2721–2736. doi:10.1111/j.1365-2966.2011.19439.x.
- [756] Mathur S, Fields D, Peterson BM, Grupe D. Supermassive Black Holes, Pseudobulges, and the Narrow-line Seyfert 1 Galaxies. *ApJ* **754** (2012) 146. doi:10.1088/0004-637X/754/2/146.
- [757] Ermash AA, Komberg BV. Morphology and Evolutionary Status of Narrow Line Seyfert (NLS) Active Galaxies. *Astrophysics* **56** (2013) 569–596. doi:10.1007/s10511-013-9309-2.
- [758] Olguín-Iglesias A, Kotilainen JK, León Tavares J, Chavushyan V, Añorve C. Evidence of bar-driven secular evolution in the gamma-ray narrow-line Seyfert 1 galaxy FBQS J164442.5+261913. *MNRAS* **467** (2017) 3712–3722. doi:10.1093/mnras/stx022.
- [759] Järvelä E, Lähteenmäki A, Berton M. Near-infrared morphologies of the host galaxies of narrow-line Seyfert 1 galaxies. *AAP* **619** (2018) A69. doi:10.1051/0004-6361/201832876.
- [760] Doi A, Kino M, Kawakatu N, Hada K. The radio-loud narrow-line Seyfert 1 galaxy 1H 0323+342 in a galaxy merger. *MNRAS* **496** (2020) 1757–1765. doi:10.1093/mnras/staa1525.
- [761] Davis BL, Graham AW, Cameron E. Black Hole Mass Scaling Relations for Spiral Galaxies. II. $M_{BH} - M_{*,tot}$ and $M_{BH} - M_{*,disk}$. *ApJ* **869** (2018) 113. doi:10.3847/1538-4357/aae820.
- [762] Sanghvi J, Kotilainen JK, Falomo R, Decarli R, Karhunen K, Uslenghi M. The black hole-host galaxy relation for very low mass quasars. *MNRAS* **445** (2014) 1261–1268. doi:10.1093/mnras/stu1822.
- [763] Bennert VN, Auger MW, Treu T, Woo JH, Malkan MA. The Relation between Black Hole Mass and Host Spheroid Stellar Mass Out to $z \sim 2$. *ApJ* **742** (2011) 107. doi:10.1088/0004-637X/742/2/107.
- [764] Mezcuca M, Civano F, Fabbiano G, Miyaji T, Marchesi S. A Population of Intermediate-mass Black Holes in Dwarf Starburst Galaxies Up to Redshift=1.5. *ApJ* **817** (2016) 20. doi:10.3847/0004-637X/817/1/20.
- [765] Fornasini FM, Civano F, Fabbiano G, Elvis M, Marchesi S, Miyaji T, et al. Low-luminosity AGN and X-Ray Binary Populations in COSMOS Star-forming Galaxies. *ApJ* **865** (2018) 43. doi:10.3847/1538-4357/aada4e.
- [766] Zou F, Brandt WN, Vito F, Chen CT, Garmire GP, Stern D, et al. X-ray properties of dust-obscured galaxies with broad optical/UV emission lines. *MNRAS* **499** (2020) 1823–1840. doi:10.1093/mnras/staa2930.
- [767] Satyapal S, Kamal L, Cann JM, Secrest NJ, Abel NP. The Diagnostic Potential of JWST in Characterizing Elusive AGNs. *ApJ* **906** (2021) 35. doi:10.3847/1538-4357/abfbaf.
- [768] Magain P, Letawe G, Courbin F, Jablonka P, Jahnke K, Meylan G, et al. Discovery of a bright quasar without a massive host galaxy. *Nat* **437** (2005) 381–384. doi:10.1038/nature04013.
- [769] Sulentic JW, Arp H. The Galaxy-Quasar Connection: NGC 4319 and Markarian 205. II. Spectroscopy. *ApJ* **319** (1987) 693. doi:10.1086/165490.
- [770] Arp H, Sulentic JW, di Tullio G. Quasars aligned across NGC 3384. *ApJ* **229** (1979) 489–495. doi:10.1086/156980.

- [771] Sulentic J, Arp HC. Are Quasars Nearby / NGC4319 and MARKARIAN205. *Sky& Tel* **65** (1983) 322.
- [772] Kim M, Ho LC, Peng CY, Im M. The Host Galaxy of the Quasar HE 0450-2958. *ApJ* **658** (2007) 107–113. doi:10.1086/510846.
- [773] Reines AE, Plotkin RM, Russell TD, Mezcua M, Condon JJ, Sivakoff GR, et al. A Candidate Massive Black Hole in the Low-metallicity Dwarf Galaxy Pair Mrk 709. *ApJL* **787** (2014) L30. doi:10.1088/2041-8205/787/2/L30.
- [774] Seth AC, van den Bosch R, Mieske S, Baumgardt H, Brok MD, Strader J, et al. A supermassive black hole in an ultra-compact dwarf galaxy. *Nat* **513** (2014) 398–400. doi:10.1038/nature13762.
- [775] van Loon JT, Sansom AE. An evolutionary missing link? A modest-mass early-type galaxy hosting an oversized nuclear black hole. *MNRAS* **453** (2015) 2341–2348. doi:10.1093/mnras/stv1787.
- [776] Barber C, Schaye J, Bower RG, Crain RA, Schaller M, Theuns T. The origin of compact galaxies with anomalously high black hole masses. *MNRAS* **460** (2016) 1147–1161. doi:10.1093/mnras/stw1018.
- [777] Savorgnan GAD, Graham AW. Explaining the reportedly overmassive black holes in early-type galaxies with intermediate-scale discs. *MNRAS* **457** (2016) 320–327. doi:10.1093/mnras/stv2713.
- [778] Merritt D, Storchi-Bergmann T, Robinson A, Batcheldor D, Axon D, Cid Fernandes R. The nature of the HE0450-2958 system. *MNRAS* **367** (2006) 1746–1750. doi:10.1111/j.1365-2966.2006.10093.x.
- [779] Lipari S, Bergmann M, Sanchez S, Terlevich R, Taniguchi Y, Mediavilla E, et al. Gemini GMOS IFU Spectroscopy of IRAS 04505-2958: A New Exploding BAL + IR + Fe II QSO. *Boletín de la Asociación Argentina de Astronomía La Plata Argentina* **50** (2007) 259–262.
- [780] Du P, Wang JM, Hu C, Ho LC, Li YR, Bai JM. The Fundamental Plane of the Broad-line Region in Active Galactic Nuclei. *ApJL* **818** (2016) L14. doi:10.3847/2041-8205/818/1/L14.
- [781] Nguyen K, Bogdanović T. Emission Signatures from Sub-parsec Binary Supermassive Black Holes. I. Diagnostic Power of Broad Emission Lines. *ApJ* **828** (2016) 68. doi:10.3847/0004-637X/828/2/68.
- [782] Volonteri M. Gravitational Recoil: Signatures on the Massive Black Hole Population. *ApJL* **663** (2007) L5–L8. doi:10.1086/519525.
- [783] Blecha L, Cox TJ, Loeb A, Hernquist L. Recoiling black holes in merging galaxies: relationship to active galactic nucleus lifetimes, starbursts and the $M_{BH}-\sigma_*$ relation. *MNRAS* **412** (2011) 2154–2182. doi:10.1111/j.1365-2966.2010.18042.x.
- [784] Schulze A, Wisotzki L. Accounting for selection effects in the BH-bulge relations: no evidence for cosmological evolution. *MNRAS* **438** (2014) 3422–3433. doi:10.1093/mnras/stt2457.
- [785] Li JIH, Shen Y, Ho LC, Brandt WN, Dalla Bontà E, Fonseca Alvarez G, et al. The Sloan Digital Sky Survey Reverberation Mapping Project: The M_{BH} -Host Relations at $0.2 \lesssim z \lesssim 0.6$ from Reverberation Mapping and Hubble Space Telescope Imaging. *ApJ* **906** (2021) 103. doi:10.3847/1538-4357/abc8e6.
- [786] McLure RJ, Jarvis MJ, Targett TA, Dunlop JS, Best PN. On the evolution of the black hole: spheroid mass ratio. *MNRAS* **368** (2006) 1395–1403. doi:10.1111/j.1365-2966.2006.10228.x.
- [787] Decarli R, Walter F, Venemans BP, Bañados E, Bertoldi F, Carilli C, et al. An ALMA [C II] Survey of 27 Quasars at $z \lesssim 5.94$. *ApJ* **854** (2018) 97. doi:10.3847/1538-4357/aaa5aa.
- [788] Merloni A, Bongiorno A, Bolzonella M, Brusa M, Civano F, Comastri A, et al. On the Cosmic Evolution of the Scaling Relations Between Black Holes and Their Host Galaxies: Broad-Line Active Galactic Nuclei in the zCOSMOS Survey. *ApJ* **708** (2010) 137–157. doi:10.1088/0004-637X/708/1/137.
- [789] Vayner A, Wright SA, Murray N, Armus L, Boehle A, Cosens M, et al. A Spatially-Resolved Survey of Distant Quasar Host Galaxies: II. Photoionization and Kinematics of the ISM. *arXiv e-prints*

- (2021) arXiv:2101.08291.
- [790] Marshall MA, Ni Y, Di Matteo T, Wyithe JSB, Wilkins S, Croft RAC, et al. The host galaxies of $z = 7$ quasars: predictions from the BLUETIDES simulation. *MNRAS* **499** (2020) 3819–3836. doi:10.1093/mnras/staa2982.
- [791] Lupi A, Haiman Z, Volonteri M. Forming massive seed black holes in high-redshift quasar host progenitors. *arXiv e-prints* (2021) arXiv:2102.05051.
- [792] Shankar F, Marulli F, Bernardi M, Mei S, Meert A, Vikram V. Size evolution of spheroids in a hierarchical Universe. *MNRAS* **428** (2013) 109–128. doi:10.1093/mnras/sts001.
- [793] Zhu P, Ho LC, Gao H. The Correlation between Black Hole Mass and Stellar Mass for Classical Bulges and the Cores of Ellipticals. *ApJ* **907** (2021) 6. doi:10.3847/1538-4357/abcaa1.
- [794] Volonteri M. Formation of supermassive black holes. *AAPRev* **18** (2010) 279–315. doi:10.1007/s00159-010-0029-x.
- [795] Trakhtenbrot B. What do observations tell us about the highest-redshift supermassive black holes? *arXiv e-prints* (2020) arXiv:2002.00972.
- [796] Hirschmann M, Somerville RS, Naab T, Burkert A. Origin of the antihierarchical growth of black holes. *MNRAS* **426** (2012) 237–257. doi:10.1111/j.1365-2966.2012.21626.x.
- [797] Zhao Y, Ho LC, Shangguan J, Kim M, Zhao D, Gao H. The Diverse Morphology, Stellar Population, and Black Hole Scaling Relations of the Host Galaxies of Nearby Quasars. *arXiv e-prints* (2021) arXiv:2102.09190.
- [798] Dullo BT, Bouquin AYK, Gil de Paz A, Knapen JH, Gorgas J. The Black Hole Mass-Color Relations for Early- and Late-type Galaxies: Red and Blue Sequences. *ApJ* **898** (2020) 83. doi:10.3847/1538-4357/ab9dff.
- [799] Mathur S. Narrow-line Seyfert 1 galaxies and the evolution of galaxies and active galaxies. *MNRAS* **314** (2000) L17–L20. doi:10.1046/j.1365-8711.2000.03530.x.
- [800] Sulentic JW, Marziani P, Dultzin-Hacyan D. Phenomenology of Broad Emission Lines in Active Galactic Nuclei. *ARA&A* **38** (2000) 521–571. doi:10.1146/annurev.astro.38.1.521.
- [801] Fraix-Burnet D, Marziani P, D'Onofrio M, Dultzin D. The phylogeny of quasars and the ontogeny of their central black holes. *Frontiers in Astronomy and Space Sciences* **4** (2017) 1. doi:10.3389/fspas.2017.00001.
- [802] Gravity Collaboration, Amorim A, Bauböck M, Brandner W, Clénet Y, Davies R, et al. The spatially resolved broad line region of IRAS 09149-6206. *AAP* **643** (2020) A154. doi:10.1051/0004-6361/202039067.
- [803] Heinz S, Sunyaev RA. The non-linear dependence of flux on black hole mass and accretion rate in core-dominated jets. *MNRAS* **343** (2003) L59–L64. doi:10.1046/j.1365-8711.2003.06918.x.
- [804] Merloni A, Heinz S, di Matteo T. A Fundamental Plane of black hole activity. *MNRAS* **345** (2003) 1057–1076. doi:10.1046/j.1365-2966.2003.07017.x.
- [805] Ünal C, Loeb A. On Spin dependence of the Fundamental Plane of black hole activity. *MNRAS* **495** (2020) 278–284. doi:10.1093/mnras/staa1119.
- [806] Schindler JT, Fan X, Novak M, Venemans B, Walter F, Wang F, et al. A Closer Look at Two of the Most Luminous Quasars in the Universe. *ApJ* **906** (2021) 12. doi:10.3847/1538-4357/abc554.
- [807] Valtonen MJ, Ciprini S, Lehto HJ. On the masses of OJ287 black holes. *MNRAS* **427** (2012) 77–83. doi:10.1111/j.1365-2966.2012.21861.x.
- [808] Sulentic JW, Stirpe GM, Marziani P, Zamanov R, Calvani M, Braitto V. VLT/ISAAC spectra of the $H\beta$ region in intermediate redshift quasars. *A&Ap* **423** (2004) 121–132. doi:10.1051/0004-6361:20035912.

- [809] Sulentic JW, Repetto P, Stirpe GM, Marziani P, Dultzin-Hacyan D, Calvani M. VLT/ISAAC spectra of the $H\beta$ region in intermediate-redshift quasars. II. Black hole mass and Eddington ratio. *A&Ap* **456** (2006) 929–939. doi:10.1051/0004-6361:20054153.
- [810] Sillanpaa A, Haarala S, Valtonen MJ, Sundelius B, Byrd GG. OJ 287 - Binary pair of supermassive black holes. *ApJ* **325** (1988) 628–634. doi:10.1086/166033.
- [811] Mehrgan K, Thomas J, Saglia R, Mazzalay X, Erwin P, Bender R, et al. A 40 Billion Solar-mass Black Hole in the Extreme Core of Holm 15A, the Central Galaxy of Abell 85. *ApJ* **887** (2019) 195. doi:10.3847/1538-4357/ab5856.
- [812] Mirabel IF, Rodríguez LF. A superluminal source in the Galaxy. *Nat* **371** (1994) 46–48. doi:10.1038/371046a0.
- [813] Boroson TA, Green RF. The emission-line properties of low-redshift quasi-stellar objects. *ApJS* **80** (1992) 109–135. doi:10.1086/191661.
- [814] Sulentic JW, Zwitter T, Marziani P, Dultzin-Hacyan D. Eigenvector 1: An Optimal Correlation Space for Active Galactic Nuclei. *ApJL* **536** (2000) L5–L9. doi:10.1086/312717.
- [815] Zamfir S, Sulentic JW, Marziani P, Dultzin D. Detailed characterization of $H\beta$ emission line profile in low- z SDSS quasars. *MNRAS* **403** (2010) 1759. doi:10.1111/j.1365-2966.2009.16236.x.
- [816] Popović LČ, Kovačević J. Optical Emission-line Properties of a Sample of the Broad-line Active Galactic Nuclei: The Baldwin Effect and Eigenvector 1. *ApJ* **738** (2011) 68. doi:10.1088/0004-637X/738/1/68.
- [817] Kruczek NE, Richards GT, Gallagher SC, Deo RP, Hall PB, Hewett PC, et al. C IV Emission and the Ultraviolet through X-Ray Spectral Energy Distribution of Radio-quiet Quasars. *AJ* **142** (2011) 130. doi:10.1088/0004-6256/142/4/130.
- [818] Grupe D, Nousek JA. Is There a Connection between Broad Absorption Line Quasars and Narrow-Line Seyfert 1 Galaxies? *AJ* **149** (2015) 85. doi:10.1088/0004-6256/149/2/85.
- [819] Shen Y, Ho LC. The diversity of quasars unified by accretion and orientation. *Nat* **513** (2014) 210–213. doi:10.1038/nature13712.
- [820] Peterson BM, Wandel A. Keplerian Motion of Broad-Line Region Gas as Evidence for Supermassive Black Holes in Active Galactic Nuclei. *ApJL* **521** (1999) L95–L98. doi:10.1086/312190.
- [821] Sulentic JW, Zamfir S, Marziani P, Bachev R, Calvani M, Dultzin-Hacyan D. Radio-loud Active Galactic Nuclei in the Context of the Eigenvector 1 Parameter Space. *ApJL* **597** (2003) L17–L20. doi:10.1086/379754.
- [822] Zamfir S, Sulentic JW, Marziani P. New insights on the QSO radio-loud/radio-quiet dichotomy: SDSS spectra in the context of the 4D eigenvector1 parameter space. *MNRAS* **387** (2008) 856–870. doi:10.1111/j.1365-2966.2008.13290.x.
- [823] Ganci V, Marziani P, D'Onofrio M, del Olmo A, Bon E, Bon N, et al. Radio loudness along the quasar main sequence. *AAP* **630** (2019) A110. doi:10.1051/0004-6361/201936270.
- [824] Wang J, Wei JY, He XT. A Sample of IRAS Infrared-selected Seyfert 1.5 Galaxies: Infrared Color $\alpha(60, 25)$ -dominated Eigenvector 1. *ApJ* **638** (2006) 106–119. doi:10.1086/498667.
- [825] Dultzin-Hacyan D, Taniguchi Y, Uranga L. Where is the Ca II Triplet Emitting Region in AGN? Gaskell CM, Brandt WN, Dietrich M, Dultzin-Hacyan D, Eracleous M, editors, *Structure and Kinematics of Quasar Broad Line Regions* (1999), *Astronomical Society of the Pacific Conference Series*, vol. 175, 303.
- [826] Martinez-Aldama ML, Dultzin D, Marziani P, Sulentic JW, Bressan A, Chen Y, et al. O I and Ca II Observations in Intermediate Redshift Quasars. *ApJS* **217** (2015) 3. doi:10.1088/0067-0049/217/1/3.

- [827] Panda S, Martínez-Aldama ML, Marinello M, Czerny B, Marziani P, Dultzin D. Optical Fe II and Near-Infrared Ca II triplet emission in active galaxies: (I) Photoionization modelling. *arXiv e-prints* (2020) arXiv:2004.05201.
- [828] Sulentic JW, Marziani P, Zwitter T, Dultzin-Hacyan D, Calvani M. The Demise of the Classical Broad-Line Region in the Luminous Quasar PG 1416-129. *ApJL* **545** (2000) L15–L18. doi:10.1086/317330.
- [829] Reichard TA, Richards GT, Schneider DP, Hall PB, Tolea A, Krolik JH, et al. A Catalog of Broad Absorption Line Quasars from the Sloan Digital Sky Survey Early Data Release. *AJ* **125** (2003) 1711–1728. doi:10.1086/368244.
- [830] Bachev R, Marziani P, Sulentic JW, Zamanov R, Calvani M, Dultzin-Hacyan D. Average Ultraviolet Quasar Spectra in the Context of Eigenvector 1: A Baldwin Effect Governed by the Eddington Ratio? *ApJ* **617** (2004) 171–183. doi:10.1086/425210.
- [831] Śniegowska M, Kozłowski S, Czerny B, Panda S, Hryniewicz K. Quasar Main Sequence in the UV Plane. *ApJ* **900** (2020) 64. doi:10.3847/1538-4357/aba620.
- [832] Baskin A, Laor A. What controls the CIV line profile in active galactic nuclei? *MNRAS* **356** (2005) 1029–1044. doi:10.1111/j.1365-2966.2004.08525.x.
- [833] Richards GT, Vanden Berk DE, Reichard TA, Hall PB, Schneider DP, SubbaRao M, et al. Broad Emission-Line Shifts in Quasars: An Orientation Measure for Radio-Quiet Quasars? *AJ* **124** (2002) 1–17. doi:10.1086/341167.
- [834] Richards GT, Croom SM, Anderson SF, Bland-Hawthorn J, Boyle BJ, De Propris R, et al. The 2dF-SDSS LRG and QSO (2SLAQ) Survey: the $z < 2.1$ quasar luminosity function from 5645 quasars to $g = 21.85$. *MNRAS* **360** (2005) 839–852. doi:10.1111/j.1365-2966.2005.09096.x.
- [835] Wang T, Brinkmann W, Bergeron J. X-ray properties of active galactic nuclei with optical FeII emission. *A&Ap* **309** (1996) 81–96.
- [836] Grupe D, Thomas HC, Beuermann K. X-ray variability in a complete sample of Soft X-ray selected AGN. *AAp* **367** (2001) 470–486. doi:10.1051/0004-6361:20000429.
- [837] Bensch K, del Olmo A, Sulentic J, Perea J, Marziani P. Measures of the Soft X-ray Excess as an Eigenvector 1 Parameter for Active Galactic Nuclei. *Journal of Astrophysics and Astronomy* **36** (2015) 467–474. doi:10.1007/s12036-015-9355-8.
- [838] Mao YF, Wang J, Wei JY. Extending the Eigenvector 1 space to the optical variability of quasars. *Research in Astronomy and Astrophysics* **9** (2009) 529–537. doi:10.1088/1674-4527/9/5/004.
- [839] Bon N, Bon E, Marziani P. AGN Broad Line Region variability in the context of Eigenvector 1: case of NGC 5548. *Frontiers in Astronomy and Space Sciences* **5** (2018) 3. doi:10.3389/fspas.2018.00003.
- [840] Sulentic JW, Zamfir S, Marziani P, Dultzin D. Our Search for an H-R Diagram of Quasars. *Revista Mexicana de Astronomia y Astrofisica Conference Series* (2008), vol. 32, 51–58.
- [841] Sulentic J, Marziani P, Zamfir S. The Case for Two Quasar Populations. *Baltic Astronomy* **20** (2011) 427–434.
- [842] Sulentic J, Marziani P. Quasars in the 4D Eigenvector 1 Context: a stroll down memory lane. *Frontiers in Astronomy and Space Sciences* **2** (2015) 6. doi:10.3389/fspas.2015.00006.
- [843] Wildy C, Czerny B, Panda S. Quasar main sequence: A line or a plane. *AAp* **632** (2019) A41. doi:10.1051/0004-6361/201935620.
- [844] Sulentic JW, Marziani P, Zamanov R, Bachev R, Calvani M, Dultzin-Hacyan D. Average Quasar Spectra in the Context of Eigenvector 1. *ApJL* **566** (2002) L71–L75. doi:10.1086/339594.
- [845] Eracleous M, Halpern JP. Completion of a Survey and Detailed Study of Double-peaked Emission Lines in Radio-loud Active Galactic Nuclei. *ApJ* **599** (2003) 886–908. doi:10.1086/379540.

- [846] Eracleous M, Halpern JP. Accurate Redshifts and Classifications for 110 Radio-Loud Active Galactic Nuclei. *ApJS* **150** (2004) 181–186. doi:10.1086/379823.
- [847] Strateva IV, Strauss MA, Hao L, Schlegel DJ, Hall PB, Gunn JE, et al. Double-peaked Low-Ionization Emission Lines in Active Galactic Nuclei. *AJ* **126** (2003) 1720–1749. doi:10.1086/378367.
- [848] Richards GT, Kruczek NE, Gallagher SC, Hall PB, Hewett PC, Leighly KM, et al. Unification of Luminous Type 1 Quasars through C IV Emission. *AJ* **141** (2011) 167–+. doi:10.1088/0004-6256/141/5/167.
- [849] Lipari S, Terlevich R, Macchetto F. Extreme optical Fe II emission in luminous IRAS active galactic nuclei. *ApJ* **406** (1993) 451–456. doi:10.1086/172456.
- [850] Graham MJ, Clowes RG, Campusano LE. A quasar with ultrastrong, ultraviolet Fe II emission. *MNRAS* **279** (1996) 1349–1356.
- [851] Wang JM, Du P, Hu C, Netzer H, Bai JM, Lu KX, et al. Supermassive Black Holes with High Accretion Rates in Active Galactic Nuclei. II. The Most Luminous Standard Candles in the Universe. *ApJ* **793** (2014) 108. doi:10.1088/0004-637X/793/2/108.
- [852] Sun J, Shen Y. Dissecting the Quasar Main Sequence: Insight from Host Galaxy Properties. *ApJL* **804** (2015) L15. doi:10.1088/2041-8205/804/1/L15.
- [853] Panda S, Czerny B, Adhikari TP, Hryniewicz K, Wildy C, Kuraszkiwicz J, et al. Modeling of the Quasar Main Sequence in the Optical Plane. *ApJ* **866** (2018) 115. doi:10.3847/1538-4357/aae209.
- [854] Panda S, Marziani P, Czerny B. The Quasar Main Sequence Explained by the Combination of Eddington Ratio, Metallicity, and Orientation. *ApJ* **882** (2019) 79. doi:10.3847/1538-4357/ab3292.
- [855] Richards GT. CIV Emission as a Probe of Accretion Disk Winds. Chartas G, Hamann F, Leighly KM, editors, *AGN Winds in Charleston* (2012), *Astronomical Society of the Pacific Conference Series*, vol. 460, 67.
- [856] Marziani P, Martínez Carballo MA, Sulentic JW, Del Olmo A, Stirpe GM, Dultzin D. The most powerful quasar outflows as revealed by the Civ λ 1549 resonance line. *ApSpSci* **361** (2016) 29. doi:10.1007/s10509-015-2611-1.
- [857] Marziani P, Sulentic JW, Negrete CA, Dultzin D, Zamfir S, Bachev R. Broad-line region physical conditions along the quasar eigenvector 1 sequence. *MNRAS* **409** (2010) 1033–1048. doi:10.1111/j.1365-2966.2010.17357.x.
- [858] Negrete CA, Dultzin D, Marziani P, Esparza D, Sulentic JW, del Olmo A, et al. Highly accreting quasars: The SDSS low-redshift catalog. *AAp* **620** (2018) A118. doi:10.1051/0004-6361/201833285.
- [859] Bon E, Popović LČ, Gavrilović N. The Hidden Disk Emission in the Single Peaked Sy1 Balmer Emission Lines. Popovic LC, Dimitrijevic MS, editors, *Spectral Line Shapes in Astrophysics* (2007), *American Institute of Physics Conference Series*, vol. 938, 59–64. doi:10.1063/1.2800153.
- [860] Bon E, Popović LČ, Gavrilović N, Mura GL, Mediavilla E. Contribution of a disc component to single-peaked broad lines of active galactic nuclei. *MNRAS* **400** (2009) 924–936. doi:10.1111/j.1365-2966.2009.15511.x.
- [861] Du P, Brotherton MS, Wang K, Huang ZP, Hu C, Kasper DH, et al. Monitoring AGNs with H β Asymmetry. I. First Results: Velocity-resolved Reverberation Mapping. *ApJ* **869** (2018) 142. doi:10.3847/1538-4357/aaed2c.
- [862] Bon N, Bon E, Marziani P, Jovanović P. Gravitational redshift of emission lines in the AGN spectra. *ApSpSci* **360** (2015) 7. doi:10.1007/s10509-015-2555-5.
- [863] Wang JM, Du P, Brotherton MS, Hu C, Songsheng YY, Li YR, et al. Tidally disrupted dusty clumps as the origin of broad emission lines in active galactic nuclei. *Nature Astronomy* **1** (2017) 775–783. doi:10.1038/s41550-017-0264-4.

- [864] Chen K, Halpern JP. Structure of Line-emitting Accretion Disks in Active Galactic Nuclei: ARP 102B. *ApJ* **344** (1989) 115. doi:10.1086/167782.
- [865] Elvis M. A Structure for Quasars. *ApJ* **545** (2000) 63–76. doi:10.1086/317778.
- [866] Marziani P, del Olmo A, D' Onofrio M, Dultzin D, Negrete CA, Martiinez-Aldama ML, et al. Narrow-line Seyfert 1s: what is wrong in a name? *ArXiv e-prints* (2018).
- [867] Mineshige S, Kawaguchi T, Takeuchi M, Hayashida K. Slim-Disk Model for Soft X-Ray Excess and Variability of Narrow-Line Seyfert 1 Galaxies. *PASJ* **52** (2000) 499–508.
- [868] Sądowski A. Slim accretion disks around black holes. *ArXiv e-prints* (2011).
- [869] Sądowski A, Narayan R, McKinney JC, Tchekhovskoy A. Numerical simulations of super-critical black hole accretion flows in general relativity. *MNRAS* **439** (2014) 503–520. doi:10.1093/mnras/stt2479.
- [870] Marziani P, Sulentic JW, Zwitter T, Dultzin-Hacyan D, Calvani M. Searching for the Physical Drivers of the Eigenvector 1 Correlation Space. *ApJ* **558** (2001) 553–560. doi:10.1086/322286.
- [871] Boroson TA. Black Hole Mass and Eddington Ratio as Drivers for the Observable Properties of Radio-loud and Radio-quiet QSOs. *ApJ* **565** (2002) 78–85. doi:10.1086/324486.
- [872] Ai YL, Yuan W, Zhou HY, Wang TG, Dong XB, Wang JG, et al. Dependence of the Optical/Ultraviolet Variability on the Emission-line Properties and Eddington Ratio in Active Galactic Nuclei. *ApJL* **716** (2010) L31–L35. doi:10.1088/2041-8205/716/1/L31.
- [873] Xu D, Komossa S, Zhou H, Lu H, Li C, Grupe D, et al. Correlation Analysis of a Large Sample of Narrow-line Seyfert 1 Galaxies: Linking Central Engine and Host Properties. *AJ* **143** (2012) 83. doi:10.1088/0004-6256/143/4/83.
- [874] Panda S, Czerny B, Wildy C. The physical driver of the optical Eigenvector 1 in Quasar Main Sequence. *Frontiers in Astronomy and Space Sciences* **4** (2017) 33. doi:10.3389/fspas.2017.00033.
- [875] Netzer H. *The Physics and Evolution of Active Galactic Nuclei* (Cambridge University Press) (2013).
- [876] Shang Z, Brotherton MS, Wills BJ, Wills D, Cales SL, Dale DA, et al. The Next Generation Atlas of Quasar Spectral Energy Distributions from Radio to X-Rays. *ApJS* **196** (2011) 2. doi:10.1088/0067-0049/196/1/2.
- [877] Pennell A, Runnoe JC, Brotherton MS. Updating quasar bolometric luminosity corrections - III. [O III] bolometric corrections. *MNRAS* **468** (2017) 1433–1441. doi:10.1093/mnras/stx556.
- [878] Nemmen RS, Brotherton MS. Quasar bolometric corrections: theoretical considerations. *MNRAS* **408** (2010) 1598–1605. doi:10.1111/j.1365-2966.2010.17224.x.
- [879] Netzer H. Bolometric correction factors for active galactic nuclei. *MNRAS* **488** (2019) 5185–5191. doi:10.1093/mnras/stz2016.
- [880] Elvis M, Wilkes BJ, McDowell JC, Green RF, Bechtold J, Willner SP, et al. Atlas of quasar energy distributions. *ApJS* **95** (1994) 1–68. doi:10.1086/192093.
- [881] Woo JH, Urry CM. Active Galactic Nucleus Black Hole Masses and Bolometric Luminosities. *ApJ* **579** (2002) 530–544. doi:10.1086/342878.
- [882] Richards GT, Lacy M, Storrie-Lombardi LJ, Hall PB, Gallagher SC, Hines DC, et al. Spectral Energy Distributions and Multiwavelength Selection of Type 1 Quasars. *ApJS* **166** (2006) 162. doi:10.1086/506525.
- [883] Marziani P, Sulentic JW, Stirpe GM, Zamfir S, Calvani M. VLT/ISAAC spectra of the H β region in intermediate-redshift quasars. III. H β broad-line profile analysis and inferences about BLR structure. *A&Ap* **495** (2009) 83–112. doi:10.1051/0004-6361:200810764.
- [884] Marziani P, Zamanov RK, Sulentic JW, Calvani M. Searching for the physical drivers of eigenvector 1: influence of black hole mass and Eddington ratio. *MNRAS* **345** (2003) 1133–1144. doi:10.1046/j.

1365-2966.2003.07033.x.

- [885] Giustini M, Proga D. A global view of the inner accretion and ejection flow around super massive black holes. Radiation-driven accretion disk winds in a physical context. *AAp* **630** (2019) A94. doi:10.1051/0004-6361/201833810.
- [886] Zamanov R, Marziani P. Searching for the Physical Drivers of Eigenvector 1: From Quasars to Nanoquasars. *ApJ* **571** (2002) L77–L80. doi:10.1086/341367.
- [887] Ferland GJ, Hu C, Wang J, Baldwin JA, Porter RL, van Hoof PAM, et al. Implications of Infalling Fe II-Emitting Clouds in Active Galactic Nuclei: Anisotropic Properties. *ApJL* **707** (2009) L82–L86. doi:10.1088/0004-637X/707/1/L82.
- [888] Narayan R, Yi I. Advection-dominated Accretion: Underfed Black Holes and Neutron Stars. *ApJ* **452** (1995) 710. doi:10.1086/176343.
- [889] Marziani P, Sulentic JW. Quasars and their emission lines as cosmological probes. *Advances in Space Research* **54** (2014) 1331–1340. doi:10.1016/j.asr.2013.10.007.
- [890] Martínez-Aldama ML, Del Olmo A, Marziani P, Sulentic JW, Negrete CA, Dultzin D, et al. Highly accreting quasars at high redshift. *Frontiers in Astronomy and Space Sciences* **4** (2018) 65. doi:10.3389/fspas.2017.00065.
- [891] Diamond-Stanic AM, Fan X, Brandt WN, Shemmer O, Strauss MA, Anderson SF, et al. High-redshift SDSS Quasars with Weak Emission Lines. *ApJ* **699** (2009) 782–799. doi:10.1088/0004-637X/699/1/782.
- [892] Negrete A, Dultzin D, Marziani P, Sulentic J. BLR Physical Conditions in Extreme Population A Quasars: a Method to Estimate Central Black Hole Mass at High Redshift. *ApJ* **757** (2012) 62.
- [893] Temple MJ, Ferland GJ, Rankine AL, Hewett PC, Badnell NR, Ballance CP, et al. Fe III emission in quasars: evidence for a dense turbulent medium. *MNRAS* **496** (2020) 2565–2576. doi:10.1093/mnras/staa1717.
- [894] Abramowicz MA, Czerny B, Lasota JP, Szuszkiewicz E. Slim accretion disks. *ApJ* **332** (1988) 646–658. doi:10.1086/166683.
- [895] Li YR, Wang JM, Ho LC, Du P, Bai JM. A Bayesian Approach to Estimate the Size and Structure of the Broad-line Region in Active Galactic Nuclei Using Reverberation Mapping Data. *ApJ* **779** (2013) 110. doi:10.1088/0004-637X/779/2/110.
- [896] Li H, Mao S, Cappellari M, Ge J, Long RJ, Li R, et al. SDSS-IV MaNGA: global stellar population and gradients for about 2000 early-type and spiral galaxies on the mass-size plane. *MNRAS* **476** (2018) 1765–1775. doi:10.1093/mnras/sty334.
- [897] Wang JM, Qiu J, Du P, Ho LC. Self-shadowing Effects of Slim Accretion Disks in Active Galactic Nuclei: The Diverse Appearance of the Broad-line Region. *ApJ* **797** (2014) 65. doi:10.1088/0004-637X/797/1/65.
- [898] Padovani P, Rafanelli P. Mass-luminosity relationships and accretion rates for Seyfert 1 galaxies and quasars. *AAp* **205** (1988) 53–70.
- [899] Matsuoka Y, Kawara K, Oyabu S. Low-Ionization Emission Regions in Quasars: Gas Properties Probed with Broad O I and Ca II Lines. *ApJ* **673** (2008) 62–68. doi:10.1086/524193.
- [900] Dultzin D, Marziani P, de Diego JA, Negrete CA, Del Olmo A, Martínez-Aldama ML, et al. Extreme quasars as distance indicators in cosmology. *Frontiers in Astronomy and Space Sciences* **6** (2020) 80. doi:10.3389/fspas.2019.00080.
- [901] Czerny B, Martínez-Aldama ML, Wojtkowska G, Zajaček M, Marziani P, Dultzin D, et al. Dark energy constraints from quasar observations. *arXiv e-prints* (2020) arXiv:2011.12375.

- [902] Marziani P, Dultzin D, Del Olmo A, D'Onofrio M, de Diego JA, Stirpe GM, et al. The quasar main sequence and its potential for cosmology. *arXiv e-prints* (2020) arXiv:2002.07219.
- [903] Teerikorpi P. On Öpik's distance evaluation method in a cosmological context. *AAp* **531** (2011) A10. doi:10.1051/0004-6361/201116680.
- [904] Wang JM, Du P, Valls-Gabaud D, Hu C, Netzer H. Super-Eddington Accreting Massive Black Holes as Long-Lived Cosmological Standards. *Physical Review Letters* **110** (2013) 081301. doi:10.1103/PhysRevLett.110.081301.
- [905] La Franca F, Bianchi S, Ponti G, Branchini E, Matt G. A New Cosmological Distance Measure Using Active Galactic Nucleus X-Ray Variability. *ApJL* **787** (2014) L12. doi:10.1088/2041-8205/787/1/L12.
- [906] Czerny B, Beaton R, Bejger M, Cackett E, Dall'Ora M, Holanda RFL, et al. Astronomical Distance Determination in the Space Age. Secondary Distance Indicators. *Space Science Reviews* **214** (2018) #32. doi:10.1007/s11214-018-0466-9.
- [907] Cabanac RA, de Lapparent V, Hickson P. Classification and redshift estimation by principal component analysis. *Astronomy and Astrophysics* **389** (2002) 1090–1116. doi:10.1051/0004-6361:20020665.
- [908] Recio-Blanco A, Aparicio A, Piotto G, de Angeli F, Djorgovski SG. Multivariate analysis of globular cluster horizontal branch morphology: searching for the second parameter. *Astronomy and Astrophysics* **452** (2006) 875–884. doi:10.1051/0004-6361:20053006.
- [909] Ellis SC, Driver SP, Allen PD, Liske J, Bland-Hawthorn J, De Propris R. The Millennium Galaxy Catalogue: on the natural subdivision of galaxies. *Mon. Not. R. Astron. Soc.* **363** (2005) 1257–1271. doi:10.1111/j.1365-2966.2005.09521.x.
- [910] Chattopadhyay T, Chattopadhyay AK. Objective Classification of Spiral Galaxies Having Extended Rotation Curves Beyond the Optical Radius. *The Astronomical Journal* **131** (2006) 2452–2468. doi:10.1086/503160.
- [911] Chattopadhyay T, Chattopadhyay AK. Globular clusters of the Local Group - statistical classification. *Astronomy and Astrophysics* **472** (2007) 131–140. doi:10.1051/0004-6361:20066945.
- [912] Chattopadhyay AK, Chattopadhyay T, Davoust E, Mondal S, Sharina M. Study of NGC 5128 Globular Clusters Under Multivariate Statistical Paradigm. *The Astrophysical Journal* **705** (2009) 1533–1547. doi:10.1088/0004-637X/705/2/1533.
- [913] Fraix-Burnet D, Davoust E, Charbonnel C. The environment of formation as a second parameter for globular cluster classification. *Mon. Not. R. Astron. Soc.* **398** (2009) 1706–1714. doi:10.1111/j.1365-2966.2009.15235.x.
- [914] Sánchez Almeida J, Aguerri JAL, Muñoz-Tuñón C, de Vicente A. Automatic Unsupervised Classification of All Sloan Digital Sky Survey Data Release 7 Galaxy Spectra. *The Astrophysical Journal* **714** (2010) 487–504. doi:10.1088/0004-637X/714/1/487.
- [915] Fraix-Burnet D. Multivariate evolutionary analyses in astrophysics. Starck JL, Saber Naceur M, Murtagh R, editors, *ADA 6 - Sixth Conference on Astronomical Data Analysis* (2010), 27.